Studies of Excited State Dynamics, Third Order Optical Nonlinearity and Nonlinear Absorption in C_{60}, Porphyrins, and Phthalocyanines Using Incoherent Laser Spectroscopy

Thesis submitted for the degree of

Doctor of Philosophy

by

Sonia Venugopal Rao

School of Physics
University of Hyderabad
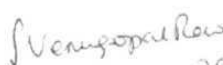**Hyderabad - 500 046 India**
March 2000.

For my Parents

DECLARATION

I hereby declare that the matter embodied in this thesis entitled **"Studies of Excited State Dynamics, Third Order Optical Nonlinearity, and Nonlinear Absorption in C_{60}, Porphyrins and Phthalocyanines Using Incoherent Laser Spectroscopy"** is the result of investigations carried out by me in the School of Physics, University of Hyderabad, India, under the supervision of Dr. D. Narayana Rao
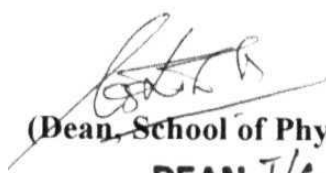
Place Hyderabad

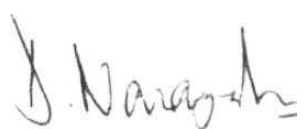Date: 29-3-2000

(Soma Venugopal Rao)

CERTIFICATE

This is to certify that the work described in this dissertation entitled **"Studies of Excited State Dynamics, Third Order Optical Nonlinearity and Nonlinear Absorption in C_{60}, Porphyrins and Phthalocyanines Using incoherent Laser Spectroscopy"** has been carried out by **Mr. Soma Venugopal Rao** under my direct supervision for the full period prescribed under PhD. ordinances of the University and the same has not been submitted for any other degree or diploma at this or any other University.

Place:　　　Hyderabad

Date:　　　**27-3.2000**

(Dean, School of Physics)

DEAN I/C
School of Physics
University of Hyderabad
Hyderabad-500 046, INDIA

(Dr. D. Narayana Rao)

Dr. D. NARAYANA RAO
Reader
School of Physics
University of Hyderabad
Hyderabad-500 046, India

ACKNOWLEDGEMENTS

Table of Contents

CHAPTER 6 C_{60}: Studies of Third-order Nonlinearity,Excited State Dynamics using DFWM-IL and Dispersion Studies of Nonlinear Absorption using Z-scan techniques

CHAPTER 7 Phthalocyanines: DFWM-IL Results

CHAPTER 1

Introduction

In this chapter we introduce the concepts and applications of third-order nonlinear susceptibility. A comparison is made between the different classes of materials, which have been investigated, for numerous technological applications. The materials chosen for the present study are C_{60}, Porphyins, and Phthalocyanines and the motivation for choosing these materials and techniques are explained in detail. The topics covered in each chapter are highlighted.

1.1 Introduction to Nonlinear Optics and its Applications

The latter half of the twentieth century was marked by the development of electronics based on semiconductor industry and technology. However, the speed and memory of the present devices used in communication, information processing and other areas, will reach their limit thereby not being able to cater the needs of the future. It is expected that the 21st century will be an era for wide application of all optical technologies since, in an information society, it is necessary to rapidly transmit, receive and process a large amount of information For large bandwidths optical sources will serve the purpose and extensive development of Optronics (optics + electronics) and Photonics is being undertaken. Optical devices have the advantages since they posses the important properties like high frequencies, broad spectral range, ultra-high speed (~ few fs), capability of parallel processing and high electromagnetic noise resistance.

Third-order nonlinear optical properties provide the means to control light with light, to change the frequency of colour of light, to amplify one source of light, switch it, or alter its transmission characteristics through a medium [I]. The intensity dependant refractive index provides the mechanism for control in most of the third-order nonlinear optical materials based devices. The discover)' of the phenomena of optical bistability gave a boost to the idea of exploiting the large bandwidth (~ 10^{12} Hz) For realisation of photonics era the search for novel materials has gained utmost importance Studies of optical materials with large third order nonlinearities and ultrafast response times has received increasing attention of the researchers over the last two decades for their potential applications in the area of optical communications,

optical data processing, opto-electronics and many other related fields [2-18]. Progress in the realising the potential of these materials depends on (a) Obtaining a fundamental understanding of the basic physics of nonlinear processes (b) Based on the understanding, optimisation at molecular level and later at the bulk level (c) Using these materials to engineer viable integrated devices. These steps include a unique blend of theoretical modelling, chemical synthesis, materials processing, complete characterisation and investigation of device application, and to provide an interactive feedback between different stages for more effective optimisation [19-23] The research of nonlinear optical effects can be mainly divided into two branches (a) Measurement of the magnitude, sign, and wavelength-dependence of nonlinear susceptibility (b) Investigation *of* the temporal, spatial, spectral, and polarization properties of input and output light. For broadband and ultra-fast response, non-resonant purely electronic nonlinearity is required. This is also desirable since no optical loss from absorption and subsequent thermal effects are present.

1.2 Nonlinear Optical Materials

Unlike second-order materials there are no symmetry' requirements to observe nonlinearity in third-order materials. This allows different kinds of materials like liquids, thin films, glasses, and crystals to exhibit the nonlinearity Kobayashi in his review article [4] on introduction to nonlinear optical materials describes the importance of the materials and their classification Over the last two decades variety of resonant and non-resonant materials have been investigated for various NLO applications, which include molecule-based materials (molecular crystals, conjugated polymers etc.), band-based materials (semiconductors, quantum dots, multiple quantum wells and related materials), bond-based materials (saturated organic molecules etc), bio-molecules (bacteriorhodopsin etc.) and several others Although several materials with large nonlinearities were discovered (InSb with a $x^{(3)}$ of 0.3 esu. and GaAs with a $x^{(3)}$ of 0.04 esu [3]) the response times (~ 400 ns and 20 ns respectively for InSb and GaAs) were severely short of the requirement An ideal material for any device application should possess non-resonant nonlinearity [$x^{(3)}$] in the range of 10^{-5} - 10^{-4} esu and the response time in the ps - fs domain. Some of the

major drawbacks, although possessing larger nonlinearities, in materials other than organics are (a) Difficulty in fabrication (b) Limitation in operational wavelength (c) Slower response times (d) Requires significant investment in terms of equipment and expertise, and (e) Lower damage threshold. Although the nonlinearity of organic materials is still less than the actual requirement and the optical quality much inferior there is still much interest owing to the ease with which one can 'tailor' these materials accordingly and due to their good mechanical, chemical, thermal, and optical stability In contrast to inorganic materials that consist of covalent or ionic bond of atoms over the entire expansion of solids, organic materials are based on independent molecules and characterised by weak intermolecular interactions. Further flexibility is offered by these molecular materials at the bulk and microstructure levels where they can be formed as crystals, solution cast or vacuum deposited films, Langmuir Blodgett films offering the ultimate design with mono-molecular resolution, polymeric films, glasses and gels Organic dyes and polymeric materials possess lower dielectric constant, responsible for faster response times, than their inorganic counterparts. Different forms of organic/polymeric materials that have been thoroughly investigated in the recent past include dye aggregates, guest-host systems, sol-gels, organic crystals, dye doped polymers etc. Some of the prototype devices already demonstrated using organic third-order nonlinear materials include a bistable device, frequency doublers. electro-luminescent devices, directional coupler, nonlinear Bragg mirror, and wave-guides [5-12],

Nalwa in his extensive review article [5] on organic materials for nonlinear optics and techniques for measurement has outlined the advantages / disadvantages all the materials and techniques studied for third-order nonlinearity. Several materials including organic liquids, molecular solids, conjugated polymer and related compounds, organometallic compounds, and organic composites have been thoroughly investigated Among these we have chosen C_{60}, Porphyrins and Phthalocyanines for our study of excited state dynamics, nonlinearity and nonlinear absorption measurements. These materials have shown promising nonlinearity ($y \sim 10^{-28}$ esu), an ultra-fast response (~ few tens of fs) [5] and high damage threshold. In these rc-conjugated systems large charge separation can be achieved through the easy de-

localisation of the n electron cloud leading to very large and fast nonlinearity since it requires only electronic motion, which could be in few fs.   Moreover these chromophores are easily amenable to structural modifications and possess tremendous applications (Complete details of which have been provided in subsequent chapters).

1.3 Techniques for measurement of excited state dynamics

The applications of organic materials fall into two broad categories: those that rely on multi-photon absorption (MPA) and those that utilise nonlinear refractive index (NR1) change.   Many optical limiting schemes rely on MPA whereas devices targeted for signal processing applications rely on the NR1 changes.   A complete insight into the magnitude, cause of nonlinearity, which includes an improved understanding of the relationship between the molecular structure and the microscopic optical nonlinearities, and dynamics *of* different excited states, contributing to the total nonlinearity, is essential for any material to be identified for device making.   To understand the microscopic dynamics *of* these materials, studies of relaxation processes after light excitation are basically important.   Studies on the relaxation processes associated with excited states *of* such materials are also important in understanding/investigating fundamentals of light-matter interaction

Relaxation processes in condensed matter such as liquids and solids are, generally, in the order of few tens of ps to few tens of fs   Probing such time scales would require very expensive ps/fs laser systems.   Most of these materials due to their complex energy level structure have a large number of vibrational and rotational bands leading to very fast non-radiative transitions within each electronic band   These relaxations normally occur in ps and fs domain   Different spectroscopic methods [24] like Dynamic Light Scattering Spectroscopy, tunable Laser Induced Grating Spectroscopy, Hole Burning Spectroscopy have been developed and served for measuring these ultra-fast relaxation times with time resolution of less than 100 fs [25] These methods are indirect, cumbersome and the obtained data requires careful interpretation   Alternative time-resolved nonlinear spectroscopic methods such as Photon Echoes, Transient DFWM, Induced Transient Grating, Optical Kerr Shutter,

Pump-Probe Technique etc. have time resolution determined by the width of the input pulse used [26]. Moreover the difficulties involved with conventional methods using ultrashort pulses are

- Lasers for generation of such short pulses, with required intensities for spectroscopic studies, are very complicated and expensive.

- Wavelength of such short pulses is limited to a short spectral region (615 to 625 nm) due to limitation in appropriate combination of gain medium and Saturable absorber. Synchronously pumped dye lasers with about 100 fs pulse width tuneable in the red region are available. Recent prominent developments have enabled us to obtain sub-100 fs pulses from Ti^{3+}-doped sapphire laser and could generate white light from these pulses. But these systems are very sophisticated and the cost involved is exorbitant.

- The power spectrum, which is the inverse of pulse width, of such pulses is very broad and leads to broadening effects due to linear/nonlinear dispersion within the optical components in the path of the pulses Even though there is a possibility of recompression by negatively dispersive optical components, such as grating pairs, prism pairs etc, perfect recompression is not very easy and can affect the intensity of the pulses drastically.

1.4 Incoherent Laser Spectroscopy: Tool for measuring excited state dynamics in the ps / fs domain

To overcome the above shortcomings, a new spectroscopic method was developed in the mid-eighties by Morita and Yajima [27] in which a temporally incoherent light, derived usually from ns pulses, is used as the source This technique has been extensively applied for the studies of both dephasing times (T_2) in fs domain and longitudinal relaxation times (T_1) in the ps domain [28] Kobayashi et al. [29] later derived a generalised formula for calculating the relaxation times when one of the beams, in the standard Degenerate Four Wave Mixing (DFWM), is delayed with respect to the other beams. Okamoto [30] extended the work of Morita and Yajima to systems with more than two levels, like organic dyes, having different excited and

ground state relaxation times and showed that the population relaxation times can be obtained, in the standard DFWM technique, using non zero delay of beam 2.

A temporally incoherent light has very short coherence and hence correlation time. This kind of light appears as a short pulse of duration τ_c in auto-correlation measurements, and is, therefore expected to play similar role to a short pulse in the non linear regime utilising the correlation technique. Accordingly, experiments with extremely high resolution can be performed with incoherent light. Here the time resolution is independent of pulse width Some of the advantages of this technique are

• Incoherent light (broadband dye laser pulses) is much easier to generate compared to ps/fs lasers   It is also easier to construct, operate and maintain an ns laser. For example it is relatively simple to generate laser pulses with line width of ~ 10 nm, which corresponds in the visible region to ~ 30-40 fs sub-pulses.

• Tunability is very large with such systems (By appropriately changing the dye species and concentration, solvent, pumping source and power etc.).

• Since the input pulse is of ns time duration the time resolution is not degraded by dispersion.

1.5 Aim and scope of the thesis

The aim of the present thesis is three folds.

1   To apply Incoherent Laser Spectroscopy for the study of different relaxation times, (phase and population) which occur in the ps and fs domain, in different materials like C_{60}, Porphyrins, Phthalocynaines etc , which have potential applications on the technological side

2   To develop a theoretical model based on three/four levels, which will satisfactorily explain the experimental observations of the DFWM-IL measurements, in these exotic molecules.

3. To study the third-order nonlinear optical properties, through DFWM technique, and nonlinear absorption mechanisms, through Z-scan technique, in these materials

and to gain an insight into the excited state parameters/dynamics, their behavior with external parameters like wavelength, intensity, concentration etc. for their applications in optical limiting and switching.

This thesis is organized into seven chapters including introduction Chapter II will introduce the concepts of Degenerate Four Wave Mixing (DFWM) and Z-scan techniques and their application for the measurement of third-order optical nonlinearity, relaxation time and nonlinear absorption measurements. This chapter also includes the complete details of the experimental setup, using incoherent light and 35 ps pulses, for each of these techniques Our initial DFWM results, with incoherent light, on the standard samples like liquid CS_2 and Rh B are also included.

Chapter III has the theoretical formulation for the observed DFWM signals in Porphyrins, C_{60}. Black Ink and other organic materials in general. A double peak structure observed in the PC signal, recorded as a function of delay of beam 3. is explained in terms *of* the relaxation of the different excited states involved Earlier models included either two levels or three levels (open two-level system) only. Here we consider a more general 4-level model for these molecules (based on energy level structure of a typical organic molecule. comprising of S_0. S_1. S_{1N}. and S_n states) and obtain, numerically, the DFWM signal as a function of delay time of the probe pulse for different delays *of* the backward pump The obtained numerical results, with similar parameters, are then compared with the experimental data

Chapter IV summarizes the results of $\chi^{(3)}$ measurements of several metalloporphyrins obtained with both ns and ps pulses in the standard DFWM configuration A total of seventeen porphyrins are studied and a comparison is made between the nonlinearity in the ns and the ps domain The origin of large nonlinearity observed with ns pulses is identified as due to strong excited state absorption, the higher excited states get populated resulting in the enhancement. Earlier studies on excited state enhancement used a strong pump beam to modify the population distribution and a subsequent beam probes the nonlinearity. In our case the strong ESA probes the nonlinearity of high-lying states A comparison is also made with

other class of porphyrins and we find that Tetra Tolyl Porphyrins are superior to many others. The nonlinear absorption studies, performed using Z-scan, indicate large, negative nonlinearity and the results are detailed.

Chapter V includes our results on the relaxation time measurements using DFWM with incoherent light for the same porphyrins, which showed large nonlinearity. The observed signals are explained in terms of the relaxation rates of the different excited states. Time-resolved data is also obtained, using DFWM in PC configuration, with 35 ps pulses and a comparison is made with the dynamics obtained with incoherent light While most of the ps and ns data agree with each other some of the results obtained using ps pulses differ from those obtained using the ns pulses and this is explained in terms of the different relaxation pathways of the molecule excited with different pulses. We also compare our DFWM-IL results with those quoted in literature for similar compounds.

Chapter VI incorporates our results on $\chi^{(3)}$ and DFWM-IL measurements on the sample C_{60} (xylene) We observe a large nonlinearity at 600 nm and attribute it to the strong two-photon absorption at that wavelength The results on the excited state dynamics obtained using incoherent light match very well with those obtained using ultra-short pulses (150 fs pulses) An experimental study of dispersion of nonlinear absorption is carried out using a ns OPO. The open aperture Z-scans are obtained in the spectral region of 440 nm to 640 nm A theoretical model (comprising of five levels, including both excited state and two-photon absorption) is developed and fitted to the observed data Different excited state absorption cross-sections have been evaluated and the effect of various parameters, like lifetimes, intersystem crossing etc, on the behavior of the scans is discussed in detail

Chapter VII deals with some of the results on excited state dynamics obtained in matallophthalocyanines. We conclude the thesis with (a) Summary of the results obtained (b) Advantages, shortcomings in the present DFWM-IL technique (c) Further improvements, suggestions in theoretical modeling for better understanding of the experimental results.

1.6 References

1. H.M Gibbs, *Optical Bistability: Controlling Light with Light,* Academic Press, Orlando, FL, 1985

2 R.W. Boyd, *Nonlinear Optics,* Academic Press, New York, USA, 1993

3. J.V. Moloney, A.C Newell, *Physica* **D44,** 1, 1990; Y.R Shen, *Rev. Mod. Phys.* 48, 1, 1976

4 T Kobayashi, *Nonlinear Opt.* 1, 91, 1991; T. Kobayashi, *Nonlinear Optics of Organics and Semiconductors,* Springer-Verlag, Berlin, 1989.

5. H.S Nalwa, Ed *Handbook of Organic Conductive Molecules and Polymers,* Volumes 1-4, John Wiley and Sons Ltd , New York, 1997; H.S. Nalwa and S Miyata, Ed 's *Nonlinear Optics of Organic Molecules and Polymers,* CRC Press Inc., USA, 1997 and references therein

6 G.J. Ashwell and D Bloor, Ed's *Organic Materials for Nonlinear Optics III.* Royal Society of Chemistry, Cambridge, 1993.

7. S R Marder, J E Sohn, and G D Stucky, Ed 's *Materials for Nonlinear Optics: Chemical Perspectives,* ACS Symposium Series 455, American Chemical Society, Washington, DC 1991

8 P.N Prasad and D.J Williams, *Introduction to nonlinear optical effects in molecules and polymers,* John Wiley, New York. 1991; J. Messier. F Kazjar. P.N Prasad and D Ulrich, Ed's *Nonlinear Optical Effects in Organic Polymers,* Kluwer Academic Publishers. Netherlands. 1989. P.N Prasad and D.R Ulrich. Ed "s *Nonlinear Optical and Electroactive Polymers,* Plenum, New York, 1998

9 D.S Chemla, J Zyss, Ed 's, *Nonlinear Optical Properties of Organic Molecules and Crystals,* Vol.'s 1 and 2, Academic Press. Orlanda, FL, USA. 1987.

10 S. Tripathy, E Cavicchi, J Kumar, and R.S Kumar, *Chemtech* **19,** 747. 1989; Y Shirota,./. *Mater. Chem.* **10.** 1, 2000.

11 R A Hann, D Bloor, Ed 's, *Organic Materials for Nonlinear Optics* Royal Society of Chemistry. London, 1989

12 A J Heeger, J Orenstein, and D.R Ulrich, *Nonlinear Optical properties of Polymers,* Materials Research Society Proceedings, Materials Research Society, Pittsburgh, **109,** 1988

13. NJ. Long, *Angew. Chem. Int. Ed. Engl.* 34, 21, 1995 and references therein.

14. D.J. Williams, *Angew. Chem. Int. FA. Engl* 23, 690, 1984 and references therein.

15. H. Nakanishi, *Nonlinear Opt.* 1, 223, 1991; P.N. Prasad, *Nonlinear Opt* 13, 91, 1995; P.N. Prasad, ME. Orczyk, J. Zieba, *Nonlinear Opt.* 14, 127, 1995.

16. M. Pope, *Mol. Cryst. Liq. Cryst.* **228,** 1, 1993; D. Bloor, *Physica Scripta* **T39**, 380, 1991; D Bloor, *Physics World* 36, 1991

17. D.F Eaton, *Science* **251,** 281, 1991 and references therein; *Physics World,* Special Issue on *Molecular Materials and Devices,* March 1999.

18 E V Keuren, H Mohwald, S Rozouvan, W. Schrof, V. Belov, H. Matsuda, and S. Yamada, *J. Chem. Phys.* **110,** 3584, 1999

19 A.D Walser, G Coskun, and R Dorsinville in *Electrical and Optical Polymer Systems,* Ed.'s D L Wise, G.E Wnek, D J Trantolo, T.M Cooper, and J.D. Gresser, Dekker, Inc , New York, US, 423, 1998.

20 J L Bredas, *Science* **263,** 487, 1994.

21. P.N. Prasad, *Nonlinear Optics: Fundamentals, Materials, and Devices* Ed S. Miyata. Elsevier Science Publication. 283, 1992.

22 A.F. Garito. J.R Heflin, K.Y. Wong. O Zamani-Khamiri. *Organic Materials for Nonlinear Optics,* Royal Society of Chemistry, 16, 1989

23 A Ganto, R F Shi. and M Wu. *Physics Today* 51. 1994.

24 K A Nelson, R Casalegno, R J Dwayne Miller, and M.D. Fayer, *J. Chem. Phys.* *11,* 1144, 1982, H Souma, T Yajima, and Y Taira, *J. Phys. Soc. Jpn.* **48,** 2040, 1980; R Trebino. C.E. Barker, and A Siegman. *IEEE J. Quant. Electron.* **QE-22,** 1413, 1986, J J Song, J.H Lee. and M.D. Levenson, *Phys. Rev.* **A17,** 1439. 1978; B M Kharlamov, R.I. Personov, and LA. Bykovskaya, *Opt. Commun.* **12,** 191, 1974

25 C.B Harris, E.P. Ippen, G.A Mourou, and A.H Zewail, Ed s *Ultrafast Phenomena I to IX,* Springer Verlag, Berlin; *Ultrashort light pulses: picosecond techniques and applications,* S.L Shapiro ed., Springer, Berlin, 1977; *Ultrashort light pulses and their applications,* W Kaiser, ed , Springer Berlin. 1988, *Spectroscopy and excitation dynamics of condensed molecular systems,* ed.'s V M Agronovitch, and R.M Hochstrasser, North-Holland, Amsterdam, 1983; A. Laubereau and W Kaiser, *Rev. Mod. Phys.* **50,** 607, 1978

26. *Picosecond phenomena, Vol. 's I to VII,* Springer Series in Chemical Physics, Springer, Berlin; K.A Drenser, R.J. Larsen, F.P. Strohkendl, and L.R. Dalton, *J. Phys. Chem.* **A103**, 2290, 1999

27 N. Morita and T. Yajima, *Phys. Rev.* **A30**, 2525, 1984; N. Morita, T. Tokizaki, and T. Yajima,./. *Opt. Soc. Am.* **B4,** 1269, 1987

28. A. Kummrow and A. Lau, *Appl. Phys.* **B63,** 209, 1996 and references therein.

29. T. Kobayashi, A. Terasaki, T Hattori, K. Kurokawa, *Appl. Phy.* **B47,** 107, 1988, T Kobayashi, *Modern Nonlinear Optics,* Part 3, Ed 's M Evans and S Kielich, Advances in Chemical Physics Series, Vol. LXXXV, John Wiley and Sons, Inc., 1994

30. H. Okamoto,./. *Opt. Soc. Am.* **B10,** 2353, 1994.

CHAPTER 2

Experimental Techniques and Details: Degenerate Four Wave Mixing and Z-scan

This chapter presents the details of the experimental techniques employed for different studies carried out. A brief introduction to Degenerate hour Wave Mixing (DFWM) and Z-scan techniques, their applicability to dynamics and nonlinear absorption studies is given. The complete details of the experimental set-up for both the techniques, using different configurations, are highlighted. A brief introduction to the photo-physics of a typical organic molecule is presented. Our initial DFWM results on the samples Rhodamine B (RhB) and CS_2 using the incoherent light are also presented.

2.1 Introduction

The magnitude and response of third-order nonlinear susceptibility are important parameters in characterising and determining the applicability of any material as a nonlinear optical device. There are several techniques [1-7] for measuring these parameters that include

(a) Degenerate Four Wave Mixing: For measurement of both magnitude and response time of the third-order nonlinearity

(b) Third Harmonic Generation. For measurement of magnitude of third-order nonlinearity only.

(c) Z-scan For measurement of sign, magnitude of third-order nonlinearity.

(d) Electro-Absorption technique. Dispersion studies of third-order nonlinearity

(e) Time-resolved Optical Kerr Effect and Transient Absorption techniques For the study of photo-physical processes determining the nonlinearity.

Among these DFWM is one of the most important and versatile technique, which provides information about the magnitude and response of the third-order nonlinearity. In this process, three coherent beams incident on a nonlinear medium generate a fourth beam due to the third order nonlinearity. The strength of this fourth beam is dependent on a coupling constant that is proportional to effective $x^{(3)}$ and hence measurements on PC signal will yield information about the $x^{(3)}$ tensor components of the medium [8-

16]. DFWM can be employed in backward (or generally called the Phase Conjugate), forward or boxcar configurations, with the choice on the experimental conditions and the requirements Using different polarizations of the three beams it is possible to measure all the independent $\chi^{(3)}$ tensor components of an isotropic material. Some of the several advantages of this technique being

- The Phase Conjugate signal is distinguishable from others by simple spatial separation
- The detected signal has a characteristic dependence on the input intensities, which can be used for verification of the experiment.
- The sample could be in any form (isotropic) and all the independent tensor components of $\chi^{(3)}$ can be measured in a single experiment
- Beams other than true Gaussian modes can be employed.
- The time dependence of the probe beam gives information about the response times of the nonlinearity.

2.1.1 Degenerate Four Wave Mixing (DFWM)

A Four Wave Mixing experiment can also be considered as an interaction of three optical fields in a medium The presence of a third-order optical nonlinear susceptibility $\chi^{(3)}$ leads to the creation of various components of material polarisation, giving rise to new optical fields If the phase-matching condition is fulfilled (i.e. the phase relation between the waves emitted by different parts of the nonlinear medium leads to constructive build up of the resulting wave), new beams of light are created If the fields are of identical frequencies, the process is termed as Degenerate Four Wave Mixing and the output beam will have the same frequency The time resolution of the FWM measurements depends on two parameters The first is related to the time duration of the laser pulses and the second is related to the coherence time of the laser pulses.

The whole process can be looked in another way and treating it as creation of the transient gratings by interference of pairs of waves and Bragg diffraction of the

other wave from the grating formed in the material by it's nonlinear response to spatially modulated light intensity. At the crossing of two beams, the spatial modulation of their electric fields varies due to constructive and destructive interference. The molecules in the interaction region experience varying electric field intensities according to their position and this leads to the formation of a transient grating of polarised molecules in space. The formation of the grating does not require that the two crossing beams coincide in time as long as the coherence is maintained in the sample. Based on the relative timing of the three fields one can envision different gratings formed as shown in fig 2 1 [1]. The grating formed by $\mathbf{k_1}$ and $\mathbf{k_2}$ waves gets diffracted by $\mathbf{k_3}$ beam to yield the output at $\mathbf{k_3} \pm (\mathbf{k_1} - \mathbf{k_2})$. The one formed by $\mathbf{k_2}$ and $\mathbf{k_3}$ gets diffracted by $\mathbf{k_1}$ to yield the output at $\mathbf{k_1} \pm (\mathbf{k_2} - \mathbf{k_3})$. They are illustrated in the fig 2 1 for the special case of $\mathbf{k_1} = -\mathbf{k_2}$. The output waves are expected in the directions $-\mathbf{k_3}$ and $\mathbf{k_3} \pm \mathbf{k_1}$. The generation of output in $-\mathbf{k_3}$ direction is phase-matched, and is known as phase conjugate signal, while in the $\mathbf{k_3} \pm \mathbf{k_1}$ directions is not. Thus usually only the output at $\mathbf{k_4} = -\mathbf{k_3}$ needs to be considered.

In the phase conjugate configuration, the backward pump is delayed with respect to other to observe the decay of the grating. For small values of 8 the grating written" by the forward pump and probe pulses will have a large spatial period $A = \lambda/(2n_{0}\mathrm{Sin}(\theta/2))$ When the pulses coincide in time two other gratings are also formed, a small period grating generated by the interaction of the backward pump and the probe pulses and a two-photon temporal coherence grating. However the spacing of the small-period grating (given now by $A = \lambda/(2n_{0}\mathrm{Sin}((\pi - \theta)/2))$ is considerably smaller than the large-period one. In our case the spacing of the large-period grating is found to be ˜ 2 - 3 μ (depending on the angle 8 and the refractive index of the solvent) and for the small-period grating it is calculated to be 0 2 - 0.3 μ If diffusive processes are present the small-period grating washes out rapidly. The contribution of the two-photon grating is usually negligible, and can be observed under special conditions of strong enhancement due to two-photon resonance

The applications of Four-Wave Mixing (FWM) can be divided into three categories. First, the creation of a dynamic grating via a material excitation and the
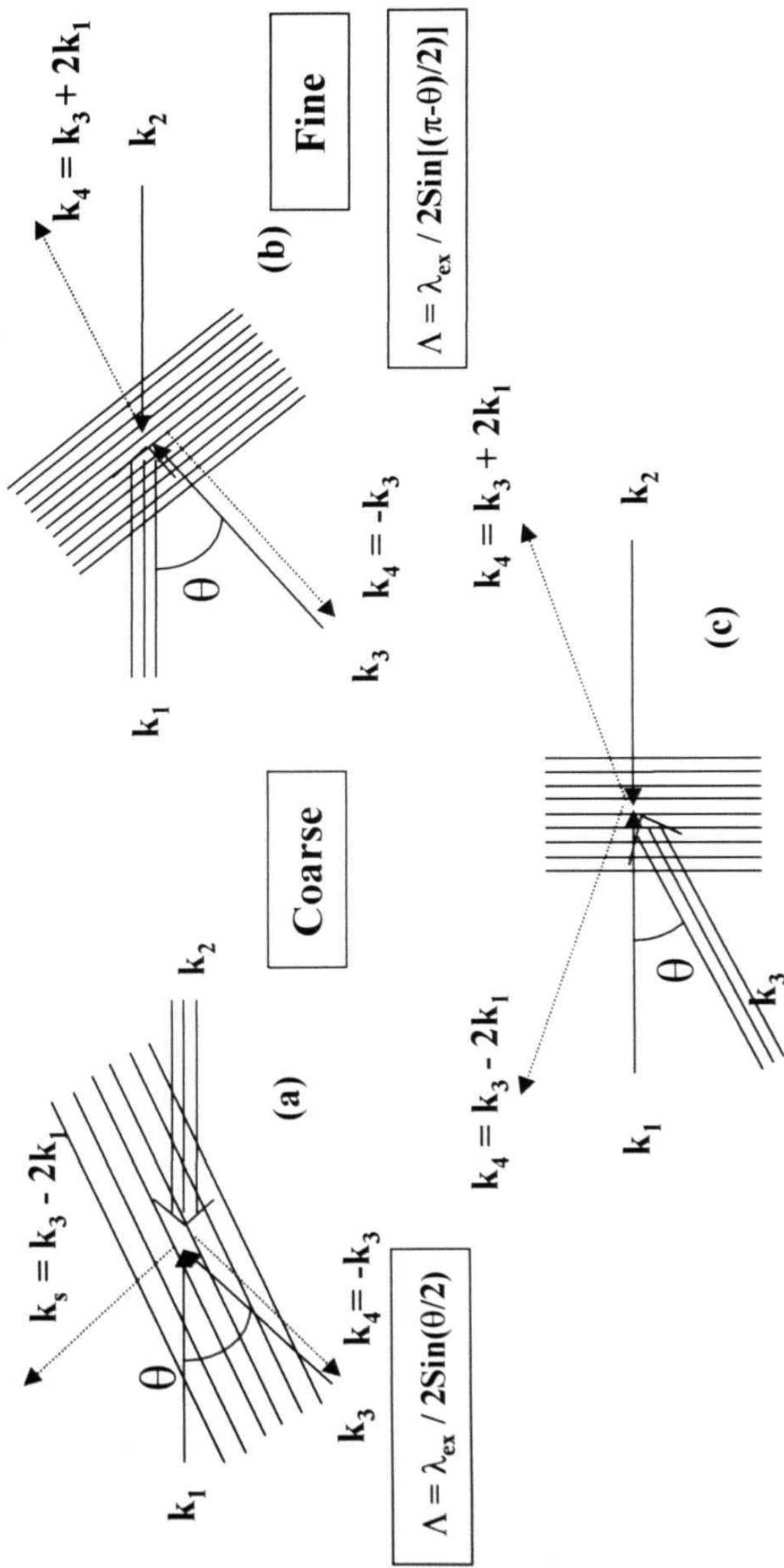
Fig. 2.1 Different gratings formed with interference of any two beams

subsequent probing of the grating using another beam allow us to study the material excitation processes. Such a spectroscopic technique is versatile and extremely powerful, and has found many applications in various disciplines [17,18]. Second, under specific conditions with the creation of a static grating, the output of FWM is a phase-conjugate (PC) signal. This is the real time holography and can be used in real-time image construction in different applications like optical image and data processing. Third, the possible generation of new frequency components in FWM permits the extension of coherent light sources to new frequency regions in the IR, UV, and XUV where there are not many available.

2.2 Degenerate **Four** Wave Mixing **with Incoherent Light (DFWM-IL)**

2.2.1 Characterisation of the Broadband Dye Laser

The source for incoherent light for all the experiments is a home-built broad band dye laser [19] The versatility and utility of organic dye lasers in science and technology continue to increase even long after the inception of the dye laser. High average power and narrow pulse width dye lasers are developed for spectroscopic studies, communications, atmospheric propagation studies, isotope separation and many other applications. New laser dyes are also being developed which provide high efficiency, designed at low cost and chemical stability for dye lasers at wavelengths ranging from the near infrared to the ultraviolet. Construction and operation of organic dye lasers depend on the photo-physical and chemical properties of the dye solutions, which are used as the gain medium. The structural and spectroscopic properties of efficient laser dyes and detailed information on their lasing properties are listed in the data sheets of dye manufacturers [20]. The most important criteria in selecting components for the dye laser system are the chemical inertness and the construction materials. The safest materials that can be used are glass or quartz, stainless steel and Teflon. One of the most attractive properties of the dye laser is its tunability. The emission spectra of fluorescent dyes are broad permitting the lasing wavelength to be tuned to any chosen value within a broad range. Moreover the number of fluorescent dyes is very large and different compounds can be chosen for

emission over the entire spectral range. Rhodamine 6G and Rhodamine B are still the best dyes available for laser applications Some of the important parameters related to these dyes are detailed in reference [20].

Fig. 2.2 shows the schematic of the dye laser set-up used for different studies. It has an oscillator and a single stage amplifier Rhodamine B (RhB) in methanol (107 mg/lit) is used as the gain medium and a pump is used to circulate the liquid (at the rate of 1 litre/minute) to minimise the laser scattering and reduce the possibility of decomposition during the experiment. 8% of the frequency doubled Nd: YAG (Continuum 660 B-10, 532 nm, 10 Hz, 6 ns FWHM, 100 mJ/pulse) laser power split by a plane glass plate, is first expanded by a plano-concave lens of f $\sim$ 50 mm and then focused by a cylindrical lens of f $\sim$ 50 mm into the dye cell of approximately 3 mm (diameter) X 15 mm (length) dimensions The oscillator cavity consists of a 100% R mirror and ~ 8% R glass plate which produces output of maximum bandwidth The total length of the oscillator cavity is $\sim$ 17 cm With both the high reflectivity mirror and the output coupler window being parallel, the resonator cavity is barely stable and hence the alignment has to be made very carefully to avoid any spurious feedback and intensity fluctuations Necessary care is taken to avoid mechanisms leading to the formation of cavity modes, which leads to undesirable structure in the laser spectrum. The output pulses from the oscillator are amplified using the remaining 92% of the power Concentration of solution used for amplification is 37 4 mg/lit The maximum average power that could be achieved after amplification is $\sim$ 20 mW The output has a FWHM of 7 - 8 nm [fig 2 3 (a)] and the corresponding τ_c calculated, from the relation $\Delta v^* \tau_c \sim 1$, is $\sim$ 170 fs. The auto-correlation function obtained by recording the PC signal, as a function of beam 3 delay, in the sample Rhodamine B (in methanol) is shown in fig 2 3 (b).

If the mirror in the cavity is replaced by a highly dispersive element like a high-resolution grating the spectral width is decreased thereby increasing the correlation time of the pulses The grating used in our configuration for tuning the dye laser is a reflection type holographic grating (Bausch and Lomb) with 600 grooves/mm and blazed at 54 It has five orders of diffraction and is oriented in the Littrow position

(a)

Mirror (R ~ 99%)   Dye Cell   Glass Wedge

Dye laser Output

Pump Beam at 532 nm

(b)

High Resolution
Grating   Dye Cell

Output
Window

Dye laser Output

Pump Beam at 532 nm
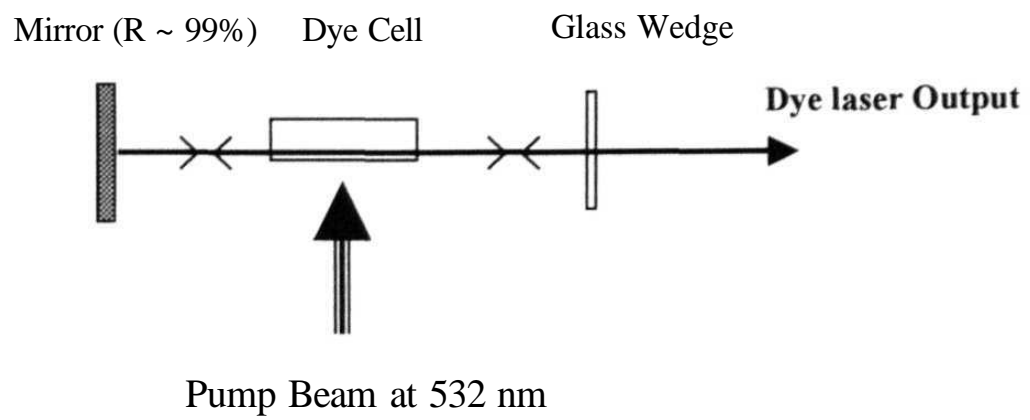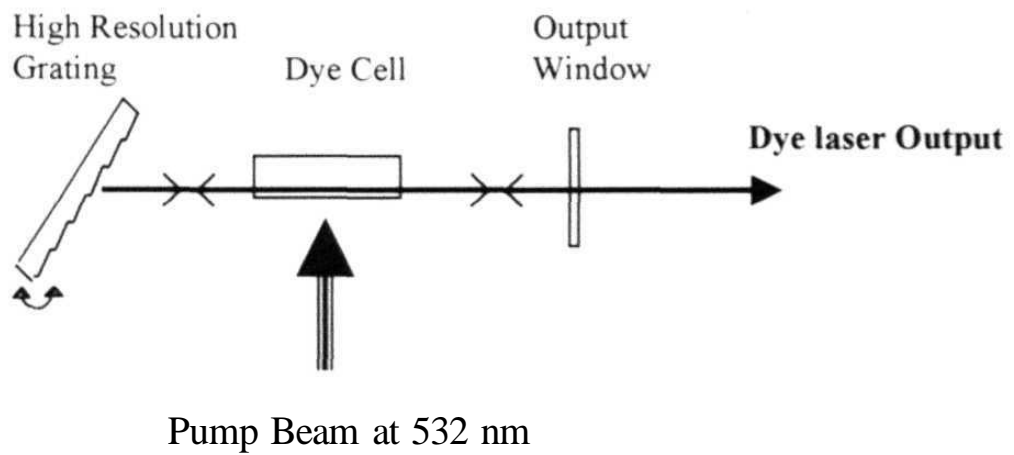
Fig. 2.2 Home built dye laser with (a) Grating and (b) Prism-Mirror
as tuning elements and the corresponding spectra.
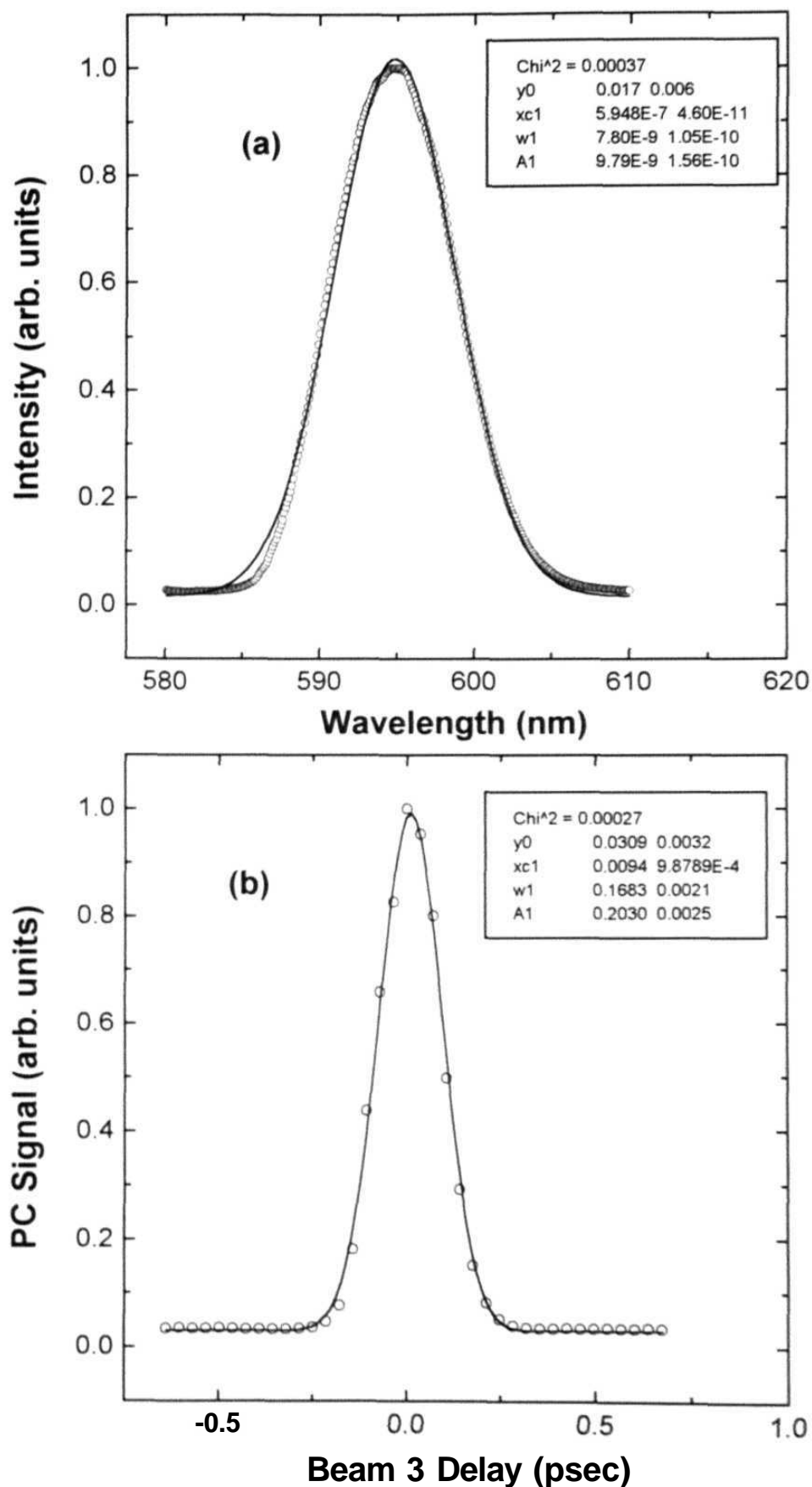
Fig. 2.3 (a) Emission Spectrum of the dye RhB (in methanol) Open circles
are experimental data and the line is a fit to gaussian with a width of 7.8 nm
(b) Autocorrelation function : Time - resolved signal in the same solution.
Solid line is a fit to gaussian of width ~168 fs

[21], for which the incident light and the diffracted light of a given wavelength lie along the same direction The spectral line narrowing, in the ns pulse, is avoided by using a glass plate of 8% R as output coupler, which also limits the number of passes in the cavity during the short excitation time (6 ns). The spectral recording of the output laser with the grating in cavity is shown in fig. 2.4 (a). The PC signal obtained in the sample RhB with grating in the cavity is shown in fig 2.4 (b).

2.2.2 Phase-Conjugate Configuration

Figure 2.5 shows the complete details of the degenerate four-wave mixing (DFWM) experimental set-up using incoherent light. The beam is initially collimated using two convex lenses and an aperture is used to cut the scattered background before splitting it into three beams Two beam splitters (30-70, 50-50) are used to obtain three beams of almost equal intensity All the three beams have a diameter of ~ 2.5 - 3 mm and could be varied further with an aperture In the phase conjugate configuration, beam 1 is fixed whereas beams 2 and 3 pass through variable delays. Beam 1 (k_1) is designated as forward pump, beam 2 (k_2) is backward pump and beam 3 (k_3) is the probe Beam 2 passes through a variable delay (either a micrometer screw or an optical bench, both of which are controlled manually). Beam 3 passes through another delay line mounted on a micrometer screw and connected to a stepper motor, which is controlled with a PC The maximum resolution we could achieve in both the cases is   5 μ corresponding to 33 fs in time (with a retro-reflector it will be twice the actual path length) The angle between the forward pump and the probe is ~ 10 - 15°. All the beams are focused into the sample contained in 1-mm thick quartz/glass cell using lenses of focal length of- 20 cm.

Beam waist at the focus is estimated to be ~ 80 -100 μ (using the formula 4fλ / 7tD, where f is the focal length of the lens, λ is the wavelength, and D is the input beam diameter The beam waist measured using a knife-edge technique, at low power densities of the laser beam, is ~ 70 μ. The polarisation state of each individual beam is controlled using a Half Wave Plate (HWP). Proper care is taken to ensure that the counter-propagating and the probe beams are overlapped in the sample, both spatially
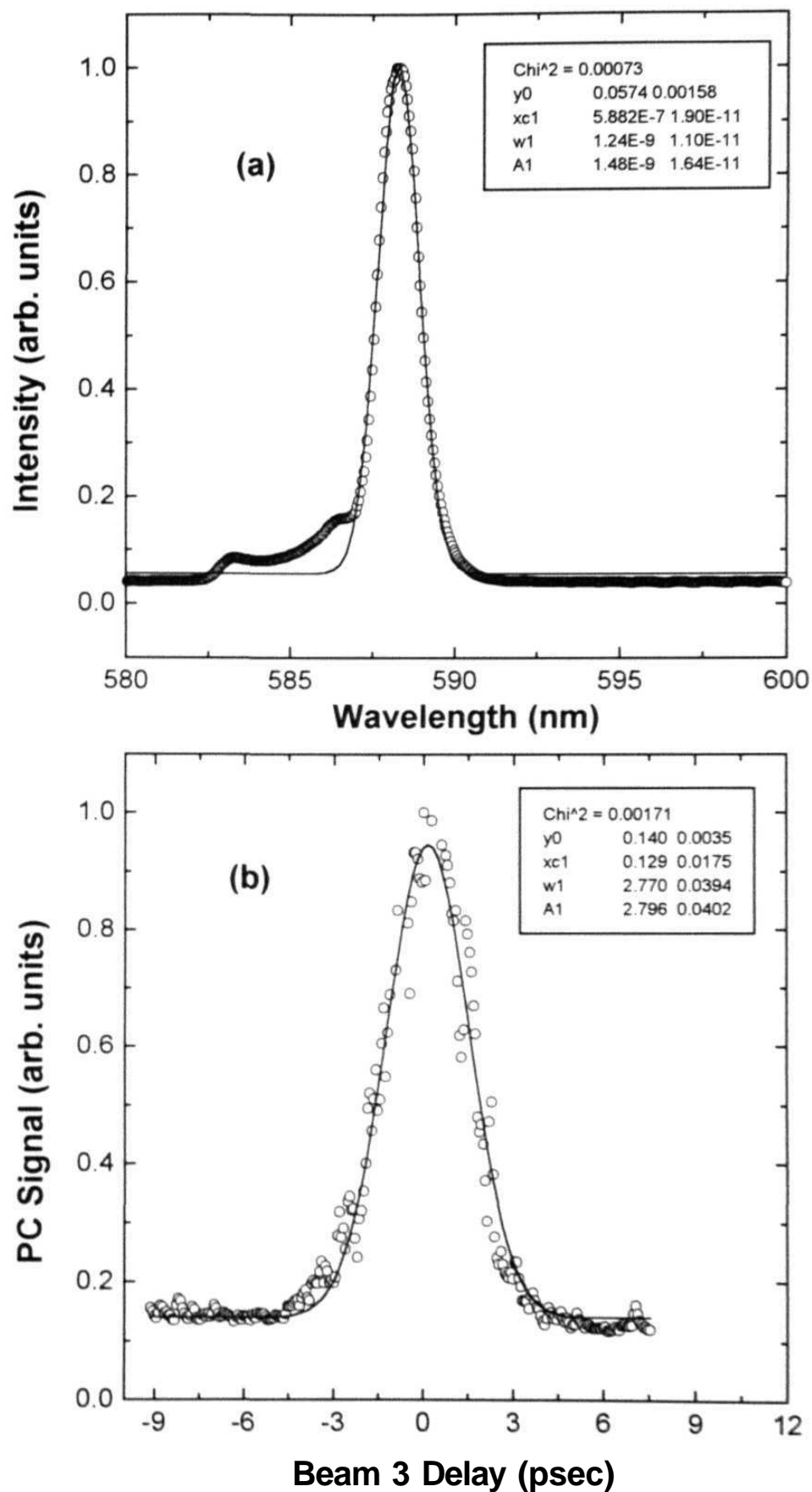
Fig. 2.4 (a) Emission spectrum of the dye laser with grating in the cavity. Solid line is fit to a gaussian. (b) PC Signal in the sample CS_2. No decay observed and solid line is fit to gaussian of width 2.78 psec.
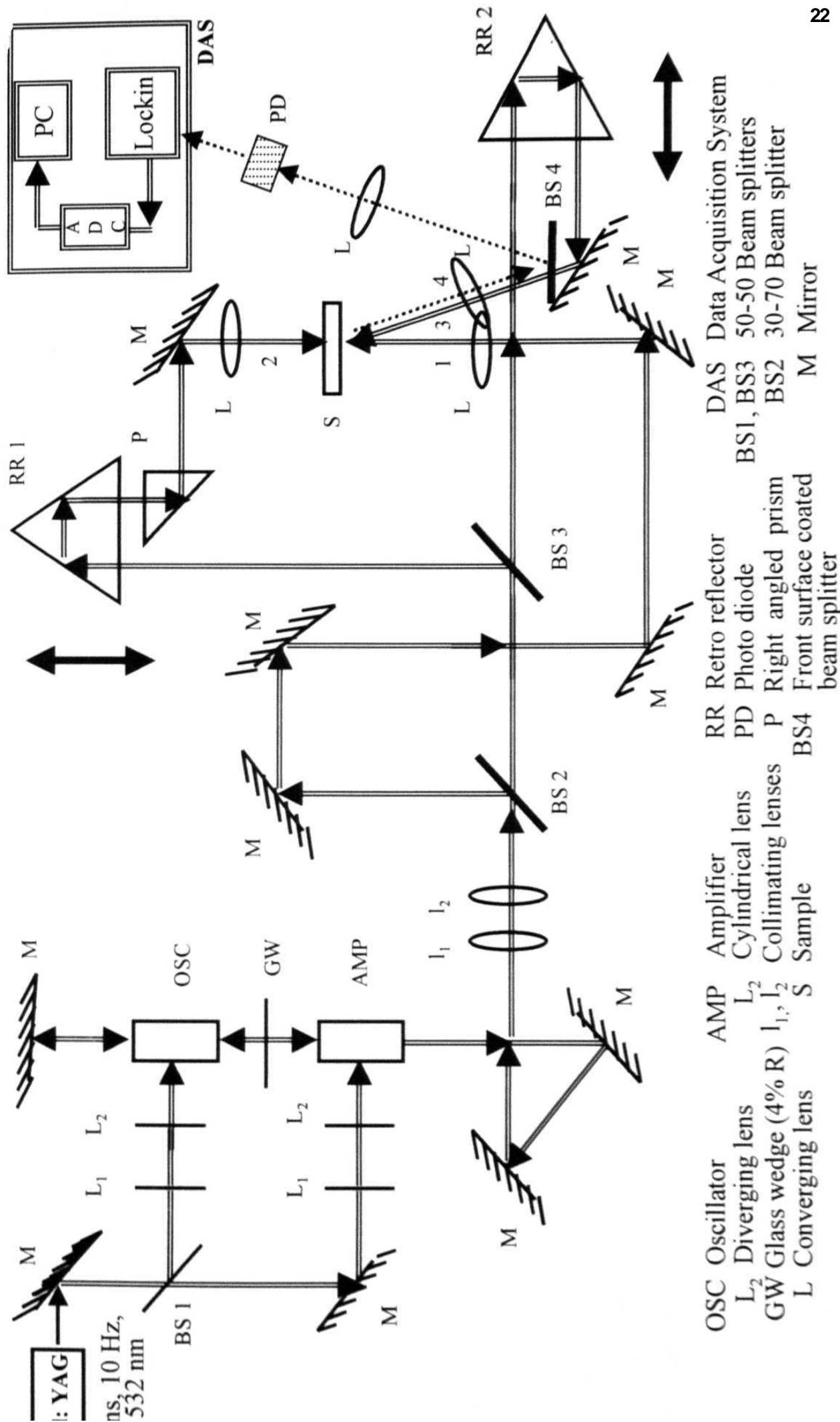
Fig. 2.5 Experimental setup for Degenerate Four Wave Mixing with Incoherent Light

OSC   Oscillator   AMP   Amplifier   RR   Retro reflector   DAS   Data Acquisition System
L_2 Diverging lens L_2 Cylindrical lens   PD   Photo diode   BS1, BS3   50-50 Beam splitters
GW   Glass wedge (4% R) l_1, l_2 Collimating lenses   P   Right angled prism   BS2   30-70 Beam splitter
L   Converging lens   S   Sample   BS4   Front surface coated   M   Mirror
                                                                                          beam splitter

and temporally. Using a pinhole at the sample position and maximising the transmission through pinhole facilitates spatial alignment. Temporal overlap is accomplished by varying the path length of each of the beams to maximise the PC signal in a standard sample like CS_2 or RhB.

The phase conjugate signal (in -k_3 direction) is isolated using a beam splitter and is passed through an aperture (to reduce the scattered background) and focused on to a fast photodiode (FND 100, rise time ~ 1 ns) Various neutral density filters (NDF) are used for attenuating the probe and the signal beams. The signal collected using a fast photodiode (PD, FND 100, rise time ~ 2 ns) is observed on a large bandwidth oscilloscope (Tektronix 2465 B, 400 MHz or Tektronix TDS 210, 60 MHz) to ensure the PD does not get saturated (In the initial stages of the present work the signal is recorded using a Digitising Camera System [TEK], which records the pulse trace onto the PC and the averaging is done using the PC software). This effect is clearly seen in the signals obtained in the samples Zinc meso-tetraphenyl porphyrin (ZnmTPP), Zinc meso-tetra- (p-methoxyphenyl) tetrabenzporphyrin (ZnmpTBP) in the initial stages and other Porphyrins in the later stages In the later stages the signal is fed to a lock-in amplifier (SRS 830) and to the ADC card where it is averaged several times (typical averages are ~ 300). The output of the ADC card finally gets recorded in a PC A GWBASIC program performs the stepper motor movement and the data averaging simultaneously.

2.2.3 Boxcar Configuration

For the Boxcar configuration, the same set-up is retained with slight modifications The second beam is diverted using another retro-reflector and it comes parallel to the first beam but at lesser height than the first beam Since the probe and forward pump are in same plane, the second beam forms the third corner of the square and the signal is seen at the fourth corner of the square Schematic of the set-up is shown in fig 2 6 The delays of beams 2 and 3 could be varied using the stepper motor. Observing and optimising the diffracted signals, in both horizontal and vertical directions, ensured the zero delay of different beams The signal(s) obtained
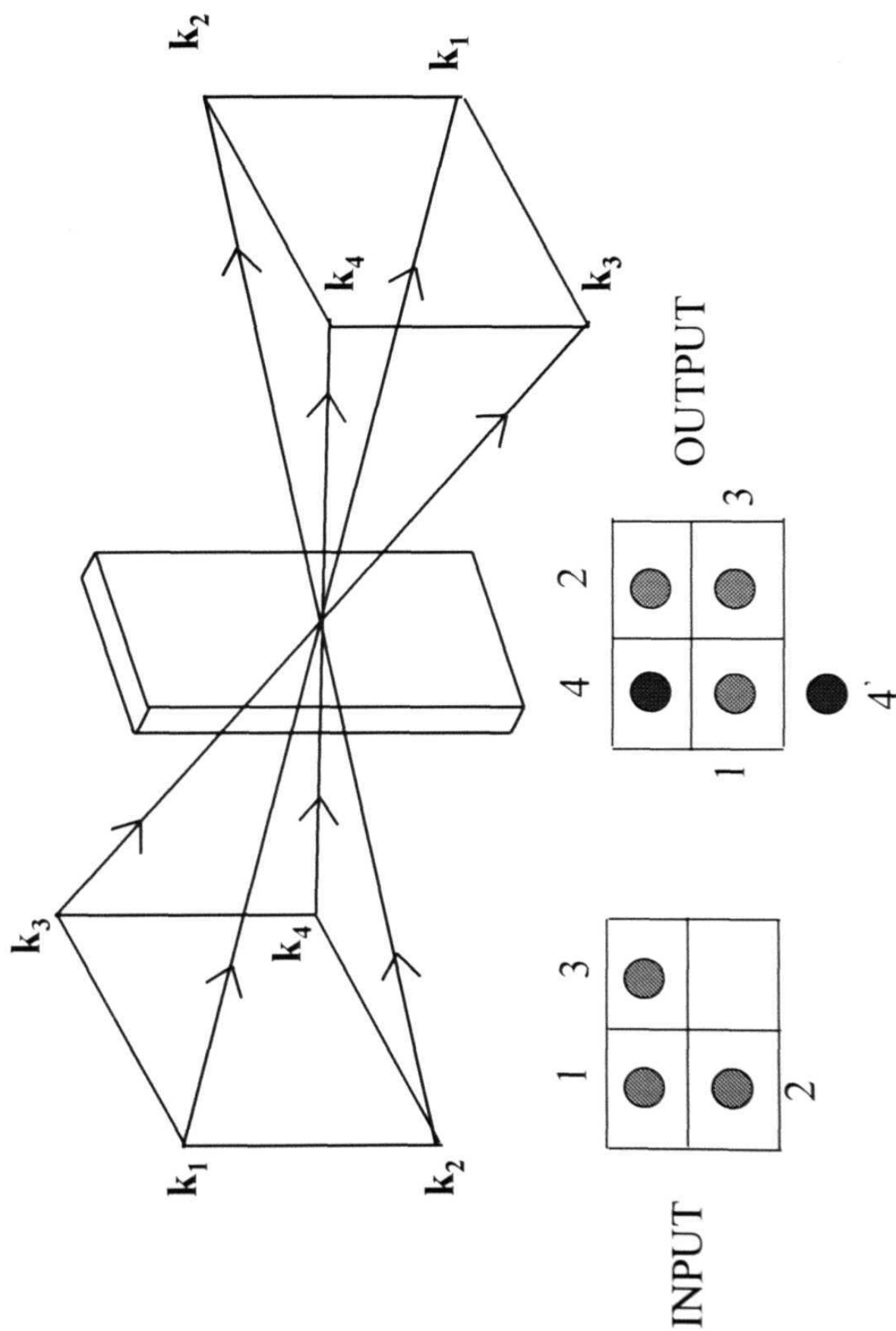
Fig. 2.6 DFWM set-up in the boxcar configuration. 4 and 4' are the signals

are spatially filtered before being fed to the fast PD to lock-in and to ADC which finally gets recorded in the computer.

2.2.4 Self-Diffraction Configuration

In the self-diffraction/forward four-wave mixing configuration the backward pump beam is blocked and the signals are obtained aligning the beams 1 and **3** The angle between the forward pump ($\mathbf{k_1}$) and probe beams ($\mathbf{k_2}$) is ~ 5 - 10^0 and the first order diffracted signals are obtained in $2\mathbf{k_1}$ - $\mathbf{k_2}$ and $2\mathbf{k_2}$ - $\mathbf{k_1}$ directions, as shown in fig. 2.7, due to the third order nonlinearity Beams 3, which is the probe passes through variable delay, as described above. and the signal(s) is (are) collected using similar Photodiodes The signals and recorded as a function of the delay of beam 3

2.3 Degenerate Four-Wave Mixing with 35 ps pulses (DFWM-PS)

The experimental set-up for the $\chi^{(3)}$ measurements and time-delayed four wave mixing using the ps pulses is shown in fig 2.8. The input beam is from a hybrid mode-locked Nd YAG laser emitting 532 nm and the pulses are of 35 ps duration at 10 Hz. The maximum pulse energy is ~ 30 mJ The input beam is passed through an aperture to get a spatially filtered beam of ~ 7 mm diameter. Using a beam splitter a part of it is split and used for the backward pump (beam 3, which goes through a microprocessor controlled, high precision delay line) and is focused using a 1m lens. The rest of the beam is again split using another beam splitter The second beam, which is the probe, (beam 2) goes through a delay line (micrometer screw) and comes at an angle to the forward pump Beam 1 (forward pump) reaches the sample at a fixed delay and is focused onto the sample using a 2m focal length lens All the beams have Neutral Density Filters in their paths to change the intensities accordingly The angle between the forward pump (beam 1) and the probe (beam 2) is measured to be ~ 5.1^0 A half wave plate (HWP) is introduced in the probe beam to change its state of polarisation A part of the forward pump is picked up by a photodiode (NRC **818J-09B)** to monitor the pulse to pulse fluctuations All the samples, in the form of solution, are placed in a 1-mm quartz/glass cuvette
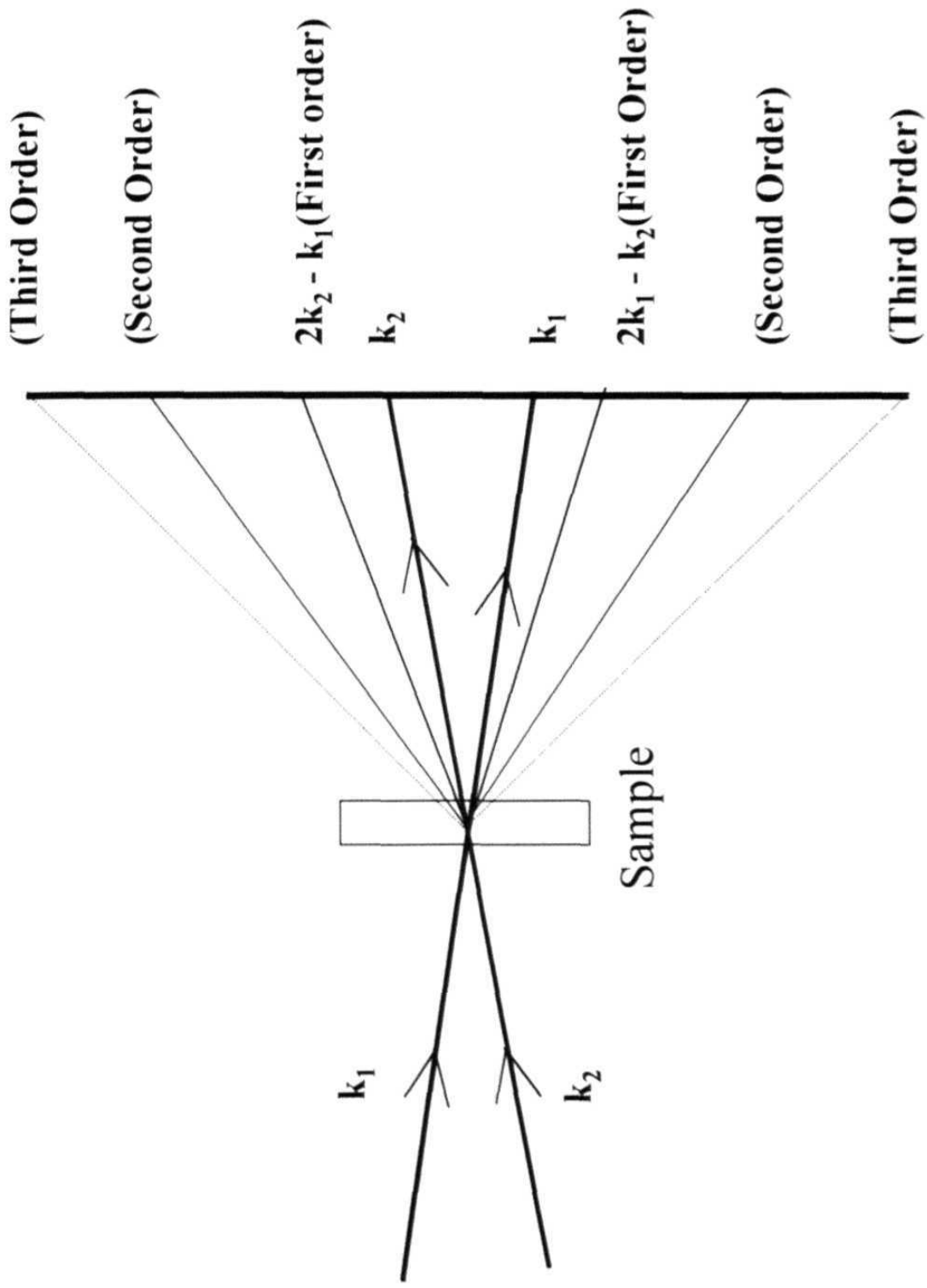
Fig. 2.7 Experimental setup for the Forward Four Wave Mixing
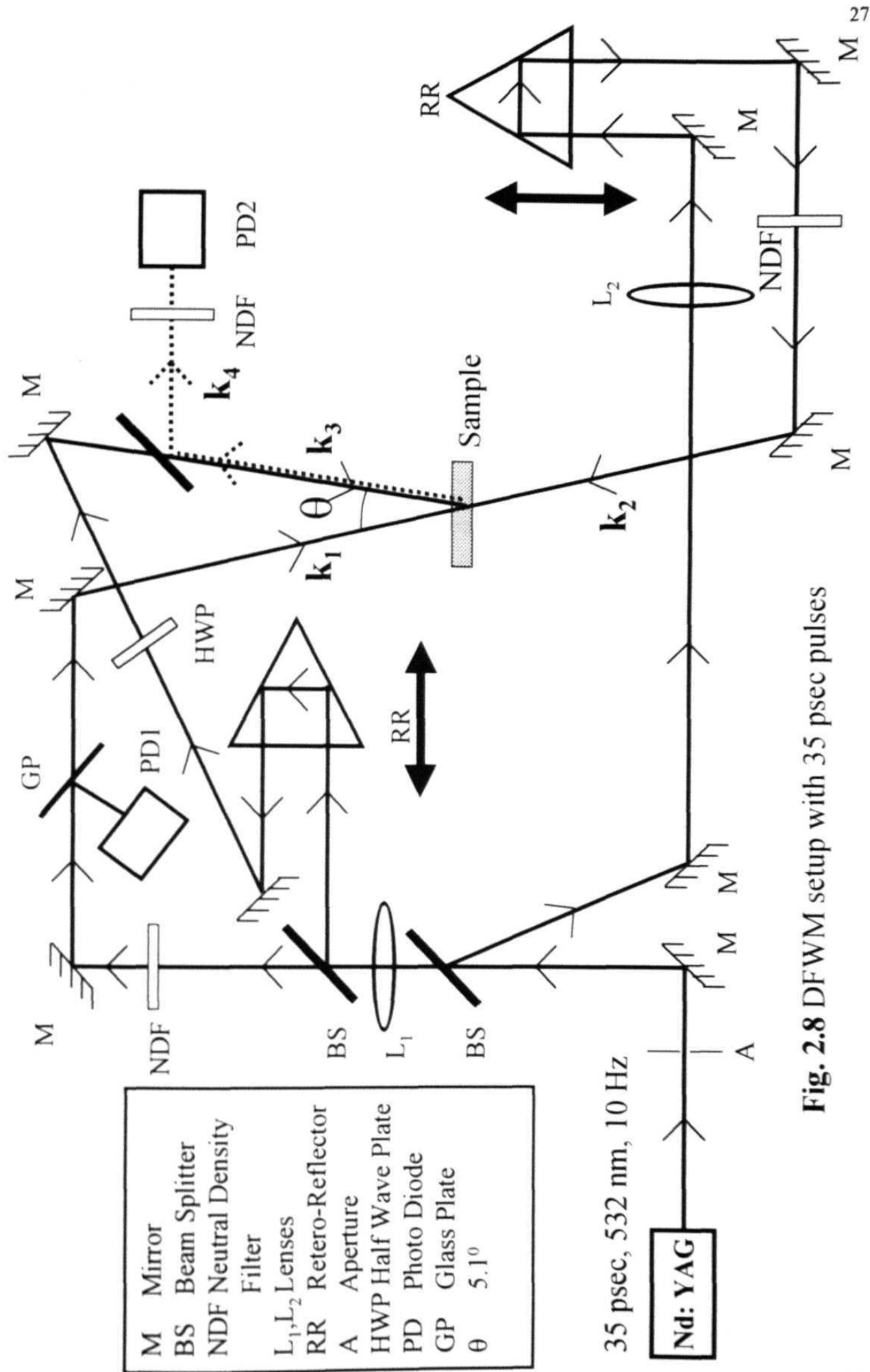
Fig. 2.8 DFWM setup with 35 psec pulses

M	Mirror
BS	Beam Splitter
NDF	Neutral Density Filter
L_1, L_2	Lenses
RR	Retero-Reflector
A	Aperture
HWP	Half Wave Plate
PD	Photo Diode
GP	Glass Plate
θ	5.1^0

35 psec, 532 nm, 10 Hz

Nd: YAG

2.4 Z-Scan

2.4.1 **Closed aperture** scan for sign and refractive nonlinearity

The Z-scan technique is a simple, sensitive, single beam method that uses the principle of spatial beam distortion to measure both the sign and the magnitude of refractive nonlinearities of optical materials. The experiment uses a Gaussian beam from a laser in tight focus geometry to measure the transmittance of a nonlinear medium through a finite aperture in the far field as a function of the sample position z, from the focal plane In addition to this, the sample transmittance without an aperture is also measured to extract complementary information about the absorptive nonlinearities of the sample The transmittance characteristics of the sample with a finite aperture depend on the nonlinear refractive index, as elucidated below.

Consider, for instance, a material with a negative nonlinear refraction and of thickness smaller than the diffraction length ($\pi \omega_0^2 / \lambda$) of the focused beam being positioned at various positions along the Z-axis (fig 2 9). This situation can be regarded as treating the sample as a thin lens of variable focal length due to the change in the refractive index at each position ($n = no + n_2 I$) When the sample is far from the focus and closer to the lens, the irradiance is low and the transmittance characteristics are linear Hence the transmittance through the aperture is fairly constant in this region As the sample is moved closer to the focus, the irradiance increases inducing a negative lensing effect A negative lens before the focus tends to collimate the beam. This causes the beam narrowing leading to an increase in the measured transmittance at the aperture A negative lens after the focus tends to diverge the beam resulting in the decrease of transmittance As the sample is moved far away from the focus, the transmittance becomes linear in Z as the irradiance becomes low again Thus the curve for Z versus transmittance has a peak followed by a valley for a negative refractive nonlinearity The curve for a positive refractive nonlinearity will give rise to the opposite effect, i.e. a valley followed by a peak. This technique has several *advantages,* some of which are

- Simplicity: No complicated alignment except for keeping the beam centered on aperture.

- Simultaneous measurement of both sign and magnitude of nonlinearity.

- Data analysis is quick and simple except for some particular conditions.

- Possible to isolate the refractive and absorptive parts of nonlinearity unlike in **DFWM**

- High sensitivity, capable of resolving a phase distortion of A/300 provided the sample is of high optical **quality**

- Close similarity between the Z-scan the Optical Power Limiting geometry.

Some of the *disadvantages* include

- Stringent requirement of high quality Gaussian TEM_{00} beam for absolute measurements

- For non-Gaussian beams the analysis is completely different. Relative measurements against a standard samples allows relaxation on requirements of beam shape

- Beam walk-off due to sample imperfections, tilt or distortions

- Not suitable for measurement of off-diagonal elements of the susceptibility tensor except when a second non-degenerate frequency beam is employed.

The Z-scan technique has been used extensively to study different materials like semiconductors, nano-crystals, semiconductor-doped glasses, liquid crystals, organic materials, biomaterials etc To enhance it's sensitivity and applicability new extensions have been added A two color Z-scan is used to perform the studies of non-degenerate optical nonlinearities A much more sensitive technique. EZ-scan (eclipsed Z-scan), has been developed which utilizes the fact that the wings of a circular Gaussian beam are much more sensitive to the far-field beam distortion. A reflection Z-scan technique was introduced to study the optical nonlinearities of surfaces Z-scan with top-hat beams, elliptical Gaussian beams have been performed resulting in better sensitivity. The dual wavelength (two-color) extension of the standard Z-scan technique has been used to measure the non-degenerate nonlinearities This has been further used to time-resolve the dynamics of the nonlinear process by introducing a delay between the pump

and probe beams. A comprehensive review of different techniques of Z-scan could be found in any of the references listed in [22].

2.4.2 Open aperture scan for absorptive nonlinearity

In the above discussion a purely refractive nonlinearity was considered assuming that absorptive nonlinearities are absent. The presence of multi-photon (two or more) absorption suppresses the peak and enhances the valley, while saturation of absorption produces the opposite effect The sensitivity of the experiment to refractive nonlinearities is entirely due to the aperture The removal of the aperture will make the Z-scan sensitive to absorptive nonlinearities alone Thus by doing the Z-scan with and without aperture both the refractive and absorptive nonlinearities of the sample can be studied Z-scan studies of the all the samples are performed using broadband source / ns pulses / ps pulses The details of the experimental set-up are shown in fig. 2.9. Spatially filtered input beam is focused using a lens of focal length ~ 80 mm For Z-scan with ps pulses a longer focal length lens is used since the peak intensities are large compared to ns pulses The sample placed in a 1-mm cuvette is scanned across the focus using a stepper motor controlled by PC A part of the input beam split using a glass plate is monitored using a PD The transmitted light is then collected using another lens (large area) of f ~ 100 mm and another fast photodiode The output beam is again split using a beam splitter For the closed aperture Z-scans an aperture of known size is placed after the cell and the light passing through the aperture is collected using a similar photo-diode Different neutral density filters are used for attenuation of the transmitted beam to ensure that the photodiode does not get saturated The photodiode output is fed to a lock-in amplifier (SRS 830 or Princeton Applied Research) and finally gets recorded in a PC The output data is averaged several times (typical number of averages is 300) The step size used is 0.25 / 0.5 mm.

2.5 Photo-physics of a typical organic molecule

In molecules, the absorption of electromagnetic radiation results in the excitation of an electron from a lower to a higher molecular quantum state The

Fig. 2.9 Z-scan (closed and open aperture) experimental setup.
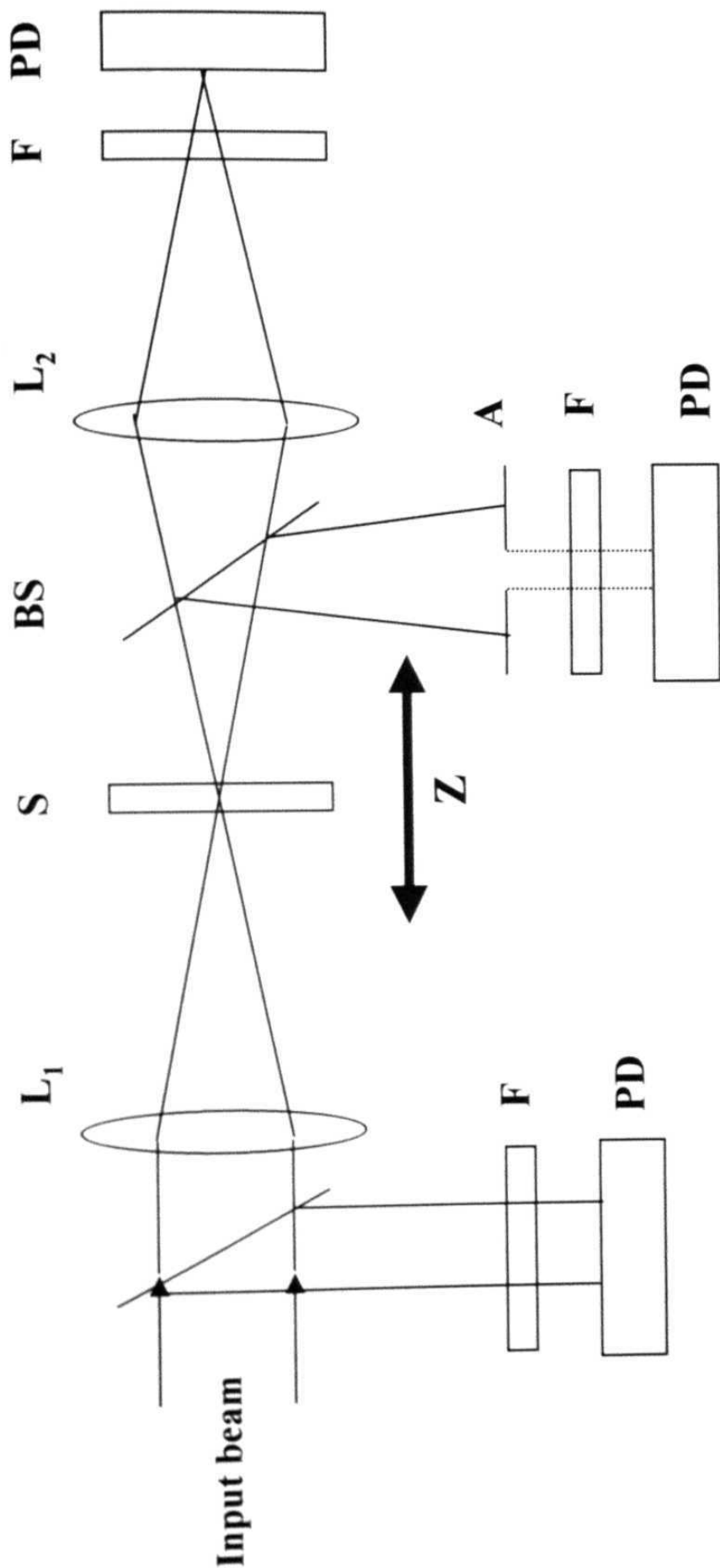
L_1, L_2 - Lenses   S - Sample   BS - 50-50 beam splitter
F - Neutral density filter   A - Aperture   PD - Photodiode

electronically excited molecule is energetically unstable with respect to ground state. If the molecule does not rearrange or fragment it will find some way of losing its excitation energy to the ground state In fact, there are number of different possible de-excitation pathways and the ones that are most favourable depend on the type of molecule and the nature of electronic states involved [23] The de-excitation pathways are often characterised by very rapid rates One of the most interesting properties of electronically excited molecules is their tendency to re-emit radiation on returning to the ground state The absorption of ultraviolet or visible light by an organic molecule causes the excitation of an electron from an initially occupied, low energy orbital to a high energy, unoccupied orbital The energy of the absorbed photon is used to energise an electron and cause it to jump to a higher energy orbital Two excited electronic states derive from the electronic orbital configuration produced by light absorption In one state, the electron spins are paired (anti-parallel) and in the other state the electron spins are unpaired (parallel). The state with paired spins has no resultant spin magnetic moment A state with paired spins remains a single state in the presence of a (laboratory) magnetic field, and is termed as singlet state A state with unpaired spins interacts with a (laboratory) magnetic field and splits into three quantized states, and is termed as triplet state An energy diagram is a display of the relative energies of the ground state, the excited singlet states, and triplet states of a molecule for a given, fixed nuclear geometry

An energy level diagram characteristic of a typical organic dye molecule is shown in fig 2 10 The electronic ground state of the molecule is a singlet state, designated as S_0, which spans a range of energies determined by the quantized vibrational and rotational excitation of the molecule The typical energy between the vibrational levels is of the order of 100 cm^{-1} The rotational levels provide a near continuum of states between the vibrational levels The higher singlet states are denoted as S_1 and S_n Each electronic state has similar broad continuum of levels and the optical transitions between these continua leads to broad absorption and emission spectra Transition between singlet states are spin-allowed, giving rise to strong absorption bands When a laser pulse is incident, the molecules are excited from the lowest levels of the ground state S_1 to the highest vibrational states of S_1 (S_{1v}). The decay from S_{1v} to S_{10} is non-radiative and occurs within few ps. From S_{10} the
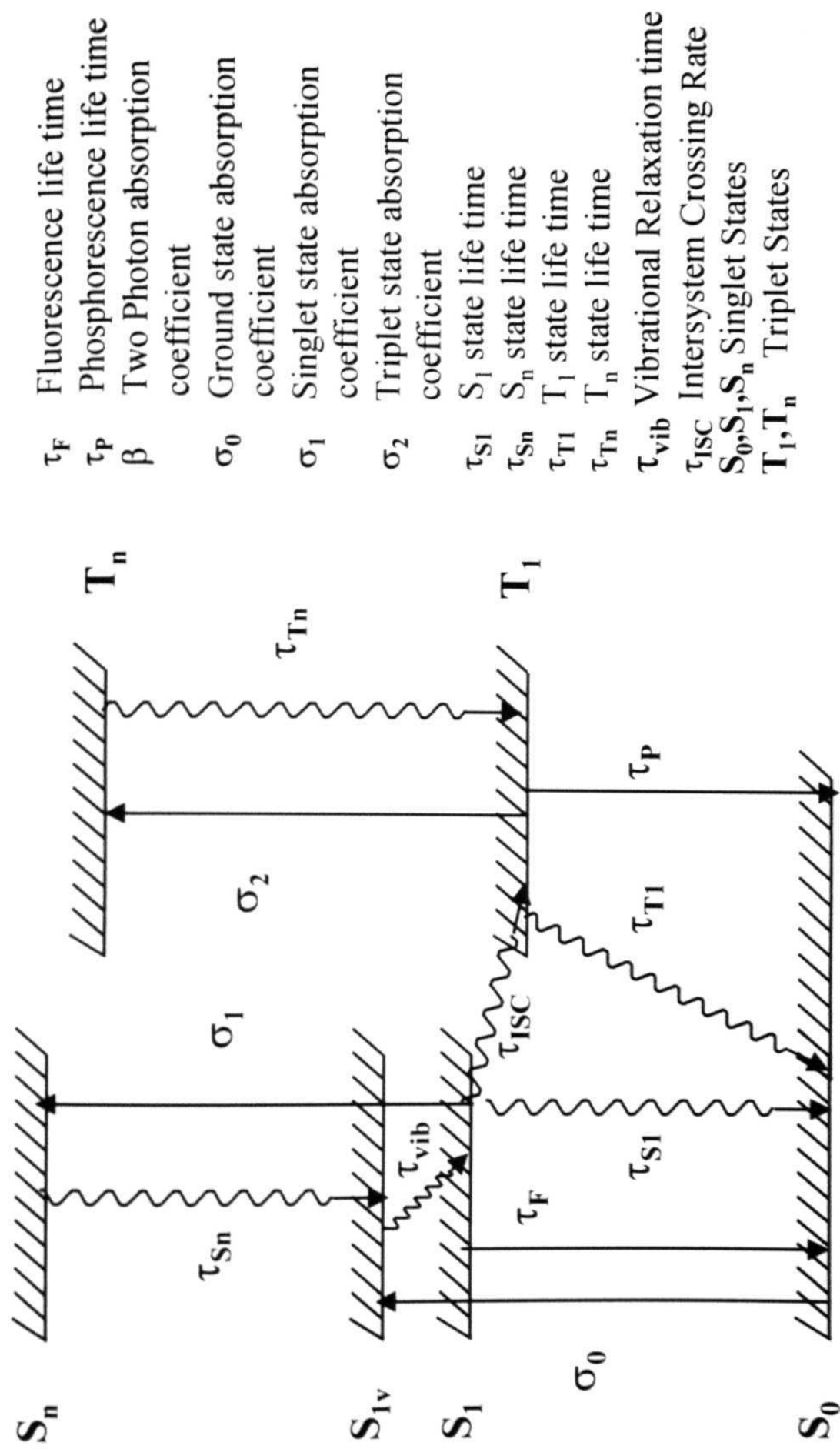
Fig. 2.10 Energy level diagram of a typical organic molecule

τ_F Fluorescence life time
τ_P Phosphorescence life time
β Two Photon absorption
     coefficient
σ_0 Ground state absorption
     coefficient
σ_1 Singlet state absorption
     coefficient
σ_2 Triplet state absorption
     coefficient
τ_{S1} S_1 state life time
τ_{Sn} S_n state life time
τ_{T1} T_l state life time
τ_{Tn} T_n state life time
τ_{vib} Vibrational Relaxation time
τ_{ISC} Intersystem Crossing Rate
S_0, S_1, S_n Singlet States
T_1, T_n Triplet States

molecules can relax back to the ground state radiatively or non-radiatively to the ground state or crossover to the triplet state (Intersystem Crossing). The radiative decay, which is spontaneous, from S_{10} to S_0 is known as Fluorescence and is governed by the lifetime of the S_1 state. For organic molecules the lifetime is typically of the Order of few ns. The energy difference between absorption and emission processes is taken by the non-radiative decay in the S_1 and S_0 states and the relaxation of the molecules from S_{10} to the lowest triplet state T_1 is governed by the intersystem crossing rate. The intersystem crossing rate constant is typically 10^{11} to 10^7 s^{-1} due to spin restriction factor. Another important process of de-activation of the S_1 state is the **Internal** Conversion which is the non-radiative decay of S_{10} to S_0. The decay from T_1 to S_0 can be radiative or non-radiative and is termed as Phosphorescence if it is the former type. Typical phosphorescence life times are in the range of ms to μs. The lifetime of the triplet state T_1 is generally large since the triplet-singlet transition is dipole forbidden.

In the first excited singlet and triplet states, under special experimental conditions (higher intensities), the molecule may be promoted to the higher states S_n and T_n respectively. These higher states relax back to the S_1 and T_1 on a very fast time scale (few hundred fs) and in the process generate a vibrationally excited state (Kashas rule). Higher triplets can also be populated by intersystem crossing from higher singlet states if the rate constants are competitive for internal conversion and intersystem crossing in the upper states. Thus, although direct absorption from ground singlet to triplet state is forbidden by selection rules, it can be populated indirectly. We will be using vibrational relaxation time also to represent the dephasing time for the S_n and S_1 states. This is so because of band of vibrational levels, closely spaced, in the S_n states leading to very fast dephasing time T_2. Since the vibrational levels in S_1 state are far more separated the dephasing (τ_{vib}) is expected to slow compared to the S_n states.

2.6 Results on the samples Rhodamine B and CS_2

Standard samples of CS_2 and RhB are studied in order to test the validity of the present Incoherent Laser Spectroscopy technique to measure the ns and ps relaxation

times through DFWM. In the first stage we studied the dynamics of RhB dissolved in methanol. The phase conjugate signal recorded as a function of delay of beam 3, with beam 2 delay at zero, is shown in fig. 2.3 (b). The curve obtained is a symmetric one with no decay observed for both positive and negative delays (convention used throughout the thesis is, if pulse arrives in the sample early it is denoted as negative delay and if it arrives late it is denoted as positive delay). Since the phase relaxation in such dyes is very fast, typically less then 100 fs [24], we do not observe any decay in the profile. In other words the curve we observed was just the auto-correlation curve. Beyond 170 fs delay time (FWHM of the curve) no two pulses are correlated and hence there is no signal. Background signal consists of the scattered light collected by the photo-diode. τ_c obtained from the theoretical calculations agrees very well with experimental value.

In the second stage we studied the relaxation times in liquid CS_2. CS_2 is one of the most familiar and simplest optical Kerr media. Fig. 2.11 (a) depicts the signal in CS_2 (open circles) and it is found to be asymmetric with three components having different life times. The intense component is due to the coherence spike as it coincides with the auto-correlation function (solid line). There are two more components with short and the long decay times. Figure 2.11 (b) shows the values obtained through least squared fitting of the data (0.18 ps for the short component and 1.8 ps for the long component). Ps and sub-ps relaxation times measurement of the optical Kerr effect was done with more accuracy with the advent of ps/fs laser systems. The ps relaxation in CS_2 is considered to be associated with orientational randomisation by rotational diffusion of molecules subsequent to their alignment by an external electric field. Several mechanisms have been proposed [25] to explain the sub-ps response like the a) damped librational motion, b) the time dependant behaviour resulting from collisions which induce an anisotropic polarizability in colliding pairs of atoms or molecules, c) short time behaviour associated with the rotational diffusion motion of molecules possessing a large anisotropic polarizability etc. Our values match perfectly with most of the reported values proving the validity of the present set-up for the measurement of different relaxation times.
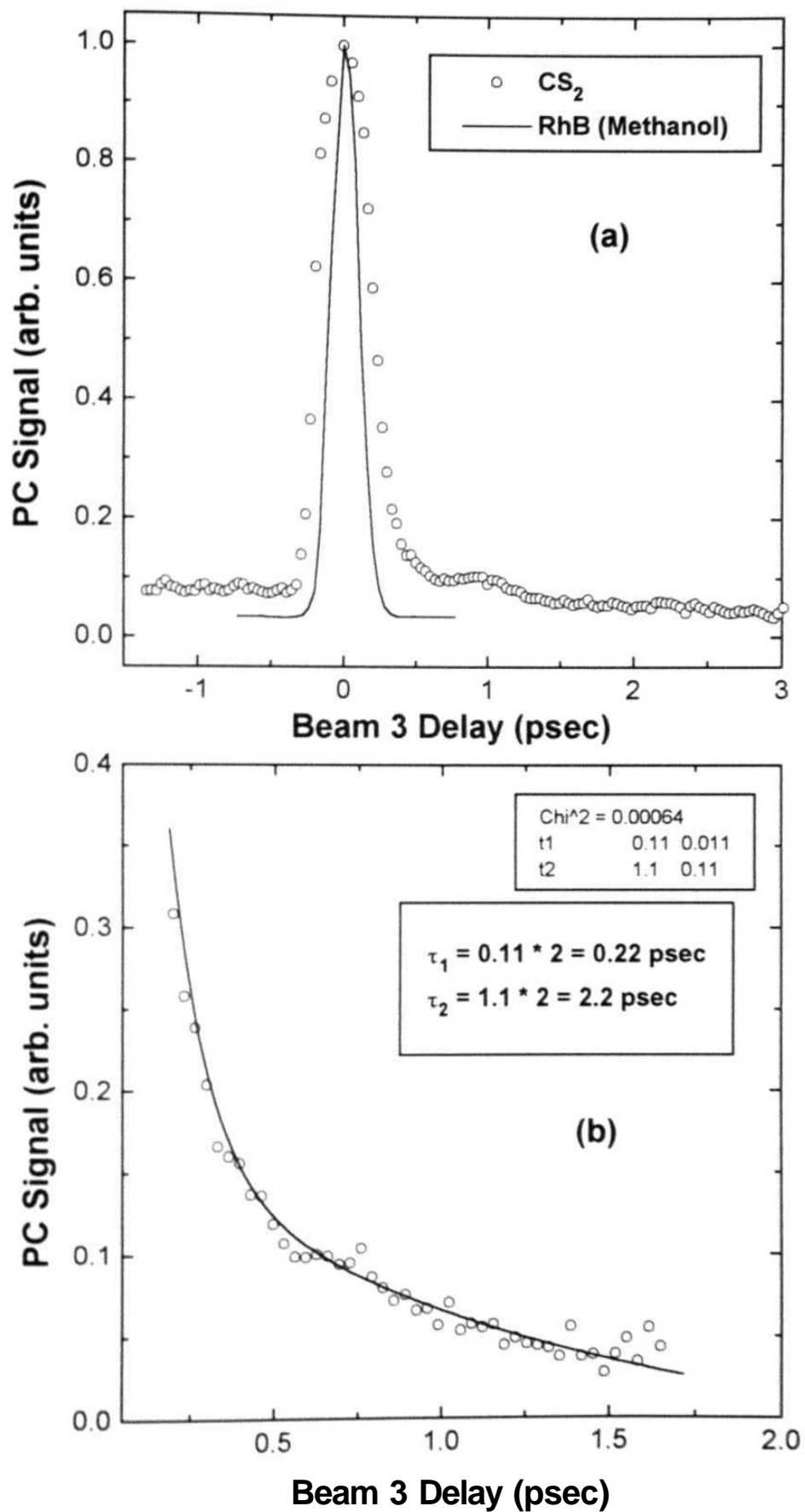
Fig. 2.11(a) The time-resolved signals obtained for CS_2 and RhB (methanol).

(b) Double exponential fit of the PC Signal. The two lifetimes are 0.22 psec and 2.2 psec. Open circles are data and the line is the fit.

2.7 Conclusions

1. The home-built dye laser with different elements (mirror and grating) in the cavity has been tried and the resulting broadband laser pulses are used for different DFWM and Z-scan experiments.

2 With RhB as the gain medium and a mirror in the cavity we obtained the correlation time as - 170 fs through time-resolved studies as well as from the inverse of bandwidth, obtained through the spectral recording, of the laser pulses.

3 When the mirror is replaced by a high-resolution grating we could get a correlation time of ~ 2.8 ps obtained from the DFWM signal in RhB and CS_2.

4 The initial results of phase relaxation measurements and oreintational relaxation measurements in RhB and CS_2 respectively match very well with those reported in literature thereby calibrating our experimental set-up for the measurement of ps and sub-ps relaxations using an incoherent laser source

2.8 References

1. Y.R. Shen, *The Principles of Nonlinear Optics,* New York: Wiley, USA, 1984, Chap 14 - 15, Y.R. Shen, *IEEE J. Quant. Electron.* 22, 1196, 1986.

2. N. Bloembergan, *Nonlinear Optics,* Benjamin, New York, 1977.

3. M.D. Levenson, *Introduction to Nonlinear Laser Spectroscopy,* New York: Academic, 1982

4   R A Fischer, *Optical Phase Conjugation,* New York: Academic, USA, 1983.

5. H.J Eichler, P Gunter, and D.W Pohl, *Laser-Induced Dynamic Gratings,* Springer-Verlag, Berlin, Heidelberg, Germany, 1986.

6   B.Ya Zeldovich, N.F. Philipetsky, V V Shkunov, *Principles of Phase Conjugation,* Springer series in optical sciences, Vol. 42, Springer, Berlin, Gemany, 1985

7. D.M Pepper, Ed *Opt. Engg.* 21, 2, 1982

8   A.D Walser, G Coskun, and R Dorsinville, *Electrical and Optical Polymer Systems,* ed.'s D L Wise, G.E Wnek, D J Trantolo, T.M Cooper, and J.D Gresser, Marcel Deccer Inc., New York, 423-452

9   M Zhao, Y Cui, M Samoc, P.N. Prasad. M.R Unroe, and B.A. Reinhardt, *J. Chem. Phys.* 95, 3991, 1991, S.K Ghoshal, P. Chopra, B.P. Singh, J Swiatkiewicz, and P N Prasad,*J. Chem. Phys.* 90, 5078, 1989.

10 M -T Zhao. B.P.Singh, and P.N. Prasad,*J. Chem. Phys.* 89, 5535, 1988.

11 B.P. Singh, M Samoc, H S Nalwa, and P.N Prasad, *J. Chem. Phys.* 92. 2756, 1990

12 Y Pang, M. Samoc. and P.N. Prasad,*J. Chem. Phys.* 94, 5282, 1991.

13 B.P Singh. P.N. Prasad. and F.E Karasz, *Polymer* 29, 1940, 1988.

14 M Samoc and P N Prasad.,*J. Chem. Phys.* 91, 6643, 1989.

15 Y Cui, M Zhao, G S He and PN. Prasad,*J. Phys. Chem.* 95, 6842, 1991.

16 M.K Casstevens, M Samoc, J Pfleger, and P N Prasad, *J. Chem. Phys.* 92, 2019, 1990

17 R.R Rojo, Ph D Thesis, Heriott-Watt University, April 1994, UK.

18 F J Aranda, Ph.D. Thesis, University of Massachusetts, Lowell, USA, 1995.

19 V.N. Kumar, Ph D Thesis. University of Hyderabad, January 1997.

20. M. Maeda, Laser Dyes, Academic Press, New York, 1984; U. Brackmann, Lambda Chrome Laser Dyes, Lambda Physik, Gottingen, 1986.

21. G. Yamaguchi, F Endo, S Murakawa, S Okamura, and C. Yamanaka, *Japn. J. Appl. Phys.* 7, 179, 1968; F.P. Schafer, in *Dye Lasers*, F.P. Schafer Ed., Springer Verlag, 1977, F P Schafer, *Liquid Lasers* in Laser handbook, Edited by FT. Areechi and E.O. Schulz-Dubois (North-Holland, 1972), Vol. 1.

22 P.B. Chappie, J.M Staromlynska, J A. Hermann, and T.J. McKay, *./. Nonlinear Opt. Phys. and Mat.* 3, 251, 1997; T Xin, D J. Hagan, M. Sheik-Bahae, and E.W. Van Stryland, *Opt. Lett.* 19, 317, 1994; D V Petrov,*./. Opt. Soc. Am.* **B13,** 1491, 1996, J –G Tian, W –P Zang, and G Zhang, *Opt. Commun.* **107,** 415, 1994; S.M. Mian, B Taheri, and J P Wicksted, *./. Opt. Soc. Am.* **B13,** 856, 1996 (and references therein), M Sheik-Bahae, A A Said, D.J. Hagan, M.J Soileau, and E.W. Van Stryland, *Opt. Engg.* 30, 1228, 1991, S V Kershaw, *./. Mod. Opt.* 42, 1361, 1995

23 N.J Turro, "Modern Molecular Photo-Chemistry", The Benjamin/Cummings Publishing Co Inc., 1978, K K Rohatgi-Mukherjee, "Fundamentals of Photo-Chemistry", Wiley Eastern Ltd., New Delhi. 1992.

24 H Souma, E.J Heilweil, and R M Hochstrasser, *J. Chem. Phys.* 76, 5693, 1982, A.M. Weiner and E P Ippen, *Chem. Phys. Lett.* **114,** 456, 1985; A.M. Weiner, S. De Silvestri, and E P Ippen, *./. Opt. Soc. Am.* B2, 654, 1985; A Kummrow and A. Lau. *Appl. Phys.* **B63,** 209, 1996 and references therein

25 C.E. Barker, R Trebino, A G Kostenbauder, and A E Stegeman, *J. Chem. Phys.* 92, 4740, 1990, C Kalpouzos, W T Lotshaw, D McMorrow, and G A Kenney-Wallace. *./. Phys. Chem.* **91,** 2028, 1987, B.I. Greene and R C Farrow, *Chem. Phys. Lett.* 98, 273, 1983, J Etchepare, G Grillion, and A. Antonetti, *Chem. Phys. Lett.* **107,** 489, 1984, B.1. Greene and R C Farrow, *J. Chem. Phys.* 77, 4779, 1982, J -M Halbout and C L Tang, *Appl. Phys. Lett* **40,** 765, 1982; C.L. Tang and J -M Halbout, in *Picosecond Phenomena Vol.* 3, ed.'s K B. Eisenthal, R M. Hochstrasser, W Kaiser, and A Laubereau, Springer, Berlin, 1983, 212; C.L. Tang and J -M Halbout. *Time Resolved Vibrational Spectroscopy,* Academic Press Inc., 73, 1983

CHAPTER 3

Theoretical Model for DFWM Signals Observed in Materials Exhibiting Reverse Saturable Absorption

This chapter presents the basics of Incoherent Laser Spectroscopy and its applications for the measurement of different relaxation times in the ultra-short time domain. The two different techniques, Degenerate Four Wave Mixing using incoherent light (DFWM-IL) and 35 ps pulses (DFWM-PS), employed for measurement of population and phase relaxation in different organic materials are explained in detail. The DFWM signals obtained in some of the materials investigated show different behavior compared to the previously reported materials. We develop a new theoretical model based on, more general, four levels in these systems, taking into account the excited singlet slates, and numerically compute the PC signal as a function of the delay between the forward pump and the probe beams. The data generated through numerical simulations is compared with the observed experimental results.

3.1 Introduction

The nonlinear optical (NLO) properties of various solid-state, inorganic and organic materials have been, and are being, extensively investigated for their use in photonic and optoelectronic applications. Ultrafast and large nonlinearity is needed to realize NLO devices, such as optical switches and information processors. From scientific view point NLO processes can be used to study the optical properties of these materials   Through the NLO response we can obtain information about the electronic structure, dynamics of excitations in materials with high sensitivity and time resolution. When laser light interacts with the matter different excited states are 'prepared'   The lime evolution of electronic excited states are generally discussed in terms of two relaxation processes. Depopulation (or Longitudinal Relaxation time) and Dephasing (Transverse Relaxation time) [1]   Depopulation is the decay of the population change induced by the absorption of light to the thermal equilibrium state of the population distribution. The population decay time (T_1) is sometimes called the energy relaxation time. Dephasing (T_2) is the disappearance of the macroscopic polarization, sometimes called as polarization decay.   Coherently induced microscopic polarizations constructively interfere with each other, resulting in a finite macroscopic polarization. Once the incident light is off, the phases of these

microscopic polarizations become gradually random because of scattering, so that they destructively interfere and the macroscopic polarization decays. The other molecular dynamical processes include molecular vibrations, photo dissociation reactions, electron transfer reactions, vibrational dephasing etc. Developments in Ultrafast Spectroscopy [2-3] with improved time-resolution has clarified the detailed mechanisms of the relaxation processes in various materials like quantum well structures, metals, polymers, organic liquids, molecules dissolved in solution or adsorbed on solid surfaces, and biological systems But the practical difficulties involved with techniques using conventional short pulses have forced the researchers to look out for alternative, indirect techniques.

3.2 DFWM-IL for ultra-fast relaxation measurements

In the early eighties a new spectroscopic technique was proposed by Morita and Yajima [4] in which a temporally incoherent light is used as the source for the measurement of T» and T_2 This technique has been successfully applied to the studies of both dephasing times in fs domain, longitudinal relaxation times in the ps domain [5] using ns pulses The other time-domain techniques using incoherent light which have been amazingly successful are coherent anti-Stokes Raman Scattering (CARS), coherent Stokes Raman Scattering (CSRS), time-resolved pump-probe Raman Spectroscopy, and Optical Kerr Gate, and Forced Light Scattering [6-8] In the frequency domain, novel ultra sharp spectral poles` have been discovered [9]. Morita et al [5] working with time-delayed four wave mixing obtained, theoretically and experimentally, the population relaxation time in DQOC1 using incoherent light and ps pulses Kobayashi et al [10] derived a generalized formula for calculating the relaxation times when one of the beams, in the standard degenerate four wave mixing (DFWM), is delayed with respect to the other beams and applied it for the measurement of Kerr relaxation in liquids like CS_2 and Nitrobenzene Okamoto [11] extended the work of Morita and Yajima to systems with more than two levels, like organic dyes, having different excited and ground state relaxation times and showed, both theoretically and experimentally, that the population relaxation time can also be obtained using non zero delay of beam 2 When the ground state and excited state relaxations are equal he could get back the equations obtained by Morita et al. [5] for

their two-level model He obtained a T_1 value of ~ 70 ps for the sample pararosaniline using ns pulses with a correlation time of ~ 200 fs using the DFWM technique in the boxcar geometry.

Over the last decade there have been several experimental results describing FWM processes in different materials and under different conditions. Liu et al [12] investigated the ps relaxation processes in Cresyl Violet and obtain a ground state recovery time (T_1) of - 160 ps using DFWM with incoherent light having a correlation time of ~ 53 ps Nakatsuka et al. [13] studied the fluorescence lifetime measurement of Cresyl Violet using incoherent light gated optical Kerr shutter technique and obtained a value of 160 ps PfeifTer et al [14] investigated both theoretically and experimentally, the fifth order nonlinear response of nuclear motion in liquids using incoherent light with fs auto-correlation time under non-resonant conditions Kummrow et al [15] reports the optical dephasing in neat liquids and liquid crystals using Forced Light Scattering (FLS) with incoherent light and fs time resolution Puech et al [16] measured the dephasing time of gold nanoparticles to be less than 20 fs using incoherent light possessing a coherence time of 86.5 fs. Similarly Maciel et al [17] reported the dephasing time in polyaniline liquid solution to be ~ 10 fs using pulses having a coherence time of 150 fs. Nomura et al. [18] performed theoretical and experimental studies on the profile of pump-probe time-resolved intensity correlation spectroscopy with incoherent light and shown that this spectroscopy is applicable to study population relaxation time and electronic pure dephasing processes.

Several other measurements using incoherent light include fs electronic dynamics in Azulene and Iodine [19], fluorescence lifetime measurements of semiconductor doped glasses [20], and orientational relaxation times in benzene and nitrobenzene [21] Phase relaxation times have been measured in Nile blue [22], Ruby [23], and semiconductor micro crystal [24] Kozich et al. [25] measured the light-induced homogenous broadening in a dye solution Measurements of dephasing times have also been performed using incoherent photon echoes with time resolution limited by the coherence time of the input pulses rather than the pulse width itself [26] Several review articles [27] have discussed, in more detail, the applications of incoherent light for the measurement of different excited state dynamics. Here we

attempt to study the dephasing and population relaxation measurements in different organic materials, with potential applications in optical information processing and communication, using DFWM technique with incoherent light as the source.

3.3 Results and Discussion

The complete details of the DFWM experimental setup using incoherent light have been provided in chapter II. Figures 3.1 (a) and (b) shows the absorption spectra for the samples, CoTTP (in chloroform), Black Ink (in distilled water), Erythrosin B (methanol) and Rhodamine B (methanol), ZnmTPP (chloroform), ZnmpTBP (chloroform) NimpTBP (chloroform) and Cresyl Violet (methanol) Inset of fig. 3.1 (b) shows the structure of the Porphyrins used in the study. All the spectra are recorded using a Jasco UV/Visible spectrometer (Model no. 7800) The solvents used for dissolving the samples are of high purity and spectroscopic grade. Fresh samples are prepared and used for every new measurement to avoid any complications arising from the photo-degradation of the samples All the measurements have been carried out with the concentrations of the samples in the 10^{-4} to 10^{-5} M range corresponding to an absorbance of less than 20% (OD ~ 0.2). The typical peak intensities (at the focal point) are calculated to be 400 - 700 MW/Cm^2. Figures 3.2 and 3.3 show time-resolved profiles, for different values of 5. in the samples ZnmpTBP and ZnmTPP Figure 3 4 shows the PC signal recorded for different compounds TTP, CoTTP. and NiTTP The main and intense peak appears at r = 0 and is found to be due to the coherence of beams 1 & 3 and has a width (FWHM) of ~ 170 fs. This width coincides with the width of the auto-correlation curve (recorded in the sample Rhodamine B) Though earlier reports showed the second peak to have the same width as the first peak we have observed, for the first time in Porphyrins and other dyes, that the second peak as much broader than the correlation time and the first peak

The physical interpretation of Degenerate Four Wave Mixing has been detailed in Chapter 2 Initially all the experiments are performed in the phase conjugate configuration where the delay time between k_1 and k_2 is denoted as 5 and that of k_1 and k_3 as τ The signal is recorded as a function of T, for different values of
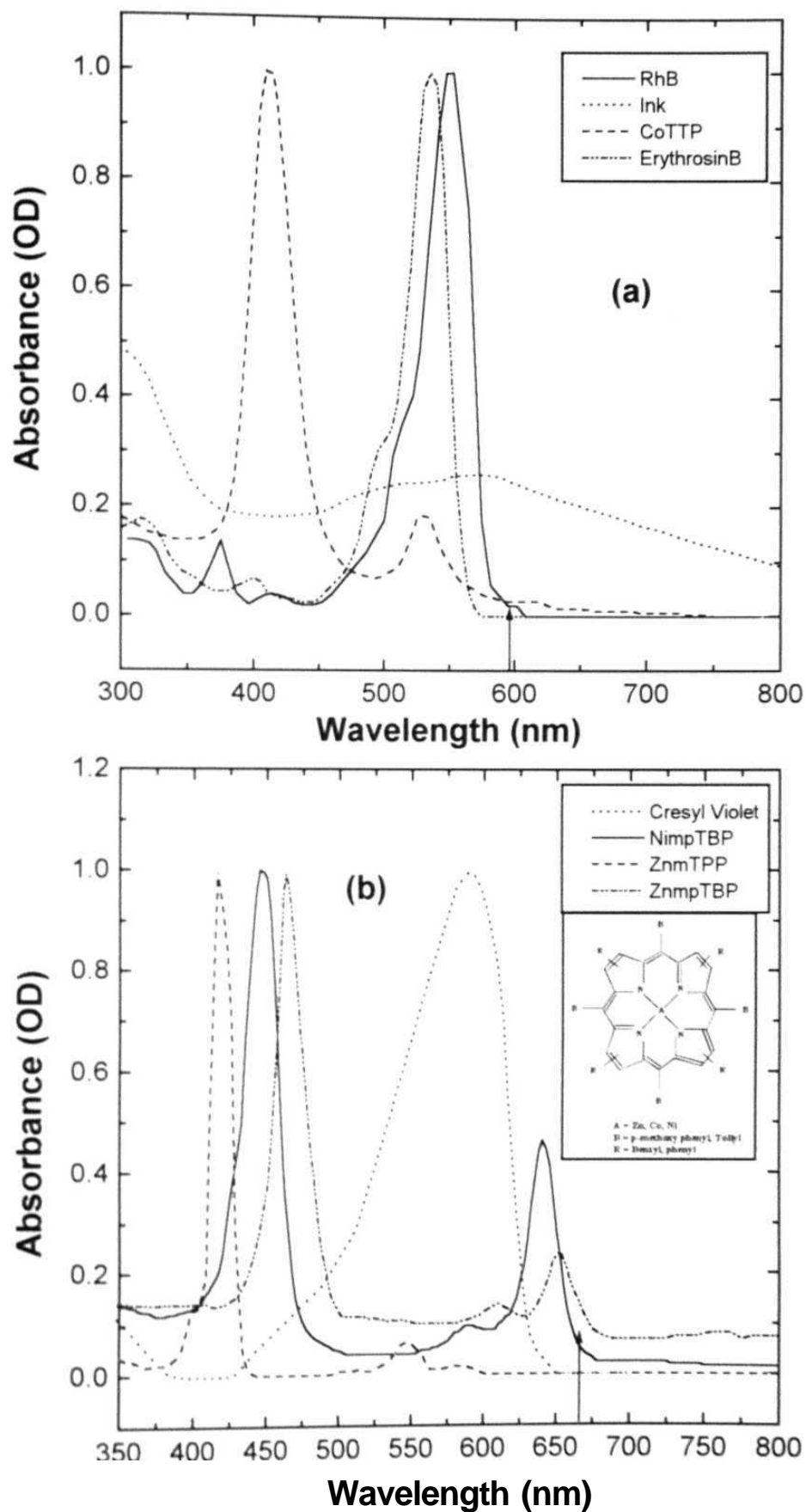
Fig. 3.1(a) Absorption spectra of RhB (Methanol), ErythrosinB **(Methanol),**
Black Ink (Distilled Water), CoTTP (Chloroform) (b) Absorption spectra **of**
Cresyl Violet (Methanol), NimpTBP, NimTPP, and NimpTBP in THF. Inset
shows the structure of the compounds used in **the study**
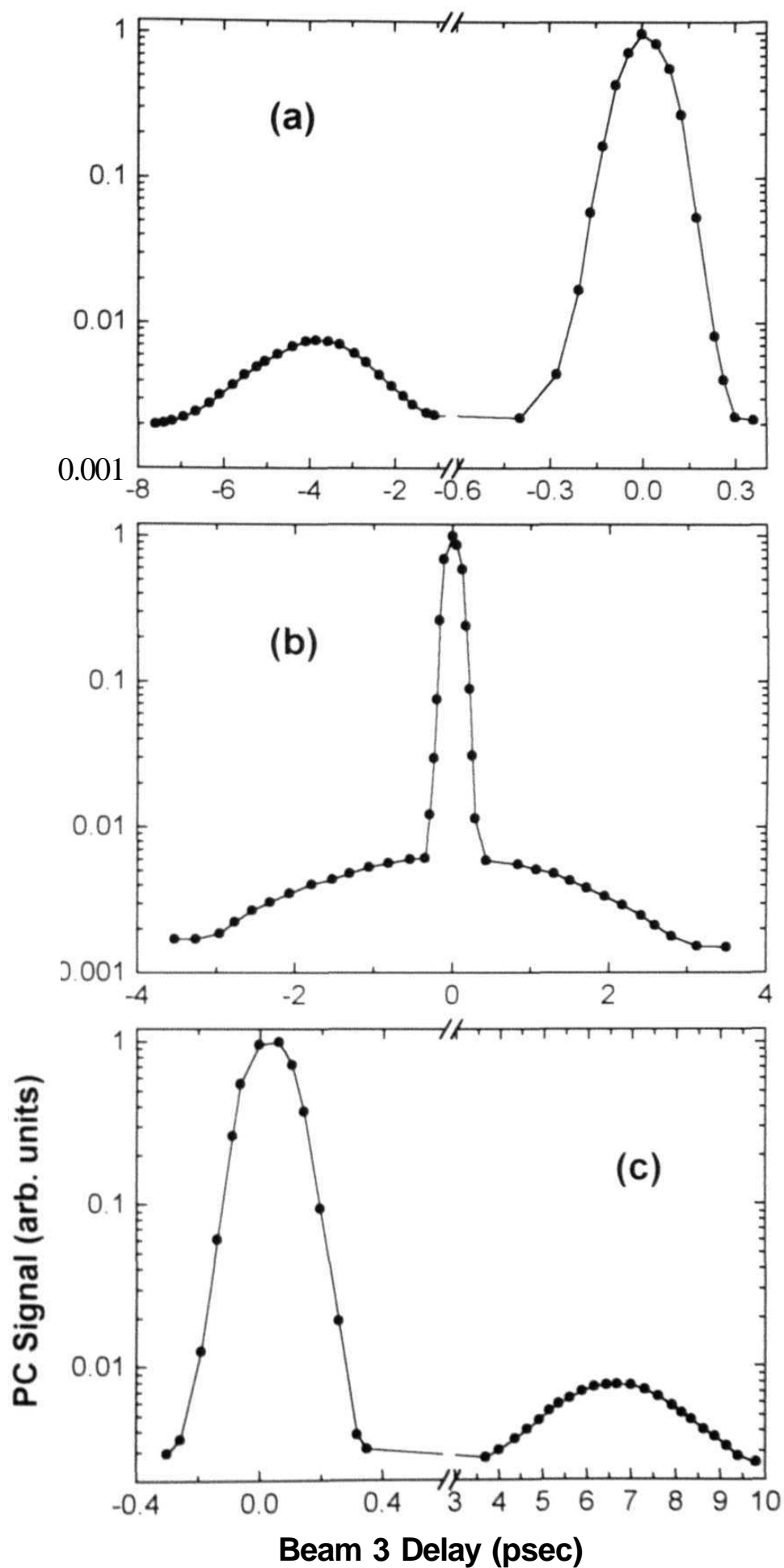
Fig. 3.2 Time-resolved DFWM-IL signals in ZnmpTBP (THF) (a) δ = -4.0 psec
(b) δ = 0.0 psec (c) δ = 6 5 psec. Solid line is for visual clarity.
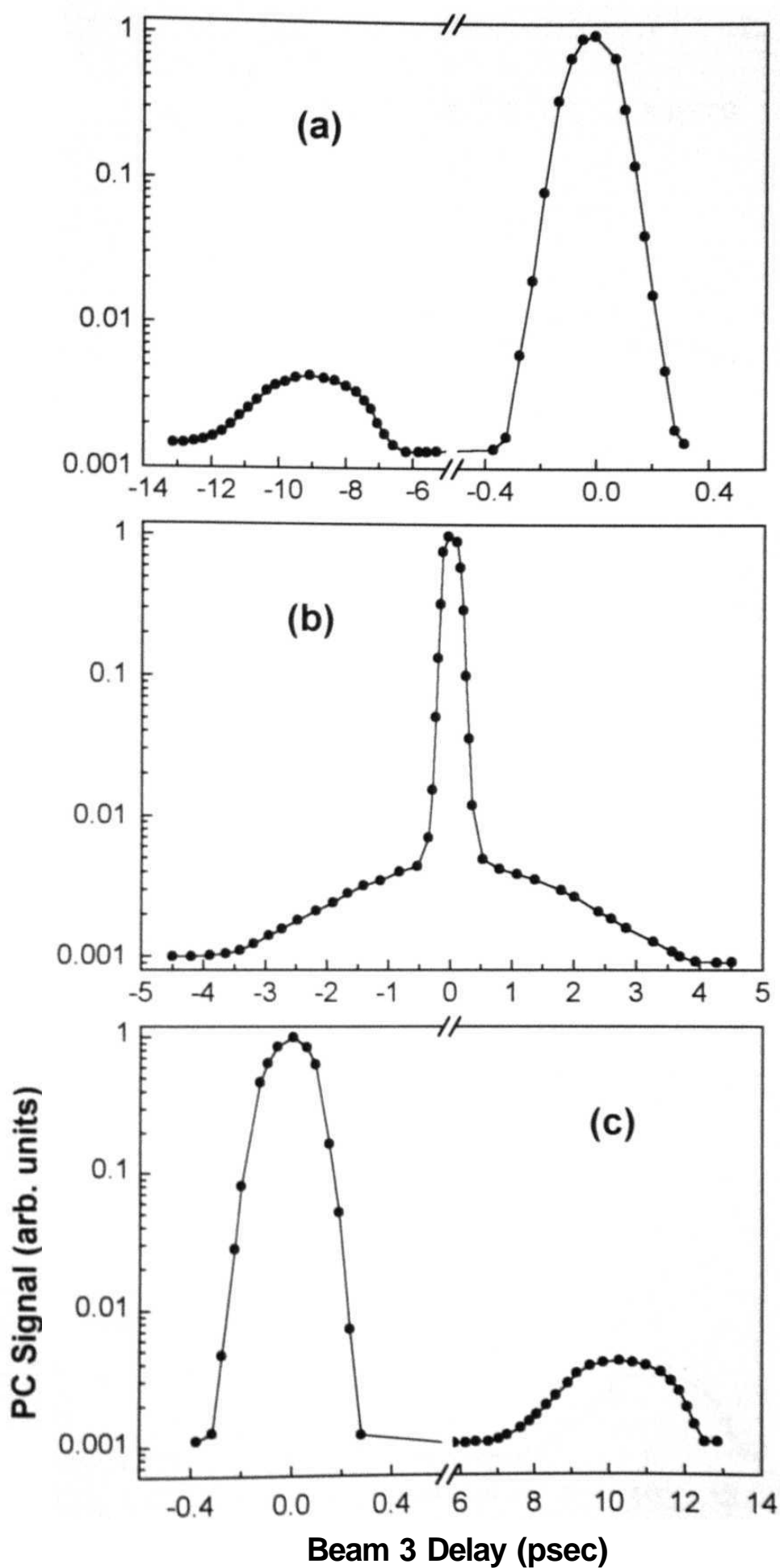
Fig. 3,3 Time - resolved DFWM-IL signal in **ZnmTPP (THF) (a)** δ **= -9 psec**
(b) 6 **= 0 psec and (c)** δ **= 10 psec.** Solid line is for visual clarity
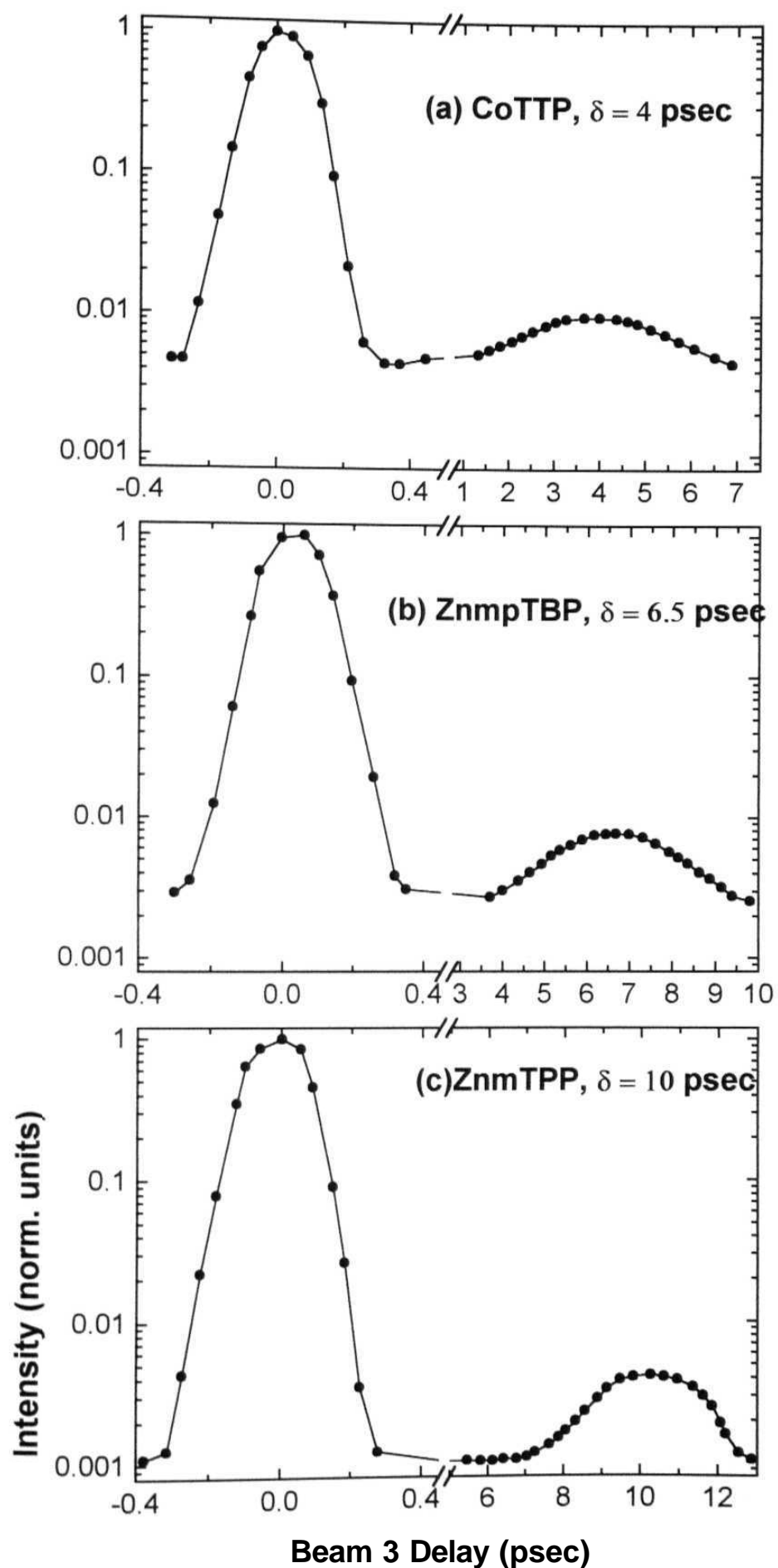
Fig. 3.4 PC Signal for different samples showing the variation in the height of second peak and background level. Solid line is for visual clarity.

6, for several samples like Rhodamine B (methanol), Erythrosin B (methanol), Black Ink (Distilled water), and CoTTP (chloroform). The salient features observed in the PC signals of all the samples [28] are

1. All the profiles, shown in fig. 3.5, had two peaks, except for the sample Rhodamine B, viz. an intense, narrow peak and a weak, broader peak. The intensity of the signal background (apart from the scattered background) was approximately equal to the intensity of the second peak. (for some samples it was 1:1 and for others it was ~ 1 : 2)

2. The main, intense peak is found to be due to the coherence of beams 1 & 3 and has a width (Full Width at Half Maximum, FWHM) of ~ 170 fs. There is no decay observed in the coherence peak, due to beams 1 and 3. Any delay, in either of the beams, beyond 170 fs, resulted in the signal going down to zero. This has been also confirmed from the fact that when the sample is replaced with RhB in methanol, we get the auto correlation function. It is well known that RhB has very fast dephasing time (T_2 ~ 50 fs) and very slow population relaxation time (T_1 ~ns) [29] and hence we see only the auto-correlation.

3. The broader and weaker peak is due to the coherence of beams 2 & 3 and has a width (FWHM) of ~ 0 17-6 ps. Again the signal vanished for any delays in the beams 2 and 3 which are greater than 10 ps.

4. The second peak moves symmetrically across the main peak with delay of beam 2 appearing exactly at $\tau = |5|$. The separation between the peaks is found to be exactly 5. The width of the second peak remained constant for large values of 5 (~ 1000 ps).

There are very few reports on the observation of two peaks in the PC signal recorded as a function of the delay of one *of* the beams with others at zero delay. Though earlier report by Okamoto et al. [11] showed the second peak to have the same width as the first peak, we have observed for the first time in porphyrin, ink and other dyes the broader second peak. Liu et al. reports T_1 (~ 160 ps) measurements on the sample Cresyl Violet with incoherent light possessing a correlation time of 53 ps. At lower power densities in the sample they do observe two peaks in the PC signal
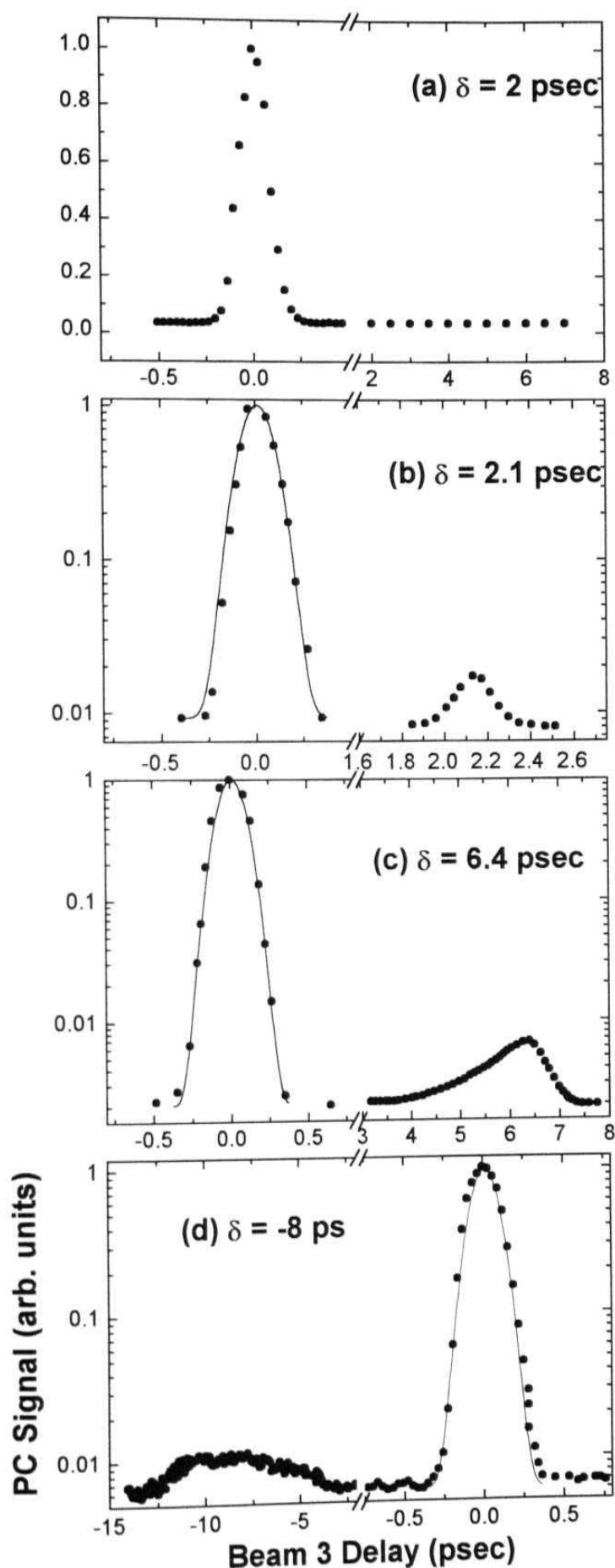
Fig. 3.5 Time-resolved PC signals in (a) **RhB** (Methanol) (b) **ErythrosinB** (Methanol) **(c) Black Ink** (Distilled Water) (d) **CoTTP** (Chloroform). **Solid** line is autocorrelation curve in RhB

structure. The widths of the two peaks are same and the ratio (we calculated from the graph) is ~ 3 indicating that the T_1, if calculated, according to Okamoto's theory will be 53 * 3 ~ 160 ps. The reason for the appearance of the peaks at low power densities only was not well explained. Fleitz et al. [30] observe the double peak structure in PC signal, obtained using ns pulses, for their samples diphenyl polyenes and attribute it to the slow grating formed as a consequence of thermal grating resulting from two photon absorption. The ratio of the peaks varied with pump energy, which is not the same in our case, and the width of the second peak was found to be ~ns. Sutherland et al. [31] made similar observations in diphenylbutadiene and attributes it to the thermal grating resulting from Two Photon Absorption. Brown et al. [32] observe two peak-structure in their femtosecond transient grating experiments with samples like benzene, toluene. They attribute the two peaks to the coherence coupling feature at time zero and rotational dephasing. Difference in amplitudes of these two components has been related to the isotropic and anisotropic components of the molecular polarizability In our case the presence of second peak is not due to thermal grating, rotational dephasing or reorientational relaxation times but is related to the presence of population of excited states as shown in the following sections. Reorientational relaxation times are very sensitive to the solvent viscosity, while lifetimes are, in general, similar in different solvent [33].

3.4 Measurement of Population Relaxation Time (T_1)

For transient gratings, signal in the direction $\mathbf{k_s} = \mathbf{k_1} + \mathbf{k_2} - \mathbf{k_3}$ has contribution from two different gratings (as depicted in fig. 3.6 with $t_1 < t_2 < t_3$)

1. $\mathbf{k_2}$ at time t_3 gets diffracted by the grating formed with the fields in directions of $\mathbf{k_3}$ and $\mathbf{k_1}$ at t_1 and t_2 respectively.

2. $\mathbf{k_1}$ at time t_3 gets diffracted by the grating formed with the fields in directions $\mathbf{k_3}$ and $\mathbf{k_2}$ at t_1 and t_2 respectively. The total electric field is given by the expression

$$E(t) = \varepsilon(t-\tau)\exp\{-i\omega_o(t-\tau) + i\mathbf{k_1}.\mathbf{r}\} + \varepsilon^*(t-\delta)\exp\{-i\omega_o(t-\delta) + i\mathbf{k_2}.\mathbf{r}\}$$

$$+ \varepsilon(t)\exp\{-i\omega_o t + i\mathbf{k_3}.\mathbf{r}\} + \text{Complex Conjugate} \qquad (3.1)$$

where e(t) = V(t)R(t). Amplitude function s(t) is expressed as the product of a slowly varying regular pulse envelope function V(t) and a complex random modulation function R(t) describing the temporal incoherence of the fields.
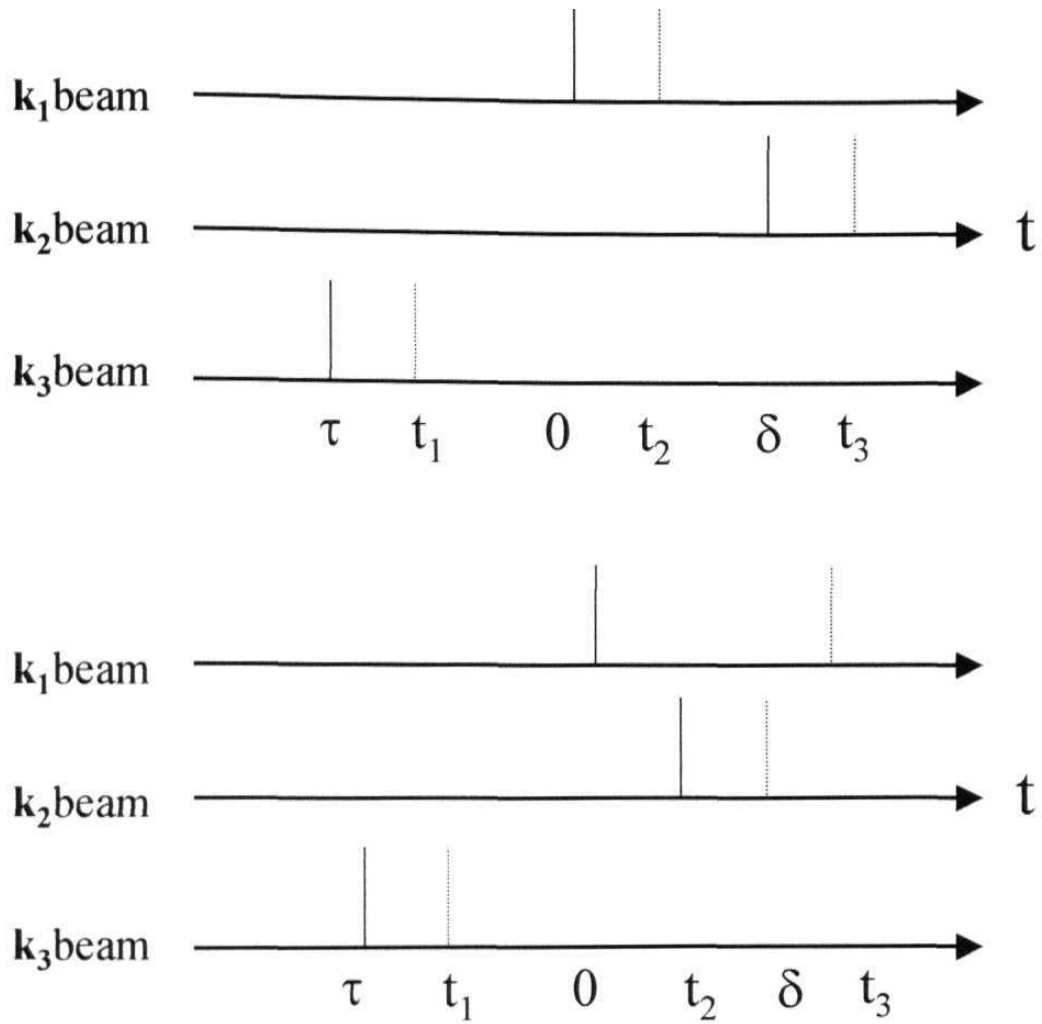
Fig. 3. 6 Timing diagram of different pulses. (a) Beam k_2 gets scattered by grating formed by (k_1, k_3) grating. (b) Beam k_1 gets scattered by grating formed by (k_2, k_3) grating.

The third-order nonlinear polarization in the $\mathbf{k_s}$ direction will be integral over $t_1, t_2,$ and t_3 and the integral limits are $t_1(-\infty, t_2)$, $t_2(-\infty, t_3)$, and $t_3(-\infty, t)$. When two or more levels are present in the system we should consider the effect of excited state relaxation which is generally not the same as ground state relaxation. The signal due to excited state relaxation may be buried in the signal due to ground state relaxation if the ground state relaxation is slow enough. The signal intensity is proportional to

$$J(\tau, \delta) = \int_{-\infty}^{\infty} dt_0 < |P_3(t_0:\tau,\delta)|^2 > \tag{3.2}$$

where $< >$ denotes statistical average.

Assuming the homogenous broadening limit, the total signal intensity is given by the expression

$$J(\tau,\delta) \propto \sum_{i=1}^{15} \int_0^{\infty} dx \int_0^{\infty} dy [\exp(-\gamma_{gg}x) + \exp(-\gamma_{ee}x)] * [\exp(-\gamma_{gg}y) + \exp(-\gamma_{ee}x)] S_i(x,y;\tau,\delta)$$

$$\tag{3.3}$$

In the above equation γ_{gg} and γ_{ee} are the ground state and excited state lifetimes respectively. Under the limiting condition that excited state relaxation is much faster than ground state relaxation (and for large values of 5) the intensities of main peak, second peak and that of background asymptotically reach a certain value given by

$$I_0 \propto [4/(\gamma_{ee} + \gamma_{gg}) + 1/\gamma_{gg} + 1/\gamma_{ee}](1/\tau_c)$$

$$I_\delta \propto [(1/\gamma_{gg} + 1/\gamma_{ee})^2(1/\tau_c)^2 + (1/\gamma_{gg} + 1/\gamma_{ee})](4/\tau_c)$$

$$I_b \propto [4/(\gamma_{ee} + \gamma_{gg}) + 1/\gamma_{gg} + 1/\gamma_{ee}](1/\tau_c) + 8$$

and the ratio

$$I_0:I_\delta:I_b = (1/\gamma_{gg}\tau_c):1:1 \quad \Rightarrow 1/\gamma_{gg} = T_1 = (I_0/I_\delta)\,\tau_c \tag{3.4}$$

leads to estimation of population relaxation time from the 5 dependence of the signal intensity provided it is longer than the correlation time.

A typical energy level diagram for an organic material indicating the different absorption and relaxation mechanisms has been discussed in chapter 2. The input pulses excite molecules from the ground state So into the higher vibrational states of the excited singlet state S_{1v}. The relaxation of the molecules out of this state occurs rapidly, within few ps, into an equilibrium level in the singlet state S_1. This level relaxes either by non-radiative decay into first Triplet state T_1 (intersystem crossing rate K_{isc}) or by both radiative and non-radiative decay within the singlet system. Depending on the intersystem crossing rates, the excited state absorption may be from Singlet S_1 or Triplet states T_1 into S_n or T_n respectively. In our case, since the time scales probed are in the order of few ps/fs, there is less probability of intersystem crossing at such short time scales. However, since we are using ns pulses, the situation is much more complicated than with ps pulses. A ns pulse can create a non-zero population in the first excited state which may get transferred to the triplet state T_1 before the observation of the ps/fs coherent signals. We can, however, imagine the system consisting of three or four levels if we assume that the S_1 - S_n and the T_1 - T_n band structures and relaxation times (S_n - S_1 and T_n - T_1) are similar. The only major difference would be the relaxation of the T_1 state ($\sim \mu s$ to ms) and the S_1 state (ps to ns). A simple three/four level model is imagined for these molecules. A five-level model is considered for Z-scan studies where the population in different excited states plays an important role in nonlinear absorption.

Pumping of the molecules, with sufficient intensity, can lead the population directly to the excited state S_n. These upper states S_n will relax back to the S_1 state on a fs time scale and in the process generate a vibrationally excited state (Kasha's rule). Different line shapes for the observed signal can be explained if we take the S_n levels as the excited upper state and S_1 as the excited lower level (ground state as given in the theory by Okamoto et al. [11]), γ_{ee} and γ_{gg} as the relaxation rates of S_n and S_1 respectively. Because of the fast response time in fs, we attribute the signal at peak 1 as due to the dephasing of excited states S_n. The relaxation within the vibrational levels, in most organic materials in general, is reported to be in the order of few ps. Femtosecond pump-probe studies on different dye molecules revealed the presence of sub-ps transients, which have been attributed to redistribution of excitation energy among the vibrational modes in, excited states S_1 of the molecule. The width of the

second peak, which is of the order of few ps, is attributed to the vibrational relaxation. The ratio of the peaks is directly related to the population relaxation time as shown in equation (3.4).

The second peak is found to be symmetric in all samples, but for the sample Black Ink there is a clear asymmetry observed which could be due to the complex relaxation mechanism in these classes of dyes. The variations in the intensities of the two peaks can be explained as due to the efficiencies of the two gratings. The difference in the signal intensities can be seen as the difference in the diffraction efficiencies of the two gratings. The difference in the intensities of the two peaks can be explained as due to the efficiencies of the two gratings. Peak 1 is due to coherence of beams 1 and 3, while beam 2 gets diffracted in k_4 direction and can be imagined as a transmission grating. Whereas the broader peak 2 is due to the coherence of beams 2 and 3 and beam 1 gets diffracted in k_4 direction and can be imagined as a reflection grating.

By changing the polarization of the probe beam such that it is perpendicular to pump polarization, the signal intensity in peak 1 dropped to 6-8 times whereas the peak 2 almost disappeared indicating that the grating formed is due to excited state population. A constant background in the signal appears in all of the profiles. The thermal effects, which occur in the slower (ns) time scales, lead to this background signal, over which the signals due to coherent processes override. The values of T_1 calculated using eqn. (5) are of 48 ps, 32 ps, 37 ps, and 34 ps for the samples **ZnmTPP** (Zinc meso-tetraphenyl porphyrin), **ZnmpTBP** (Zinc meso-tetra- (p-methoxyphenyl) tetrabenzporphyrin), CoTTP (Cobalt Tetratolyl Porphyrin), and **NimpTBP** (Zinc meso-tetra- (p-methoxyphenyl) tetrabenzporphyrin) respectively. The vibrational relaxation times calculated for these samples are summarized in table 3.1. The widths of the two peaks are calculated, by fitting the data, using an equation

$$Y = \left(\frac{A}{\omega * \sqrt{\frac{\pi}{2}}} * \exp\left(\frac{-2 * (X - X_c)^2}{\omega^2} \right) + Y_0 \right) \tag{3.5}$$

where A is the amplitude and ω is the width of the Gaussian. The ratio of I_δ to I_b is found to be 1 to 2, which is in good agreement with previously reported theory of

Okamoto [11] and Morita [5]. The signal profile recorded with different solvents such as Tetra Hydro Furan (THF), Dichloro Methane (DCM), Benzene, and Chloroform did not show any significant changes.

Open aperture Z-scans are obtained for all the materials to assess their nonlinear absorption and a few results are shown in fig. 3.7. Reverse Saturable absorption in Tetra phenyl Porphyrins, implying that there is excited state absorption, is well established. Open aperture Z-Scan studies of ZnmpTBP, ZnmTPP, CoTTP, NiTTP, TPP and Ink show reverse saturation absorption whereas, Rhodamine B and Rose Bengal show Saturable absorption. Materials that exhibited reverse Saturable absorption showed two peaks. For Rhodamine B solution, we do not observe any second peak. Experiments were also conducted for other dyes such as Rose Bengal, which shows Saturable absorption, and for which we did not observe the second peak. To confirm our observations, we replaced the porphyrin dye with commercial blue ink, which exhibits reverse Saturable absorption. The signal recorded once again showed two peaks. The width of the broader peak in this system, however, was ~ 1.5 ps. This supports our argument that the second peak appears whenever there is excited state absorption. We observed similar recordings for other Porphyrins such as CoTTP, NiTTP, and TTP. The width of the second peak varied from sample to sample. This variation in the width of second peak is attributed to the difference in dephasing/decay mechanisms in the excited states of different samples.

We have also performed similar measurements on other samples like Cresyl Violet Acetate, DQOCI (diethylquinolyloxacarbocyanine, in Ethylene Glycol)), and Brilliant Green (Ethylene Glycol) dyes. The dual peak structure is seen for all the samples with difference in the ratio of the peaks and the width of the second peak. The values of the phase and population relaxation times, vibrational relaxation are summarized in table1 DFWM-IL measurements [fig. 3.8(a)] on Cresyl Violet Acetate indicate an excited state lifetime of ~ 30 ps while measurements with 35 ps pulses [fig. 3 8(b)] on the same sample shows a lifetime of ~ 58 ps which, matches well with the value obtained with incoherent light. The value of T_1 reported by others does not match with our measured value. This could be partially due to the difference in the samples used (we used Cresyl Violet Acetate) and limitation of dynamic range in the present setup. For a T_1 value of 160 ps the ratio should be ~ 1000 which is not
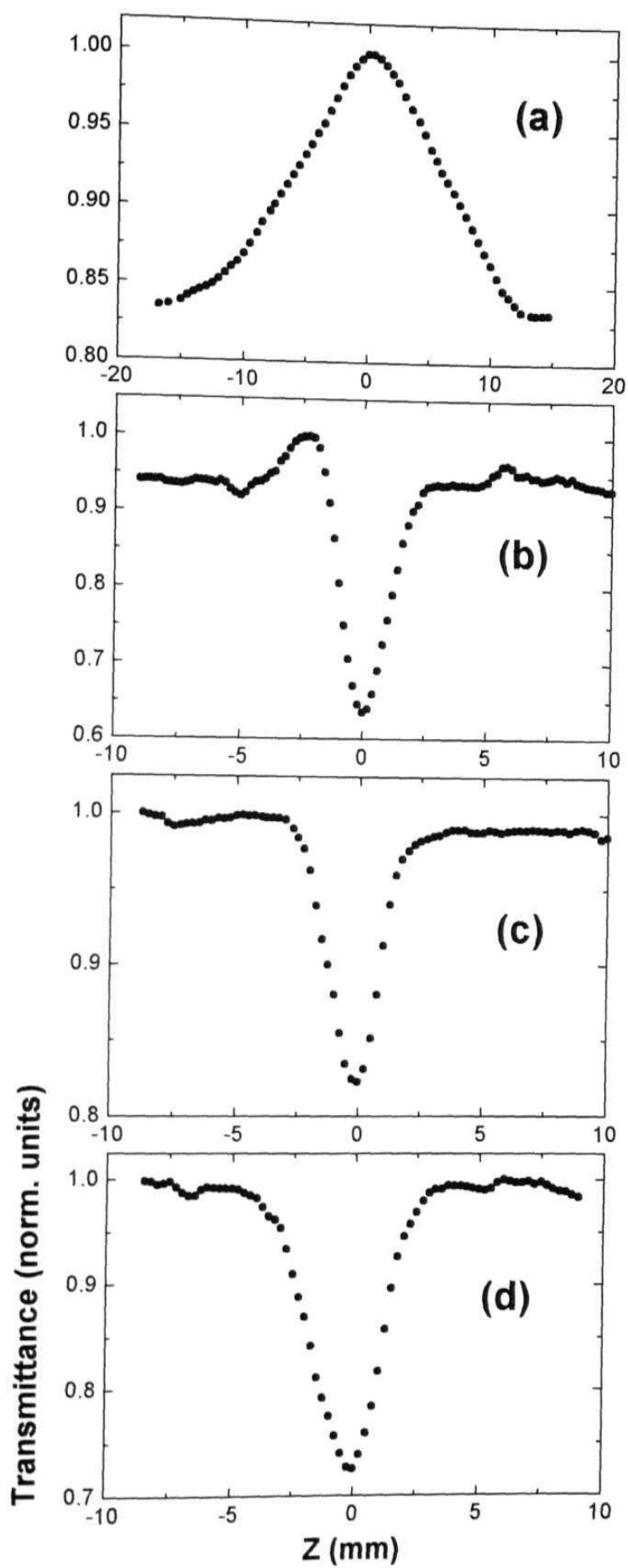
Fig. 3.7 Open aperture Z-scan for (a) RhB (b) ErythrosinB
(c) Black Ink and (d) CoTTP
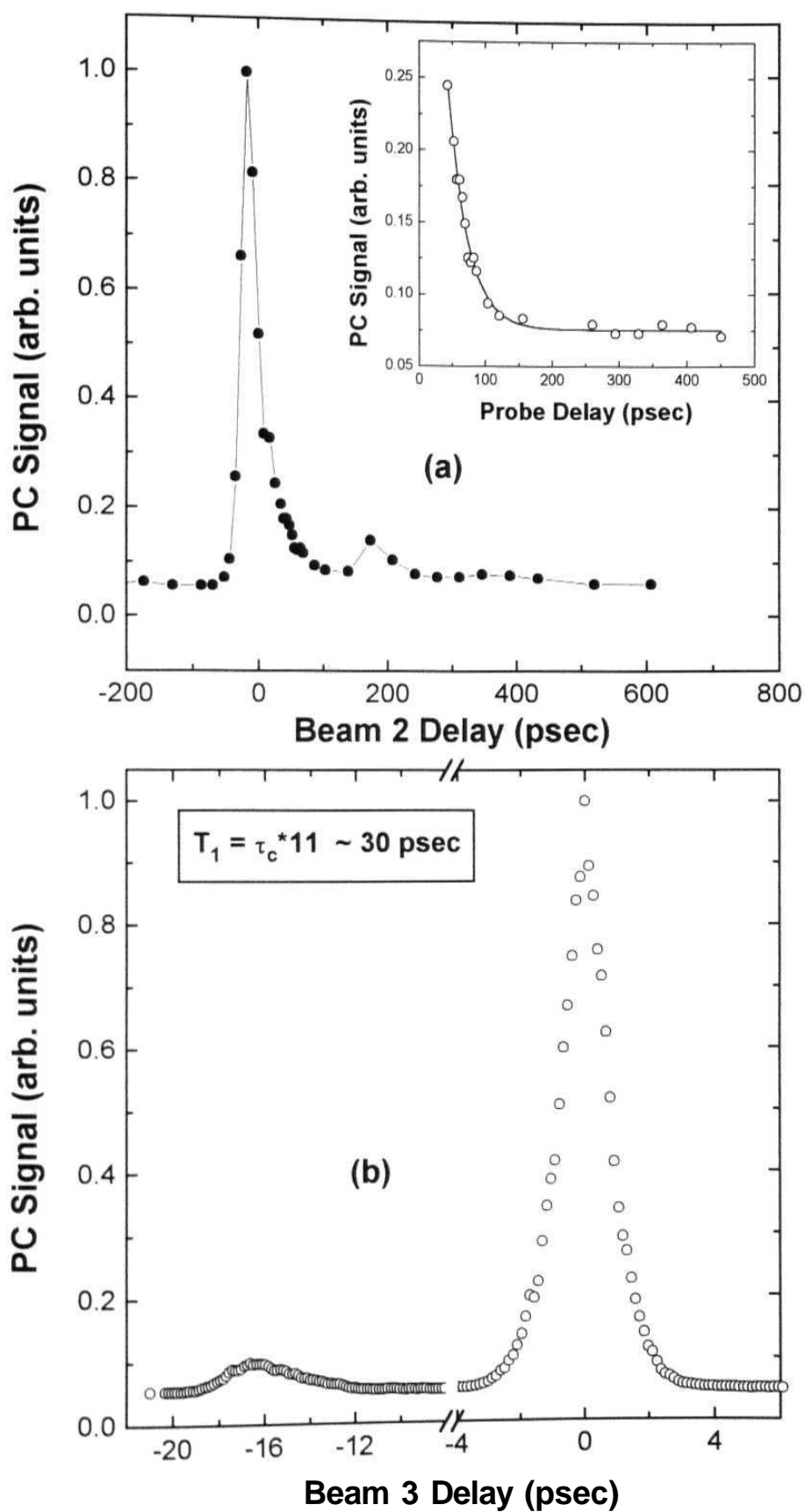
Fig. 3.8 (a)   PC Signal in Cresyl Violet Acetate (Methanol) with
35 psec pulses. Inset shows fit to the decay part. (b) PC signal
in the same sample with incoherent light of τ_c = 2.7 psec.

possible in our case (the signal to background ratio will be very small in that case). Similarly for the sample DQ0C1 we do not see perfect matching of the reported and measured values. DFWM-IL measurements [fig. 3.9 (a)] yield a lifetime of ~ 43 ps and DFWM-PS measurements [fig. 3.9 (b)] yield ~ 102 ps. The value reported by Morita et al. [5] is ~ 83 ps using both incoherent light and short pulses.

To confirm the arguments proposed in terms of the lifetimes for the appearance of the two peaks, we also measured the DFWM-IL signals with incoherent light possessing a different correlation time. By placing a highly dispersive element like a grating in the cavity, we could achieve a narrow band (~ 1.5 nm) output with a higher correlation time (~ 2.7 ps). The DFWM-IL measurements performed on the same samples, with similar experimental conditions, indicate similar structure and lifetimes again, within the experimental error.

3.4.1 Rhodamine B: Concentration dependent PC Signal

For further understanding of the structure of peaks in DFWM-IL we performed concentration and intensity dependent measurements for all the samples. Except for RhB all the samples showed similar structure of the signal and values of the lifetimes, within experimental errors. In case of RhB we observed a second peak, shown in fig. 3.10 (a) and (b), for either very large concentrations of the sample (starting from 10^{-3} M and above) used or large input intensities (for peak intensities above 800 MW/Cm^2) This could be due to the formation of aggregates at higher concentrations and thereby reducing the S_1 state lifetime. Fig. 3.10 inset shows the absorption spectra recorded at two different concentrations. With higher concentration the absorption edge spreads to 600 nm, our working wavelength, which could lead to significant population in the S_1 state. Open aperture Z-scans performed at two different concentrations, one at very low and the other at very high concentrations, show different behavior [fig's 3.11 (a) and (b)]. At lower concentrations the curve shows saturation kind of behavior and at high concentrations/intensity the curve shows RSA (not completely, but partly RSA within SA). At higher intensities the population could be excited into higher states (S_n) due to two-photon absorption which is a intensity dependent process. The decay route,
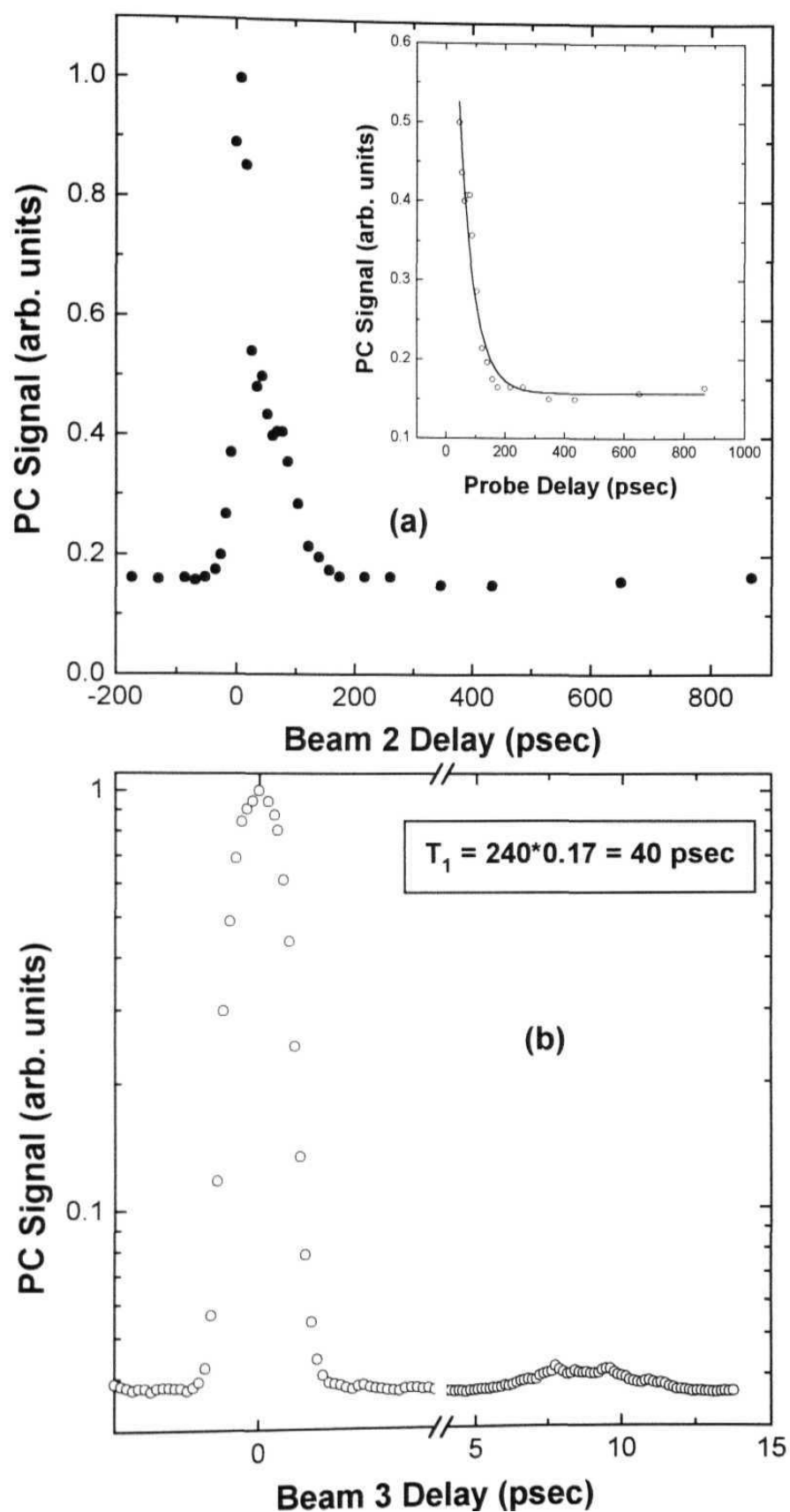
Fig. 3.9 (a) PC Signal in DQOCl (using 35 psec pulses). Inset shows fit to the decay part. (b) PC signal in the same sample obtained with incoherent light
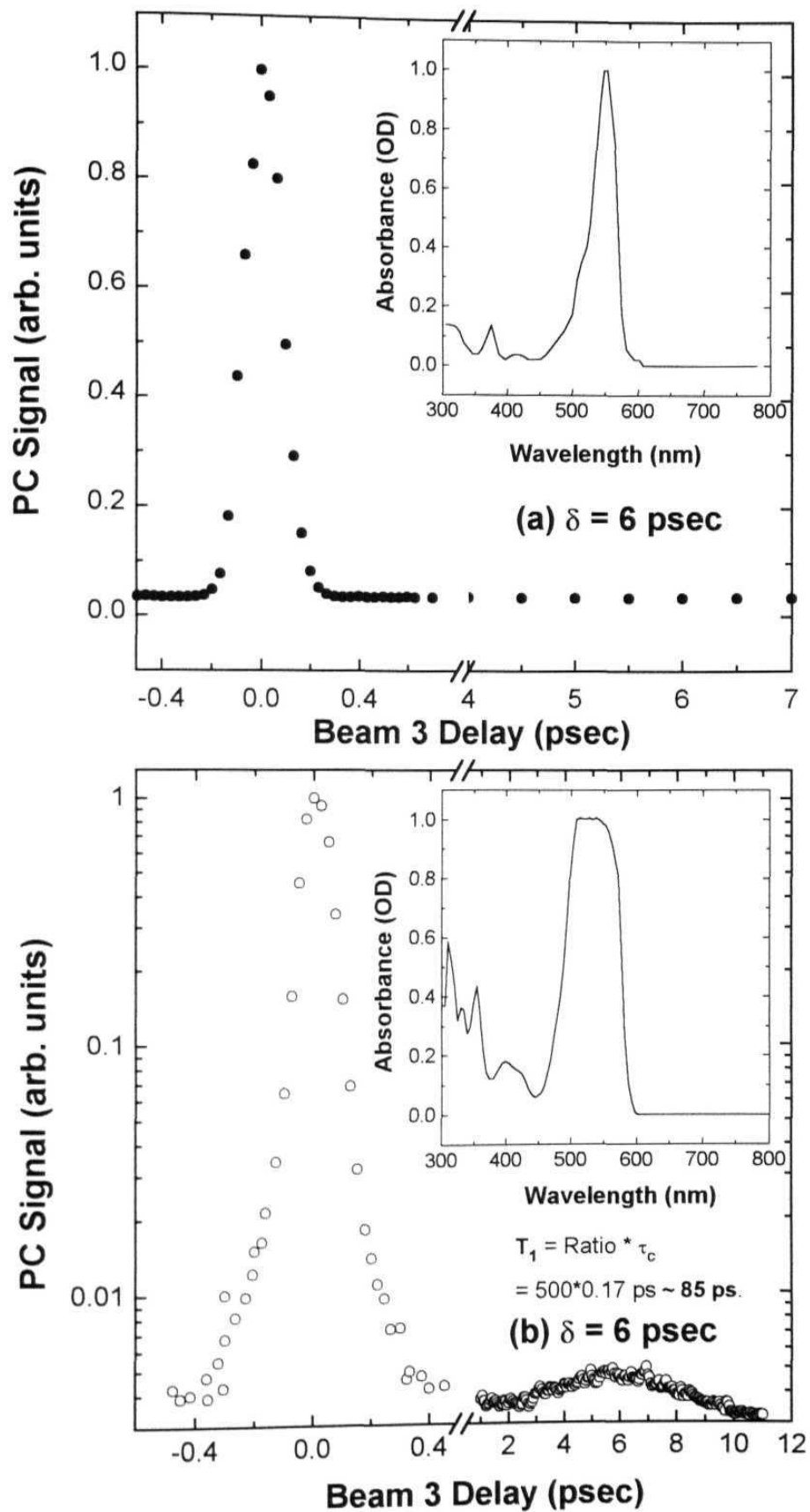
Fig. 3.10 (a) PC signal in the sample RhB (Methanol) at a concentration of ~ 5.25*10⁻⁴ M (b) PC signal in the same solution with a concentration of ~ 5 25*10⁻³ M. Inset shows the absorption spectra.
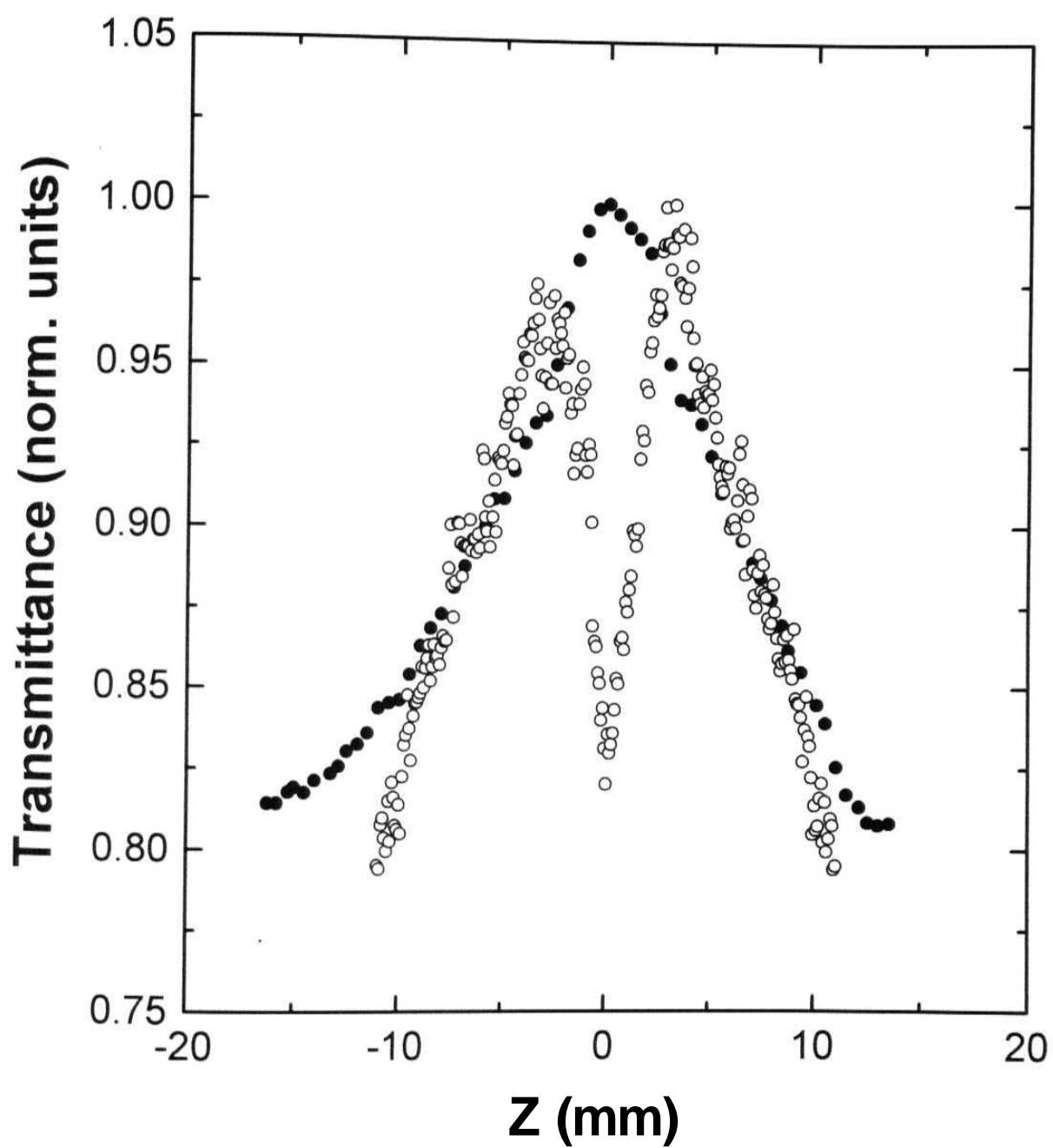
Fig. **3.11** Concentration dependent open aperture Z-scan curves in RhB (Methanol). Scan with closed circles is obtained for lower concentration and with open circles for higher concentration

then, of the population from S_n would be into the SJO state through S_{1v} state and finally to the So state as argued earlier. Earlier studies [33,34] do indicate the quenching of the S_1 state lifetime at higher concentrations. Smirl et al. [35] reports the excited state lifetime of ~ 100 ps of the RhB dimer. In our case the value of T_1 calculated using the ratio of two peaks is ~ 85 ps. The vibrational relaxation in the S_1 state is found to be 3.5 ps. There is less probability of the triplet states being involved in our time-resolved measurements since (1) The correlation time of the pulses is ~ 170 fs and the intersystem crossing rate is ~ few hundreds of ps which is much larger compared to the correlation time, τ_c. (2) The lifetime of the T_1 state is very long that the second peak will be too weak to observe.

3.4.2 DFWM signals in the Boxcar geometry

Fig's 3.12 (a) and (b) show the boxcar signal in CS_2 as a function of beam 2 delay The signal clearly shows a decay and a double exponential fit reproduces the two orientational relaxation times (~ 0.16 fs and 1.50 ps). We have measured the DFWM signal for the sample CuTTP in the boxcar geometry (details of the setup have been provided in Chapter 2) as a function of delay of one of the beams, either 1 or 3. The signal structure is shown in fig. 3.13 (a). There is no obvious decay observed indicating that the phase relaxation time (T_2) is much less than the coherence time Fig. 3.13 (b) shows the PC signal when beam 2 is delayed with beam1 fixed and beam 3 at a positive delay of ~ 3 ps. A double peak structure is observed and the two peaks have same width of ~ 170 fs. The ratio of the peaks is small (~ 15 - 20) compared to that obtained in the PC configuration (~ 250 - 300). This could be, probably, due to the misalignment or improper calibration of the setup. Also the signal recorded as a function of the delay of beam 2 did not show any decay.

3.4.3 PC signals recorded with cells of different thickness

Since there was some discrepancy with the results obtained in PC and boxcar configurations the PC signal is recorded with different cell thickness. (500 μ, 1-mm, and 2 mm). For all the configurations the variation in the widths of second peak (i.e width increasing in order for samples Erythrosin B, Black Ink, and CoTTP) is clear
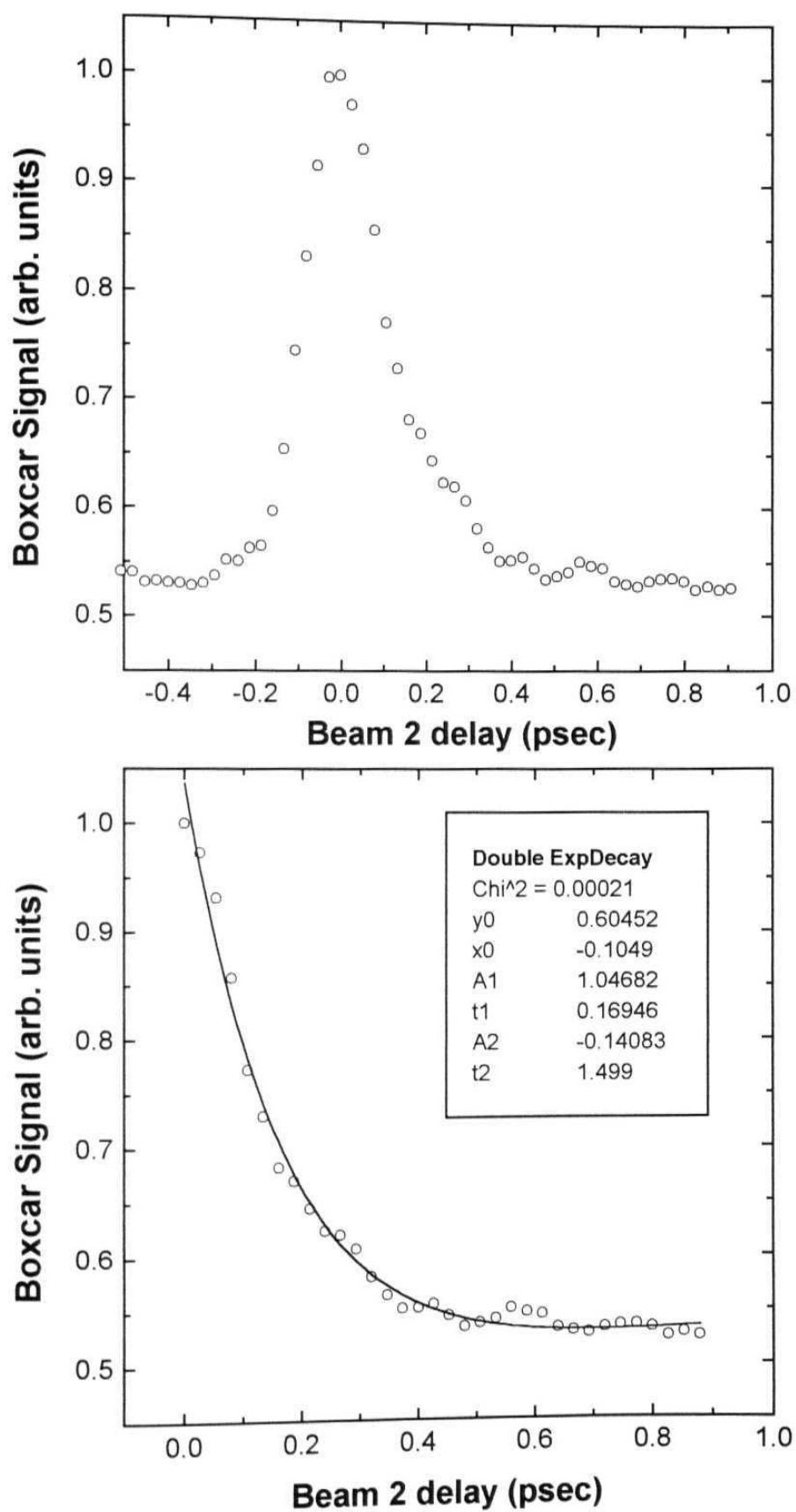
Fig. **3.12(a)** Boxcar signal obtained in the sample CS_2. (b) Double exponential
fit to the decay part yields two lifetimes of 0.16 psec and 1.499 psec.
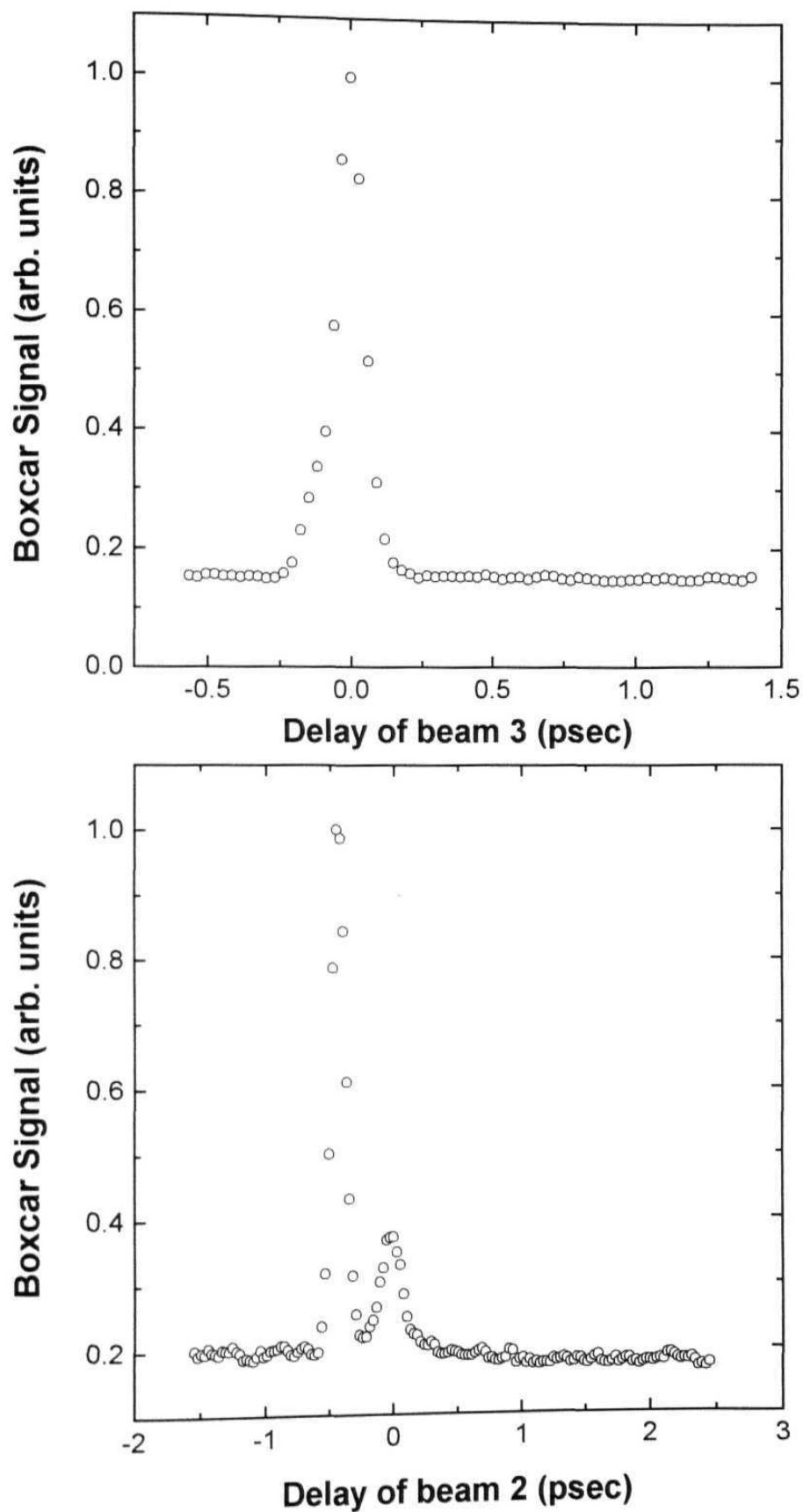
Fig. **3.13(a)** Boxcar signal in the sample CuTTP with beam 3 delayed and beams 1 and 2 at zero delay. (b) Beam 2 is delayed with beam 3 at δ = -0.5 psec and beam 1 at zero delay.

although the absolute numbers were different in each case. Figure 3.14 shows the variation clearly obtained using 500 um cell (the ratio of the peaks is not to scale). This could be explained as due to the interaction region of the interfering beams 1 and 3 in each case. It has been shown that for beams of diameter 2ω that intersect at an angle 6, the maximum sample thickness is determined by L < 2© / Sin (0) [36] which is 1.2 mm in our case. For the case of 500 μ cell the interaction region (~ 0.9 mm) is more the thickness of the cell [depicted in fig. 3.15 (a)] and for the case of 2 mm cell the interaction region is within the thickness of the cell [depicted in fig. 3.15 (c)]. The optimum thickness of the cell, with probe making an angle of ~ 10° with the forward pump, for completely including the interaction region within the cell is 1-mm [depicted in fig. 3.15 (b)] All the values for relaxation times quoted in this thesis are a result of the measurements with cells of 1-mm thickness.

3.5 Theoretical modeling of the line shapes observed in the experiments

Since the discovery of FWM for the use of ultra-fast measurements there have been several theoretical models developed for different samples, excited with different sources of light and under different experimental conditions [37-53]. Apart from the theoretical models proposed by Morita et al. [4], Kobayashi et al [10], and Okamoto et al. [11] there have been several other reports. Mi et al. [37] proposed multi-level theory of time-delayed DFWM with incoherent light in the absorption bands. Ulness et al. [38] calculated the analytic solution for Four Wave Mixing in Bloch two-level system with incoherent light having a Lorentzian spectral density. Tchenio et al. [39] reports the theory to interpret the power effects that occur during the resonant excitation of the sample by time-delayed, correlated, broadband laser pulses. Hartmann et al. [40] calculated the time-delayed FWM response of an inhomogenously broadened optical multilevel system. Vemuri et al. [41] considered the generation of FWM signals by an ensemble of two-level atoms interacting with broadband, correlated, pump and probe fields in the forward geometry. Alber et al. [42] calculated the theory of resonant DFWM with broadband lasers. Meacher et al. [43] looked at the steady-state theory of DFWM with incoherent light and calculated the intensity dependence and the saturation behavior of DFWM with pulsed lasers.
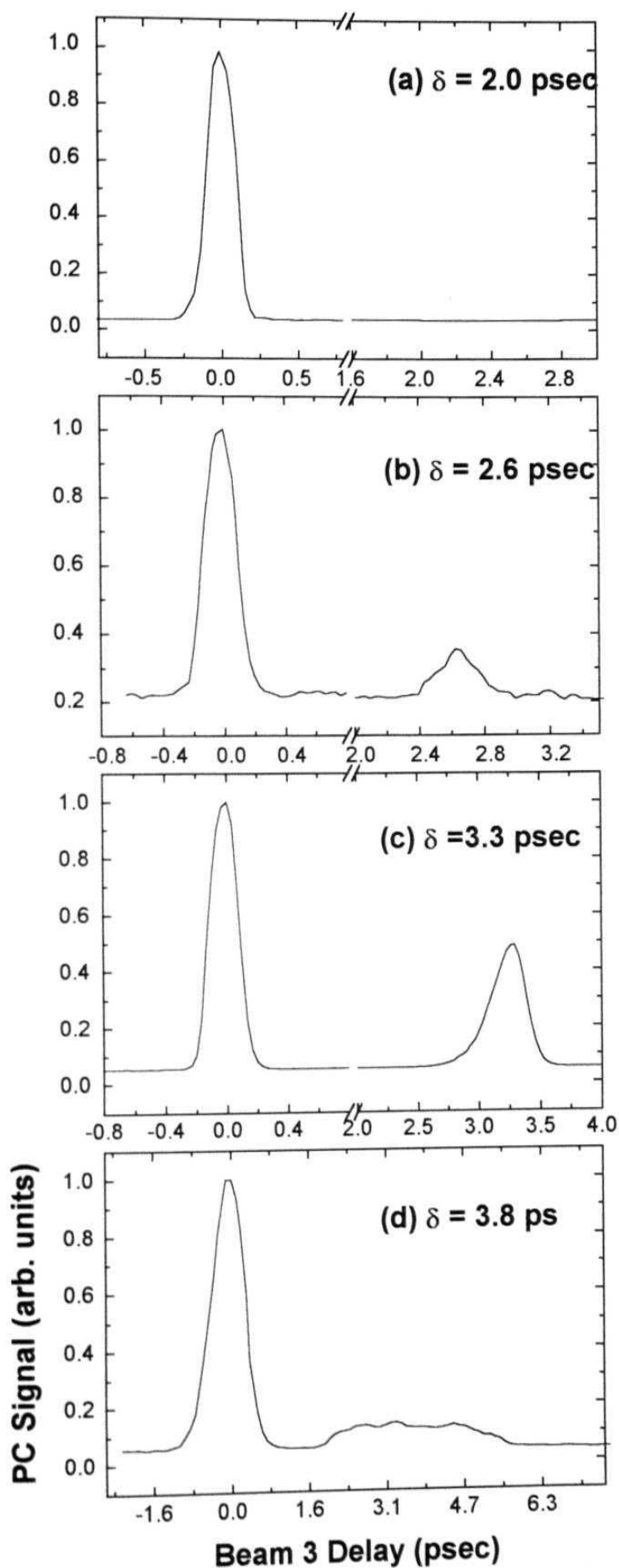
Fig. 3.14 Time - resolved PC signals in (a) RhB (Methanol) (b) ErythrosinB (Methanol) (c) Black Ink (Distilled Water) and (d) CoTTP (Chloroform) using 500 μ think cell. The ratios of the peaks are not to scale.
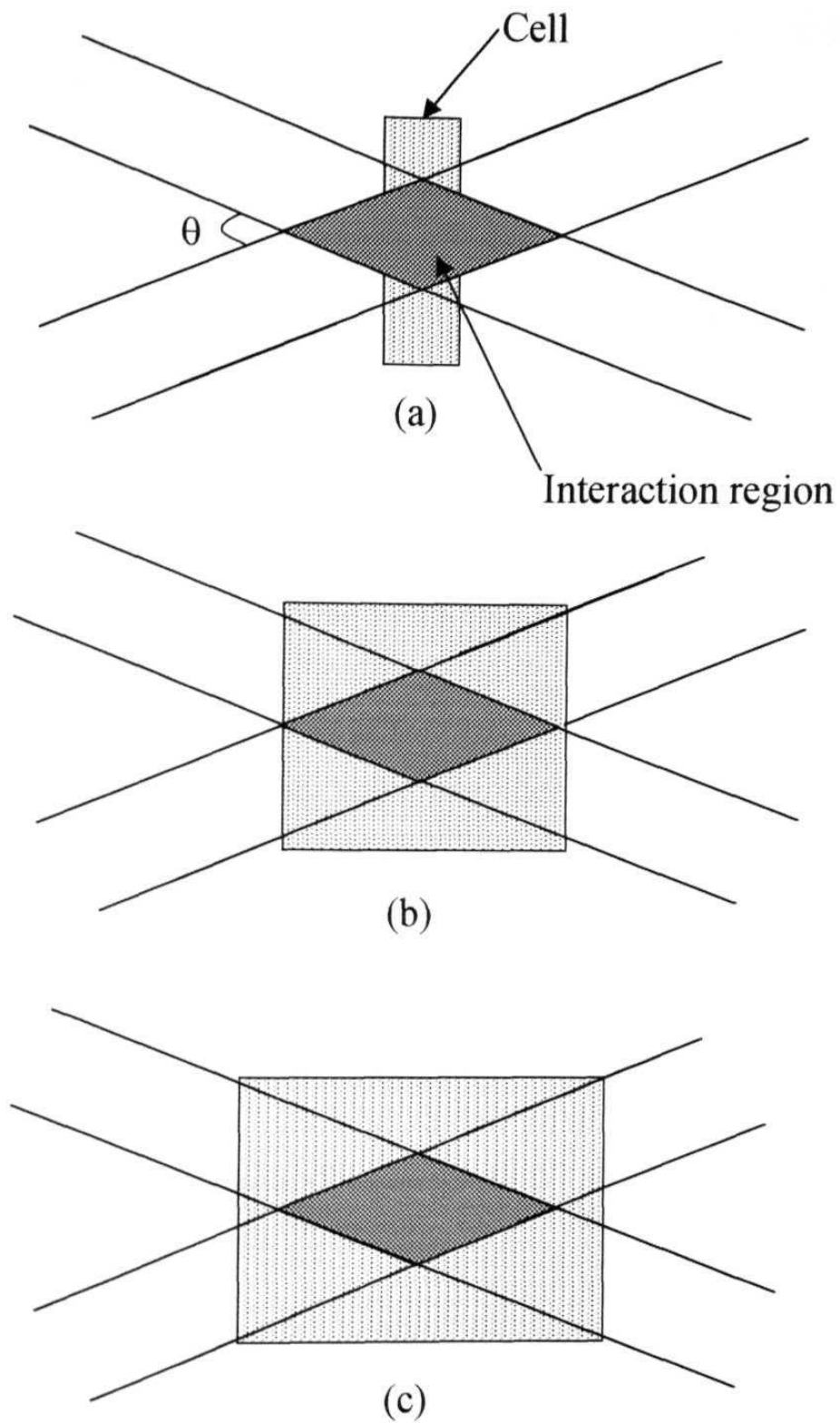
Fig. 3.15 Interaction region of the forward pump and probe beams inside the cell (a) $500\,\mu m$ (b) $1mm$ and (c) $2\,mm$ thickness. θ is the angle between the forward pump and the probe beams.

Abrams and Lind [44] have provided one of the landmarks in FWM theory in absorbing media.

Part of our results obtained could be successfully explained with Okamoto's theory (Ratio being related to the population relaxation time) but the observed large width of second peak could not be explained. We develop here, based on the energy level structure of a typical organic molecule, a homogeneously broadened four-level model, comprising of S_0, S_{10}, S_{1v}, S_n states. Figure 3.16 (a) shows the four-level model used for the theoretical simulations of the observed DFWM signal, in different samples, showing different widths for the second peak. S_i's denote the singlet states. γ_{43}, γ_{32}, γ_{21} denote the decay rates of the respective singlet states. ε_a, ε_b, and ε_c are the three degenerate fields with frequencies ω_a, ω_b, ω_c respectively. The total electric field is given by the expression:

$$\vec{E} = \varepsilon_a(t)\exp(i[\vec{k}_a.\vec{r} - \omega_a t]) + \varepsilon_b(t-\delta)\exp(i[\vec{k}_b.\vec{r} - \omega_b(t-\delta)])$$

$$+ \varepsilon_c(t-\tau)\exp(i[\vec{k}_c.\vec{r} - \omega_c(t-\tau)]) \tag{3.6}$$

$$\vec{E} = \tilde{\varepsilon}_a \exp(-i\omega_a t) + \tilde{\varepsilon}_b \exp(-i\omega_b(t-\delta)) + \varepsilon_c \exp(-i\omega_c(t-\tau))$$

where $\tilde{\varepsilon}_a = \varepsilon_a(t).\exp(i\vec{k}_a.\vec{r})$; $\tilde{\varepsilon}_b = \varepsilon_b(t-\delta).\exp(i\vec{k}_b.\vec{r})$ and

$$\tilde{\varepsilon}_c = \varepsilon_c(t-\tau).\exp(i\vec{k}_c.\vec{r}) \tag{3.7}$$

T is the delay of beam 3 (with respect to beam 1) and δ is the delay of beam 2 (with respect to beam 1)

The frequency separation between two energy levels E_j and E_k is defined as

$$\omega_{jk} = \frac{E_j - E_k}{\hbar} = \omega_j - \omega_k$$

The total Hamiltonian is given by $H_{OS} + H'$ where H' is the interaction Hamiltonian in the Schrodinger picture

$$H_{OS} = \sum_{i=1}^{4} E_i |i\rangle\langle i| \tag{38a}$$

$$H' = -\vec{d}.\vec{E} \tag{3.8b}$$

$$\vec{d} = \sum_i \sum_j |i\rangle\langle i|\vec{d}|j\rangle\langle j| = \sum_i \sum_j \vec{d}_{ij} |i\rangle\langle j| \tag{38c}$$
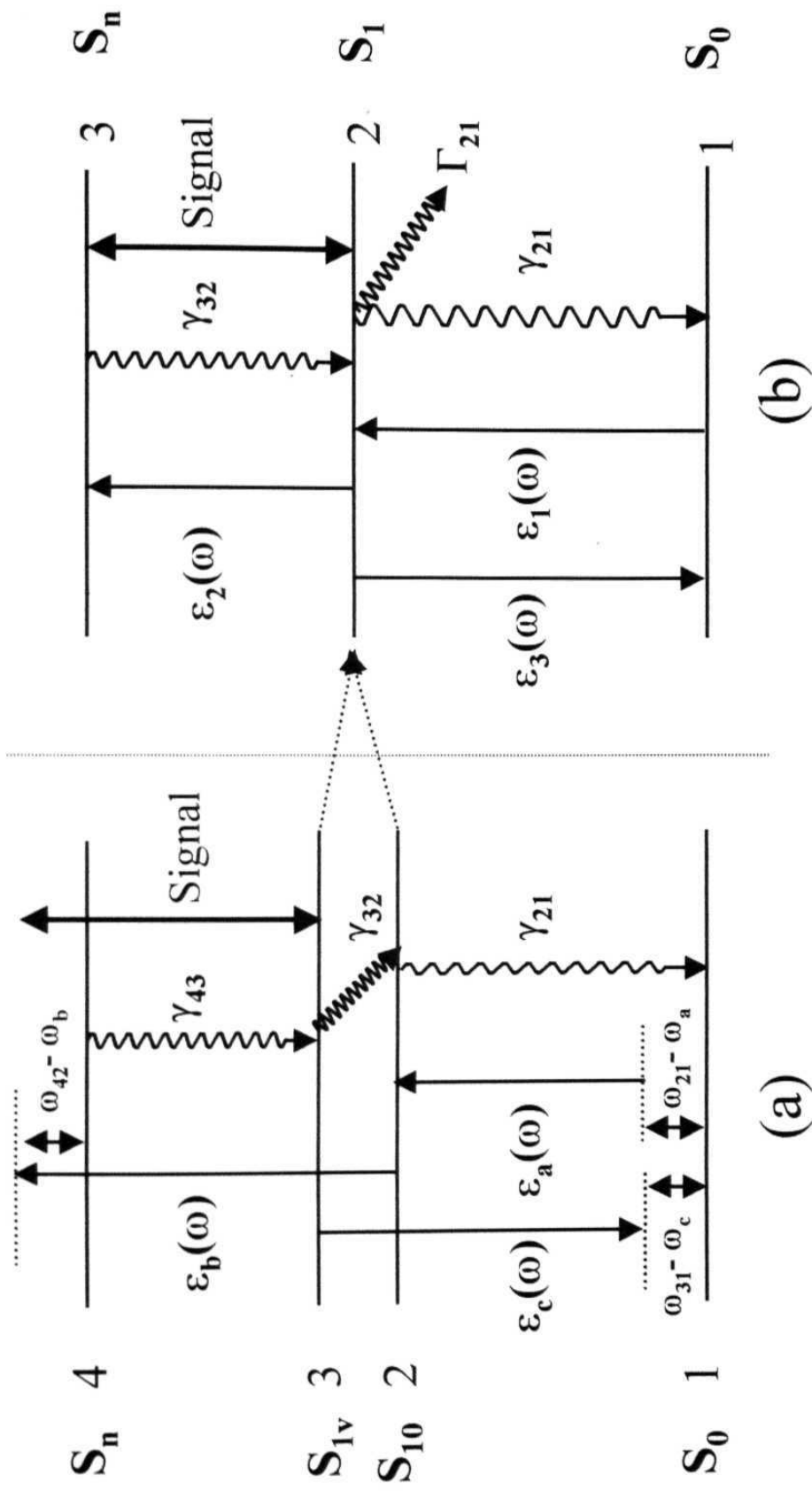
Fig. 3.16 (a) Four-level model for theoretical simulations. γ_{43} is the decay rate of level 4 to level 3, γ_{32} is the decay rate of level 3 to level 2, γ_{21} is decay rate of level 2 to level 1. $\varepsilon_1(\omega)$, $\varepsilon_2(\omega)$, and $\varepsilon_3(\omega)$ are three different fields at same frequency.**(b)** An effective three-level model when the separation between upper vibrational level S_{1v} and lower vibrational level S_{10} is small. Γ_{21} is the effective dephasing of the S_1 state.

where **d** is the dipole operator in the bare atom states basis. In the interaction picture the state vector and the operators transform as

$$|\alpha_I(t)\rangle = e^{\left(\frac{iH_{0S}t}{\hbar}\right)}|\alpha_S(t)\rangle$$

$$H_I(t) = e^{\left(\frac{iH_{0S}t}{\hbar}\right)} H_S\, e^{-\left(\frac{iH_{0S}t}{\hbar}\right)}$$

where the subscripts I and S denote Interaction and Schrodinger picture respectively. The Schrodinger equation in the interaction picture is

$$i\hbar\frac{d}{dt}|\alpha_I(t)\rangle = H_I^{'}|\alpha_I(t)\rangle$$

Taking the hermitian conjugate we get

$$-i\hbar\frac{d}{dt}\langle\alpha_I(t)| = \langle\alpha_I(t)|H_I^{'}$$

Combining the above equations we get

$$i\hbar\left(\frac{d}{dt}|\alpha_I(t)\rangle\langle\alpha_I(t)|\right) = H_I^{'}|\alpha_I(t)\rangle\langle\alpha_I(t)| - |\alpha_I(t)\rangle\langle\alpha_I(t)|H_I^{'} = \left[H_I^{'},\rho^I\right]$$

where $\rho^I = |\alpha_I(t)\rangle\langle\alpha_I(t)|$ which gives $i\hbar\frac{d}{dt}\rho^I = \left[H_I^{'},\rho^I\right]$

$$i\hbar\left(\frac{d}{dt}|\alpha_I(t)\rangle\right)\left(\langle\alpha_I(t)|\right) = H_I^{'}|\alpha_I(t)\rangle\langle\alpha_I(t)| \text{ and}$$

$$-i\hbar\left(|\alpha_I(t)\rangle\right)\left(\frac{d}{dt}|\alpha_I(t)\rangle\right) = -|\alpha_I(t)\rangle\langle\alpha_I(t)|H_I^{'}$$

Expanding operator d in terms of bare-atom eigenstates we get

$$\vec{d} = \sum_{i,j}\vec{d}_{ij}|i\rangle\langle j| \quad \text{where } \vec{d}_{ij} = \langle i|\vec{d}|j\rangle$$

$$= \vec{d}_{12}|1\rangle\langle 2| + \vec{d}_{13}|1\rangle\langle 3| + \vec{d}_{24}|2\rangle\langle 4| + \text{Hermitian Conjugate}$$

In the interaction picture we have

$$H_I'(t) = e^{\left(\frac{iH_{0S}t}{\hbar}\right)} (-\vec{d}_I^S . \vec{E}) \, e^{-\left(\frac{iH_{0S}T}{\hbar}\right)} = -\vec{d}^I . \vec{E}$$

$$\text{where } \vec{d}^I = e^{\left(\frac{iH_{0S}T}{\hbar}\right)} \vec{d}^S \, e^{-\left(\frac{iH_{0S}T}{\hbar}\right)}$$

on substituting for $\vec{d}^S$ from eqn. (3.8c) we get

$$\vec{d}^I = \sum_j \sum_k e^{\left(\frac{iH_{0S}t}{\hbar}\right)} |j\rangle\langle k| \, e^{-\left(\frac{iH_{0S}t}{\hbar}\right)}$$

$$= \sum_j \sum_k e^{\left(\frac{iE_j t}{\hbar}\right)} |j\rangle\langle k| \, e^{-\left(\frac{iE_k t}{\hbar}\right)}$$

$$= \sum_j \sum_k e^{\left(i\omega_{jk}t\right)} |j\rangle\langle k| \qquad (3.9)$$

$$\vec{d}^I = \vec{d}_{12}^S \exp(-i\omega_{21}t)|1\rangle\langle 2| + \vec{d}_{13}^S \exp(-i\omega_{31}t)|1\rangle\langle 3|$$

$$+ \vec{d}_{24}^S \exp(-i\omega_{42}t)|2\rangle\langle 4| + \text{Hermitian Conjugate}$$

where $\omega_{21} = \omega_2 - \omega_1$; $\omega_{31} = \omega_3 - \omega_1$; and $\omega_{42} = \omega_4 - \omega_2$

$$H_1' = -\vec{d}^I . \vec{E} = -d^I \{\varepsilon_a(t)\exp(i[k_a r - \omega_a(t-\tau)])$$

$$+ \varepsilon_b(t-\delta)\exp(i[k_b r - \omega_b(t-\delta)])$$

$$+ \varepsilon_c(t-\tau)\exp(i[k_c r - \omega_c(t)]) + c.c\}$$

In Rotating Wave Approximation (RWA), we obtain the interaction Hamiltonian as

$$H_1' = -d_{12}^S \exp(-i\omega_{21}t) \, [\tilde{\varepsilon}_a^* \exp(i\omega_a(t))]|1\rangle\langle 2|$$

$$- d_{21}^S \exp(i\omega_{21}t) \, [\tilde{\varepsilon}_a \exp(i\omega_a(t))]|2\rangle\langle 1|$$

$$- d_{13}^S \exp(-i\omega_{31}t) \, [\tilde{\varepsilon}_c^* \exp(i\omega_c(t-\tau))]|1\rangle\langle 3|$$

$$- d_{31}^S \exp(i\omega_{31}t) \, [\tilde{\varepsilon}_c \exp(i\omega_c(t-\tau))]|3\rangle\langle 1|$$

$$- d_{24}^S \exp(-i\omega_{42}t) \, [\tilde{\varepsilon}_b^* \exp(i\omega_b(t-\delta))]|2\rangle\langle 4|$$

$$- d_{42}^S \exp(i\omega_{42}t) \, [\tilde{\varepsilon}_b \exp(i\omega_b(t-\delta))]|4\rangle\langle 2| \qquad (3.10)$$

Dropping subscript V in the following

$$i\hbar \frac{d}{dt}\rho = \left[H_I^{'}, \rho\right]$$

$$i\hbar \frac{d}{dt}\langle k|\rho|l\rangle = \langle k|[H_I^{'},\rho]|l\rangle \text{ gives } i\hbar \frac{d}{dt}\rho_{kl} = \langle k|H_I^{'}\rho^I|l\rangle - \langle l|\rho^I H_I^{'}|k\rangle$$

$$\frac{d}{dt}\langle k|\rho|l\rangle = \frac{i}{\hbar}\langle k|(d^I.E)\rho|l\rangle - \frac{i}{\hbar}\langle k|\rho(d^I.E)|l\rangle$$

Writing down the equations for density matrix elements, we have

$$i\hbar \dot{\rho}_{12} = \langle 1|H_I^{'}\rho^I|2\rangle - \langle 2|\rho^I H_I^{'}|1\rangle$$

$$\frac{d}{dt}\rho_{12} = \frac{i}{\hbar}d_{12}^S\tilde{\varepsilon}_a^* \exp(-i\omega_{21}t)\exp(i\omega_a(t))\langle 2|\rho|2\rangle$$

$$+ \frac{i}{\hbar}d_{13}^S\tilde{\varepsilon}_c^* \exp(-i\omega_{13}t)\exp(i\omega_c(t-\tau))\langle 1|\rho|3\rangle$$

$$- \frac{i}{\hbar}d_{12}^S\tilde{\varepsilon}_a^* \exp(-i\omega_{21}t)\exp(i\omega_a(t))\langle 1|\rho|1\rangle$$

$$- \frac{i}{\hbar}d_{42}^S\tilde{\varepsilon}_b \exp(i\omega_{42}t)\exp(-i\omega_b(t-\delta))\langle 2|\rho|4\rangle \qquad (3.11)$$

$$\dot{\rho}_{12} = \frac{i}{\hbar}\{d_{21}^S\tilde{\varepsilon}_a^* \exp(-i\omega_{21}t)\exp(i\omega_a(t))(\rho_{22}-\rho_{11})$$

$$+ d_{13}^S\tilde{\varepsilon}_c^* \exp(-i\omega_{31}(t-\tau))\exp(i\omega_c t))\rho_{32}$$

$$- d_{42}^S\tilde{\varepsilon}_b \exp(i\omega_{42}t)\exp(-i\omega_b(t-\delta))\rho_{32}\} - \Gamma_{12}\rho_{12} \qquad (3.12)$$

$$\dot{\rho}_{13} = \frac{i}{\hbar}\{d_{13}^S\tilde{\varepsilon}_c^* \exp(-i\omega_{31}t)\exp(i\omega_c(t-\tau))(\rho_{33}-\rho_{11})$$

$$- d_{12}^S\tilde{\varepsilon}_a^* \exp(-i\omega_{21}t)\exp(i\omega_a(t))\rho_{23}\} - \Gamma_{13}\rho_{13}$$

$$\dot{\rho}_{24} = \frac{i}{\hbar}\{d_{24}^S\tilde{\varepsilon}_b^* \exp(-i\omega_{42}t)\exp(i\omega_b(t-\delta))(\rho_{44}-\rho_{22})$$

$$- d_{21}^S\tilde{\varepsilon}_a \exp(i\omega_{21}t)\exp(-i\omega_a(t))\rho_{23}\} - \Gamma_{24}\rho_{24} \qquad (3.13)$$

$$\dot{\rho}_{34} = \frac{i}{\hbar}\{d_{31}^S\tilde{\varepsilon}_c \exp(i\omega_{31}t)\exp(-i\omega_c(t-\tau))(\rho_{14})$$

$$- d_{24}^S\tilde{\varepsilon}_b^* \exp(-i\omega_{42}t)\exp(i\omega_b(t-\delta))\rho_{32}\} - \Gamma_{34}\rho_{34} \qquad (3.14)$$

$$\dot{\rho}_{32} = \frac{i}{\hbar}\{d_{31}^S\tilde{\varepsilon}_c \exp(i\omega_{31}t)\exp(-i\omega_c(t-\tau)))(\rho_{12})$$

$$-d_{12}^S\tilde{\varepsilon}_a^* \exp(-i\omega_{21}t)\exp(i\omega_a(t))(\rho_{31})$$

$$-d_{42}^S\tilde{\varepsilon}_b \exp(i\omega_{42}t)\exp(-i\omega_b(t-\delta))\rho_{34}\} - \Gamma_{23}\rho_{32} \tag{3.15}$$

$$\dot{\rho}_{14} = \frac{i}{\hbar}\{d_{13}^S\tilde{\varepsilon}_c^* \exp(-i\omega_{31}t)\exp(i\omega_c(t-\tau))(\rho_{34})$$

$$+d_{12}^S\tilde{\varepsilon}_a^* \exp(-i\omega_{21}t)\exp(i\omega_a(t))(\rho_{24})$$

$$-d_{24}^S\tilde{\varepsilon}_b^* \exp(-i\omega_{42}t)\exp(i\omega_b(t-\delta))\rho_{12}\} - \Gamma_{14}\rho_{14} \tag{3.16}$$

Performing the perturbation expansion in fields ε_a, ε_b, and ε_c and equating terms with same coefficients, we obtain the solutions for the third order density matrix elements.

$$\dot{\rho}_{12}^{(1)}(\tilde{\varepsilon}_a^*) = \frac{i}{\hbar}d_{12}^S\tilde{\varepsilon}_a^* \exp(-i\omega_{21}t)\exp(i\omega_a(t))(\rho_{22}^{(0)} - \rho_{11}^{(0)}) - \Gamma_{12}\rho_{12}^{(1)}(\tilde{\varepsilon}_a^*)$$

$$\dot{\rho}_{13}^{(1)}(\tilde{\varepsilon}_c^*) = \frac{i}{\hbar}d_{13}^S\tilde{\varepsilon}_c^* \exp(-i\omega_{31}t)\exp(i\omega_c(t-\tau))(\rho_{33}^{(0)} - \rho_{11}^{(0)}) - \Gamma_{13}\rho_{13}^{(1)}(\tilde{\varepsilon}_c^*)$$

$$\dot{\rho}_{24}^{(1)}(\tilde{\varepsilon}_b^*) = \frac{i}{\hbar}d_{24}^S\tilde{\varepsilon}_b^* \exp(-i\omega_{42}t)\exp(i\omega_b(t-\delta))(\rho_{44}^{(0)} - \rho_{22}^{(0)}) - \Gamma_{24}\rho_{24}^{(1)}(\tilde{\varepsilon}_b^*)$$

$$\dot{\rho}_{32}^{(2)}(\tilde{\varepsilon}_a^*, \tilde{\varepsilon}_c) = \frac{i}{\hbar}d_{31}^S\tilde{\varepsilon}_c \exp(i\omega_{31}t)\exp(-i\omega_c(t-\tau))[\rho_{12}^{(1)}(\tilde{\varepsilon}_a^*)]$$

$$-\frac{i}{\hbar}d_{12}^S\tilde{\varepsilon}_a^* \exp(-i\omega_{21}t)\exp(i\omega_a(t))[\rho_{31}^{(1)}(\tilde{\varepsilon}_a^*)]$$

$$-\Gamma_{23}\rho_{32}^{(2)}(\tilde{\varepsilon}_a^*, \tilde{\varepsilon}_c)$$

$$\dot{\rho}_{14}^{(2)}(\tilde{\varepsilon}_a^*, \tilde{\varepsilon}_b^*) = \frac{i}{\hbar}d_{12}^S\tilde{\varepsilon}_a^* \exp(-i\omega_{21}t)\exp(i\omega_a(t))[\rho_{24}^{(1)}(\tilde{\varepsilon}_b^*)]$$

$$-\frac{i}{\hbar}d_{24}^S\tilde{\varepsilon}_b^* \exp(-i\omega_{42}t)\exp(i\omega_b(t-\delta))[\rho_{12}^{(1)}(\tilde{\varepsilon}_a^*)]$$

$$-\Gamma_{14}\rho_{14}^{(2)}(\tilde{\varepsilon}_a^*, \tilde{\varepsilon}_b^*)$$

$$\dot{\rho}_{34}^{(3)}(\tilde{\varepsilon}_a^*, \tilde{\varepsilon}_b^*, \tilde{\varepsilon}_c) = \frac{i}{\hbar}d_{31}^S\tilde{\varepsilon}_c \exp(i\omega_{31}t)\exp(-i\omega_c(t-\tau))[\rho_{14}^{(2)}(\tilde{\varepsilon}_a^*, \tilde{\varepsilon}_b^*)]$$

$$-\frac{i}{\hbar}d_{24}^S\tilde{\varepsilon}_b^* \exp(-i\omega_{42}t)\exp(i\omega_b(t-\delta))[\rho_{32}^{(2)}(\tilde{\varepsilon}_a^*, \tilde{\varepsilon}_c)]$$

$$-\Gamma_{32}\rho_{34}^{(3)}(\tilde{\varepsilon}_a^*, \tilde{\varepsilon}_b^*, \tilde{\varepsilon}_c) \tag{3.17}$$

Applying transformations as mentioned below, we obtain

$$\rho_{12}^{(1)} = \hat{\rho}_{12}^{(1)} \exp(-i\omega_{21}t)\exp(i\omega_a(t))$$

$$\rho_{13}^{(1)} = \hat{\rho}_{13}^{(1)} \exp(-i\omega_{31}t)\exp(i\omega_c(t-\tau))$$

$$\rho_{24}^{(1)} = \hat{\rho}_{24}^{(1)} \exp(-i\omega_{24}t)\exp(i\omega_b(t-\delta))$$

$$\frac{\partial}{\partial t}\hat{\rho}_{12}^{(1)}(\tilde{\varepsilon}_a^*) = -[\Gamma_{12} - i(\omega_{21}-\omega_a)]\hat{\rho}_{12}^{(1)}(\tilde{\varepsilon}_a^*) + \frac{i}{\hbar}d_{12}^S\tilde{\varepsilon}_a^*(\rho_{22}^0 - \rho_{11}^0)$$

$$\frac{\partial}{\partial t}\hat{\rho}_{13}^{(1)}(\tilde{\varepsilon}_c^*) = -[\Gamma_{13} - i(\omega_{31}-\omega_c)]\hat{\rho}_{13}^{(1)}(\tilde{\varepsilon}_c^*) + \frac{i}{\hbar}d_{13}^S\tilde{\varepsilon}_c^*(\rho_{33}^0 - \rho_{11}^0)$$

$$\frac{\partial}{\partial t}\hat{\rho}_{24}^{(1)}(\tilde{\varepsilon}_b^*) = -[\Gamma_{24} - i(\omega_{42}-\omega_b)]\hat{\rho}_{24}^{(1)}(\tilde{\varepsilon}_b^*) + \frac{i}{\hbar}d_{24}^S\tilde{\varepsilon}_b^*(\rho_{44}^0 - \rho_{22}^0)$$

$$\rho_{32}^{(2)} = \hat{\rho}_{32}^{(2)} \exp(i\omega_{31}t)\exp(-i\omega_c(t-\tau))\exp(-i\omega_{21}t)\exp(i\omega_a(t))$$

$$\rho_{14}^{(2)} = \hat{\rho}_{14}^{(2)} \exp(-i\omega_{42}t)\exp(-i\omega_a(t))\exp(-i\omega_{21}t)\exp(i\omega_b(t-\delta))$$

$$\rho_{34}^{(2)} = \hat{\rho}_{34}^{(2)} \exp(-i\omega_{42}t)\exp(i\omega_b(t-\delta))\exp(i\omega_{31}t)$$

$$* \exp(-i\omega_c(t-\tau))\exp(i\omega_a(t))\exp(-i\omega_{21}t)$$

$$\frac{\partial}{\partial t}\hat{\rho}_{32}^{(2)}(\tilde{\varepsilon}_a^*,\tilde{\varepsilon}_c) = -[\Gamma_{23} - i(\omega_{31}-\omega_c-\omega_{21}+\omega_a)]\hat{\rho}_{32}^{(2)}(\tilde{\varepsilon}_a^*,\tilde{\varepsilon}_c)$$

$$+\frac{i}{\hbar}d_{31}^S\tilde{\varepsilon}_c[\rho_{12}^{(1)}(\tilde{\varepsilon}_a^*)] - \frac{i}{\hbar}d_{12}^S\tilde{\varepsilon}_a^*[\rho_{31}^{(1)}(\tilde{\varepsilon}_c)]$$

$$\frac{\partial}{\partial t}\hat{\rho}_{14}^{(2)}(\tilde{\varepsilon}_a^*,\tilde{\varepsilon}_b^*) = -[\Gamma_{14} - i(\omega_{42}-\omega_b+\omega_{21}-\omega_a)]\hat{\rho}_{14}^{(2)}(\tilde{\varepsilon}_a^*,\tilde{\varepsilon}_b^*)$$

$$-\frac{i}{\hbar}d_{24}^S\tilde{\varepsilon}_b^*[\rho_{12}^{(1)}(\tilde{\varepsilon}_a^*)] + \frac{i}{\hbar}d_{12}^S\tilde{\varepsilon}_a^*[\rho_{24}^{(1)}(\tilde{\varepsilon}_b^*)]$$

$$\frac{\partial}{\partial t}\hat{\rho}_{34}^{(3)}(\tilde{\varepsilon}_a^*,\tilde{\varepsilon}_b^*,\tilde{\varepsilon}_c) = -[\Gamma_{34} - i(\omega_{42}-\omega_b-\omega_{31}+\omega_c+\omega_{21}-\omega_a)]$$

$$* \hat{\rho}_{14}^{(2)}(\tilde{\varepsilon}_a^*,\tilde{\varepsilon}_b^*,\tilde{\varepsilon}_c) + \frac{i}{\hbar}d_{31}^S\tilde{\varepsilon}_c[\rho_{14}^{(2)}(\tilde{\varepsilon}_a^*,\tilde{\varepsilon}_b^*)]$$

$$-\frac{i}{\hbar}d_{24}^S\tilde{\varepsilon}_b^*[\rho_{32}^{(2)}(\tilde{\varepsilon}_a^*,\tilde{\varepsilon}_c)] \tag{3.18}$$

To find the solution of a differential equation of the form

$$\frac{d}{dt}f(t) = -\lambda f(t) + g(t)$$

$$f(t_2) = \int_{-\infty}^{t_2} dt_1 \exp[-\lambda(t-t_2)]g(t_2)$$

$$\hat{\rho}_{12}^{(1)} = \int_{-\infty}^{t} dt' \exp-[\Gamma_{12} - i(\omega_{21} - \omega_a)](t - t') \frac{i}{\hbar} d_{12}^{S} \exp(-i\vec{k}_a.\vec{r})$$

$$* \varepsilon_a^{*}(t'-\tau)(\rho_{22}^{0} - \rho_{11}^{0})$$

Initial condition is

$$\rho_{1}^{(0)} = \text{Cons}\tan t = N_0 \,(\text{Concentration})$$

$$\rho_{22}^{(0)} = \rho_{33}^{(0)} = \rho_{22}^{(0)} = 0$$

Thus, we get

$$\hat{\rho}_{12}^{(1)}(t') = -N_0 \frac{i}{\hbar} d_{12}^{S} \exp(-i\vec{k}_a.\vec{r}) \{ \int_{-\infty}^{t'} dt'' \exp-[\Gamma_{12} - i(\omega_{21} - \omega_a)](t'-t'') * \varepsilon_a^{*}(t'') \}$$

$$\hat{\rho}_{13}^{(1)}(t') = -N_0 \frac{i}{\hbar} d_{13}^{S} \exp(-i\vec{k}_c.\vec{r}) \{ \int_{-\infty}^{t'} dt'' \exp-[\Gamma_{13} - i(\omega_{31} - \omega_c)](t'-t'') * \varepsilon_c^{*}(t''-\tau) \}$$

$$\hat{\rho}_{24}^{(1)}(t') = 0$$

$$\hat{\rho}_{32}^{(1)}(t) = \int_{-\infty}^{t'} dt' \exp-[\Gamma_{23} + i(\omega_{31} - \omega_c - \omega_{21} + \omega_a)](t - t')$$

$$\{ \frac{i}{\hbar} d_{31}^{S} \exp(i\vec{k}_c.\vec{r}) \varepsilon_c(t'-\tau) \hat{\rho}_{12}^{(1)}(t') - \frac{i}{\hbar} d_{12}^{S} \exp(-i\vec{k}_a.\vec{r}) \varepsilon_a(t') \hat{\rho}_{31}^{(1)}(t') \}$$

$$\hat{\rho}_{32}^{(2)}(t) = \int_{-\infty}^{t'} dt' \exp-[\Gamma_{23} + i(\omega_{31} - \omega_c - \omega_{21} + \omega_a)(t - t')]$$

$$\{ \frac{i}{\hbar} d_{31}^{S} \exp(i\vec{k}_c.\vec{r}) \varepsilon_c(t'-\tau) * [-N_0 \frac{i}{\hbar} d_{12}^{S} \exp(-i\vec{k}_a.\vec{r}) *$$

$$\{ \int_{-\infty}^{t'} dt'' \exp-[\Gamma_{12} - i(\omega_{21} - \omega_a)(t'-t'')] * \varepsilon_a^{*}(t'') \}]$$

$$- \frac{i}{\hbar} d_{12}^{S} \exp(-i\vec{k}_a.\vec{r}) \varepsilon_a(t'-\tau) * [-N_0 \frac{i}{\hbar} d_{13}^{S} \exp(-i\vec{k}_c.\vec{r}) *$$

$$\{ \int_{-\infty}^{t'} dt'' \exp-[\Gamma_{13} - i(\omega_{31} - \omega_c)(t'-t'')] * \varepsilon_c^{*}(t''-\tau) \}] \}$$

Substituting $t = t_3$, $t' = t_2$, and $t'' = t_1$ we get

$$\hat{\rho}_{32}^{(2)}(t_3) = \frac{N_0}{\hbar^2} d_{12}^S d_{13}^S \exp[i(\vec{k}_c - \vec{k}_a).\vec{r}]*$$

$$\int_{-\infty}^{t_3} dt_2 \exp-[\Gamma_{23} + i(\omega_{31} - \omega_c - \omega_{21} + \omega_a)(t_3 - t_2)]*$$

$$\{\int_{-\infty}^{t_2} dt_1 \exp-[\Gamma_{12} - i(\omega_{21} - \omega_a)(t_2 - t_1)]\varepsilon_c(t_2 - \tau)\varepsilon_a^*(t_1) +$$

$$\int_{-\infty}^{t_2} dt_1 \exp-[\Gamma_{12} - i(\omega_{31} - \omega_c)(t_2 - t_1)]\varepsilon_c(t_1 - \tau)\varepsilon_a^*(t_2)\}$$

$$\hat{\rho}_{14}^{(2)}(t_3) = -\frac{N_0}{\hbar^2} d_{12}^S d_{13}^S \exp[i(\vec{k}_a + \vec{k}_b).\vec{r}]*$$

$$\int_{-\infty}^{t_3} dt_2 \exp-[\Gamma_{23} + i(\omega_{42} - \omega_b + \omega_{21} - \omega_a)(t_3 - t_2)]*$$

$$\{\int_{-\infty}^{t_2} dt_1 \exp-[\Gamma_{12} - i(\omega_{21} - \omega_a)(t_2 - t_1)]\varepsilon_b^*(t_2 - \delta)\varepsilon_a^*(t_1)\}$$

$$\hat{\rho}_{34}^{(3)}(t) = \int_{-\infty}^{t} dt_3 \exp-\{\Gamma_{34} - i[(\omega_{42} - \omega_b) - (\omega_{31} - \omega_c)$$

$$+ (\omega_{21} + \omega_a](t - t_3)]\} * \{\frac{i}{\hbar} d_{31}^S \exp(i\vec{k}_c.\vec{r})\varepsilon_c(t_3 - \tau)\hat{\rho}_{14}^{(2)}(t_3)$$

$$- \frac{i}{\hbar} d_{24}^S \exp(-i\vec{k}_b.\vec{r})\varepsilon_b^*(t_3 - \delta)\hat{\rho}_{32}^{(2)}(t_3)\}$$

(3.19)

$$\hat{\rho}_{34}^{(3)}(t) = B * \int_{-\infty}^{t} dt_3 \exp-\{\Gamma_{34} - i[(\omega_{42} - \omega_b) - (\omega_{31} - \omega_c) + (\omega_{21} - \omega_a](t - t_3)]\}*$$

$$\{\int_{-\infty}^{t_3} dt_2 \exp-[\Gamma_{14} - i(\omega_{42} - \omega_b + \omega_{21} - \omega_a)(t_3 - t_2)]*$$

$$\int_{-\infty}^{t_2} dt_1 \{\exp-[\Gamma_{12} - i(\omega_{21} - \omega_a)(t_2 - t_1)]\varepsilon_c(t_3 - \tau)\varepsilon_b^*(t_2 - \delta)\varepsilon_a^*(t_1) +$$

$$\int_{-\infty}^{t_3} dt_2 \exp-[\Gamma_{23} - i\{(\omega_{31} - \omega_c) - (\omega_{21} - \omega_a)\}(t_3 - t_2)]$$

$$\int_{-\infty}^{t_2} dt_1 \{\exp-[\Gamma_{12} - i(\omega_{21} - \omega_a)(t_2 - t_1)]\varepsilon_c(t_2 - \tau)\varepsilon_b^*(t_3 - \delta)\varepsilon_a^*(t_1) +$$

$$\exp-[\Gamma_{12} + i(\omega_{31} - \omega_c)(t_2 - t_1)]\varepsilon_c(t_1 - \tau)\varepsilon_b^*(t_3 - \delta)\varepsilon_a^*(t_2)\}\} \tag{3.20}$$

If the electronic dephasing times, $(\Gamma_{12})^{-1}$ and $(\Gamma_{34})^{-1}$ (single photon coherence decays), are assumed to be very fast and the field detunings are zero (ε_a, ε_b, and ε_c are tuned close to resonance frequency) then the integrals involving Γ_{12} and Γ_{34} can be evaluated in the steady state by pulling the field amplitudes ε_a and ε_b out of the integral. The first peak observed in the signal is due to two-photon coherence created in the S_n states and hence we retain the Γ_{14} integral. By substituting $t_3 = t$ and $t_1 = t_2$ in the equation (3.20) we obtain

$$\hat{\rho}_{34}^{(3)}(t) = C * \int_{-\infty}^{t} dt_2 \{\exp-\{\Gamma_{14} - i[(\omega_{42} - \omega_b) + (\omega_{21} - \omega_a)](t - t_2)\}*$$

$$\varepsilon_c(t - \tau)\varepsilon_b^*(t_2 - \delta)\varepsilon_a^*(t_2) + \{\exp-[\Gamma_{23} + i\{(\omega_{31} - \omega_c) - (\omega_{21} - \omega_a)\}(t - t_2)]$$

$$[\varepsilon_c(t_2 - \tau)\varepsilon_b^*(t - \delta)\varepsilon_a^*(t_2) + \varepsilon_c(t_2 - \tau)\varepsilon_b^*(t - \delta)\varepsilon_a^*(t_2)]\}\}$$

$$\hat{\rho}_{34}^{(3)}(t) = C * \int_{-\infty}^{t} dt_2 \{\exp-\{\Gamma_{14} - i[(\Delta_{42} + \Delta_{21})](t - t_2)\}*$$

$$\varepsilon_c(t - \tau)\varepsilon_b^*(t_2 - \delta)\varepsilon_a^*(t_2) + \{\exp-[\Gamma_{23} + i\{(\omega_{31} - \omega_c)$$

$$-(\omega_{21} - \omega_a)\}(t - t_2)]*2[\varepsilon_c(t_2 - \tau)\varepsilon_b^*(t - \delta)\varepsilon_a^*(t_2)]\}\} \tag{3.21}$$

$$\hat{\rho}_{43}^{(3)}(t) = C^* * \int_{-\infty}^{t} ds_2 \{\exp-\{\Gamma_{14} + i[\Delta_{42} + \Delta_{21}](t - s_2)\}*$$

$$[\varepsilon_c^*(t - \tau)\varepsilon_b(s_2 - \delta)\varepsilon_a(s_2)] + 2\{\exp-[\Gamma_{23} - i\{\Delta_{31} - \Delta_{21}\}(t - s_2)]$$

$$*[\varepsilon_c^*(s_2 - \tau)\varepsilon_b(t - \delta)\varepsilon_a(s_2)]\}\} \tag{3.22}$$

where $\Delta_{42} = \omega_{42} - \omega_b; \Delta_{31} = \omega_{31} - \omega_c; \Delta_{21} = \omega_{21} - \omega_a$

From equation (3.22) we obtain

$$\left\langle \hat{\rho}_{43}^{(3)}(t) . \hat{\rho}_{34}^{(3)}(t) \right\rangle = |C|^2 \int\limits_{-\infty}^{t} dt_2 \int\limits_{-\infty}^{t} ds_2$$

$$([\{\exp- \{\Gamma_{14} + i[\Delta_{42} + \Delta_{21}](t - t_2)\} \{\exp- \{\Gamma_{14} - i[\Delta_{42} + \Delta_{21}](t - s_2)\}$$

$$\left\langle \varepsilon_c^*(t - \tau)\varepsilon_b(s_2 - \delta)\varepsilon_a(s_2)\varepsilon_c(t - \tau)\varepsilon_b^*(t_2 - \delta)\varepsilon_a^*(t_2) \right\rangle]$$

$$[2 * \{\exp- \{\Gamma_{14} + i[\Delta_{42} + \Delta_{21}](t - t_2)\} \{\exp- \{\Gamma_{23} - i[\Delta_{31} - \Delta_{21}](t - s_2)\}$$

$$\left\langle \varepsilon_c(t - \tau)\varepsilon_b^*(t_2 - \delta)\varepsilon_a^*(t_2)\varepsilon_c^*(s_2 - \tau)\varepsilon_b(t - \delta)\varepsilon_a(s_2) \right\rangle]$$

$$[2 * \{\exp- \{\Gamma_{23} - i[\Delta_{31} - \Delta_{21}](t - t_2)\} \{\exp- \{\Gamma_{14} + i[\Delta_{42} + \Delta_{21}](t - s_2)\}$$

$$\left\langle \varepsilon_c(t_2 - \tau)\varepsilon_b^*(t - \delta)\varepsilon_a^*(t_2)\varepsilon_c^*(t - \tau)\varepsilon_b(s_2 - \delta)\varepsilon_a(s_2) \right\rangle]$$

$$[4 * \{\exp- \{\Gamma_{23} - i[\Delta_{31} - \Delta_{21}](t - t_2)\} \{\exp- \{\Gamma_{23} - i[\Delta_{31} - \Delta_{21}](t - t_2)\}$$

$$\left\langle \varepsilon_c(t_2 - \tau)\varepsilon_b^*(t - \delta)\varepsilon_a^*(t_2)\varepsilon_c^*(s_2 - \tau)\varepsilon_b(t - \delta)\varepsilon_a(s_2) \right\rangle]) \qquad (3.23)$$

Since the fields used are incoherent the amplitude function is expressed as a product of a slowly varying regular pulse envelope function and a complex random modulation function. Expanding the above expression, we obtain the sixth-order moments of the random modulation function. If the modulation obeys a Gaussian process, the sixth-order moments are factorized into second-order moments, which satisfy the following relations

$$< R(t)R^*(s) > = f(t - s)$$
$$< R(t)R(s) > = < R(t)R(s) > = 0$$

where R(t) is the random modulation function, $f(t)$ is the correlation function for the stochastic process.

The total signal intensity, then, is given by $J(\tau, \delta)$ which is proportional to

$$J(\tau, \delta) \propto \left\langle \hat{\rho}_{34}^{(3)}(t) \hat{\rho}_{43}^{(3)}(t) \right\rangle \qquad (3.24)$$

since $\hat{\rho}_{34}^{(3)*}(t) = \hat{\rho}_{43}^{(3)}(t)$

$$J(\tau,\delta) \propto \int\limits_0^\infty dx \int\limits_0^\infty dy \{ e^{-\Gamma_{14}(x+y)} \, [f(0)f(x-y)f(x-y) + f(x+\tau-\delta)$$

$$f(x-y-\delta)f(-y+\tau) + f(x-\tau)f(x-y)f(-y+\tau) + f(0)f(x-y$$

$$-\delta)f(x-y+\delta) + f(x-\tau)f(-y+\tau-\delta)f(x-y+\delta) + f(x+\delta-\tau)$$

$$f(-y+\tau-\delta)f(x-y)] + 2e^{-\Gamma_{14}x-\Gamma_{23}y} \, [f(x)f(y)f(x-y) + f(x-\delta)$$

$$f(x-\tau+\delta)f(\tau) + f(x-\tau)f(x)f(\tau) + f(y)f(x-\delta)f(x-y+\delta)$$

$$+ f(x-\tau)f(y+\tau-\delta)f(x-y+\delta) + f(x-\tau+\delta)f(y+\tau-\delta)f(x-y)]$$

$$+ 2e^{-\Gamma_{23}x-\Gamma_{14}y} \, [f(x)f(y)f(x-y) + f(-x-\tau+\delta)f(-y+\tau)$$

$$f(x-y-\delta) + f(\tau)f(-y+\tau)f(y) + f(x)f(x-y-\delta)f(-y+\delta)$$

$$+ f(\tau)f(-y+\delta)f(-y+\tau-\delta) + f(-x-\tau+\delta)f(-y+\tau-\delta)f(x-y)] +$$

$$4e^{-\Gamma_{23}(x+y)} \, [f(-x+y)f(0)f(x-y) + f(x-\delta)f(-x-\tau+\delta)f(\tau) +$$

$$f(\tau)f(0)f(\tau) + f(-x+y)f(x-\delta)f(-y+\delta)$$

$$+ f(\tau)f(-y+\delta)f(y+\tau-\delta) + f(-x-\tau+\delta)f(y+\tau-\delta)f(x-y)] \} \qquad (3.25)$$

where we used the function $f(x) = \exp(-x^2/2\tau_c^2) = f^*(x)$ with $t - t_2 = x$ and $t - s_2 = y$. γ_{23} is the vibrational relaxation time within S_1 state (as defined in chapter 2), Γ_{14} is the dephasing time in the S_n states and τ_c is the correlation time.

3.5.1 Numerical Results and Discussion

The above equation (3.25) for the signal intensity, containing 24 terms, is solved numerically using IMSL subroutines [54] for different values of $(\Gamma_{14})^{-1}$ and $(\Gamma_{23})^{-1}$. To verify the integrity of our program we simulated the results obtained by Morita et al. [5] and Okamoto et al. [11] with the signal intensity given according to their theory. We obtain excellent agreement between the curves simulated using our program and the reported ones indicating the integrity of our program.

Fig. 3.17 shows typical curves simulated using the parameters obtained through experimental results. The structure of the different curve matches well with the experimental observations but the ratio does not since the calculations do not

account for the population relaxation. Fig. 3.17 (a) shows the auto-correlation curve for the sample RhB. All the values are normalized with τ_c and the value of τ_c used for simulations is 0.17. Typical values of integration are 0 to 200*τ_c. Figure 3.17 (b) shows the curve simulated for sample Erythrosin B where the value of τ_{14} or $(\Gamma_{14})^{-1}$ used is 0.05 (since the phase relaxation in the S_n states is much smaller than the correlation time τ_c) and the value of τ_{23} or $(\Gamma_{23})^{-1}$ used is 0.17. The curve shows two-peak structure as observed in experiments except for the ratio. The experimental ratio is ~ 200. Figure 3.17 (c) shows the curve simulated for the sample Black Ink using the same experimental parameters. Again the curve shows two-peak structure with the second peak clearly showing the asymmetry. In this case the ratio observed in both experiment and theory match well. The value of $(\Gamma_{14})^{-1}$ used is 0.05 and the value of $(\Gamma_{23})^{-1}$ used is 1.50. Figure 3.17 (d) shows the curve simulated with the observed experimental values for the sample CoTTP where the value of $(\Gamma_{14})^{-1}$ used is 0.05 and the value of $(\Gamma_{23})^{-1}$ used is 3.0 (5 = 5.2). In this case the second peak obtained is asymmetric while in experiment we observe a symmetric peak. The second peak moves symmetrically, for all the samples, across the first peak as observed in experiment. Probing the coherent signal emission, using incoherent light, in the ps/fs time scales involves correlation between various fields: (a) ε_a and ε_c correlation is significant at $\tau = 0$ which gives rise to the coherence peak at $\tau = 0$. (b) ε_b and ε_c correlation is significant around $T - 5$ which gives rise to the second peak at $T = 5$. The width of this peak is governed by the coherence time τ_{23}

Since all the three fields are degenerate, the generated FWM signal could arise via different possible mechanisms (some of which are shown in fig. 3.18 for both three-level and four-level models). We have attempted to analyze the generated DFWM signal using an open two-level system (proposed by Okamoto et al. [11]) and a four-level model, as is applicable to organic dyes in general. We find that the open two-level model (consisting of ground, excited states and a reservoir) explains the signal ratio (related to the population relaxation time T_1). But it fails to account for the large line-width of the second peak observed for several samples which possess strong Reverse Saturable Absorption. Whereas in the four-level model there is a reasonable, qualitative agreement, as far as the line shapes are concerned, for few
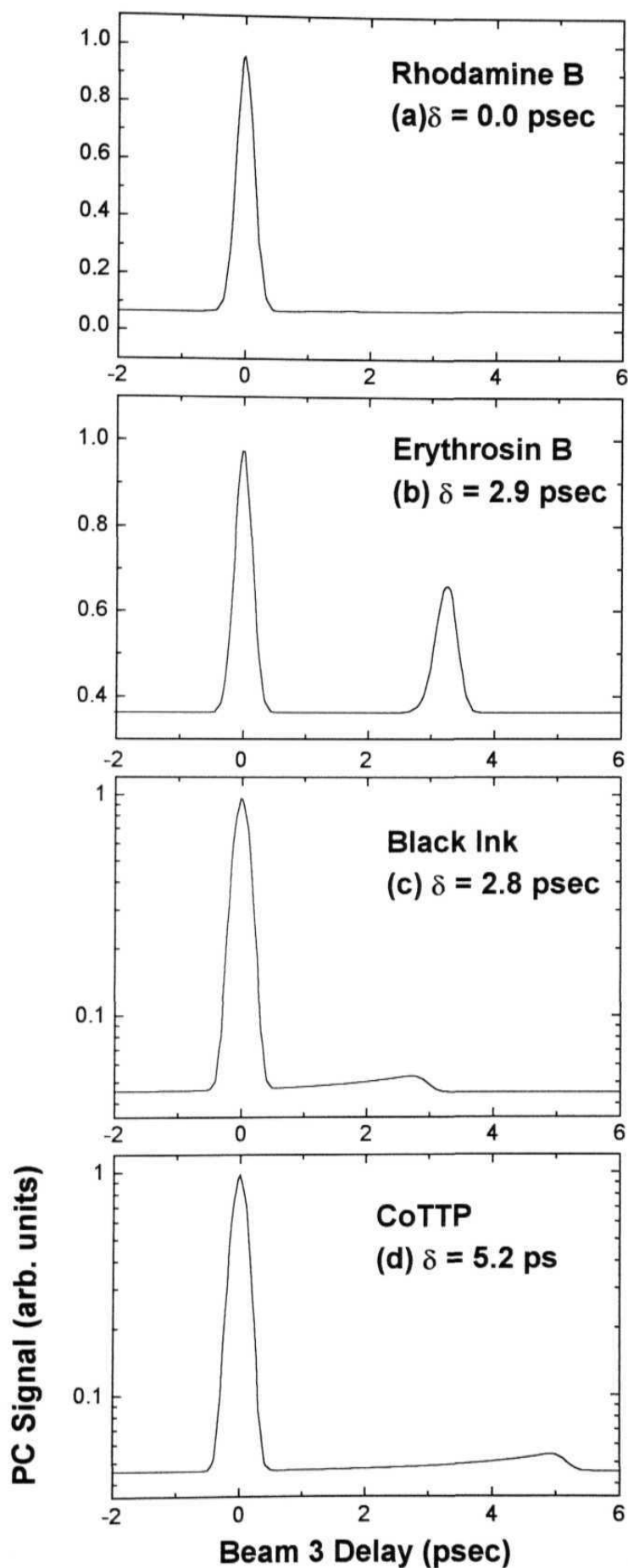
Fig. 3.17 Theoretical PC signals, calculated using eqn. 3.25, in samples (a) RhB (b) ErythrosinB (c) Black Ink and **(d)** CoTTP.
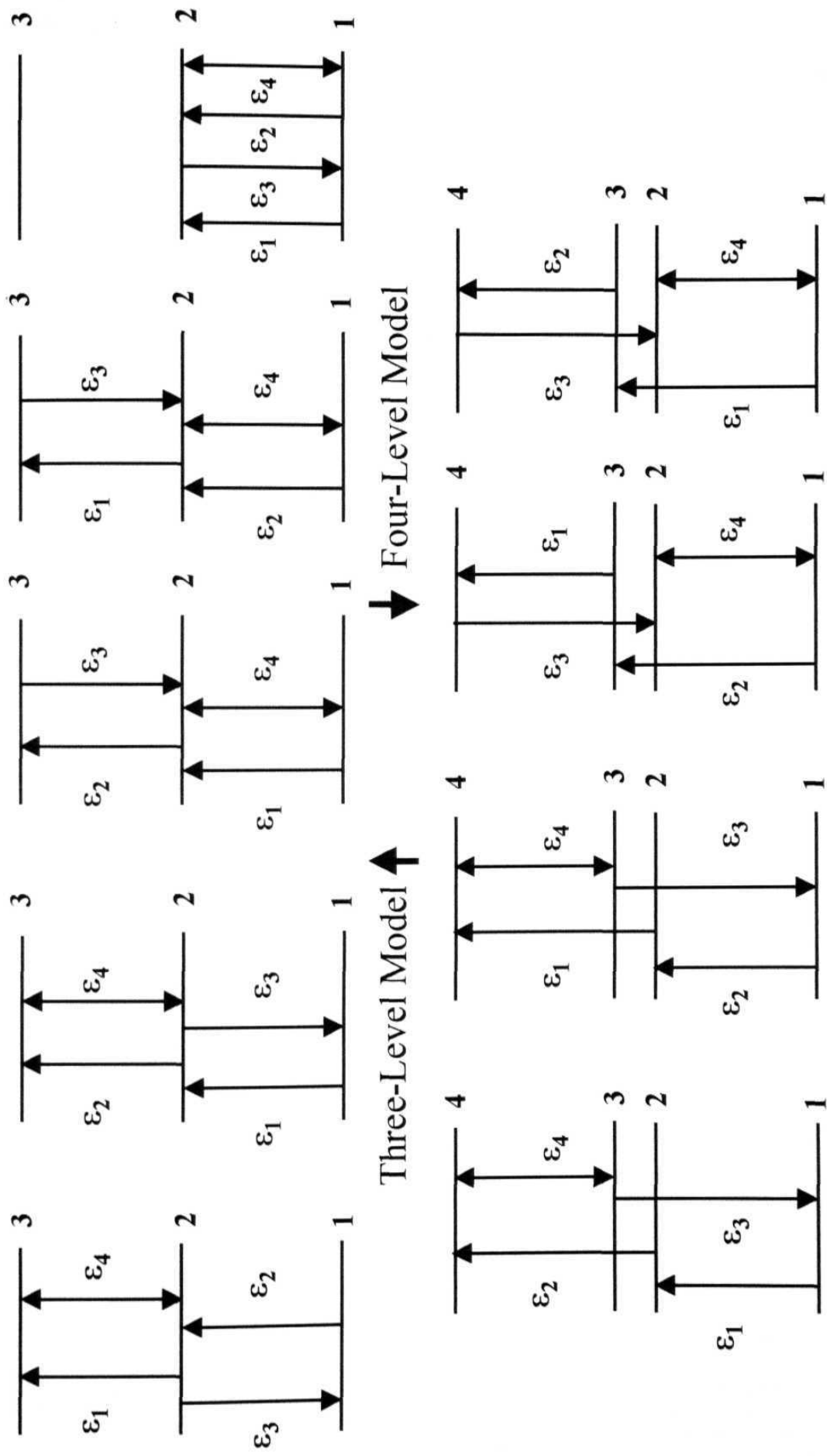
Fig. 3.18 Different possible interactions for obtaining the FWM signal with three degenerate fields ε_1, ε_2, ε_3 based on three-level and four-level models. ε_4 is the Phase Conjugate (DFWM) signal generated

Four-Level Model

Three-Level Model

samples. However, it fails to provide explanation for the observation of symmetric peak in porphyrins/related molecules and quantitative matching of the ratios. Therefore we feel that more extensive work, taking into account all the possible interaction mechanisms responsible for generation of DFWM signal, is required to interpret the observed signal structure.

We have shown, both experimentally and theoretically, that the second peak width is related to the vibrational relaxation within the S_1 state. Another possibility is to look into an effective 3-level model (consisting of S_0, S_1, and S_n, where S_1 state has two relaxation times, dephasing and depopulation, as shown in fig. 16 [b]), when the vibrational spacing between the S_{1v} and S_{10} is quite small, and obtain the signal as a function of delay of beam 3.

Sample	Dephasing of the S_n state (T_2) in fs (DFWM-IL)	Vibrational Relaxation in S_1 state (τ_{Vib}) in ps (DFWM-IL)	Population Relaxation time (T_1) in ps (DFWM-IL) (DFWM-PS)	
Rhodamine B (Methanol)	< 170	-	-	-
Rhodamine B[#] (Higher Concn.'s)	< 170	3.30 ±0.66	85.0 ±17.0	-
Erythrosin B (Methanol)	< 170	0.17 ±0.03	16.0 ±3.20	-
Black Ink (Distilled Water)	< 170	1.50 ±0.30	27.0 ± 5.40	-
CoTTP (Chloroform)	< 170	5.60 ±1.12	37.0 ± 7.40	109 ±22
ZnmTPP Tetra Hydro Furan)	< 170	3.80 ±0.76	48.0 ±9.60	-
ZnmpTBP Tetra Hydro Furan)	< 170	3.00 ±0.60	32.0 ± 6.40	-
NimpTBP Tetra Hydro Furan)	< 170	5.50 ± 1.10	34.0 ±6.80	-
Cresyl Violet Acetate (Methanol)	< 2700*	2.80 ±0.56	30.0 ±6.00	58 ± 11
DQOCI (Ethylene Glycol)	< 170	3.50 ±0.70	42.5 ±8.50	104 ±21
Brilliant Green (Ethylene Glycol)	< 170	4.50 ±0.90	34.0 ±6.80	

* Measured with Grating in the cavity.

Concentration used: $5.25 * 10^{-3} M$

Table 3.1 The phase and population relaxation times calculated for different samples using DFWM-IL.

3.6 Conclusions

1. Using Degenerate Four Wave Mixing with Incoherent Light (DFWM-IL) we attempt to study the ultra-fast relaxation times in various organic materials. Our results on some of the dyes (like black ink and porphyrin) show interesting PC signal behavior with delay of the probe (beam 3).

2. The double peak structure observed in the PC signal is understood in terms of the gratings formed by beams 1, 3 and beams 2, 3 with the other beam getting diffracted. Different excited state lifetimes derived from the widths and ratio of the two peaks are calculated for different samples using this technique.

3. The measurements performed with narrow band laser (35 ps pulses) corroborate, to most extent, our results obtained with incoherent light. However, there are some limitations with the present setup like small dynamic range.

4. We find that the widths and the ratio of the peaks are related to dephasing times and the population relaxation time. Earlier reports do not account for the width of the second peak.

5. A much better understanding of our results can be obtained based on a four-level model (comprising of S_o, S_{10}, S_{1v}, S_n levels) in these systems and develop a theory including the higher levels in the transition. However our preliminary theory does not completely account for the symmetry of the second peak. A more rigorous theory including all the possible interaction mechanisms and relaxation parameters may be essential to explain the observed results. The role of triplets also should be taken into account to develop a perfect model. Further the signal amplitude is to be estimated for both the peaks taking into the account the coherent part, background part (due to ns pulse), lifetimes of S_1, S_n, τ_{ISC}, T_1, T_n states. A detailed study, though would involve rigorous analytical and computational efforts, would be quite rewarding as a single experiment would yield results for all the levels.

3.7 References

1. H.J. Eichler, P. Gunter, and D.W. Pohl, *Laser Induced Dynamic Gratings,* Springer Verlag, Heidelberg, 1986; S. Mukamel, *Principles of Nonlinear Optical Spectroscopy,* Oxford University Press, New York, 1995.

2. Ultrafast Laser Pulses - Generation and Applications, Ed. W. Kaiser, Springer-Verlag, Berlin, 1993.

3. *Femtochemistry,* Ed. A. Zewail, World Scientific, Singapore, 1994, Vol's I and **II;** *Femtochemistry,* Ed.'s J. Manz and L. Woste, VHS, Heidelberg, 1995, Vol.'s I and II; *Femtochemistry: Ultrafast Chemical and Physical Processes in Molecules,* Ed. M. Chergui, World Scientific, Singapore, 1997.

4. N. Morita and T. Yajima, *Phys. Rev.* **A30,** 2525, 1984.

5. N. Morita, T. Tokizaki, and T. Yajima, *J. Opt. Soc. Am.* B4, 1269, 1987; K. Kurokawa, T. Hatton, and T. Kobayashi, *Phys. Rev.* **A36,** 1298, 1987; K. Misawa, T Hattori, and T Kobayashi, *Opt. Lett.* **14,** 453, 1989; N. Morita, K. Torizuka, and T. Yajima, *J. Opt. Soc. Am.* B3, 548, 1986; T. Hattori and T. Kobayashi, *Chem. Phys. Lett.* **133,** 230, 1987; M. Tomita and M. Matsuoka, *J. Opt. Soc. Am.* B3, 560, 1986; J.E Golub and T.W. Mossberg, *J. Opt. Soc. Am.* B3, 554, 1986; F. Minami and A. Hasegawa, *Appl. Phys. Lett.* 54, 978, 1989; D.C. DeMott, D.J. Ulness and A.C Albrecht, *Phys. Rev.* **A55,** 761, 1997; T. Yanagawa, K. Nagamuna, H. Kanbara, and T. Kaino, *Opt. Lett.* **21,** 318, 1996; T. Yanagawa, Y. Kurokawa, H. Kasai, and H. Nakanishi, *Opt. Commun.* **137,** 103, 1997; P.A. Apanasevich, V.P. Kozich, V.A. Orlovich, and A.I. Vodehitz, *Proc. SPIE* **2370,** 279, 1994.

6. H. Okamoto, T. Nakabayashi, and M. Tasumi, *J. Raman Spectroscopy* 25, 631, 1994, H. Okamoto, T. Nakabayashi, and M. Tasumi, *J. Phys. Chem.* **97,** 9872, 1993; MA. Dugan and A.C Albrecht, *Phys. Rev.* **A43,** 3877, 1991; M.A. Dugan, J.S. Melinger, and A.C Albrecht, *Chem. Phys. Lett,* **147,** 411, 1988; J.C. Kirkwood, D.J. Ulness, and A.C. Albrecht, *Chem. Phys. Lett.* **293,** 167, 1998; J.C. Kirkwood, A.C. Albrecht, and D.J. Ulness, *J. Chem. Phys.* **111,** 253, 1999; J.C. Kirkwood, A.C. Albrecht, and D.J. Ulness, *J. Chem. Phys.* **111,** 272, 1999

7. M.J. Stimson, D.J. Ulness, and AC. Albrecht, *Chem. Phys. Lett.* **263,** 185, 1996; M.J. Stimson, D.J. Ulness, and A.C. Albrecht, *Chem. Phys.* **222,** 17, 1997; M.J.

Stimson, D.J Ulness, and A.C. Albrecht, *J Raman Spectroscopy* **28,** 579, 1997; D.J. Ulness **and A.**C. Albrecht, *J. Raman Spectroscopy* **28,** 571, 1997; D.J. Ulness, M.J. Stimson, J.C. Kirkwood, and A.C. Albrecht,*J. Raman Spectroscopy* **28,** 917, 1997; D.J. Ulness, J.C. Kirkwood, M.J. Stimson, and A.C. Albrecht, *J. Chem. Phys.* **107,** 7127, 1997; D.J. Ulness, M.J. Stimson, J.C. Kirkwood, and A.C. Albrecht, *J. Phys. Chem.* **A101,** 4587, 1997; T. Hattori, A. Terasaki, and T. Kobayashi, *Phys. Rev.* **A35,** 715, 1987.

8. T. Hattori and T. Kobayashi, *J. Chem. Phys.* 94, 3332, 1991; A.I. Vodchits, V.P. Kozich, and B.L. Kontsevoi, *Opt. Spectr.* 70, 516, 1992; A. Kummrow, S. Woggon, and A. Lau, *Phys. Rev.* **A50,** 4264, 1994; A. Kummrow, A. Lau and K. Lenz, *Phys. Rev.* **A55,** 2310, 1997; A. Kummrow, A. Lau, H. -G. Ludewig, and S. Woggon, *Proc. SPIE* **2370,** 207, 1994.

9. A.C. Albrecht et al. *Laser Phys.* 5, 667, 1995.

10. T. Kobayashi, A. Terasaki, T. Hattori, K. Kurokawa, *Appl. Phy.* **B47,** 107, 1988; T. Kobayashi, T. Hattori, A. Terasaki, and K. Kurokawa, *Revue Phys. Appl.* **22,** 1773, 1987.

11 H. Okamoto,*J. Opt. Soc. Am.* **B10,** 2353, 1993.

12. J. Liu, S. Huang, W Qin, and J. Yu, *Opt. Commun.* **91,** 87, 1992.

13 H. Nakatsuka, Y. Katashima, K. Inouye, and R Yano, *Opt, Commun.* **69,** 169, 1988.

14. M. Pfeiffer and A. Lau, *J. Chem. Phys.* **108,** 4159, 1998; A. Lau, M. Pfeiffer V. Kozich, and F. Tschirschwitz,*J. Chem. Phys.* **108,** 4173, 1998

15. A. Kummrow, *Chem. Phys. Lett.* **236,** 362, 1995.

16. K. Puech, F.Z. Henari, W.J. Blau, D. Duff, and G. Schmid, *Chem. Phys. Lett.* **247,** 13, 1995.

17 G.S. Maciel, C.B. De Araujo, R.R.B. Correia, and W.M de Azevedo, *Opt. Commun.* **157,** 187, 1998.

18. Y. Nomura, Y. Fujimara, M. Takahashi, M. Fujii, and M. Ito, *Chem. Phys. Lett.* 197,405, 1992.

19. T. –S. Yang, R. Zhang, and A.B. Myers, *J. Chem. Phys.* **100,** 8573, 1994; T. Matsumoto, K. Ueda, and M. Tomita, *Chem. Phys. Lett.* **191,** 627, 1992.

20. T. Tokizaki, Y. Ishida, and T. Yajima, *Opt. Commun.* 71, 355, 1989; H. Nakatsuka, Y. Katsahima, K. Inouye, R. Yano, and S. Uemura, *Opt. Commun.* 74, 219, 1989.

21. P.A. Apanasevich, V.P. Kozich, and A.I. Vodschitz, *J. Mod. Opt.* 35, 1933, 1988.

22. Y. Zhang, S.R. Hartmann, and F. Moshary, *J. Chem. Phys.* **104,** 4380, 1996; F. Moshary, M. Arend, R. Friedberg and S.R. Hartmann, *Phys. Rev.* **A46,** R33, 1992.

23. R. Zhang, X. Mi, H. Zhou, and P. Ye, *Opt. Commun.* 67, 446, 1988.

24. G.L. Huang and H.S. Kwok, *J. Opt. Soc. Am.* B9, 2019, 1992.

25. V. Kozich, L. de S. Menezes, and Cid B. de Araujo, *Opt. Commun.* **171**, 125, 1999.

26. R. Beach and S.R. Hartmann, *Phys. Rev. Lett.* 53, 663, 1984; M. Fujiwara, R. Kuroda, and H. Nakatsuka, *J. Opt. Soc. Am.* 8, 1634, 1985; S. Asaka, H. Nakatsuka, M. Fujiwara, and M. Matsuoka, *Phys. Rev.* **A29,** 2286, 1984; N.V. Gruzdev, E.G. Silkis, V.D. Titov, and Y.G. Vainer, *J. Opt. Soc. Am.* 9, 941, 1992.

27. A. Kummrow and A. Lau, *Appl. Phys.* **B63,** 209, 1996; T. Kobayashi, "Measurement of femtosecond dynamics of nonlinear optical responses", *Modern Nonlinear Optics,* Part 3, Ed.'s M. Evans and S. Kielich, Advances in Chemical Physics Series, Vol. LXXXV, John Wiley and Sons Inc., 1994.

28. D. Narayana Rao, S. Venugopal Rao, F.J. Aranda, M. Nakashima and J.A. Akkara, J. Opt. Soc. Am. **B14,** 2710-2714, 1997; S. Venugopal Rao, L. Giribabu, B.G. Maiya and D. Narayana Rao, Current Science 72, 957, 1997.

29. D.W. Phillion, D.J. Kuizenga, and AE. Siegman, *Appl. Phys. Lett.* 27, 85, 1975; H. Souma, E.J Heilweil, and R.M. Hochstrasser, *J. Chem. Phys.* 76, 5693, 1982.

30. P.A. Fleitz, R.L. Sutherland, L.V. Natarajan, T. Pottenger, and N.C. Fernelius, *Opt. Lett.* 17, 716, 1992.

31. R.L. Sutherland, E. Rea, L.V. Natarajan, T. Pottenger, and P.A. Fleitz, *J. Chem. Phys.* 98,2593, 1993.

32. E.J. Brown, Q. Zhang, and M. Dantus, *J. Chem. Phys.* **110,** 5772, 1999.

33. R.W. Chambers, T. Kajiwara, and D.R. Kearns, *J. Phys. Chem.* 78, 380, 1974; H. Bottcher, O. Hertz, and M.A. Fox, *Chem. Phys. Lett.* **160,** 121, 1989.

34. G.S. Beddard, T. Doust, and G. Porter, *Chem. Phys.* **61,** 17, 1981.

35. A.L. Smirl, J.B. Clark, E.W. Van Stryland, and B.R. Russell, *J. Chem. Phys.* 77, 631, 1982 and references therein.

36. *Handbook of nonlinear optics,* R.L. Sutherland, Marcel Dekker, Inc., New York, Chapter 7, 1996.

37. P. Ye, R. Zhang, X. Mi, H. Zhou, and Q. Jiang, *Int. J. Nonlin. Opt. Phys.* 1, 223, 1992; X. Mi, H. Zhou, R. Zhang, and P. Ye, *J. Opt. Soc. Am.* **B6,** 184, 1989.

38. D.J. Ulness **and** A.C. Albrecht, Ph.D. Thesis, Cornell University, 1996; D.J. Ulness and A.C. Albrecht, *Phys. Rev.* **A53,** 1081, 1996.

39. P. Tchenio, A. Debarre, J.C. Keller, and J.L. Le Gouet, *J. Opt. Soc. Am.* B5, 1293, 1988.

40. S.R. Hartmann and J.T. Manassah, *J. Phys. B: At. Mol. Opt. Phys.* **23,** 1363, 1990.

41. G.S. Agarwal, *Phys. Rev.* **A37,** 4741, 1988; G. Vemuri, G.S. Agarwal, R. Roy, M.H. Anderson, J. Cooper and S.J. Smith, *Phys. Rev.* **A44,** 6009, 1991.

.42. G. Alber, J. Cooper, and P. Ewart, *Phys. Rev.* **A31,** 2344, 1985

43. D.R. Meacher, A. Charlton, P. Ewart, J. Cooper, and G. Alber, *Phys. Rev.* **A42,** 3018, 1990; M. Kaczmarek, DR. Meacher, and P. Ewart,./. *Mod. Opt.* **37,** 1561, 1990.

44 L. Abrams and R.C. Lind, *Opt. Lett.* 2, 94, 1978; L. Abrams and R.C. Lind, *Opt. Lett.* 3,205, 1978

45. S. Mukamel and RF. Loring, *J. Opt. Soc. Am.* B3, 595, 1986; S. Mukamel and E. Hanamura, *Phys. Rev.* **A33,** 1099, 1986.

46. P. Ye and Y.R. Shen, *Phys. Rev.* **A25**, 2183, 1982.

47. R. Trebino, E.K. Gustafson, and AE. Seigman, *J. Opt. Soc. Am.* B3, 1295, 1986.

48. V. Finkelstein and PR. Berman, *Phys. Rev.* **A41,** 6193, 1990.

49. P. Fu, Z. Hu, X. Mi and P. Ye, *J. Physique,* **48,** 2089, 1987; X. Mi, Z. Yu, Q. Jiang, and P. Fu, *Opt. Commun.* **116**, 443, 1995.

50. R Beach, D.DeBeer, and S.R.Hartmann, *Phys. Rev.* **A32,** 3467, 1985.

51. B. Do, J. Cha, S. Elliott, and S.J. Smith, *Phys. Rev.* **A60,** 508, 1999.

52. J.E. Golub and T.W. Mossberg, *Opt. Lett.* **11,** 431, 1986.

53. X. Cheng and T. Kobayashi, *Mol. Cryst, Liq. Cryst.* **182A,** 139, 1990.

54. IMSL PC based numerical subroutines, Visual Numerics Inc., USA, 2000.

CHAPTER 4

Tetra Tolyl Porphyrins: Studies of Third-order Optical Nonlinearity and Nonlinear Absorption.

This chapter contains our experimental results on the measurement of third-order optical nonlinearity in the ns and ps domain, in several tetratolyl porphyrin molecules (TTP), using degenerate four wave mixing (DFWM) and Z-Scan techniques. Our results indicate a very high value of nonlinearity for these molecules in the ns domain and reasonably high values in the ps domain. They are found to exhibit a strong nonlinear absorption at both 532 nm and 600 nm. The high value of nonlinearity for ns pulses is attributed to higher excited singlet and triplet states. Time-resolved studies indicate an ultra-fast temporal evolution of the nonlinearity in these molecules.

4.1 Introduction

The last two decades have witnessed a phenomenal growth of research in nonlinear optical properties of various conjugated polymers, molecular solids, organic/organo-metallic composites and compounds [1]. A collective effort from physicists, chemists and material scientists is in progress to understand the basic processes responsible for the nonlinearity. Current emphasis is on the synthesis of novel chemical structures that can be tailored to optimize the nonlinear response while preserving their chemical, mechanical, optical and thermal stability. Among the various organic materials Porphyrins, metalloporphyrins and their derivatives are one of the most studied group of molecules [2]. Porphyrins are a ubiquitous class of naturally occurring compounds having important biological representatives including hemes, chlorophyll and vitamin B_{12} among several others. They are also involved in oxygen binding, electron transfer, catalysis, light harvesting. Heme and chlorophyll are iron and magnesium derivatives of cyclic pyrrole pigments. Hemoglobin in blood is responsible for the transfer of molecular oxygen to tissues. Manganese derivatives are thought to be responsible for the decomposition of water via photosynthesis in organisms found in nature. Zinc Porphyrins take part in metabolic processes. Colors of feathers in some birds are due to copper derivatives of Porphyrins. In addition there are multitudes of synthetic porphyrinoid molecules that have been prepared and studied for purposes ranging from basic research to functional applications. All these

molecules share the porphyrin macrocyclic substructure in common. The basic structure of the porphyrin macrocycle, shown in fig. 4.1, consists of four pyrrolic subunits linked by four methine bridges.

Although the porphyrin ring is a macromolecule, it is highly flexible and a number of structural changes involving different central metal ions and peripheral substituents can be introduced without compromising its excellent chemical and thermal stability. This architectural aspect is relevant to nonlinear optics in developing materials with optimum nonlinearity and response times. The high n electron density, resulting in an extended electron de-localization makes Porphyrins useful for observing a variety of nonlinear optical effects. Their sharp absorption bands in the visible and NIR can be used for resonance enhancement of $\chi^{(3)}$ as well. They have enormous potential for applications on the technological front, which include optical limiting [3], optical switching, optical data processing and opto-electronic device fabrication [4]. They have also been used as organic semiconductor [5], bistable device [6], in magnetic resonance imaging and photodynamic therapy [7]. Because of these vital roles played by Porphyrins and their derivatives a vast amount of research has been directed towards understanding the detailed mechanisms responsible for nonlinearity.

Compared to other linear π-conjugated systems these cyclic structures offer advantage of more tensor components contributing to the total nonlinearity. For linear structures major contribution to $<\gamma>$ comes from γ_{xxxx} component whereas for Porphyrins and related molecules γ_{yyyy}, γ_{xxyy}, γ_{xyxy}, γ_{xyyx}, γ_{yyxx}, γ_{yxyx}, and γ_{yxxy} also contribute to the total $<\gamma>$. The nonlinear optical properties of Porphyrins and their derivatives have been previously studied in solution [8-9], spin-coated thin films and polymer hosts [10], sol-gels [11] and glass [12]. In this chapter we present our results on the measurement of the third order optical nonlinearity and nonlinear absorption studies in Tetra Tolyl Porphyrins (TTP) synthesized with sixteen different central metal ions in the porphyrin ring. Fig. 4.1 shows the structure of the compounds used, where M denotes the substituent metal ion. The techniques of Degenerate Four Wave Mixing (DFWM) [13] in the backward configuration and Z-scan [14] have been employed.
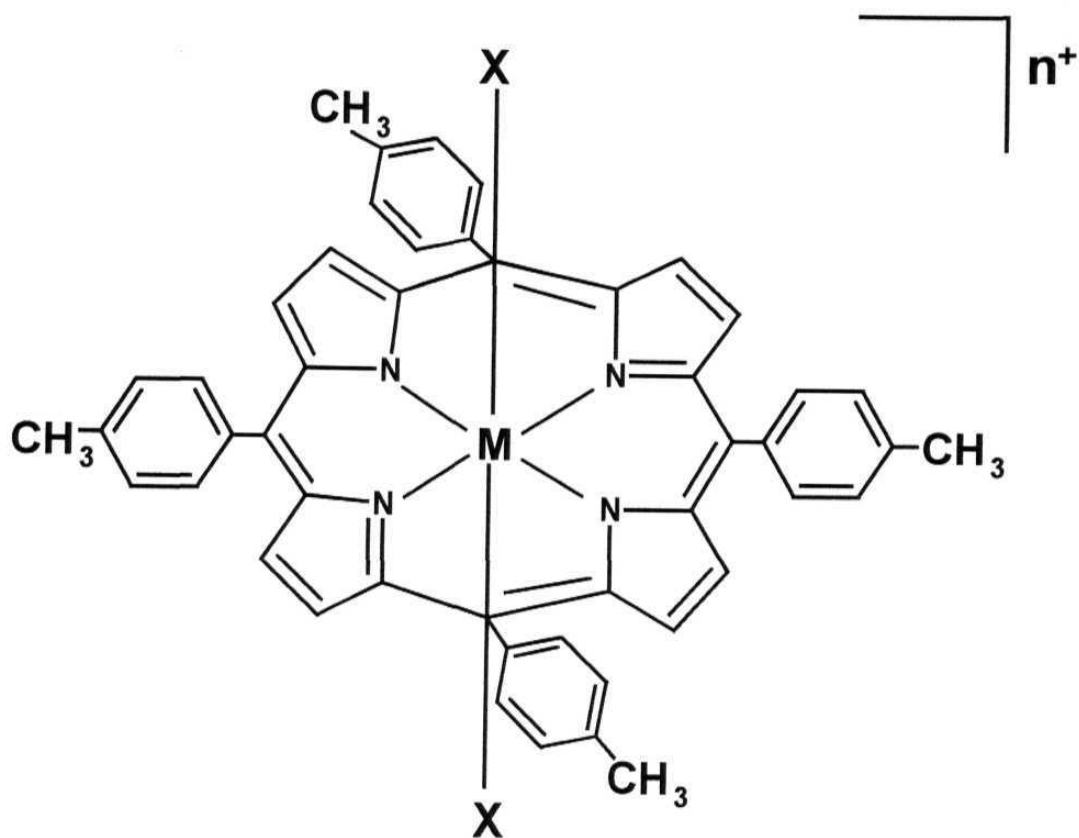
M = 2H, n = 0

M = Co, Ni, Cu, Zn, Ag, Cd or Hg, n = 0

M = Cr, Mn, Fe or Au, n = 1, X = Cl

M = In, n = 1, X = OH

M = Ge or Sn, n = 2, X = OH

M = V, n = 2, X = O

M = P, n = 3, X = OH

Fig. 4.1 Structure of the compounds used in the study

4.2 Experimental Details

The samples are synthesized and purified according to the reported procedures in literature [15]. Each sample is subjected to a column chromatographic purification process just prior to the measurements. The samples are dissolved in highly purified, spectroscopic grade chloroform and the absorption spectra are recorded using an UV-visible recording spectrophotometer (model UV-160 A, Shimadzu). In all experiments, sample solutions are taken in 1-mm quartz cuvettes. Fresh solutions are prepared for each measurement to avoid any complications arising from photo-degradation.

4.2.1 Degenerate Four Wave Mixing

We employ the standard backward DFWM geometry. All the three input beams are focussed on to the sample solution using a lens of f ~ 15 cm. The peak power densities are in the range of 400 - 800 MW/Cm^2. The angular separation is about 10^0 between the forward pump and the probe beam. The phase conjugate (PC) signal counter-propagating to the probe is split using a beam splitter, attenuated using a variable neutral density filter and focused onto a fast photodiode. The photodiode signal is fed to a digital oscilloscope (TDS 210) and readings are taken after several successive signals are averaged.

The source for ps $\chi^{(3)}$ measurements is a hybrid mode-locked Nd: YAG laser (35 ps, 532 nm, 10 Hz). The experimental set up is similar to the above, except that the beams are loosely focused by a lens of f ~200 cm to avoid large power densities inside the sample. The angle between the pump and probe beams is ~ 5°. A part of the forward pump is picked up by a fast photodiode to monitor the pulse-to-pulse fluctuations. For time-resolved measurements, the backward pump is delayed with respect to the temporally coincident forward pump and probe [In the case of experiments with ps pulses we are delaying the beam 2 which should be called the *probe* but for convention sake we call it as the backward pump only]. The zero delay of forward pump and probe is achieved by optimizing the forward FWM signals in CS2. The intensity ratio of beams 1, 2 and 3 approximately is 1:1:0.2 for nonlinearity

measurements and 1:0.2:1 for time-resolved measurements. Polarization of each beam is varied using a Half Wave Plate (HWP).

4.2.2 Z-Scan

For the Z-scan [14] studies, dye laser pulses centered at 600 nm wavelength and 6 ns duration also were used for excitation, in addition to the others. The input beam in each case is appropriately focused using different lenses to ensure the thin sample regime. The sample is scanned across the focus using a micrometer translation stage, which is controlled by a PC. A small part of the input beam is split using a glass plate to monitor the pulse-to-pulse energy fluctuation. The transmitted light is collected using a large area lens of $f \sim 100$ mm and focused on to a photodiode for open aperture data. A fraction of the transmitted beam is split and passed through a variable aperture before focusing on to another photodiode to obtain the closed aperture data.

4.3 Results and Discussion

All samples used in this study show the linear absorption features typical of metalloporphyrins, namely the high energy B (Soret) band and the low energy Q band(s). Figures 4.2 to 4.5 illustrate the UV-Visible spectra obtained for all samples. The solid line represents the data obtained at very low concentrations and the dotted line at very high concentrations to distinguish between the B and the Q bands. Table 1 summarizes the λ_{max} and log (s) (e = molar extinction coefficient) values for each porphyrin investigated. The compounds remain stable even after exposure to laser pulses for a long period of time, which is confirmed from absorption spectra recorded before and after the measurements. All the experiments are carried out with samples having a concentration in the range of 10^{-4} to 10^{-5} M corresponding to an absorbance of less than 0.3. The cubic dependence of the phase conjugate signal with the input intensity has been verified for all the samples in the low intensity range. A typical plot of the phase conjugate signal versus input intensity is shown in fig. 4.6 (a) for the sample SnTTP and the data is fitted to a cubic function. Fig. 4.6 (b) shows the linear dependence of $\chi^{(3)}$ to the sample concentration for SnTTP. The other samples also
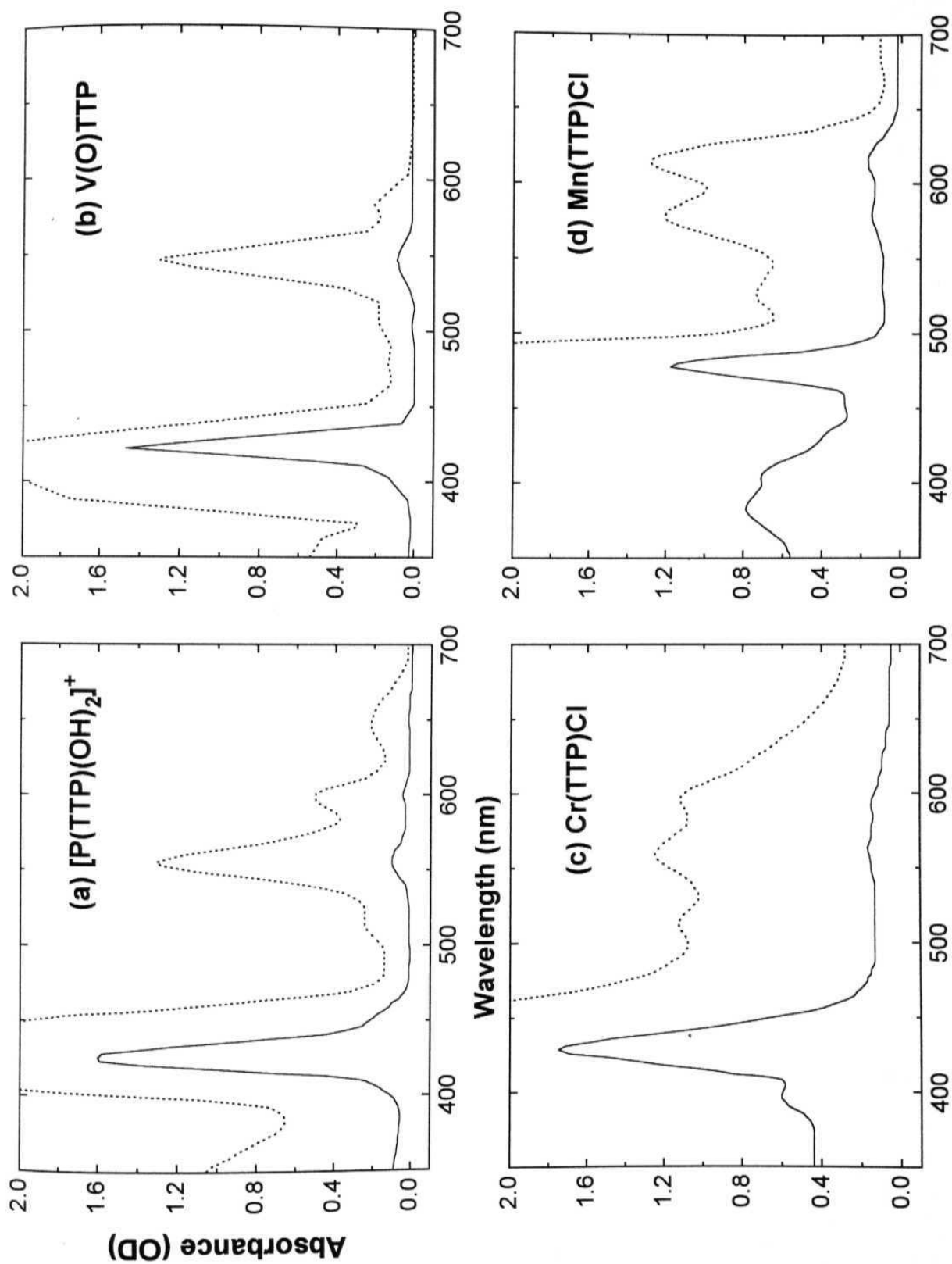
Fig. 4.2 Absorption spectra of (a) [P(TTP)(OH)$_2$]$^+$ (b) V(O)TTP (c) Cr(TTP)Cl (d) Mn(TTP)Cl
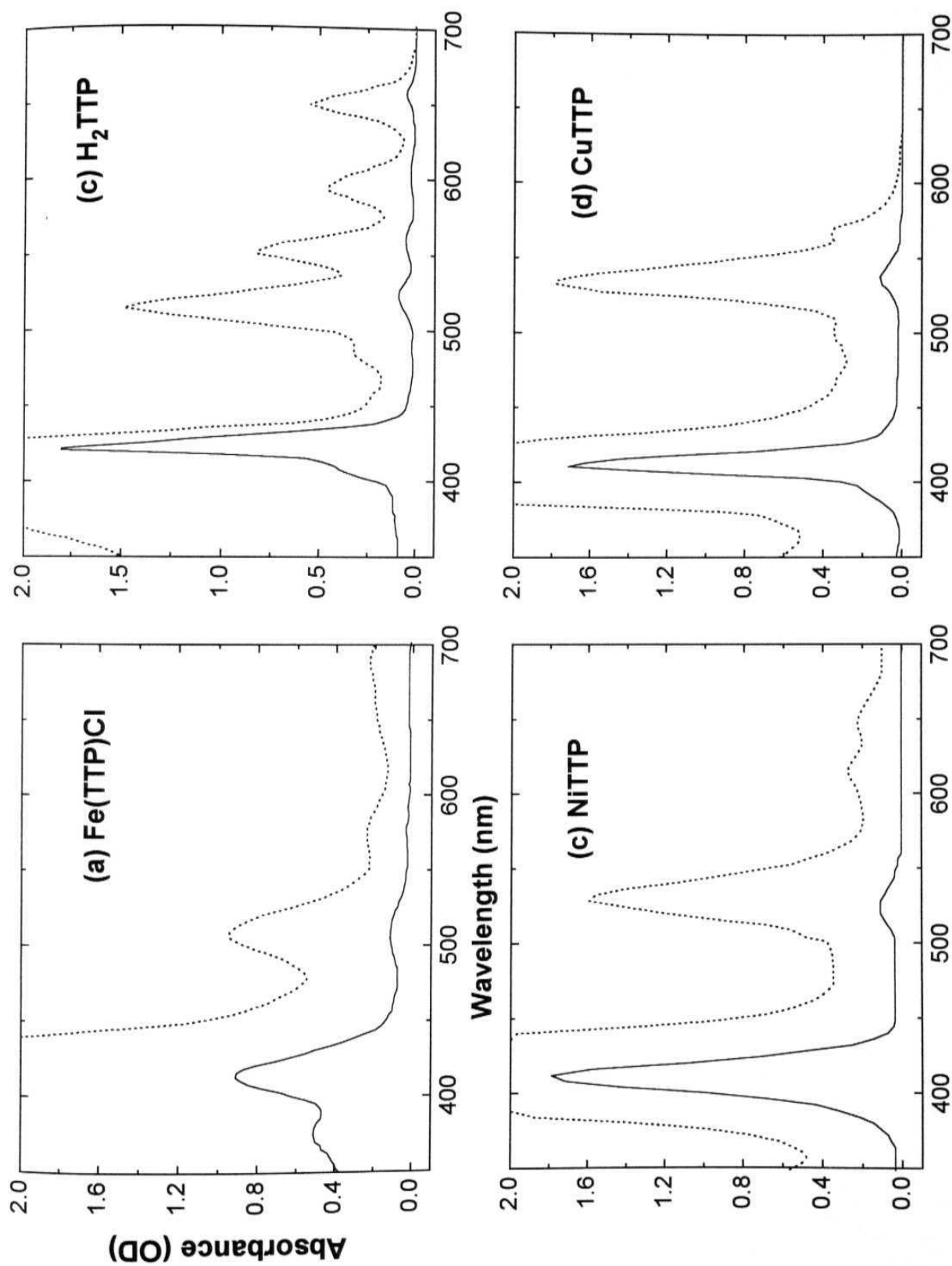
Fig. 4.3 Absorption spectra of (a) Fe(TTP)Cl (b) H_2TTP (c) NiTTP (d) CuTTP
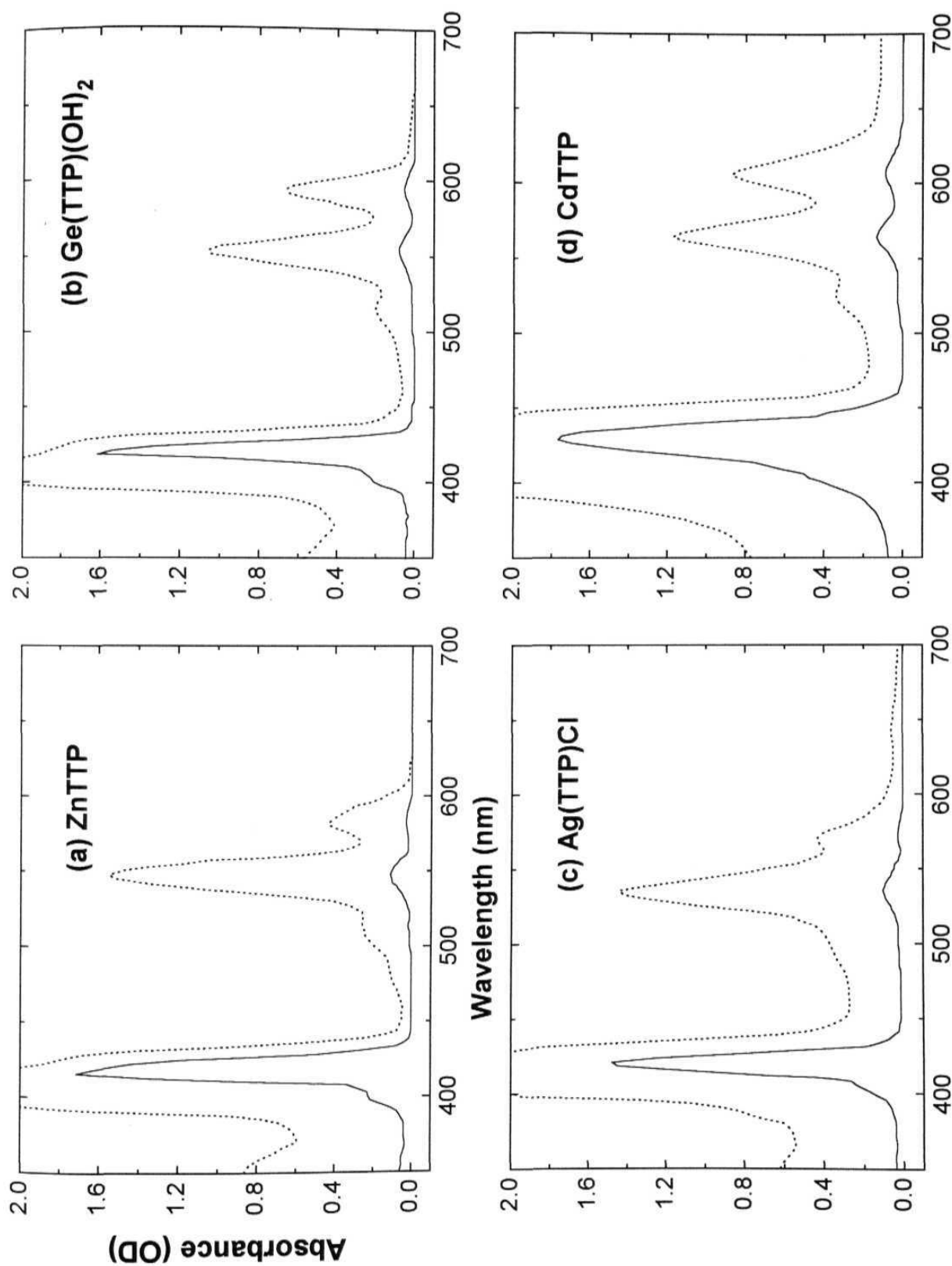
Fig. 4.4 Absorption spectra of (a) ZnTTP (b) Ge(TTP)(OH)$_2$ (c) Ag(TTP)Cl (d) CdTTP
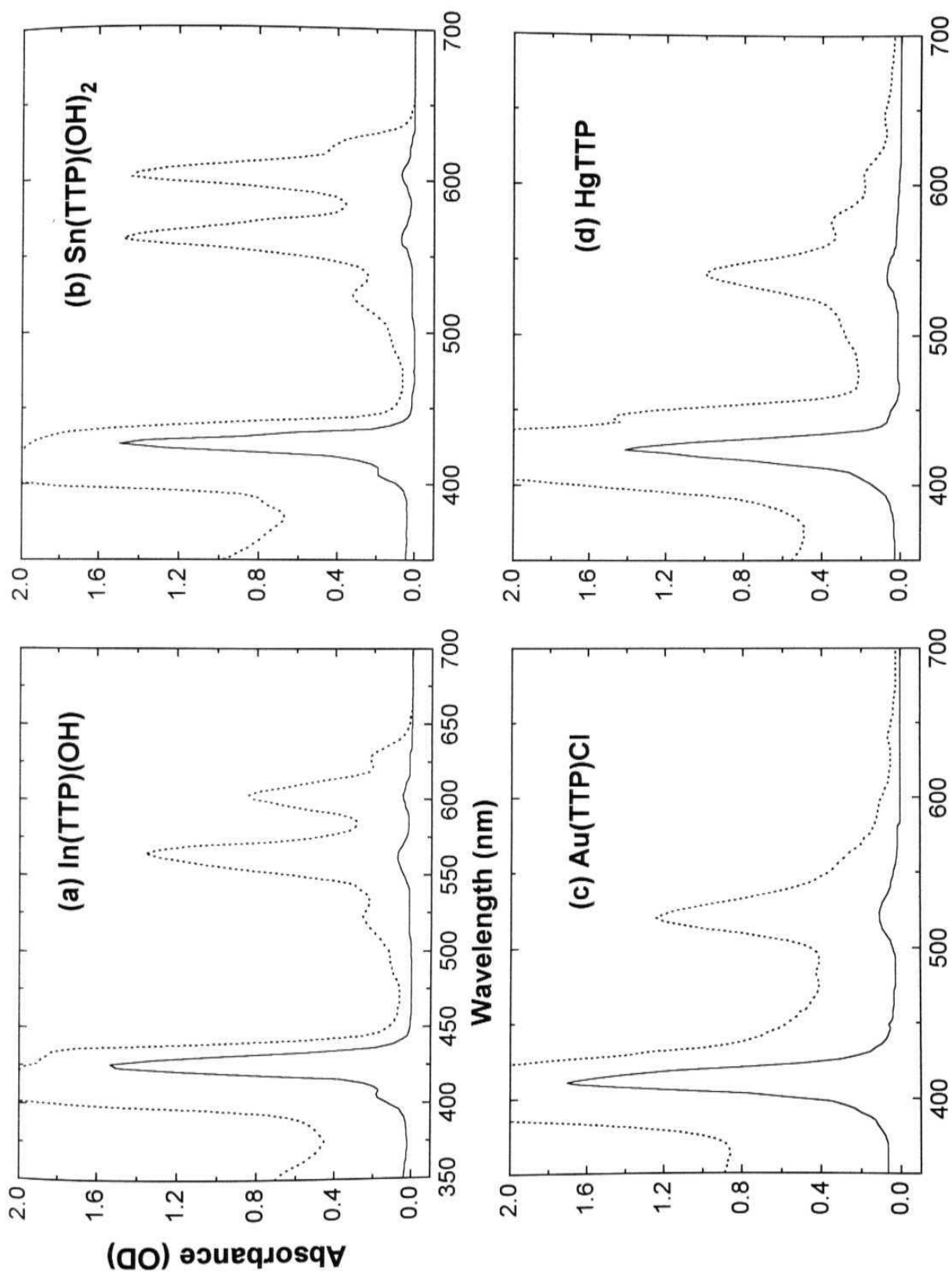
Fig. **4.5** Absorption spectra of **(a)** In(TTP)(OH) **(b)** Sn(TTP)(OH)$_2$ **(c)** Au(TTP)Cl **(d)** HgTTP
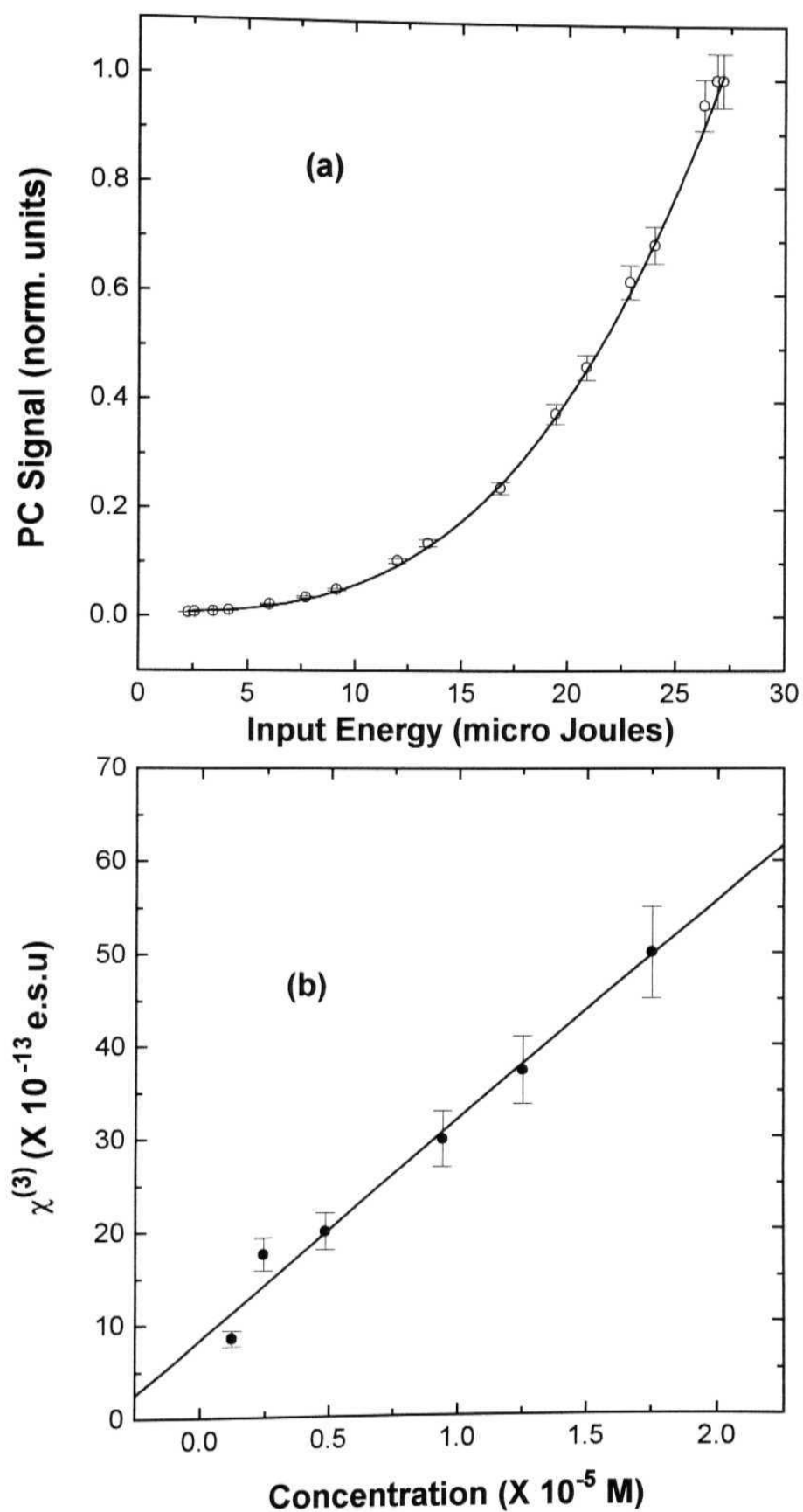
Fig. 4.6(a) Intensity dependence of the PC signal. (b) Concentration
dependence of the PC Signal.

show a similar behavior.   The calculated values of the cubic hyperpolarizability $\langle\gamma\rangle$, using equations (1) - (4), and the figure of merit F are given in table 2.   These are calculated using the equations

$$\chi_s^{(3)} = \left(\frac{n_0}{n_{ref}}\right)^2 \left(\frac{l_{ref}}{l}\right)\left(\frac{A}{A_{ref}}\right)^{\frac{1}{2}} \left(\frac{\alpha l \, \exp\left(\alpha l/2\right)}{1 - \exp(-\alpha l)}\right)\chi_{ref}^{(3)} \tag{1}$$

and

$$\langle\gamma\rangle = \frac{\chi^{(3)}}{L^4 N} \; ; \; L = \frac{n^2 + 2}{3} \tag{2}$$

Where 'n' is the refractive index, T is the length of the sample, 'A' is the coefficient of the cubic term of a least squares fit to the plot of PC signal versus input intensity, and a is the absorption coefficient.

For a solution of non-interacting particles, the effective $\chi^{(3)}$ assuming a pairwise additive model [16] is given by

$$\chi_{solution}^{(3)} = L^4 \left[N_{solvent}\,\gamma_{solvent} + N_{solute}\,\gamma_{solute}\right] \tag{3}$$

where N_{solute}, $N_{solvent}$ ate the number densities of molecules of the solute and the solvent respectively.   For dilute solutions with:

$N_{solute} = ((A*C)/M)$, we may write

$$\chi_{solution}^{(3)} = \chi_{solvent}^{(3)} + \frac{L^4 \gamma_{solute} A}{M} * C \tag{4}$$

with 'A' being the Avagadro's number, 'M' being the molecular weight and 'C' the concentration of the solute in g/ml. For lower concentrations the $|\chi^{(3)}|$ of the solution follows a linear relationship with respect to the concentration of the solute. $\chi^{(3)}$ mav have both real and imaginary components originating from the solute as well as solvent.   The real part is responsible for the nonlinear refraction whereas the imaginary part is responsible for nonlinear absorption, SA, TPA or ESA.   The real part can be positive or negative.   The figure of merit, independent of concentration, F is defined as $\chi^{(3)}/\alpha$. We have taken the value of $\chi^{(3)}$, for the reference sample CS_2, as

1.7 x 10^{-12} esu for ns pulses and 4.0 x 0^{13} esu for ps pulses [8,16] for the sake of consistency although other values of 6.8 x 10^{-12} esu for ns and 1.62 x $10''$ esu for ps pulses have been reported. L is the local field correction factor and N is the number density of the solute molecules in solution. The $\chi^{(3)}$ contribution from solvent is taken to be zero, as it is negligibly small in comparison to the solute.

Obviously, structural modifications to the porphyrin ring can be expected to result in molecules with diverse Photophysical and photochemical properties that will in turn affect their optical nonlinearity. Among the various factors involved, the atomic number of the central metal atom, redox potential of the ring and occurrence of excited-state absorption, nature of peripheral substituents, ring size require special mention [17]. The largest value of y is found to be ~ 725*10^{-30} esu for AuTTP with ns pulses and ~ 1.43*10^{-30} esu for CoTTP using ps pulses. It is also seen that for ns pulses SnTTP has the largest value of F (~ 323 x $10''^{13}$ cm.esu) whereas for ps pulses H$_2$TTP has the largest value (~ 7.24 x 10^{-13} cm.esu).

A close examination of the table 2 does not indicate any direct relation between the property and structure. Fig. 4.7 shows the variation of <y> and F as a function of the atomic number for both ns and ps pulse excitations. An examination of this figure does not reveal any heavy atom effect, and no obvious relationship can be established between the measured <y> value and the atomic number of the corresponding metal ion. Similarly the plot of <y> and F against the redox potentials (which is a measure of the extent of delocalization of π electron cloud) of the corresponding molecules, shown in fig. 4.8, also does not indicate an immediate relationship. Comparing the ns and ps y values of porphyrins, with Cr, Mn, Fe, and Ag as central metal ion, which have chlorine group attached to the axial part of the ring and same oxidation states (III), the heavy atom effect is clearly not seen. Similarly Co, Ni, Cu, Zn TTP's having an oxidation state of 11, and without any attachment to the ring, also does not show the heavy atom effect. Also since the nonlinear absorption [imaginary part of $\chi^{(3)}$] contributes to the total nonlinearity it is difficult to figure out any trend in the observed values. If there were an electron-donating (to the ring) group attached the effect would be to increase the nonlinearity. But if the one without any group has large nonlinear absorption it would also have the
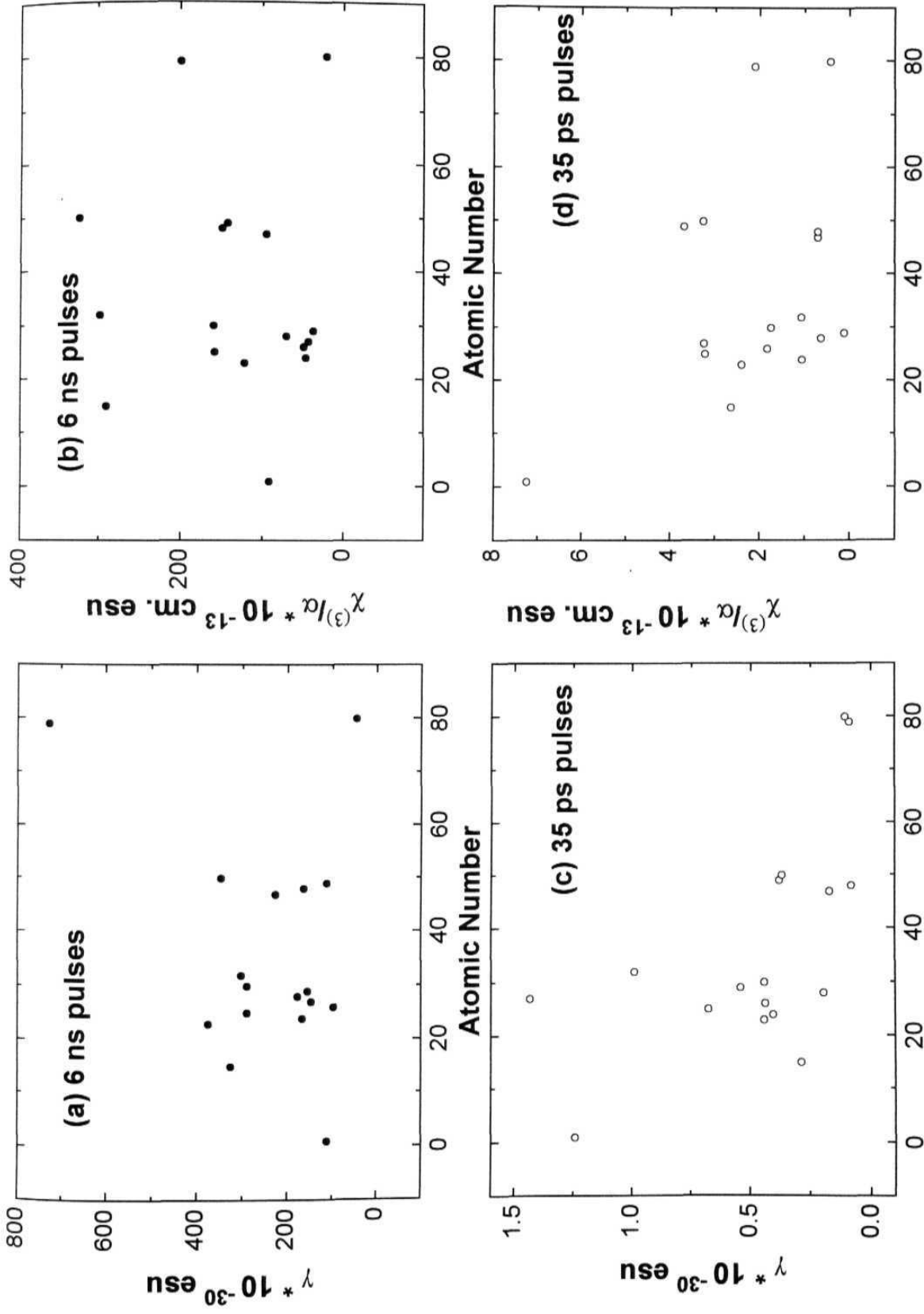
Fig. 4.7 (a),(c) γ plotted as a function of atomic number for 6 ns and 35 ps pulses (b),(d) Figure of merit $F = \chi^3 l_\alpha$ plotted as a function of atomic number for 6 ns and 35 ps pulses respectively
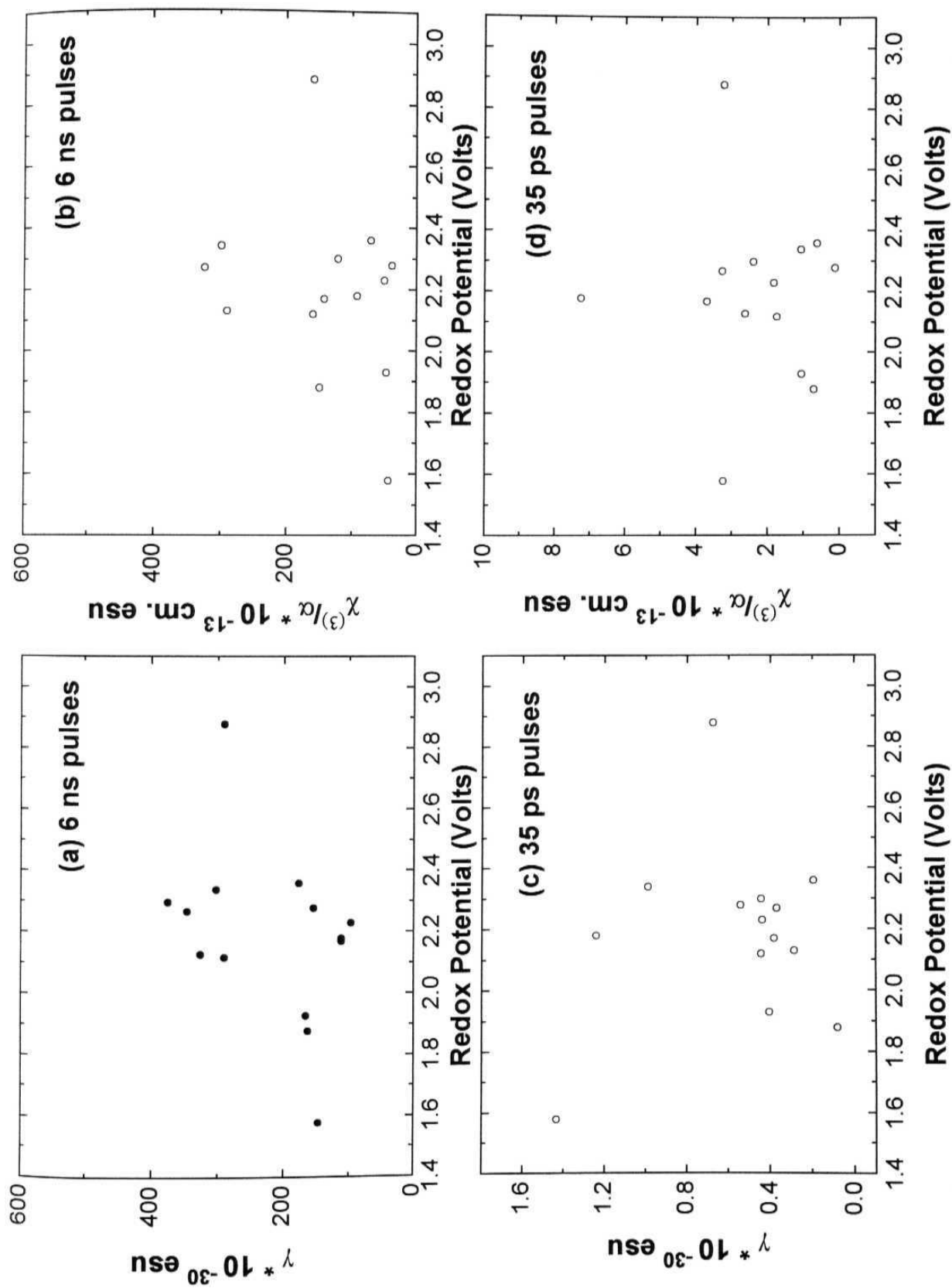
Fig. 4.8 (a),(c) γ plotted a a function of redox potential for 6 ns and 35 ps pulses (b),(d) Figure of merit $F=\chi^3 l\alpha$ plotted as a function of redox potential for 6 ns and 35 ps pulses respectively

same effect of enhancing the nonlinearity. Hence it is premature to comment on the structure-property relationship with the present date available. More detailed studies, with different pulse widths, are needed in this direction to figure out the exact relationship.

Open aperture Z-scans with ns pulses show deeper valleys for those samples which are found to have higher <y> values as measured from the DFWM experiments. Figures 4.9 (a) and 4.9 (c) shows the closed aperture Z-scans for AuTTP and NiTTP. All the samples are found to exhibit similar behavior, indicating a negative nonlinearity as evidenced by the peak occurring at negative Z values in the scan. Because of the near-resonant excitation, this negative nonlinearity in the ns time scales could be due to the thermal excitation of the medium. Figures 4.9 (b) and 4.9 (d) shows typical open aperture Z-scans, for the samples AuTTP and NiTTP. Depending on the pulse duration, pump intensity and wavelength, nonlinear absorption can be from (a) the ground state So to higher excited singlet states S_n (two-photon or multi-photon excitation), (b) the first excited singlet state S_1 to higher excited states S_n, or from (c) the T_1 to T_n states in the triplet manifold. The last two processes are known as excited state absorption (ESA), but if their cross sections are larger than that of linear absorption, then these are referred to as reverse Saturable absorption (RSA). We attribute the observed nonlinear absorption to strong ESA or RSA. Typical peak intensities at the focus are in the range of 10 to 10 W/cm . Figure 4.10 shows the open aperture Z-scan for InTTP using 35 ps pulses. In this case, however, the triplet contribution to the nonlinear absorption can be much less due to the decreased intersystem crossing (which is ~ few hundred ps) as compared to ns excitation [17,18].

4.3.1 Origin of large nonlinearity in the ns regime

On comparing the <y> values of our compounds with other Porphyrins [26-45], the ns values are found to be three orders of magnitude larger than any of them. When the probe polarization is made normal to the pump beams, the PC signal gets reduced by only one-third of the original value (when all beams are co-polarized) indicating that the nonlinearity is predominantly electronic in origin [19] and thermal
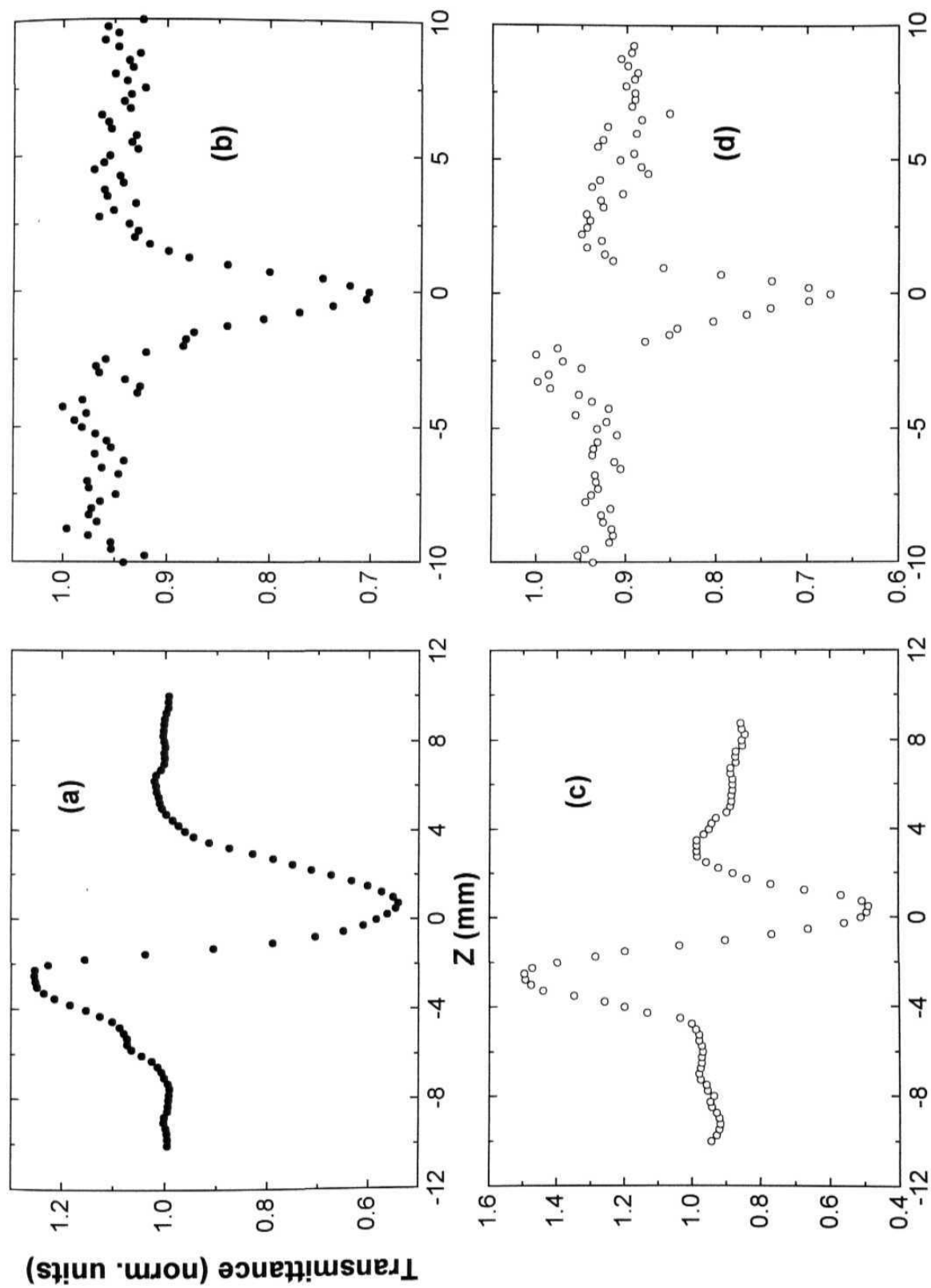
Fig. **4.9** Closed aperture scans for samples (**a**) AuTTP and (**c**) NiTTP. Open aperture scans for (**b**) AuTTP and (**d**) NiTTP
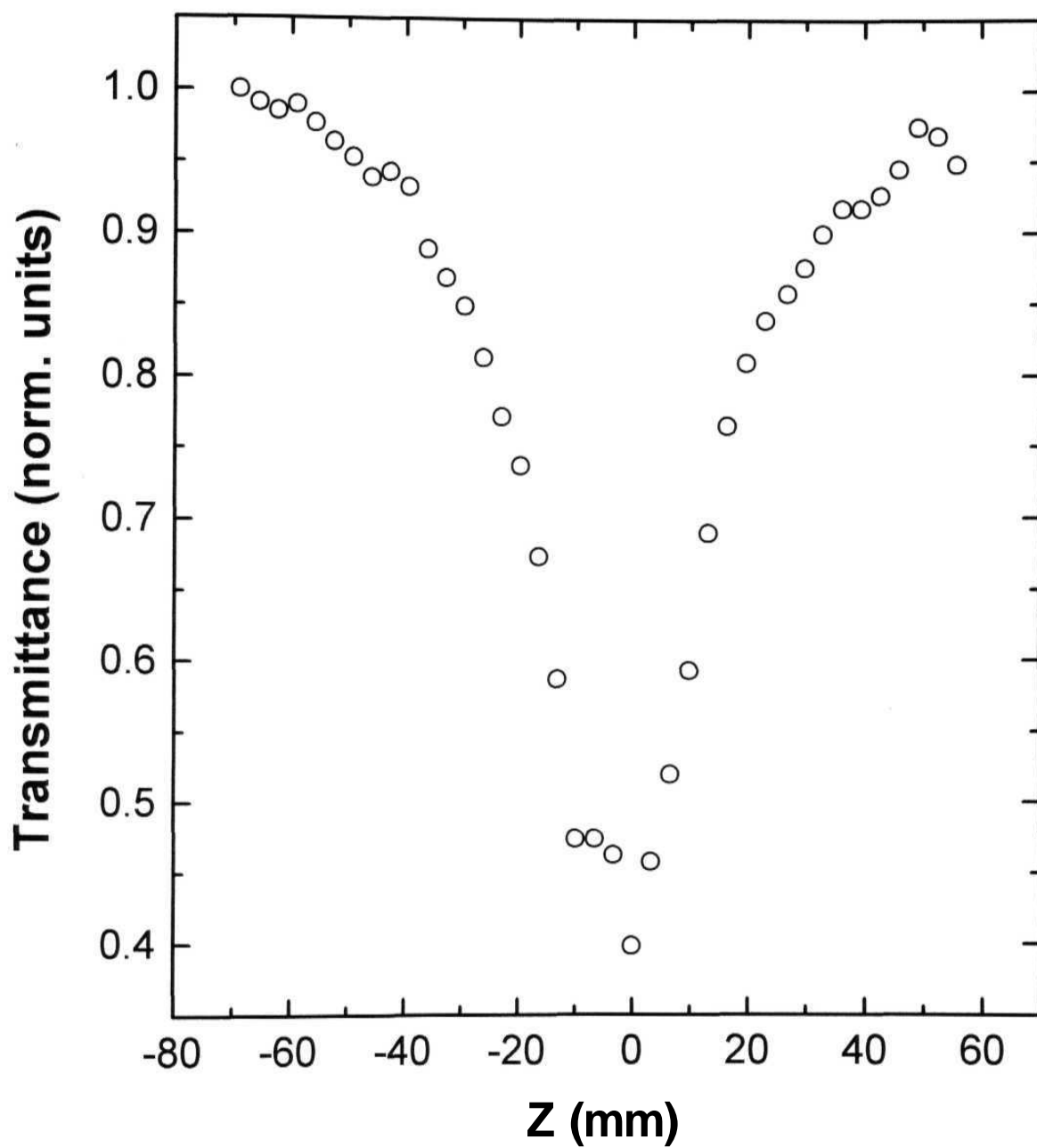
Fig. 4.10 Open aperture Z-scan of InTTP with 35 ps pulses

effects are not dominant. We observe very strong ESA, due to fast intersystem crossing rate compared to the pulse width, in all the open aperture Z-scan data recorded with the ns pulses. A significant contribution to this large value of $<\gamma>$, therefore, comes from the long-lived and excited triplet states in addition to the excited singlet states. The concentration dependence of the $\chi^{(3)}$ value [fig. 4.6 (b)] clearly indicates the strong contribution of imaginary part to the total nonlinearity compared to real part. It is well established that ESA is an intensity dependent process and will dominate at higher intensity levels. This is well supported by our $\chi^{(3)}$ measurements at different input intensity levels whereby we observe an enhancement by a factor of three to four in its value. $\chi^{(3)}$ measurements on the sample AuTTP give a value of 10 x 10^{-12} esu at an input of ~ 2 mW (corresponding peak intensity at focus is ~ 100 MW/cm^2) and a value of ~ 30 x10^{-12} esu at an input of ~ 6 mW (corresponding peak intensity at focus is ~ 300 MW/cm) for the same sample concentration. A log-log plot of input energy versus PC signal shown in fig. 4.11 gives a slope of < 3 at lower intensities and a slope of ~ 5 at higher intensities suggesting nonlinearity contributions from higher excited states.

Equally large $<\gamma>$ values have been observed using dye laser pumping also, when excited at 595 nm. At this wavelength these compounds have a stronger two-photon absorption [20-21] as compared to 532 nm. Earlier reports show the excited state enhancement of the nonlinearity in linear conjugated molecules [22] and a square planar complex [23]. Those experiments were performed in the presence of a strong pump beam. In polyphenyls [24], the observed enhancement was due to strong Two-Photon Absorption (TPA). In a porphyrin heterodimer [25] and in an azo-benzene material [26], the enhancement was due to the presence of highly populated excited states. In Porphyrins, larger excited state cross-section probes the nonlinearity due to S_n and T_n apart from S_1 and T_1 states. Time resolved studies using incoherent light and ps pulses, the results of which are presented in the next chapter, do suggest the distribution of population in different excited states and very fast relaxation time associated with these states.

Rodenberger et al. [26] found a new way to achieve large nonlinearities through excited-state population. In that case a strong pump beam acting on the
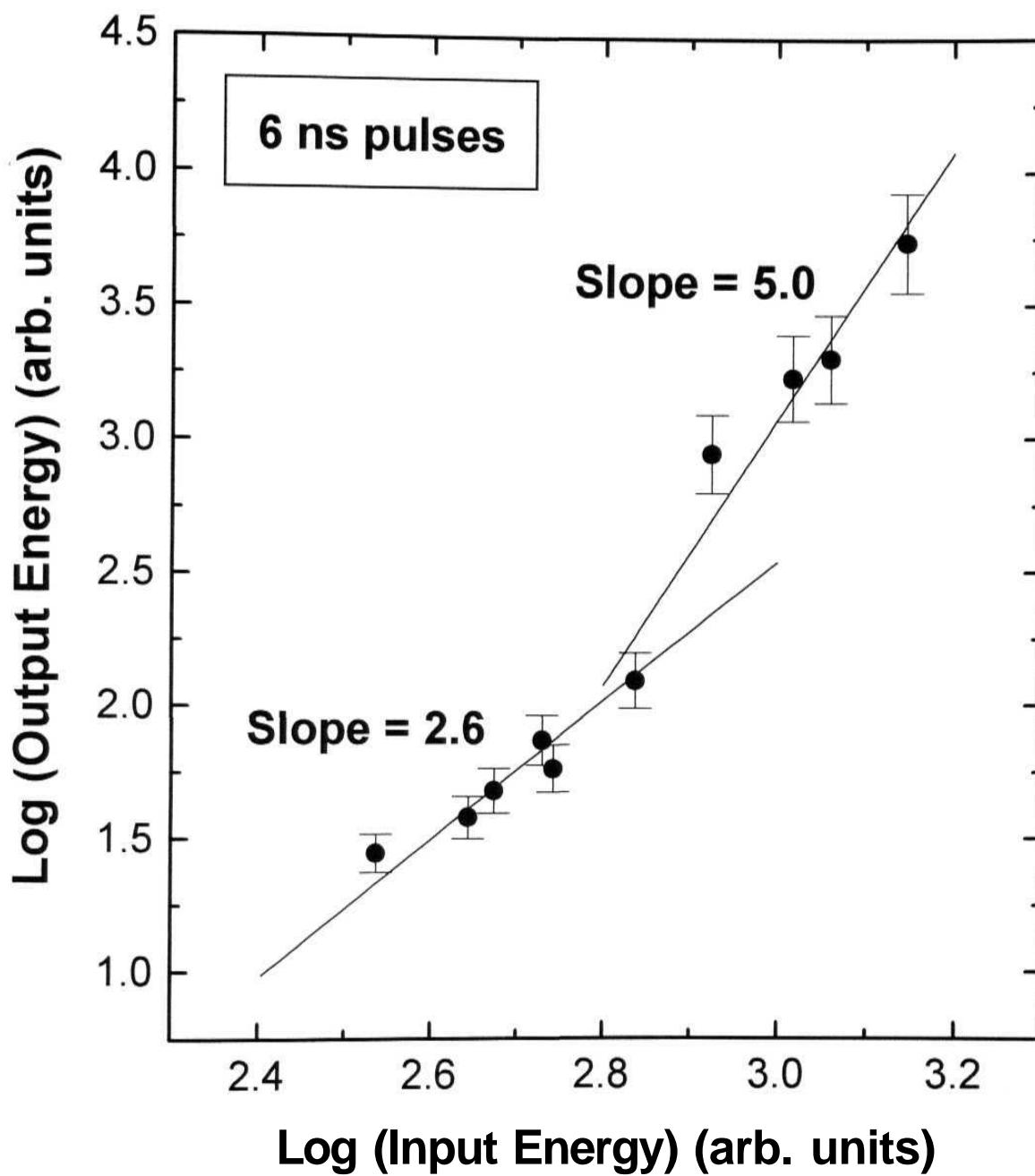
Fig. 4.11 Intensity dependence of PC signal. At lower intensities
the slope is < 3 and at higher intensities the slope is ~ 5

molecule excites the molecule to higher states and a probe is used for measurement of the nonlinearity. In our case due to strong excited state absorption the population is distributed among the excited states with the pump pulse itself. Si et al. reports the fluence dependence of nonlinear optical response of cadmium texaphyrin [27] using time-resolved DFWM at 532 nm. They argue that at lower fluences of excitation, the nonlinearity mainly arises from the first excited singlet and triplet states since the population in the higher excited states is small. In this case two response times, one fast and one slow, characterized the NLO response. The fast component was from the singlet state and the slow one from triplet state. At higher fluences the higher excited states also contribute, due to significant amount of population, to the total nonlinearity and the response will have three components, fastest one due to the higher states added to the fast and slow components observed at lower fluences. Using ns pulses we observed very large nonlinearities. It has been shown that while using ns pulses the excitation could lead the population to any of the higher excited states [28]. The time response of the PC signal, at 600 nm using ns pulses, has three components (details of the complete dynamics of excited states are presented in the next chapter) and it is found to be independent of the input intensity. This again confirms the contribution of different excited states to the total nonlinearity. With ps pulses we could achieve reasonably large nonlinearities. *By* suitable structural modifications, like increasing the intersystem crossing rate and enabling the population being transferred to triplet state, these compounds could be improved for even larger nonlinearities.

4.3.2 Comparison with other class of porphyrins

Rao et al. [7,8] report the largest γ values for some of the Tetrabenzporphyrins [10 x 10^{-30} esu. for Zinc meso-tetra-(p-dimethylaminophenyl) tetrabenzporphyrin] using 30 ps pulses. They observed that those Porphyrins having electron donating meso-phenyl groups showed large $\chi^{(3)}$ values. Our results on Tetratolyl Porphyrins using 35 ps pulses show a value of 2.4 x 10^{-30} esu for CoTTP (assuming a $\chi^{(3)}$ value of 6.8 x 10^{13} esu for CS_2) which is comparable to the TBP. Advantages of tetraarylporphyrins over tetrabenzporphyrins are that they are easy to synthesize, have a high thermal and chemical stability, and have a longer shelf life. We can also

compare the ps nonlinearity magnitudes with that observed in other kind of Porphyrins - for example those reported for basket handle Porphyrins by Kumar et al [9]. We find that the present molecules have larger nonlinearity in comparison to those Porphyrins. The difference could be attributed to the higher electron delocalization in the present set of molecules and/or due to the strong excited state absorption as argued earlier. Meloney et al. [8] reported the third order NLO properties several tetraphenylporphyrins. The samples studied were TPP, ZnTPP, and CoTPP dissolved in toluene with DFWM at 532 nm and the calculated $\chi^{(3)}$ values using thermally induced refractive index changes were $2.07*10^{-11}$ esu, $2.0*10^{-11}$ esu, and $1.21*10^{-11}$ esu respectively. Sakaguchi et al. [8] measured $\chi^{(3)}$ values for 5,10,15,20-tetrakis(4-n-pentadecylphenyl) Porphyrins containing Co, Ni, Zn, Cu, and Vo as the central metals and found that all the samples had value in the range $\sim 10^{-11}$ esu and showed a concentration dependence. The effect of central metal on the nonlinearity was found to be small and the reason could be the substitution of bulky alkyl chains on phenyl rings.

Guha et al. [8] working with ns and ps pulses on some of the benzoporphyrins reported by Rao et al. observed that imaginary part of $\chi^{(3)}$ and y was dominating compared to the real part. Hosoda et al. [9] measured $\chi^{(3)}$ values of spin-coated films of metal-free octaethyl porphyrin (H_2OEPP), MnCl-Octaethylporphyrin (MnCl-OEPP), N'N"N'"N""- tetramethyl - otcaethylporphyrin - bistriflouroacetate (TMOEPP) by THG at 1.9 μ. The $\chi^{(3)}$ value of TMOEPP was found to be 5 times larger than H_2OEPP indicating the effect of increased number of π electrons in the cyclic conjugated chain. Norwood et al. [10] working with 1 ps pulses at 598 nm observed values of $\chi^{(3)}_{xxxx}$ and $\chi^{(3)}_{xyyx}$ as $1.17*10^{-11}$ esu and $3.03*10^{-12}$ esu respectively for a magnesium octaphenyl tetrazoporphyrin (Mg-OPTAP) with 5% weight incorporated in a PMMA film. The value of $\chi^{(3)}_{xxxx}/\chi^{(3)}_{xyyx}$ was found to be ~ 3 indicating that the nonlinearity is predominantly electronic in origin. The response time measured using DFWM was ~ 44 ps.

Anderson et al. [10] performed electro-absorption measurements on soluble conjugated porphyrin polymer and measured the value of χ (-co; 0, 0, ca) as $\sim$

$7.3*10^{-8}$ esu at the peak resonance. Bao et al. [10] synthesized metal-free and Zn-containing new monomeric and polymeric Porphyrins. The $\chi^{(3)}$ value measured at 532 nm using DFWM was $\sim 10^{-10}$ esu for thin films. The polymer solutions in chloroform and THF showed $\chi^{(3)}$ values with lesser magnitude of two orders less when compared to thin films. The value of Zn-porphyrin was twice that of metal-free porphyrin in THF solution.

4.4 Conclusions

1. We have synthesized a set of Tetra Tolyl Porphyrins, with sixteen different metal ions in the ring, and studied their third order nonlinear optical properties with 6 ns and 35 ps pulses. We observe a large negative nonlinearity in these molecules when pumped by ns pulses and ps pulses.

2. For ns pulse excitation AuTTP has the highest y value of $\sim 725*10^{-30}$ esu and for ps pulse excitation CoTTP has the highest value of y of $\sim 1.4*10^{-30}$ esu. A figure of merit is defined as $F = \chi^{(3)}/\alpha$ and SnTTP has the largest value of F (~ 323 x 10^{-13} cm.esu) for ns pulses whereas for ps pulses H2TTP has the largest value (~ 7.24 x 10^{-13} cm.esu).

3. The large values of nonlinearity are attributed due to higher excited singlet and triplet states being populated through strong ESA at 532 nm and TPA at 600 nm. There is no definite trend observed in the $\chi^{(3)}$ values with respect to atomic number and redox potential. This could be due to the contribution from various factors to the total nonlinearity like the atomic number, nonlinear absorption, electron donating groups attached to the ring, and thermal part.

4. The strong nonlinear absorption at both 532 nm and 595 nm show that these molecules are promising candidates for efficient optical limiting at these and a nearby range of wavelengths. From the time-resolved DFWM data the nonlinearity is found to have an ultrafast response time in the order of fs to ps. Thus these molecules, with their large nonlinearity properly combined with ultra-fast response times, can become potential candidates for various photonic applications.

Compound	Soret band λ_{max} , nm (log ε)	Q-Bands λ_{max} , nm (log ε)			
H_2TTP	418 (5.55)	516 (4.24)	551 (3.98)	592 (3.73)	648(3.8)
$[P(TTP)(OH)_2]^+$	432 (5.35)	522 (3.48)	560 (4.20)	603 (3.79)	
V(O)TTP	424 (5.42)	547 (4.17)	584 (3.37)		
Cr(TTP)Cl	435 (5.26)	520 (4.12)	566 (4.17)	603 (4.12)	
Mn(TTP)Cl	478 (4.91)	526 (3.78)	577 (4.00)	613 (4.03)	
Fe(TTP)Cl	416 (5.01)	508 (4.11)	575 (3.52)	691 (3.50)	
CoTTP	411 (5.23)	529 (4.10)			
NiTTP	415 (5.27)	527 (3.98)	615 (3.15)		
CuTTP	415 (5.48)	538 (4.26)	570 (3.47)		
ZnTTP	419 (5.62)	549 (4.34)	588 (3.78)		
Ge(TTP)(OH)$_2$	421 (5.50)	517 (3.40)	555 (4.12)	594 (3.92)	
Ag(TTP)Cl	425 (5.17)	541 (3.99)	575 (3.47)		
CdTTP	429 (5.31)	526 (3.49)	564 (4.03)	605 (3.90)	
In(TTP)(OH)	426 (5.46)	522 (3.47)	561 (4.16)	602 (3.99)	
Sn(TTP)(OH)$_2$	426 (5.47)	523 (3.50)	562 (4.16)	603 (4.15)	
Au(TTP)Cl	412 (5.35)	522 (4.12)			
HgTTP	426 (5.17)	542 (3.92)	575 (3.47)		

Table 4.1 UV-Visible Data[a]

(a) Spectra were taken in $CHCl_3$. Error limits: λ_{max}, ± 1 nm; s, $\pm 7\%$

Compound (Redox Potential)	Y (6 ns) (10^{-30} esu)	$F = \chi^{(3)} / \alpha$ (10^{13} cm. esu)	Y (35 ps) (10^{-30} esu)	$F = \chi^{(3)} / \alpha$ (10^{13} cm. esu)
H_2TTP (2.18 V)	111.40	91.50	1.240	7.24
$[P(TTP)(OH)_2]^+$ (2.13 V)	325.50	289.33	0.286	2.62
V(O)TTP (2.30) V	375.00	121.13	0.442	2.39
Cr(TTP)Cl (1.93 V)	166.25	45.93	0.403	1.04
Mn(TTP)Cl (2.88 V)	289.5	158.01	0.674	3.21
Fe(TTP)Cl (2.23 V)	96.25	48.78	0.437	1.82
CoTTP (1.58)	146.75	42.65	1.432	3.23
NiTTP (2.36 V)	177.25	69.95	0.193	0.62
CuTTP (2.28 V)	154.25	37.05	0.541	0.11
ZnTTP (2.12 V)	289.75	158.83	0.442	1.73
$Ge(TTP)(OH)_2$ (2.34 V)	302.00	297.5	0.988	1.06
Ag(TTP)Cl '(-)	226.50	94.58	0.170	0.69
CdTTP (1.88 V)	162.50	148.53	0.079	0.70
ln(TTP)(OH) (2.17 V)	111.25	142.00	0.380	3.69
$Sn(TTP)(OH)_2$ (2.27 V)	346.25	322.75	0.368	3.26
Au(TTP)Cl (-)	725.00	198.93	0.088	2.10
HgTTP (-)	45.25	20.65	0.106	0.42

Table 4.2 Calculated values of *y* and figure of merit F using 6 nsec and 35 psec pulses.

4.5 References

1. DS. Chem la, J. Zyss, Eds., *Nonlinear Optical Properties of Organic Molecules and Crystals*, Vols., 1 and 2, Academic Press, Orlanda, FL, USA, (1987); S.R. Marder, J.E. Sohn, G.D. Stucky, Eds., *Materials for Nonlinear Optics: Chemical Perspectives*, ACS Symposium Series, American Chemical Society, Washington , DC (1991); P.N Prasad and D.J. Williams, *Introduction to Nonlinear Optical Effects in Molecules and Polymers,* Wiley, New York, (1991); H.S. Nlawa, *Adv. Mater.* 5, 341, 1993; J.L. Bredas, C. Adant, P. Tackx, and A. Persoons, Chem. Rev. 94, 243 1994; *Molecular Nonlinear* Optics, Ed. J. Zyss, Academic, NewYork, USA, 1994; Handbook *of Organic Conductive Molecules and Polymers*, Vol.'s 1-4, Ed. H.S. Nalwa, John Wiley and Sons, USA, 1997.

2. M. Gouterman, *The Porphyrins*, Vols. I-VII, D. Dolphin Ed., Academic Press, New York, (1978); K. Smith, *Porphyrins and Metalloporphyrins,* Amsterdam, The Netherlands: Elsevier/North-Holland Biomedical Press, (1976); M. Gouterman, P. Rentzepis, Ed.'s, *Porphyirns: Excited State and Dynamics*, Am. Chem. Soc. Symp. Ser. **321,** 1987; H.S. Nalwa and S. Miyata, Eds., *Nonlinear Optics of Organic Molecules and Polymers,* CRC Press Inc., USA, 1997; M. Ravikanth and G.R. Kumar, *Current Science* **68,** 1010, 1995; F.J.Aranda, *PhD. Thesis* submitted to University of Massachusetts, Boston, USA, 1995; H.L. Anderson, *Chem. Commun.* 2323, 1992

3. W. Blau, H. Byrne, W.M. Dennis, and J.M. Kelly, *Opt. Commun.* **56,** 25, 1985; J. Si, M. Yang, L. Zhang, C. Li, D. Wang, S. Dong, and W. Sun, *Appl Phys. Lett.* **64,** 3083, 1994; G.L. Wood, M.J. Miller, A.G. Mott, *Opt. Lett.* **20,** 973, 1995; A. Sevian, M. Ravikanth, G.R. Kumar, *Chem. Phys. Lett.* **263,** 241, 1996; P. Chen, I.V. Tomov, A.S. Dvornikov, M. Nakashima, J.F. Roach, DM. Alabran, and P.M. Rentzepis, *J. Phys. Chem.* **100,** 17507, 1996; N. Tang, W. Su, T. Cooper, W. Adams, D. Brandelik, M. Brant, D. McLean, and R. Sutherland, Proc. SPIE **2853,** 149, 1996; S.R. Mishra, H.S. Rawat, M. Laghate, *Optics Commun.* **147,** 328, 1998; W. Su, T.M. Cooper, and M.C. Brant, *Chem. Mater.* **10,** 1212, 1998; F.M. Qureshi, S.J. Martin, X. Long, D.D.C. Bradley, F.Z. Henari, W.J. Blau, EC. Smith, C.H. Wang, A.K. Kar, and H.L. Anderson, *Chem. Phys.* **231,** 87, 1998; K. Dou, X. Sun, X. Wang, R. Parkhill, Y. Guo, and E.T. Knobbe, *Solid State Comminucations* **107,** 101, 1998.

4. Z Bao and L. Yu, Trends in *Polymer science* 3(5), 159, 1995; R.W. Wagner and J.S. Lindsey, *J. Am. Chem. Soc.* **116,** 9759, 1994; MP. O'Neil, M.P. Niemczyk, WA. Svec, D. Gosztola, G.L. Gaines III, MR. Wasielewski, *Science* **257,** 63, 1992; M.J. Crossley, and PL. Burn,./. *Chem. Soc, Chem. Commun.* 1569, 1991; MR. Wasieleski, *Chem. Rev.*, 92, 435, 1992; H. Segawa, N. Nakayama, and T. Shimidzu,*J. Chem. Soc, Chem. Commun.* 784, 1992.

5. N. Kobayashi, W.A. Nevin, S. Mizunuma, H. Awaji and M. Yamaguchi, *Chem. Phys. Lett.* **205,** 51, 1993.

6. D.V.G.L.N. Rao, F.J. Aranda, D.E. Remy, J.F. Roach, *Int.J. Nonlinear Opt. Phys.* 3(4), 511, 1994.

7. B. Meunier, *Chem. Rev.* 92, 1411, 1992; B.W. Handerson and T.J. Dougherty, *Photodynamic therapy: Basic principles and clinical applications*, Marcel Dekker, NewYork, (1992).

8. C. Meloney, H. Byrne, W.M. Dennis, W. Blau, and J.M. Kelly, *Chem. Phys.* **121,** 21, 1988; D.V.G.L.N. Rao, F.J. Aranda, J.F. Roach and DE. Remy, Appl. Phy. Lett. **58,** 1241, 1991; S. Guha, K. Kang, P. Porter, J.F. Roach, D.E. Remy, F.J. Aranda, and D.V.G.L.N. Rao, *Opt. Lett.* **17,** 264, 1992; T. Sakaguchi, Y. Shimizu, M. Miya, T. Fukumi, K. Ohta, and A. Nagata, *Chem. Lett.* 281, 1992; J. Qin, T. Wada, and H. Sasabe,*Mol. Cryst. Liq. Cryst.* **217,** 47, 1992.

9. M. Hosoda, T. Wada, A.F. Garito, and H. Sasabe, *Jpn. J. Appl, Phys.* 31, L249, 1992; K.S. Suslick, C. -T. Chen, G.R. Meredith, and L -T. Cheng, ./. *Am. Chem. Soc.* **114,** 6928, 1992; L.X. -Q. Chen, Proc. *SP1E* **1852,** 162, 1993; F.Z. Henari, W.J. Blau, L.R. Milgrom, G. Yahioglu, D. Phillips, and J.A. Lacey, *Chem. Phys. Lett.* **267,** 229, 1997; G.R. Kumar, M. Ravikanth, S. Banrjee, A. Sevian, *Opt. Commun.* **144,** 245, 1997; M. Terazima, H. Shimizu, and A. Osuka,./. *Appl. Phys.*, **81,** 2946, 1997; K. Kandasamy, S.J. Shetty, P.N. Puntabekar, T.S. Srivastava, T. Kundu, and B.P. Singh,*J. Chem. Soc, Chem. Commun.* 1159, 1997; D. Beljonne, GE. O'Keefe, P.J. Hamer, R.H. Friend, H.L. Anderson, and J.L. Bredas, *J. Chem. Phys.*, 106,9439, 1997.

10. H.L. Anderson, S.J. Martin, and D.D.C. Bradley, *Angew. Chem. Int. Ed. Eng.* 33, 655, 1994; R.V. Honeychuck, *Polym. Preprints* 32, 138, 1992; Z. Bao and L. Yu, *Proc. ACS Meeting Polym. Mater. Sci.Eng.*, *PMSE* 71, 781, 1994; R. A. Norwood and J.R. Sounik, *Appl. Phys. Lett.* 60, 295, 1992.

11. M. Brunei, F. Chaput, S.A. Vinogradov, B. Campagne, M. Canva, J.P. Boilot, and A. Brun, *Chem. Phys.* **218,** 301, 1997; K. Dou, X. Sun, X. Wang, R. Parkhill, Y. Guo, and E.T. Knobbe, *IEEE J. Quantum Electron.* **35,** 1004, 1999.

12. K. Kandasamy, K.D. Rao, R. Deshpande, P.N. Puntabekar, B.P Singh, S.J. Shetty, and T.S. Srivastava, *Appl Phys.* **B64,** 479, 1997.

13. R. Dorsinville, L. Young, R.R. Alfano, R. Zamboni, R. Daniels, G. Ruane, and C. Taliani, *Opt. Lett.* **14,** 1321, 1989; M. Zhao, Y. Cui, M. Samoc, P.N. Prasad, M.R. Unroe, and B.A. Reinhardt, *J. Chem. Phys.* **95,** 3991, 1991.

14. M. Sheik-Bahae, A.A. Said, T. -H. Wei, D.J. Hagan, E.W. Van Stryland, *IEEE J. Quantum Electron.* 26,760, 1990.

15. J. -H. Furhorp, K.M. Smith, In *Porphyrins and Metalloporphyrins*; K.M. Smith, Ed., Elsevier : Amsterdam, 769, 1975; T. Barbour, W.J. Belcher, P.J. Brothers, C.E.F. Rickard, D.C. Ware, *Inorg. Chem.* **31,** 746, 1992; K.M. Kadish, Q.Y.Y. Xu, B.G. Maiya, J.-M. Barbe, R. Guilard, *J. Chem. Soc. Dalton Trans.*, 1531, 1989; J.E. Maskasky, M.E. Kenney, *J. Am. Chem. Soc.* **95,** 1443, 1973; R.G. Little, *J. Heterocycl. Chem.* **15**, 203, 1978.

16. M. -T. Zhao, B.P. Singh, and P.N. Prasad, J. Chem. Phys. **89,** 5535, 1988.

17. D.J. McGraw, A.E. Seigman, G.M. Wallraff, and R.D. Miller, *Appl. Phys. Lett.* **54,** 1713, 1989.

18. A. Harriman, *J.C.S. Faraday I* 76, 1978, 1980; A. Harriman, *J.C.S Faraday I* 77, 369, 1980; A. Harriman, *J.C.S. Faraday I* 77, 1281, 1980.

19. J.S. Shirk, J.R. Lindle, F.J. Bartoli, C.A. Hoffman, Z.H. Kafafi, and A.W. Snow, *App. Phys. Lett.* **55,** 1287, 1989; D.V.G.L.N. Rao, F.J. Aranda, J.F. Roach and D.E. Remy, Appl. Phy. Lett. **58,** 1241, 1991; W. Su, T.M. Cooper, K. Nguyen, M.C. Brant, D. Brandelik, and D.G. McLean, Proc. SPIE 3472, 136, 1998.

20. D.N. Rao, S.V. Rao, F.J. Aranda, D.V.G.L.N. Rao, and M. Nakashima, *J. Opt. Soc. Am.* **B14,** 2710, 1997; S.V. Rao, L. Giribabu, B.G. Maiya, and D.N. Rao, Current Science 72, 957, 1997.

21. S.V. Rao, N.K.M.N. Srinivas, L. Giribabu, B.G. Maiya, R. Philip, G.R. Kumar, and D.N. Rao, Submitted to *Opt. Commun.*; S.V. Rao, N.K.M.N. Srinivas, L. Giribabu, B.G. Maiya, R. Philip, G.R. Kumar, and D.N. Rao, Submitted to *J. Opt. Soc. Am. B*.

22. D.C. Rodenberger, J.R. Heflin, and A.F. Garito, *Nature* **359,** 309, 1992; D.C. Rodenberger, J.R. Heflin, and A.F. Garito, *Phys. Rev.* **A51,** 3234, 1995

23. J. Si, Q. Yang, Y. Wang, P. Ye, S. Wang, J. Qin, and D. Liu, *Opt. Commun.* **132,** 311, 1995.

24. M. Zhao, Y. Cui, M. Samoc, P.N. Prasad, M.R. Unroe, and B.A. Reinhardt, J. *Chem. Phys.* 95, 3991, 1991.

25. J. Si, Y. Wang, Q. Yang, P. Ye, H. Tian, Q. Zhou, and H. Xu, *Appl. Phys. Lett.* 69, 1832, 1996.

26. H. Yanping, S. Zhenrong, D. Liangen, W. Zugeng, *Chinese J. Lasers* B7, 560, 1998.

27. J. Si, Y. Wang, J. Zhao, P. Ye, D. Wang, W. Sun, And S. Dong, Appl. Phys. Lett. 67, 1975, 1995;

28. S.V. Rao, D.N. Rao, J.A.Akkara, B.S.DeCristofano, and D.V.G.L.N.Rao, *Chem. Phys. Lett.* 297,491, 1998.

CHAPTER 5

Excited State Dynamics in Tetra Tolyl Porphyrins Studied Using Incoherent Light and 35 Psec Pulses.

This chapter presents our experimental results on the excited state dynamics in several Tetra Tolyl Porphyrins (with different central metal-ions) studied using Degenerate Four Wave Mixing with incoherent light (DFWM-IL) and 35 ps pulses (DFWM-PS). Incoherent studies indicate three life times for all the samples, which have been attributed to different excited states. The shortest component, 170 fs, is due to the dephasing in the S_n states, the 3-6 ps component is due to the vibrational relaxation in the Frank-Condon states of S_1 state (S_{1v} to S_{10}) and the longest component ~ 20 - 70 ps is due to the population relaxation from S_{10} to S_0. Results obtained with ps pulses, in standard backward DFWM geometry, also indicate similar lifetimes for population relaxation substantiating our incoherent studies.

5.1 Introduction

The last two decades have witnessed an extensive research activity in the nonlinear optical, Photophysical and photochemical properties of organic materials in general and metalloporphyrins/related compounds in particular. The interest in metalloporphyrins is many-fold, some of which are (a) The part they play in some of the most important natural processes, (b) These molecules are found to have strong nonlinearities and fast response times, the desired criteria for making useful photonic devices, (c) Transition metal Porphyrins have strong electronic transitions in the visible and ultraviolet region, making them experimentally very attractive, (d) Synthetic and spectroscopic studies of these molecules provide extensive information about the bonding and the structure. Study of the nonlinearity and elucidation of the dynamics associated with excited states of such molecules is important from a fundamental as well as technological point of view. There are several reports on electronic deactivation kinetics in these molecules which provide a firm base to identify transient species existing on the ultra-short time scale [1-3]. The measured values of cubic hyperpolarizabilities are as high as 10^{-29} esu [4] and responses as fast as few hundreds of fs to ps [5-10]. Methods for the study of excited state solvation and vibrational relaxation dynamics, fluorescence from high lying states in a variety of metalloporphyrins (and similar molecules) have included transient absorption

spectroscopy, transient grating spectroscopy, pump-probe technique and Raman spectroscopy [11-20]. Different relaxation pathways as well as the effects of solvent, temperature and metal-ions have been extensively investigated using ps and fs laser pulses.

We have synthesized Tetra Tolyl Porphyins (TTP) with sixteen different metal ions in the ring and studied their third-order optical nonlinearity and nonlinear absorption using the techniques of degenerate four wave mixing (DFWM) and Z-scan. Our studies, using both ns and ps excitations, showed that these molecules exhibit a large nonlinear absorption and a strong refractive nonlinearity [21]. We extended these studies to the excited state dynamics in these molecules. It is well established that for lowest singlet and triplet states the energy dissipation is strongly affected by the characteristics of the central metal ion and the axial ligand. There are also reports on the S_2 state fluorescence in these molecules [6]. The motivation for the study of excited state dynamics in these molecules is two folds. First to identify the different response times (T_1 and T_2) and second to check the applicability of DFWM-IL for such measurements in these materials where the excited state absorption is dominant and one has to consider the contribution of population, to the total response time, in higher energy levels also. We use two different experimental methods of DFWM, namely nanosecond incoherent light spectroscopy (DFWM-IL) using a broad band dye laser operating around 600 nm, and ps time-resolved spectroscopy (DFWM-PS) using a frequency-doubled Nd: YAG laser. Time-resolved DFWM-PS experiments are performed using 35 ps pulses, at 532 nm, for the measurement of population relaxation time (T_1) in the samples and the results are compared with those obtained from incoherent light experiments. We also compare our results with those obtained through other techniques reported in literature.

5.2 Experimental Details

All the samples are dissolved in highly purified spectroscopic grade chloroform and experiments are carried out in samples of 10^{-4} to 10^{-5} M concentrations corresponding to an absorbance of less than 0.3 at both 532 nm and 600 nm. Essential details of our experimental setup [3, 22] used for DFWM - IL is as

follows. The dye laser output peaks at 594 nm, and has a line width (FWHM) of approximately 7.5 nm corresponding to a correlation time (τ_c) of ~ 170 fs. Three beams of equal intensity are derived from this beam. The pumps make an angle of 10° with each other while the probe is counter-propagating to beam 1. All three beams are focused down to a beam waist of ~ 100 μ and intersect in the sample kept in a 1-mm cuvette. The peak intensities reached are about 300-500 MW/cm , which are far off from the threshold intensity where the samples chemically decompose. Beam 1 is fixed whereas beams 2 and 3 pass through variable optical delay lines controlled by a PC. The resolution of each delay line is 5 μ, which corresponds to a temporal resolution of 33 fs (with a retro-reflector). The PC signal obtained in $-\mathbf{k_3}$ direction is recorded as a function of τ (delay between beams 1 and 3) for different values of 5 (delay between beams 1 and 2). An optional half wave plate (HWP) is used to rotate the state of polarization of any given beam as desired. Data acquisition part consists of a fast photodiode, lock-in amplifier, an ADC card and a PC.

The source for ps time-resolved four-wave mixing experiment (DFWM-PS) is a frequency-doubled, hybrid mode-locked Nd: YAG laser giving 532 nm, 35 ps pulses at a 10 Hz repetition rate. Beam geometry is the same as that for DFWM-IL. In this case beams 1 and 2 are focused using a 2 m lens and beam 3 is focused using a 1 m lens for better overlap of the pump and the probe pulses. PC signal is recorded by delaying the beam 2 with the other two at zero delay. Hence beam 2 will be the probe now. The sample is kept away from the focal point so that the peak intensities seen are limited to about 200-400 MW/cm^2. The angle between the pump beams is about 5°. The PC signal is recorded as a function of the time delay of the probe ($\mathbf{k_2}$) with respect to the temporally coincident pump beams ($\mathbf{k_1}$ and $\mathbf{k_2}$). The delay line in the probe beam is microprocessor controlled and has a maximum resolution of 1.3 microns corresponding to a temporal resolution of 4.35 fs. The DFWM signal picked up by a fast photodiode is fed to a digital storage oscilloscope where it is averaged over several successive pulses before recording. Appropriate neutral density filters are used to attenuate the probe beam and the PC signal to avoid saturation of the PD. The ratio of intensities of the beams 1, 2 and 3 are 1:1:0.2 and 1:0.2:1 for DFWM-IL (in this case beam 3 is the probe) and DFWM-PS (in this case beam 2 is the probe) measurements respectively.

5.3 Results and Discussion

Electronic spectra of metalloporphyrins are not only sensitive to the porphyrin structure and the nature of the central atom of the metal, but also depend on what axial ligand is added to the metal. The absorption spectra of all the samples have been presented in Chapter 4. The S_1 state for all the samples falls in the spectral region of 500 - 650 nm corresponding to 20,000 cm^{-1} - 15,400 cm^{-1} and S_2 state falls in 390 - 450 nm region corresponding to 25,640 cm^{-1} - 22,222 cm^{-1}. The excitation using incoherent light is centered around 595 nm (with 8 nm FWHM) corresponding to 16,806 cm^{-1} and using 35 ps pulses at 532 nm corresponding to 18,797 cm^{-1}.

5.3.1 DFWM-IL studies

Figures 5.1 to 5.4 shows the PC signal recorded as a function of τ for different values of 5. The solid line shows the auto correlation function obtained in the sample RhB/Rh6G (methanol) at low concentration and intensity. The same double-peak structure (viz. a sharp, intense peak and a broad, weak hump) has been observed in all samples. As shown in earlier chapters, the widths of the peaks and the ratio of the peak heights give information on (a) the dephasing time T_2 of the higher excited singlet states S_n, (b) the vibrational relaxation time τ_{V0} of the Franck-Condon states of the first excited singlet τ_{vib} (S_{1V} - S_{10}) and (c) the population relaxation time (T_1) of the S_1 state [3, 22]. Here it is assumed that the dynamics is limited to the singlet manifold, since the time scales involved are less than 100 ps during which time intersystem crossing (~ few hundreds of ps) plays minimal role. This assumption is valid since the lifetime of the triplet state T_1, generally, is in μs range and the ratio of the two peaks would be very large by orders of magnitude thereby reducing the second peak height much less than the noise level.

Open aperture Z-scan [23] curves, inset of figures 5.1 to 5.4, shows a valley in the scan indicating strong Two-Photon Absorption / Excited State Absorption behavior. The single photon absorption corresponds to 16,800 cm^{-1} whereas two-photon absorption corresponds to 33,600 cm^{-1}, which falls deep into the S_n states. There is no apparent decay in the PC signal while delaying the backward pump, with
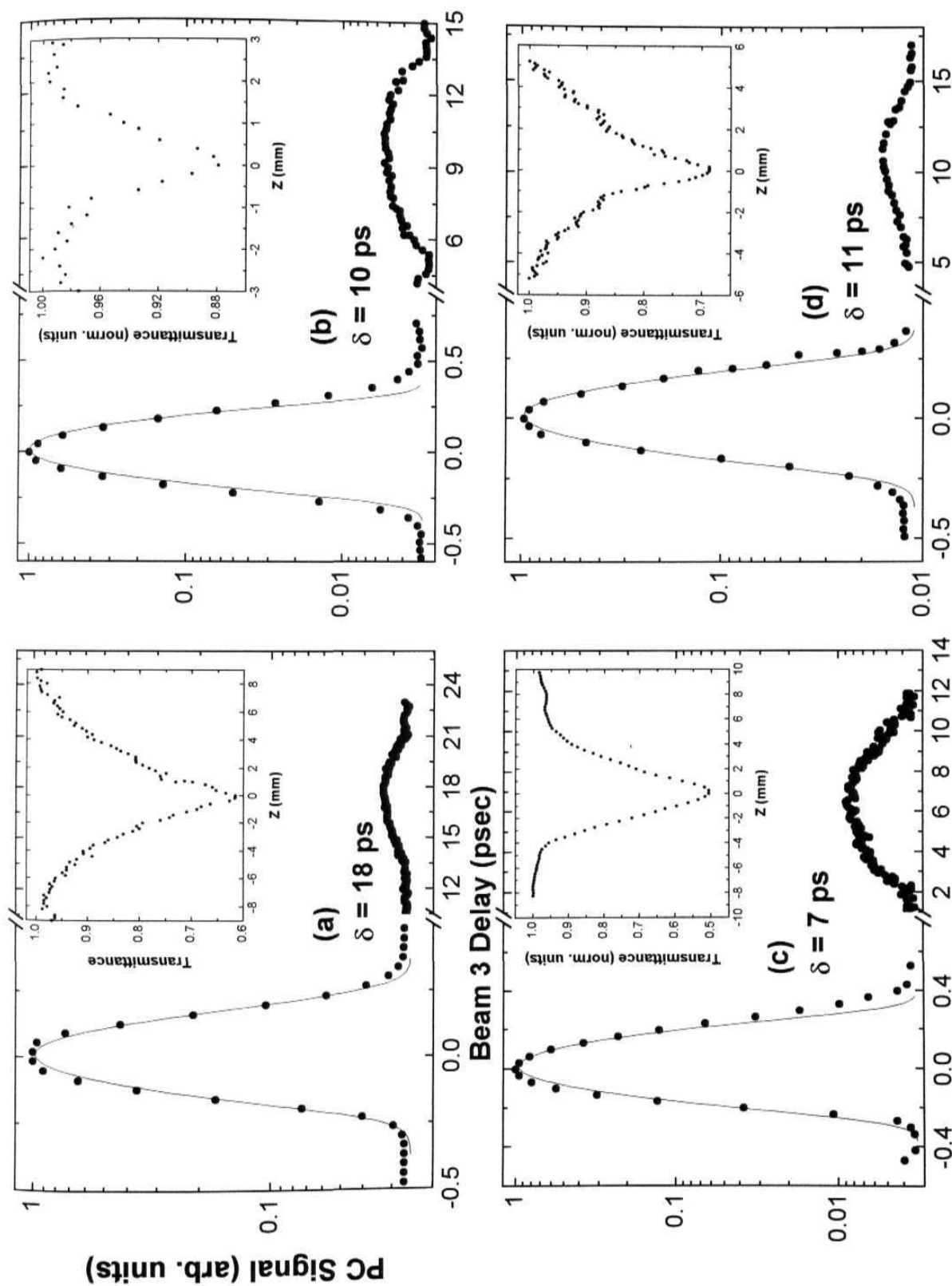
Fig. 5.1 Solid dots are the time resolved DFWM-IL signals for the samples (a) AuTTP (b) AgTTP (c) H$_2$TTP (d) CuTTP. Solid line is the autocorrelation function in RhB. Inset shows the open aperture Z-scan curves for the same samples.
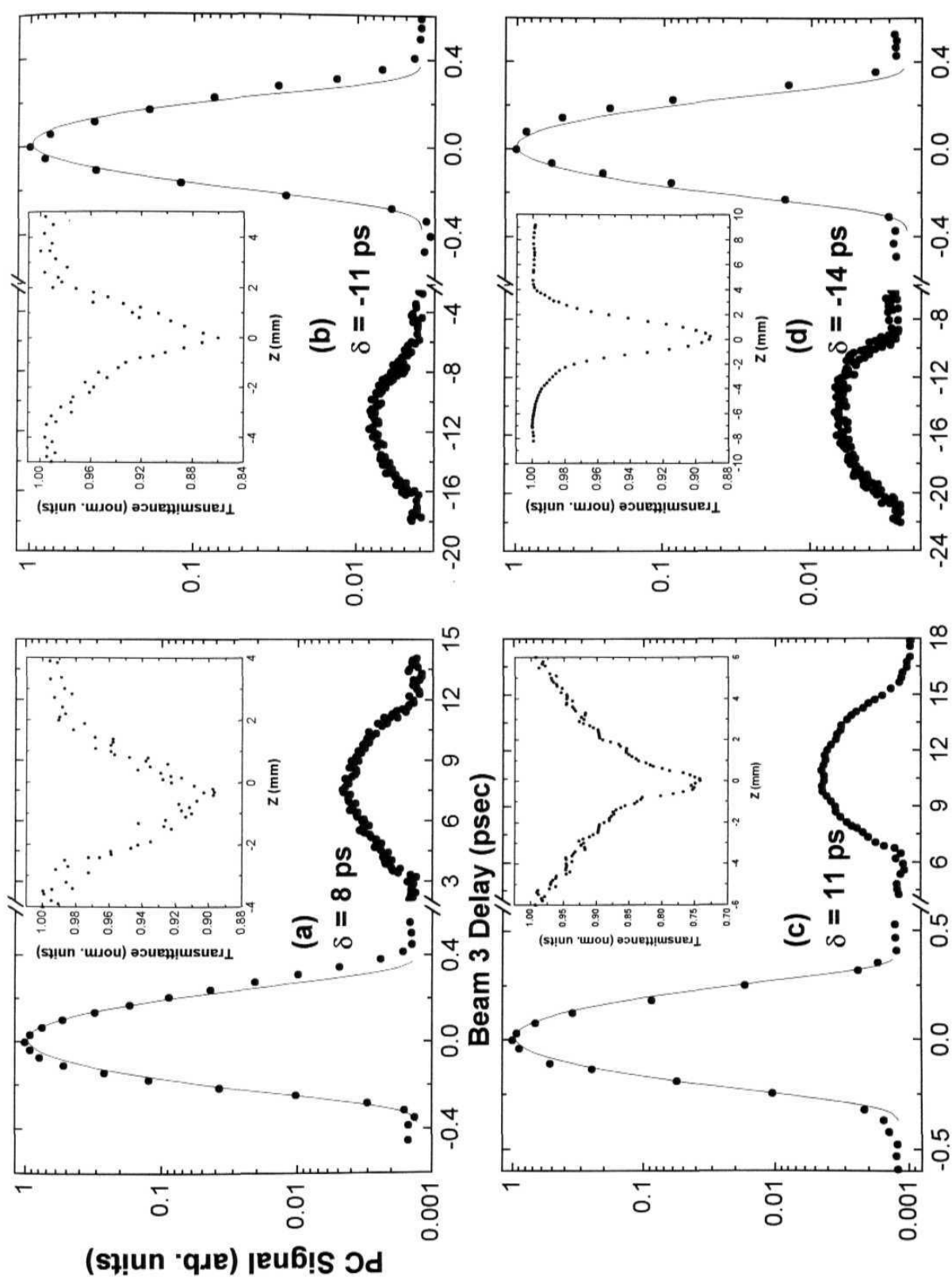
Fig. 5.2 Solid dots are the time resolved DFWM-IL signals for the samples **(a)** FeTTP **(b)** ZnTTP **(c)** SnTTP **(d)** NiTTP. Solid line is the autocorrelation function in Rhb. Inset shows the open aperture Z-scans for the same samples.
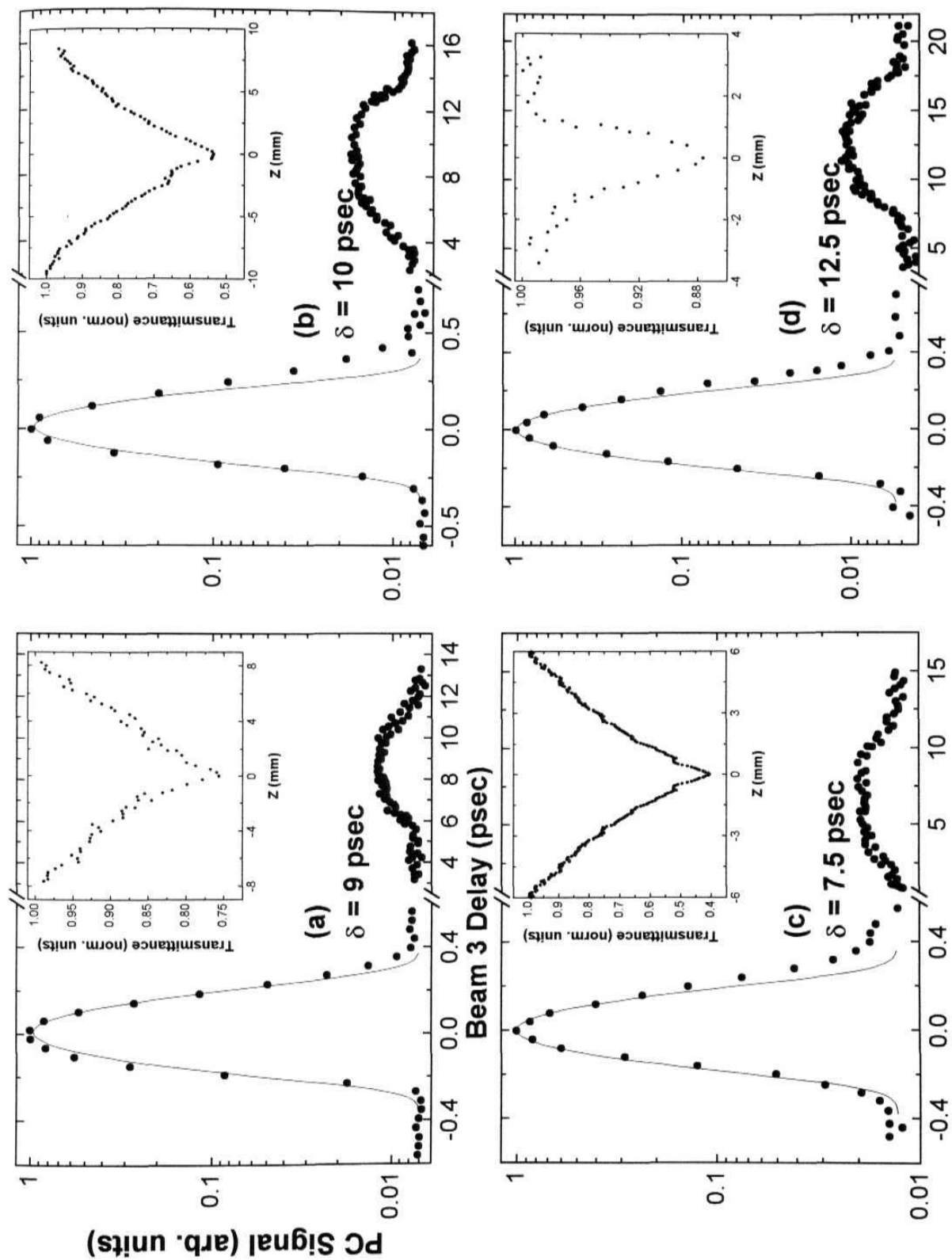
Fig. 5.3 Solid dots are the time-resolved DFWM-IL signals for the samples (a) PTTP (b) VoTTP (c) CrTTP (d) MnTTP. Line is the atuocorrelation function in RhB. Inset shows the open aperture Z-scan for the same sample.
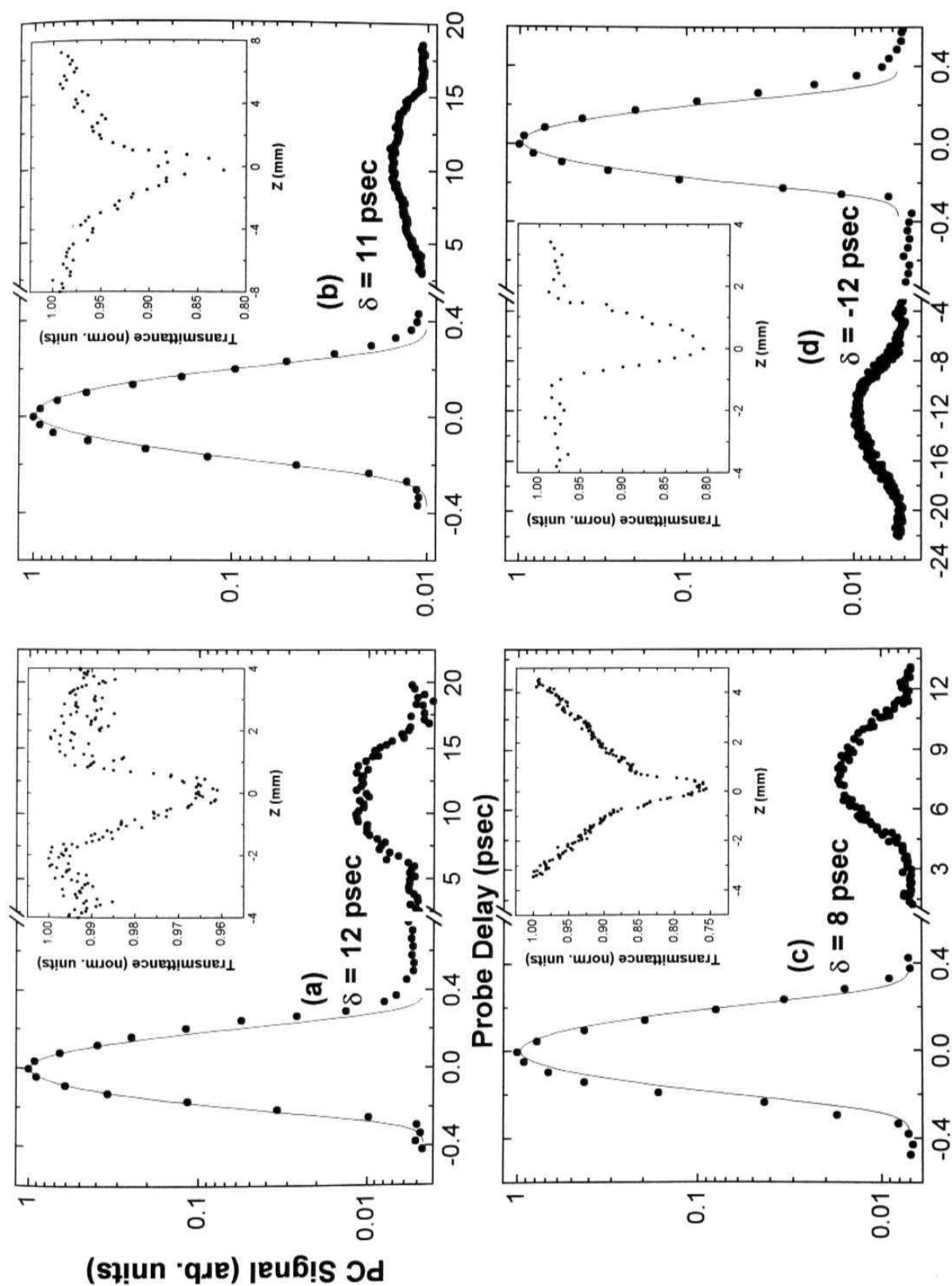
Fig. 5.4 Solid dots are the time-resolved DFWM-IL signals for the sample **(a)** GeTTP **(b)** CdTTP **(c)** InTTP **(d)** HgTTP. Line is the autocorrelation function in Rhb. Inset shows the open aperture Z-scan for the same sample.

both forward pump and probe at zero delay and this is confirmed with beam delayed to almost 1 ns. The PC signal, recorded with $\tau > 0$, is a symmetric one with FWHM of ~ 3-6 ps for different samples. The calculated lifetimes are summarized in table 1. It is clearly seen that the first peak follows the auto correlation trace indicating that dephasing time for all the samples to be less than 170 fs. It is well supported by the data obtained from self-diffraction configuration. The self-diffracted signal, obtained using beams 1 and 3, in both of the directions $2\mathbf{k_1}$ - $\mathbf{k_2}$ or $2\mathbf{k_2}$ - $\mathbf{k_1}$ is recorded as a function of the beam 3 delay. The signal shown in fig. 5(a) does not indicate any clear decay supporting that $\mathbf{T_2}$ for these samples is $< \tau_c$ (170 fs). The vibrational relaxation times in the S_1 state are about 3-6 ps and the population relaxation times are in the range of 20-70 ps. Such fast relaxation rates are expected since all these Porphyrins are either non-fluorescent or very weakly fluorescent rendering the de-excitations generally non-radiative.

The PC signal recorded with incoherent light of τ_c ~ 2.7 psec, obtained using a high-resolution grating in the cavity, also shows similar structure for the PC signal and time scales, within experimental errors. Figure 5 (b) shows one such curve obtained for the sample ZnTTP (chloroform) solution. The two-peak structure is still evident with only the ratio being changed. The lifetimes obtained with this measurement are < 2.7 ps for $\mathbf{T_2}$, ~ 5 ps for τ_{vib} and ~ 50 ps for $\mathbf{T_1}$ which are in good agreement with measurements performed with incoherent light having a τ_c of 170 fs.

5.3.2 DFWM-PS studies

Time-resolved studies using 35 ps pulses at 532 nm have been performed on the samples AuTTP, AgTTP, CoTTP, CuTTP, FeTTP, NiTTP, SnTTP, and ZnTTP. The signal obtained for different TTP's are shown in fig.'s 5.6 and 5.7 for *xxxx* polarization configuration (where all the beams have same polarization). Solid dots are the experimental data for the samples. The solid line is the auto-correlation in reference sample CS2 obtained by recording the PC signal as a function of delay of the beam 3 with other two at zero delay. Since the two orientational relaxation times of CS_2, 200 fs and 2 ps [24], are much smaller than the 35 ps, half-width of the pump pulse, the CS2 signal serves as an auto-correlation trace of the pump pulse. On the

Inset for panel (a):

Chi^2 = 0.00169
y0	0.0245	0.0090
xc1	-0.0115	0.0020
w1	0.1500	0.01
A1	0.1800	0.0043

Inset for panel (b):

$T_2 < 2.7$ psec
$\tau_{vib} = 5.0$ psec
$T_1 = 50$ psec
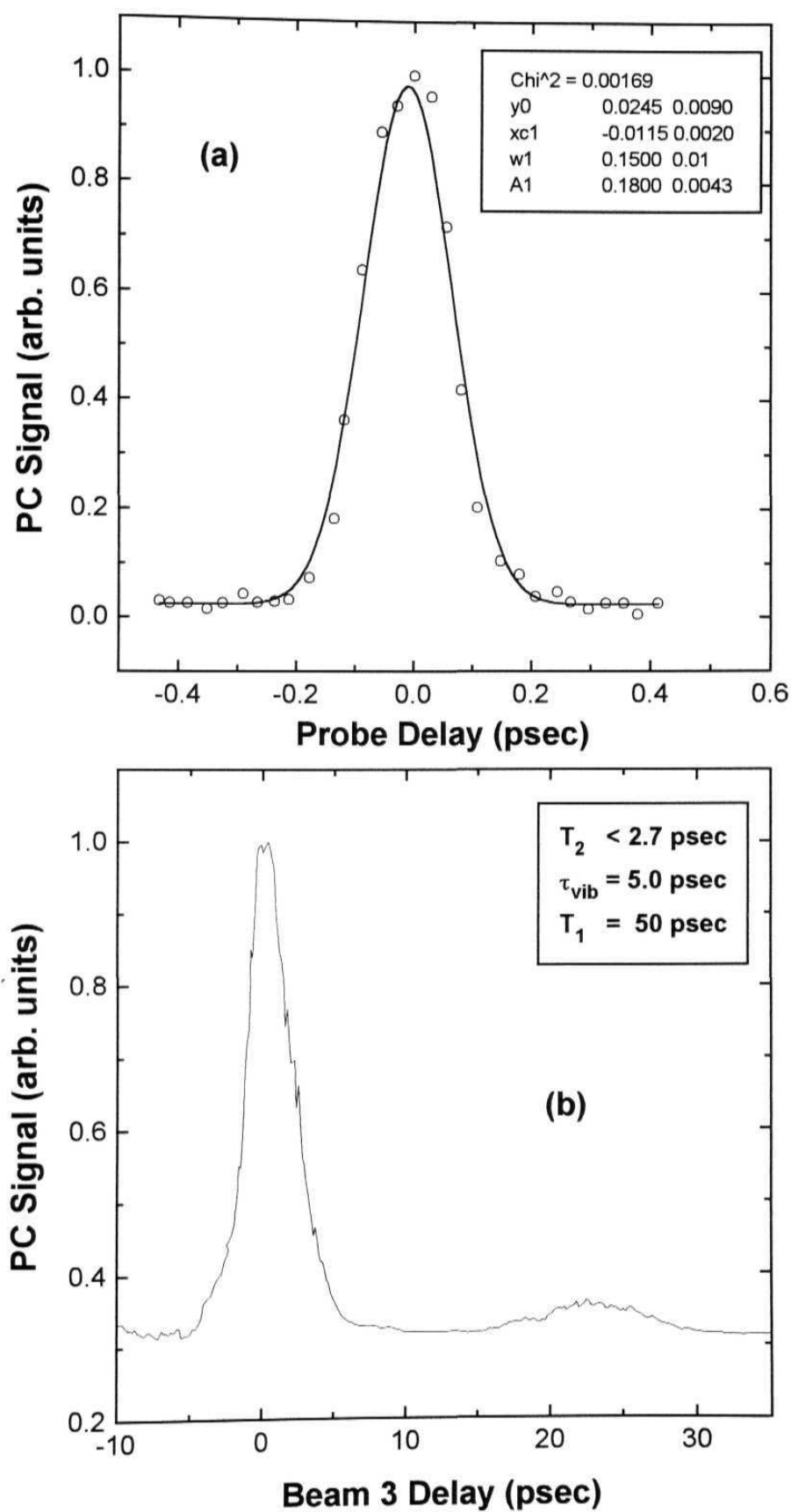
Fig. 5.5(a) Self-Diffracted signal in **H₂TTP** using incoherent light (open circles). Solid line is a gaussian fit. (b) DFWM-IL signal in **ZnTTP** with τ_c = **2.7 psec.**
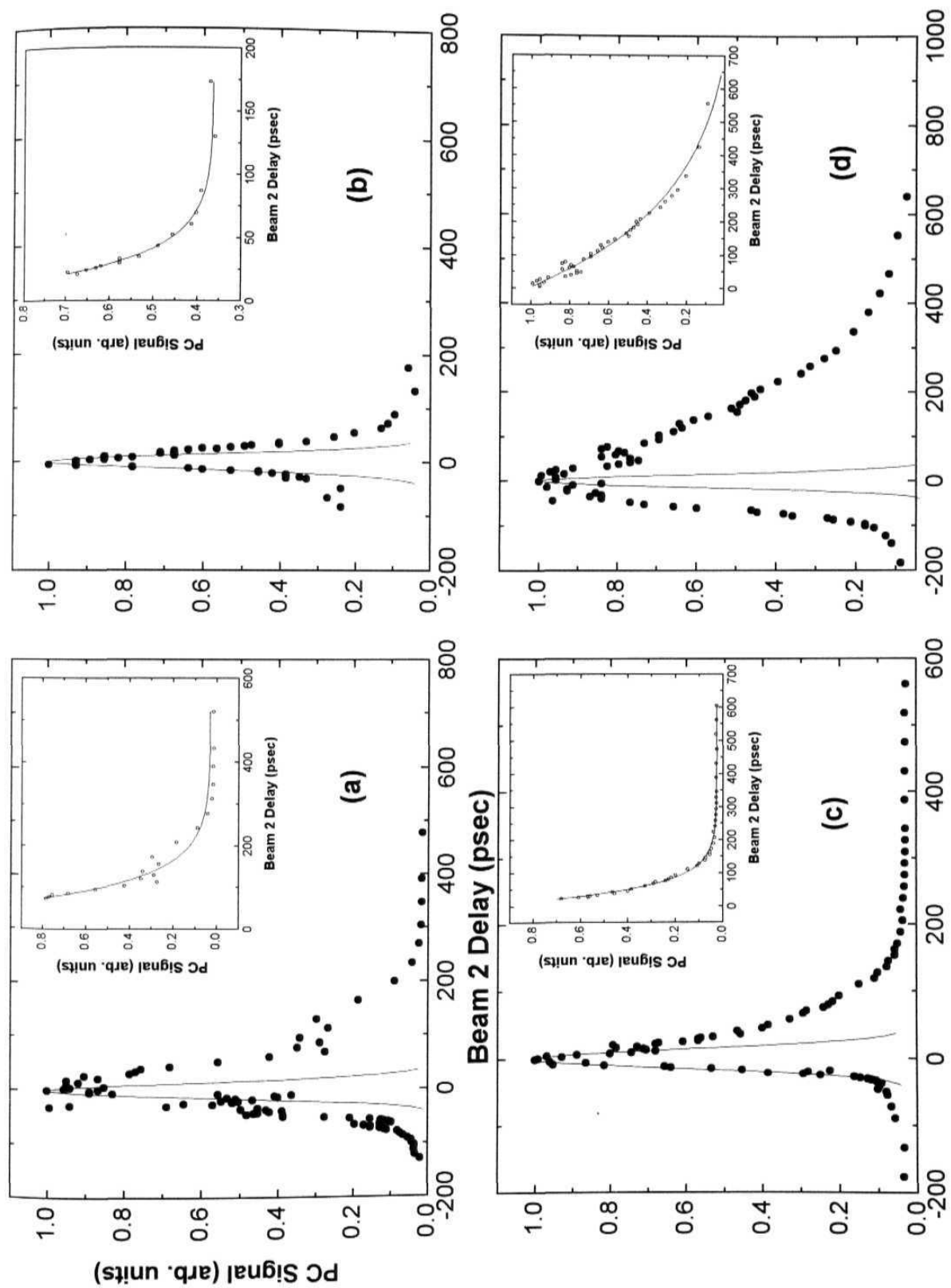
Fig. 5.6 Time-resolved PC signals in (a) AuTTP (b) AgTTP (c) CoTTP and (d) CuTTP using 35 psec pulses. Solid line is the autocorrelation curve in CS_2. Inset shows the fit to decay part
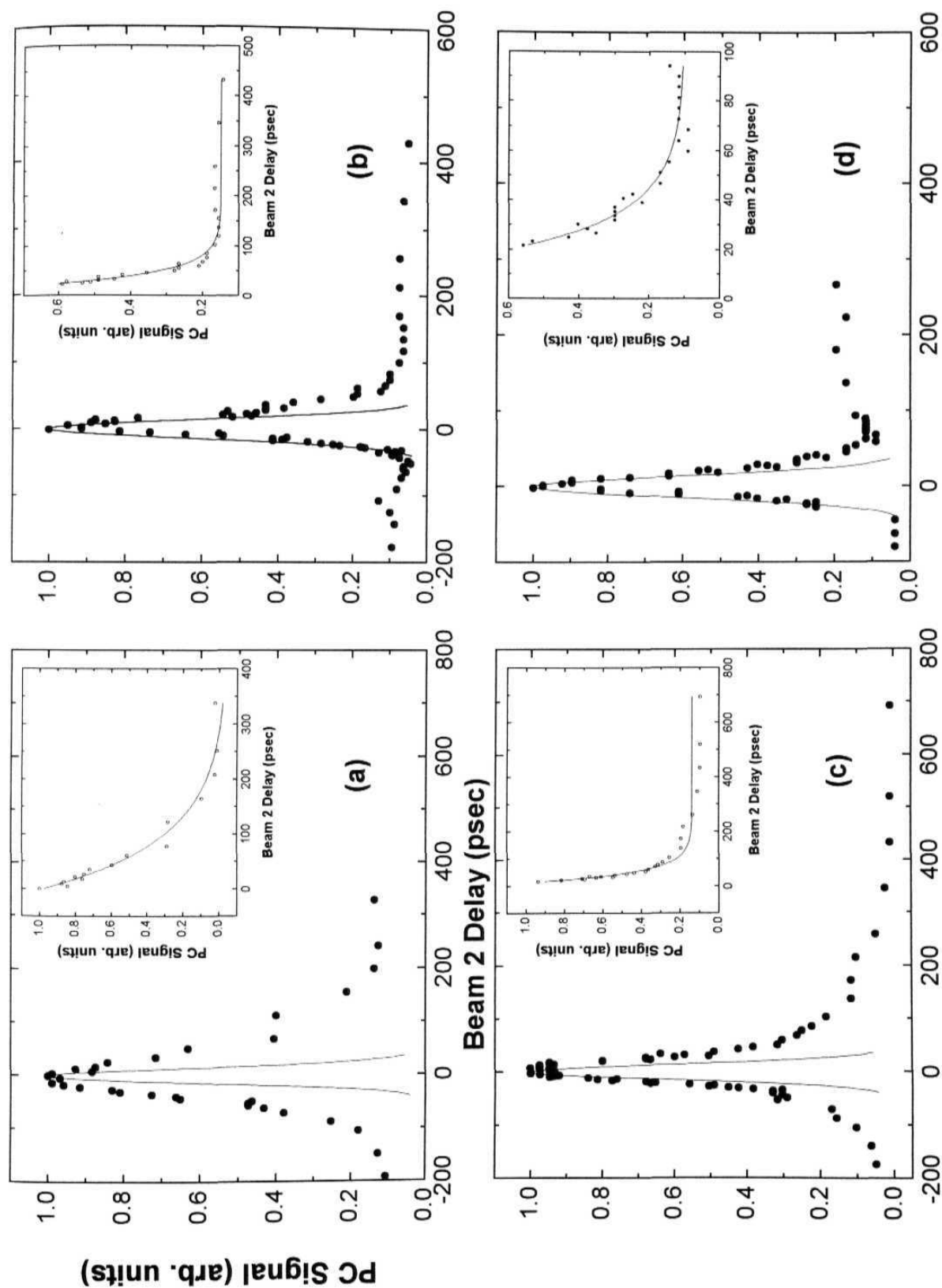
Fig. 5.7 Time-resolved PC signals in **(a)** FeTTP **(b)** ZnTTP **(c)** SnTTP and **(d)** NiTTP using 35 psec pulses. Solid line is the autocorrelation cureve in CS_2. Inset shows the fit to decay part.

other hand, for all the TTP samples there is an obvious slower component in the decay. Since we do not see any variation in the ratio of the peaks in DFWM-IL studies with different solvents, ruling out the possibility of any other decay involved, and the dephasing times in S_1 state being few ps, we assume that the long component in the observed DFWM-PS decay curve is due to population relaxation **(T_1)**. The **T_1** values are calculated by least-square fitting the decay part of the signal on positive time delays to an exponential decay. The relaxation-induced decay time of the present signal is predominantly **$T_1/2$** where as with incoherent light it is **T_1** [25] The values obtained for all the samples are summarized in table 1. Temporal evolution of the signal has been checked for all samples at longer time delays (> 400 ps) also, and no thermal contribution was observed, as has been reported previously in certain other Porphyrins (e.g. basket handle Porphyrins [2]). All the values are quoted with an experimental error of 20 - 25 % arising from the calibration of the neutral density filters, movement of the stepper motor, and the fitting procedures.

Fig's 5.1 (a) and 5.6 (a) show the signals obtained for AuTTP using both the techniques. DFWM-IL studies yield a lifetime of 4.10 + 0.82 ps for τ_{vib} and 62.0 ± 12.4 ps for **T_1**, whereas DFWM-PS studies give a very close value of 73.0 ± 15.0 ps for **T_1**. For Zn porphyrin Kobayashi et al. [26] have observed a long excited state lifetime of approximately 2.6 ns. However our results depicted in fig.'s 5.2 (b) and 5.7 (b) indicate lifetimes of 49 ± 10 ps and 55 ± 11 ps which are in excellent agreement with each other. Fig.'s 5.2 (c) and 5.7 (c) show the results for the sample SnTTP. The **T_1** values obtained are 51 ± 10.2 ps and 74 ± 14.8 ps respectively. In the case of FeTTP [fig.'s 5.2 (a) and 5.7 (a)] the values obtained are 54 ± 11 ps and 150 ± 30 ps respectively which do not match with each other. One of the previous studies in iron Porphyrins has been by Cornelius et al. [27] who observed a 100 ps transient in the relaxation, using a broadband ps continuum probe.

According to Kobayashi et al. [28] for Ag porphyrin, ps excitation to the S_1 state results in energy relaxation to $^2T_1$ state within 8 ps, which is followed by equilibrium between $^2T_1$ and $^4T_1$ with a time constant of~ 12 ps. From our incoherent light measurements **T_1** is found to be 60 ± 12 ps for AgTTP [fig. 5.1 (b)], and the corresponding value obtained from time-resolved measurements is 46 ± 9 ps [fig. 5.6

(a)]. Chirvonyl et al. [29] have observed transient species lifetimes of 250 ± 50 ps and 15 ± 8 ps respectively for Ag(II) and Ni(TI) Porphyrins respectively from flash photolysis experiments.

From ps transient absorption spectroscopy of donor-appended Co(II) Porphyrins, Loppnow et al. [30] have estimated their ground state recovery time to be less than 50 ps. Tait et al. [31] also have reported similar studies of Co^{II} and Co^{III} octaethylporphyrins (in toluene) and they observe two distinct time scales of transient absorption decay with different spectral signatures. In Co^{II} porphyrin the mixing of the state which is due to the unpaired d electron with the normal singlet and triplet states produces doublets and quartets. The ground state becomes a doublet, the lowest excited states become the singdoublet [$Q(\pi,\pi')$], the tripdoublet [$T(\pi,\pi)$], and tripquartet [$^4T(\pi,\pi^*)$]. The two lifetimes of the former were estimated to be $<$ 10 ps and 10-20 ps which were attributed to the deactivation of the $T(\pi,\pi')$ and the charge transfer state. The lifetime for Co^{III} sample was found to be $\sim$ 5 ns. Fs dynamics in Co(II)TTP were reported by Yu et al. in solvents of varying polarity and structure [5]. They have observed the relaxation time-scales to be 0.2 ps, 2 ps, and 20-200 ps in different solvents. The longest component is found to be different for each of the solvent benzene (16 ps), dichloroethane (23 ps), pyridine (40 ps) and piperidine (190 ps). This effect is attributed to the presence of a charge transfer (CT) state. Our results give T_1 values of 37 ± 7.4 ps from DFWM-IL [already shown in chapter 3, fig. 5(d)] and $109 + 22$ ps from DFWM-PS measurements [fig. 5.6(c)]. We recorded the DFWM-IL signal with two different solvents (chloroform, which is a non-polar solvent, and piperidine, which is a polar solvent), but observed no change in the signal structure and the lifetimes measured, within the limits of experimental error. Thus the involvement of a CT state in the relaxation pathway could not be inferred from our measurements.

Hilinski et al. [32] have observed that the ground state recovery time of excited Cu(II) protoporphyrins increases rapidly from highly polar solvents like pyridine ($\sim$ 45 ps) to non-polar solvents like benzene ($\sim$ 400 ps). They indicate the possibility of a CT state being involved which is possible with axial coordination of more polar solvents. For Cu(II) porphyrin Kobayashi et al. [28] have observed that

after ps excitation a Franck-Condon state of $^2S_1$ is populated which decays into the $^2T_1$ state within 8 ps. This state relaxes with time constant of ~450 ps to the $^2T_1$ state and $^4T_1$ equilibrium state from which phosphorescence is emitted. Another report is from Yan et al. [33] who found the lifetime of photoexcited CuTTP to be even longer, as high as 30 - 40 ns, and attributed it to the CT state. Jeoung et al. [34] reports the relaxation dynamics of the excited states to be completed within 100 ps for a water-soluble Cu porphyrin. The different time scales observed were 100 fs, 1.2 ps, 4 ps and 25 ps and they are attributed to the split triplet states and a new quenched state. Our measurements for CuTTP yielded a τ_{V0} of 4 $\pm$ 0.8 ps and T_1 of 37 $\pm$ 7.4 ps from DFWM-IL, and T_1 of 535 $\pm$ 107 ps from DFWM-PS [fig's 5.1 (d) and 5.6 (d)]. Again the effect of solvent polarity could not be established from DFWM-IL experiments. The 535 ps lifetime obtained by DFWM-PS is in good agreement with that reported by Hilinski et al. However, the present DFWM-IL setup is not ideally suited for measuring large lifetimes of this order. This is because T_1 is calculated from the ratio of the peaks (T_1 = Ratio * τ_c), and to obtain a lifetime of 535 ps with a τ_c of 170 fs the ratio has to be as high as 3000 which is beyond the dynamic range of our experiment. If one uses a dye which has a correlation time of about 50 - 100 psec (or use a grating in the dye laser cavity to reduce line width) there is a possibility of measuring the 500 ps component. Moreover the excitation at 532 leads the population to S_1 state primarily whereas the excitation at 600 nm leads the population directly to the S_n states through TPA. It is well understood that the effect of unpaired electrons in Cu is to split the singlet S_1 and the triplet T_1 thereby creating new pathways of relaxation (which includes the presence of a CT state or metal state). Therefore the decay mechanism could be entirely different in these two cases and each of them could be detecting different mechanism. More detailed studies, using fs/ps pulses and at different wavelengths, are necessary to resolve this discrepancy.

Kim et al. [35] have previously investigated the ps photophysics and photochemistry of Ni(II) porphyrin. While studying its conformational dynamics using time-resolved Raman and absorption spectroscopy, Courtney et al. [36] have observed relaxation processes on a ps time scale. In addition, the fs transient absorption studies of Eom et al. [37] have yielded lifetimes of 1 ps and 250 ps for NiTTP in toluene. Fig.'s 5.2 (d) and 5.7 (d) show our results for NiTTP giving T_1

values of 45 ± 9 ps and 30 + 6 ps, which are in good agreement with each other and also with the reported values of Kobayashi et al. [28]. According to Drain [38], the metal excited state of NiT(t-Bu)P exhibits a lifetime that is critically dependent on the solvent dielectric properties and temperature. He found that the lifetime varied from 2 ps in highly polar solvents to about 50 ns in non-polar solvents, and increased to several microseconds in both kinds of solvents as the temperature was reduced to 80 K. Brodard et al. [39] reports the ground state recovery time of ~250 ps for NiTPP, dissolved in toluene, THF, DCM, and DCE, using various transient grating techniques. Findsen et al. [40] investigated the photo-dynamics of nickel Porphyrins in non-coordinating solvents using Transient Raman Spectroscopy with 10 ns pulses. They observe lifetime of ~250 ps for the metal-centered excited state similar to the one probed by Kim et al. [35]. They argue that appreciable population of the excited-state species is present during the relatively longer pulse, allowing the detection of sub-ns lifetimes with ns laser pulses.

Temperature dependence has been investigated by Gentemann et al. [10] also, who reported that H_2T (alkyl) Porphyrins have ultra-short lifetimes of 10–50 ps at 296 K which slow down to 10-15 ns at 78 K. According to them it is the ability of the non-planar ruffled Porphyrins to undergo additional structural deformations in the excited state that is responsible for the dramatically enhanced rates of internal conversion, which leads to this slowing down. Our results indicate lifetimes of 40.00 ± 8.00 ps in H_2TTP, with incoherent light [shown in fig. 5.1 (c)]. Akimoto et al. [41] measured fluorescence rise and decay times of Zinc porphyrin and free-base porphyrin using fs florescence spectroscopy. They observed three exponentials in the decay curve: 150 fs, 600 fs, and 15 ns for ZnP; and 90 fs, 15 ps, and 12 ns for H2P. They associate the two short components150 fs and 600 fs for ZnP to the B (S_n) to Q (S_1) internal conversion and the vibrational relaxation within the Q state. For H_2P they attribute the 90 fs and 15 ps components to the $\mathbf{Q_y}$ to $\mathbf{Q_x}$ internal conversion and the vibrational relaxation in the $\mathbf{Q_x}$ state respectively.

J. Si et al. [42] reports the fluence dependence of nonlinear optical response of cadmium texaphyrin using time-resolved DFWM at 532 nm. They argue that at lower fluences of excitation, the nonlinearity mainly arises from the first excited singlet and

triplet states since the population in the higher excited states is small. In this case two response times, one fast and one slow, characterized the NLO response. The fast component was from the singlet state and the slow one from triplet state. They observe life times of 100 ps and 4.7 ps which they attribute to the first singlet state and higher singlet excited state. We observe values of 5.7 ± 1.1 ps and $40 + 8$ ps for the vibrational relaxation in the S_1 state and the population relaxation respectively which match very well with those reported by Si et al. In their case they attribute the 4.7 ps component to the S_2 to S_1 relaxation whereas in our case it is the S_{1v} to S_{10} relaxation.

In DFWM-PS studies, the PC signal dropped by about six times for cross polarization of the pump (beam 1) and probe beams (beam 2) with the signal structure remaining the same for all the samples.

5.4 Conclusions

1. We have investigated the excited state dynamics in several Tetra Tolyl Porphyrins using the DFWM-IL technique with nanosecond incoherent excitation, and the time-resolved DFWM technique with ps excitation.

2. Our studies with incoherent light show that there are three response times for the photoexcited molecules (derived from the widths and the ratio of the two peaks in the DFWM signal). These are explained using a typical 4-level model (S_0, S_{10}, S_{1v}, and S_n). The fastest response (< 170 fs), limited by the correlation time, is attributed to the S_n state dephasing, the slower component (~ 3-6 ps) is attributed to the $S_{1v\text{-}10}$ relaxation and the slowest component (~ 20 -70 ps) is attributed to the population relaxation.

3. The values obtained using incoherent light with $\tau_c \sim 2.7$ ps corroborate our earlier results obtained using pulses of $\tau_c \sim 170$ fs. The DFWM signal in the forward geometry indicates the dephasing time to be < 170 fs.

4. Most of the earlier reports discuss the presence of metal-centered states, charge-transfer (CT) states and the splitting of the excited states due to presence of unpaired d electron in the metal ion. However, in our case we do not observe any such state. This could be due to the fact that we excite all the molecules directly into the S_n states and in the process generate a higher vibrational state in the S_1 level. Another reason could be that our technique/setup allows measuring only the ps (few tens of ps) component and not the longer ones.

5. Time-resolved data obtained for some of the samples using 35 ps pulses agree with the results of incoherent light experiments except for the sample CuTTP. The discrepancy for this sample is explained partly in terms of the splitting of the excited states leading to a different relaxation mechanism using ps pulses and partly by the inadequacy in the present DFWM-IL setup to measure very long relaxation times.

Sample	Dephasing time of the S_n state (T_2) in fs	Vibrational Relaxation in S_1 state (X32) in ps	Population Relaxation time (T_1) in ps (DFWM-IL)	Population Relaxation time (T_1) in ps (35 ps pulses)
H_2TTP	< 170	5.40 ± 1.08	40.0 ±8.00	
$[P(TTP)(OH)_2]^+$	< 170	3.50 ±0.70	27.0 ±5.40	
V(O)TTP	< 170	5.30 ±1.06	22.0 ±4.40	
Cr(TTP)Cl	< 170	5.10 ±1.02	30.6 ±6.10	
Mn(TTP)Cl	< 170	4.90 ±0.98	32.6 ± 6.60	
Fe(TTP)Cl	< 170	5.10 ± 1.02	54.0 ± 10.8	211.0 ±42.0
CoTTP	< 170	5.60 ± 1.12	37.0 ±7.4	109.0 ±22.0
NiTTP	< 170	5.00 ± 1.00	45.0 ±9.0	40.0 ±8.0
CuTTP	< 170	4.50 ±0.90	37.0 ±7.4	535.0 ± 107.0
ZnTTP	< 170	5.50 + 1.10	49.0 ±9.8	55.0 ± 11.0
Ge(TTP)(OH)$_2$	< 170	5.70 ±1.14	30.0 ±6.0	
Ag(TTP)Cl	< 170	4.20 ±0.84	60.0 ± 12.0	46.0 ±9.0
CdTTP	< 170	5.70 ±1.14	40.0 ±8.0	
In(TTP)(OH)	< 170	3.80 ±0.76	21.0 + 4.2	
Sn(TTP)(OH)$_2$	< 170	5.20 ± 1.04	51.0 ± 10.2	74.0 ± 15.0
Au(TTP)Cl	< 170	4.10 ±0.82	62.0 ± 12.4	73.0 ± 15.0
HgTTP	< 170	5.40 ± 1.08	37.6 ±0.75	

Table 5.1 The life times of different excited states calculated using DFWM-IL and 35 psec pulses:

5.5 References

1. B.M. Dzhagarov, VS. Chirvonyi, and G.P. Gurinovich, "*Laser picosecond spectroscopy and photochemistry of bio-molecules*", Ed. VS. Letekhov, The Adam Hilger series on Optics and Opto-electronics, Bristol, 1987, UK and references therein; H.S. Nalwa, *"Nonlinear Optics of Organic molecules and Polymers,"* Eds. H.S. Nalwa and S. Miyata, CRC Press Inc., USA (1997) and references therein; J.L. Bredas, C. Adant, P. Tackx, and A. Persoons, *Chem. Rev.* 94, 243, 1994 and references therein.

2. M. Ravikanth and G.R. Kumar, *Current Science* **68,** 1010, 1995; G.R. Kumar, M. Ravikanth, S. Banerjee, and A. Sevian, *Opt. Commun.* **144,** 245, 1997.

3. D. Narayana Rao, S. Venugopal Rao, F.J. Aranda, D V.G.L.N. Rao, and M. Nakashima, *J. Opt. Soc. Am.* **B14,** 2710, 1997.

4. D.V.G.L.N. Rao, F.J. Aranda, D.E. Remy, J.F. Roach, *Int. J. Nonlinear Opt. Phys.* 3, 511, 1994.

5. H.Z Yu, J.S. Baskin, B. Steiger, C.Z. Wan, F.C. Anson, and A.H. Zewail, *Chem. Phys. Lett.* **293,** 1, 1998.

6. S. Tobita, Y. Kaizu, H. Kobayashi, and I. Tanaka, *J. Chem. Phys.* **81,** 2962, 1984; S. Tobita and 1. Tanaka, *Chem. Phys. Lett.* 96, 517, 1983; O. Ohno, Y. Kaizu, and H. Kobayashi, *J. Chem. Phys.* 82, 1779, 1985.

7. A. Harriman, *J.C.S.Faraday I* 76, 1978, 1980; A. Harriman, *J.C.S.Faraday J* **11,** 369, 1981; A. Harriman, *J.C.S.Faraday* I 77, 1281, 1981.

8. G.G. Gurzadyan, T. -H. Tran-Thi, and T. Gustavsson, *J. Chem. Phys.* **108,** 385, 1998; Q. Zhong. Z. Wang, Y. Liu, Q. Zhu, and F. Kong, *J. Chem, Phys.* **105,** 5377, 1996; Y. Kurabayashi, K. Kikuchi, and H. Kokubun, *J. Phys. Chem.* **88,** 1308, 1984.

9. MP. Tsvirko, G.F. Stelmakh, V.E. Pyatosin, K.N. Solovyov, T.F. Kachura, A.S. Piskarska, and R.A. Gadonas, *Chem. Phys.* **106,** 467, 1986; I.V. Rubtsov, Y. Kobuke, H. Miyaji, and K. Yoshihara, *Chem. Phys. Lett.* **308,** 323, 1999; H. Stiel, A. Volkmer, 1. Ruckmann, A. Zeug, B. Ehrenberg, and B. Roder, *Opt. Commun.* **115,** 135, 1998.

10. N. Serpone, TX. Netzel, and M. Gouterman, *J. Am. Chem. Soc.* **104, 246,** 1982; S. Gentemann, C.J. Medforth, T. Ema, N.Y. Nelson, K.M. Smith, J. Fajer, and D. Holten, *Chem. Phys. Lett.* **245,** 441, 1995; S.I. Yang, J. Li, H.S. Cho, D. Kim,

D.F. Bocian, D. Holten, and J. Lindsey, *J. Mater. Chem.* **10,** 283, 2000 and references therein.

11. J. Aaviskoo, A. Freiberg, S. Savikhin, G.F. Stelmakh, and M.P. Tsvirko, *Chem. Phys. Lett.* **111,** 275, 1984; C. Galli, K. Wynne, S.M. LeCours, M.J. Therien, and R.M. Hochstrasser, *Chem. Phys. Lett,* **206,** 493, 1993.

12. R. Kumble, S. Palese, VS. -Y. Lin, M.J. Therien, and RM. Hochstrasser, *J. Am. Chem. Soc.* **120,** 11489, 1998

13. J. Si, Y. Wang, Q. Wang, P. Ye, H. Tian, Q. Zhou, and H. Xu, *Appl, Phys. Lett.* 69, 1832, 1996; J. Si, Y. Wang, J. Zhao, P. Ye, D. Wang, W. Sun, And S. Dong, Appl. Phys. Lett. 67, 1975, 1995.

14. P. Chen, I.V. Tomov, AS. Dvornikov, M. Nakashima, J.F. Roach, DM. Alabran, and P.M, Rentzepis, *J. Phys. Chem.* **100,** 17507, 1996

15. R.F. Khairutdinov and N. Serpone, /. *Phys. Chem.* **B103,** 763, 1999; J.R. Andrews and R.M. Hochstrasser, *Chem. Phys. Lett.* 76, 213, 1980.

16. D. Kim, D. Holten, M. Gouterman, and J.W. Buchler, /. *Am. Chem. Soc.* **106,** 4015, 1984; L.Genberg, Q. Bao, S. Gracewski, and R.J.D. Miller, *Chem. Phys.* **131,** 81, 1989.

17. MM. Devane, *Opt. Commun.* 52, 136, 1984; O. Bilsel, J. Rodriguez, and D. Holten, *J. Phys. Chem.* 94, 3508, 1990; D. LeGourrierec, M. Andersson, J. Davidsson, E. Mukhtar, L. Sun, and L. Hammarstrom, *J. Phys. Chem.* **A103,** 557, 1999.

18. GE. O'Keefe, G.J. Denton, E.J. Harvey, RT. Phillips, R.H. Friend, and H.L. Anderson, /. *Chem. Phys.* **104(3),** 805, 1996; A.Yu, Chikishev, V.F.Kamalov, N.l.Koroteev, V.V. Kvach, A.P.Shkurinov, and B.N. Toleutaev, *Chem. Phys. Lett,* **144,** 90, 1988.

19. K. Susumu, K Kunimoto, H. Segawa, and T. Shimidzu, *J. Phys. Chem.* 99, 29, 1995; H. Chosrowjan, S. Tanigichi, T. Okada, S. Takagi, T. Arai, and K. Tokumara, *Chem, Phys. Lett.* **242,** 644, 1995.

20. J. Rodriguez, C. Kirmaier and D. Holten, *J. Chem. Phys.* 94, 6020, 1994; J. Rodriguez, C. Kirmaier and D. Holten, *J. Am. Chem. Soc.* **111,** 6500, 1989; J. Rodriguez, and D. Holten, *J. Chem. Phys.* 91, 3525, 1989.

21. S. Venugopal Rao, N.K.M.N. Srinivas, L. Giribabu, B.G. Maiya, R. Philip, G.R. Kumar and D. Narayana Rao, Submitted to *Optics Communications.*

22. S. Venugopal Rao, L. Giribabu, B.G. Maiya, and D.N. Rao, *Current Science* 72, 957, 1997

23. M. Sheik-Bahae, A.A. Said, T. -H. Wei, D.J. Hagan, E.W. Van Stryland, *IEEE Journal of Quantum Electronics,* 26,760, 1990.

24. Charles E. Barker, Rick Trebino, A.G.Kostenbauder, and A.E.Stegeman, J. Chem. Phys. 92, 4740, 1990; B.I.Greene and R.C.Farrow, J.Chem. Phys. 77, 4779, 1982; **B.I.Greene** and R.C.Farrow, Chem. Phys. Lett. 98, 273, 1983.

25. N. Morita, T. Tokizaki, and T. Yajima, J. Opt. Soc. Am. B4, 1269, 1987; Y. Cui, M. Zhao, G.S. He, and P.N. Prasad, *J. Phys. Chem.* 95, 6842, 1991; E.P. Ippen and C.V. Shank, "Techniques for measurement" in *Ultrashort Light Pulses,*, S.L. Shapiro ed., Springer-Verlag, Berlin, 83, 1977.

26. T. Kobayashi, D. Huppert, K.D. Straub, and P.M. Rentzepis, *J. Chem. Phys.* 70, 1720, 1979.

27. P.A. Cornelius, A.W. Steele, D.A. Chernoff, and R.M. Hochstrasser, *Chem. Phys. Lett.* **82,9,** 1981.

28. T. Kobayashi, K.D. Straub, and P.M. Rentzepis, *Photochem. Photobiol,* 29, 925, 1979.

29. V. Chirvonyl, B.M. Dzhagarov, Y.V. Timinskii, and G.P. Gurinovich, *Chem. Phys. Lett.* 70, 79, 1980.

30. G.R. Loppnow, D. Melamed, A.L. Leheny, A.D. Hamilton, and T.G. Spiro, *J. Phys. Chem.* 97, 8969, 1993.

31. C.D. Tait, D. Holten, and M. Gouterman, *Chem. Phys. Lett,* **100,** 268, 1984.

32. E. Hilinski, K.D. Straub, and P.M. Rentzepis, *Chem. Phys. Lett,* **111**, 333, 1984.

33. X. Yan and D. Holten, *J. Chem. Phys.* 92, 5982, 1988.

34. S.C. Jeoung, S. Takeuchi, T. Tahara, and D. Kim, *Chem. Phys. Lett.* **309,** 369, 1999.

35. D. Kim, C. Kirmaier, and D. Holten, *Chem. Phys.* 75, 305, 1983.

36. S.H. Courtney, T.M. Jedju, J.M. Friedman, L. Rothberg, R.G. Alden, M.S. Park, and M.R. Ondrias, *J. Opt. Soc. Am.* B7, 1610, 1990; S.H. Courtney, T.M. Jedju, J.M. Friedman, R.G. Alden, and M.R. Ondrias, *Chem. Phys. Lett.* **164,** 39, 1989.

37. H.S. Eom, S.C. Jeoung, D. Kim, J. -H. Ha, and Y. -R. Kim, *J. Phys. Chem.* **A101,** 3661, 1997.

38. CM. Drain, S. Gentemann, J.A. Roberts, N.Y. Nelson, C.J. Medforth, S. Jia, M.C. Simpson, KM. Smith, J. Fajer, J.A. Shelnutt, and D. Holten, *J. Am. Chem. Soc.* **120,** 3781, 1998.

39. P. Brodard and E. Vauthey, *Chem. Phys. Lett.* **309,** 198, 1999.

40. E.W. Findsen, J.A. Shelnutt, and M.R. Ondrias, *J. Phys. Chem.* 92, 307, 1988.

41. S. Akimoto, T. Yamazaki, I. Yamazaki, and A. Osuka, *Chem. Phys. Lett.* **309,** 177, 1999.

42. J. Si, Y. Wang, J. Zhao, P. Ye, D. Wang, W. Sun, And S. Dong, Appl. Phys. Lett. 67, 1975, 1995; J. Si, Q. Yang, Y. Wang, P. Ye, S. Wang, J. Qin, and D. Liu, *Opt. Commun.* **132,** 311, 1995.

CHAPTER 6

C$_{60}$: Studies of Third-order Nonlinearity, Excited State Dynamics using DFWM-IL and Dispersion of Nonlinear Absorption using Z-scan techniques

Third-order optical nonlinearity, excited state dynamics and dispersion studies of nonlinear absorption of C$_{60}$ have been studied using standard backward Degenerate Four Wave Mixing (both with incoherent light and coherent light) and Z-scan techniques. We observe a large nonlinearity at 600 nm and it is attributed to strong two-photon absorption. We estimate the population relaxation T$_1$ (of the lower excited singlet state S$_1$) and phase relaxation time T$_2$ (of the higher excited singlet state S$_n$) of the sample. The vibrational relaxation (τ_{vib}) in the S$_1$ state is found to be ~ 5 ps. Our results are found to be in good agreement with those obtained using 150 fs pulses. We also present our open aperture Z-scan data at 600 nm using the broadband source and our experimental and theoretical results on the dispersion studies of non-linear absorption in C$_{oo}$ solution. Open aperture Z-scans are performed over the visible region (440 nm to 660 nm) using an ns OPO and the obtained results are interpreted using a 5-level model taking into account both the excited state absorption and two-photon absorption processes. Results indicate that excited state absorption dominates in the shorter wavelength region (440 nm to 560 nm) whereas two-photon absorption dominates in the longer wavelength region (580 nm to 660 nm).

6.1 Introduction

The progress of modern optical technology for all-optical, electro-optical, acousto-optical, and opto-mechanical devices demands the ability to control the intensity of light in a predetermined and predictable manner. Some of the important requirements of materials for the realisation of photonic devices are a) Large nonlinearity b) Ultrafast response time (in ps and fs domain) c) Low dielectric constant and linear losses d) High resistance to laser radiation ~ GW/Cm^2 e) Ease in chemical tailoring of physical and optical properties f) Ability to process into thin films, fibres g) Mechanical strength and flexibility h) Compatibility with semiconductor-integrated structures and i) Compactness and cost-effectiveness. Extensive research in recent years suggests organic and organo-metallic materials to be the best candidates for 'tailoring' the material properties. Since its discovery and availability in milligrams [1], fullerenes and their derivatives have received extraordinary attention from physicists,

chemists and material scientists who have been extensively investigating their optical, physical and chemical properties for fundamental understanding and technological applications. Fullerenes are fascinating owing to their chemistry and unique physics coupled with material science. It has been well established that organic molecules with highly de-localised π-electron system exhibit large optical nonlinearity [2]. Fullerenes are also found to have a very high value of $\chi^{(3)}$ with small absorption coefficient, fast nonlinear response and high chemical stability. Although there is considerable variation in the reports on measurements of experimental and theoretical $\chi^{(3)}$ values of fullerenes in solution/thin films [3-21], they are found to have very high potential in device applications. Earlier studies indicate C_{60} and it's derivatives (doped in glass matrix, sol-gels, polymers, etc.) as potential candidates for optical limiting [22-36], optical bistability [37] optical switching [38] and higher harmonic generation [39]. Owing to their electronic structure, fullerenes also find unique applications in photoconductivity, electroluminescence, ferromagnetism, superconductivity, cancer therapy, and in biological use [40]. Understanding the origin, magnitude of nonlinearity and excited state dynamics in such an exotic molecule is very important both from the fundamental point of view and its wide range of applications. We study the third order optical nonlinearity, excited state dynamics, which occur in fs and ps domain, and nonlinear absorption of C_{60} dissolved in xylene/toluene.

6.2 Degenerate Four Wave Mixing

6.2.1 $\chi^{(3)}$ Measurements

Although there is wide literature available [3-21] on the measurement of $\chi^{(3)}$, there is also a wide range of values reported (~ 10^{-8} to 10^{12} esu). Most of the nonlinearity measurements were performed in the NIR spectral region, far away from one-photon resonance. We have measured $\chi^{(3)}$ using a broad band laser peaking at 595 nm and having a width of ~ 8 nm. Complete details of the experimental set-up have been reported in earlier chapters. The laser line width (FWHM), when the mirror is present in the cavity, is found to be ~ 8 nm (RhB in methanol) [41]. This corresponds to a correlation time (τ_c) of ~ 170 fs measured from the inverse of bandwidth as

well as from the width of PC signal in RhB (since in RhB, $\mathbf{T_1}$ is very large, ~ few ns, we see only a symmetric auto-correlation curve). When the mirror in the cavity is replaced by a dispersive element like a high resolution grating the line width is reduced and is found to be ~ 1.3 nm with the corresponding correlation time is ~ 2.7 ps (measured from the width of PC signal in RhB and CS2). The correlation time measured by using the relation $\Delta v * \tau_c = 1$ is ~ 900 fs.

Beam 1 ($\mathbf{k_1}$) is forward pump, beam 2 ($\mathbf{k_2}$) is backward pump and beam 3 is the probe. The sample is placed in a 1-mm thick cuvette and different parts of the cell are exposed, for different measurements, to the laser beam to avoid any degradation of the sample. Beam 1 is fixed whereas beams 2 and 3 pass through variable delays. Beam 2 passes through a retro-reflector mounted on a micrometer which is delayed manually whereas beam 3 passes through another retro-reflector mounted on a micrometer controlled by a stepper motor interfaced to a computer. In both the cases the maximum resolution we could achieve (i.e. minimum distance that could be moved with this delay) is ~ 5 um which corresponds to ~ 33 fs in time (with a retro-reflector). Beam 3, which is the probe in our case, makes an angle of ~ 10° with the forward pump. The sample is dissolved in spectroscopic grade, highly purified xylene/toluene. All the beams have same polarisation and the change in polarisation in each of the beams is achieved using a Half Wave Plate (HWP).

C_{60} (> 99% pure) was purchased from Strem Chemicals, USA and is used without further purification. Fig. 6.1 (a) shows the absorption spectrum, recorded using a UV/VIS spectrometer (Jasco, model 7800), of the sample dissolved in xylene and it matches well with those reported in literature. The main features are a strong band around 335 nm, very small and almost constant absorption in the visible region. An OD of < 0.2 at 600 nm is chosen for recording the signals in all measurements. The cubic dependence (at lower input intensities) of the PC signal with varying input is verified before each measurement. The PC signal plotted as a function of the sample concentration, shown in fig. 1 (b), clearly follows a linear dependence. $\chi^{(3)}$ and γ are calculated using the standard relations as described in previous chapter. $\chi^{(3)}$ value at a concentration of $3.47*10^{-4}$ M is found to be ~ $2.5*10^{-11}$ esu (at 600 nm). γ is found
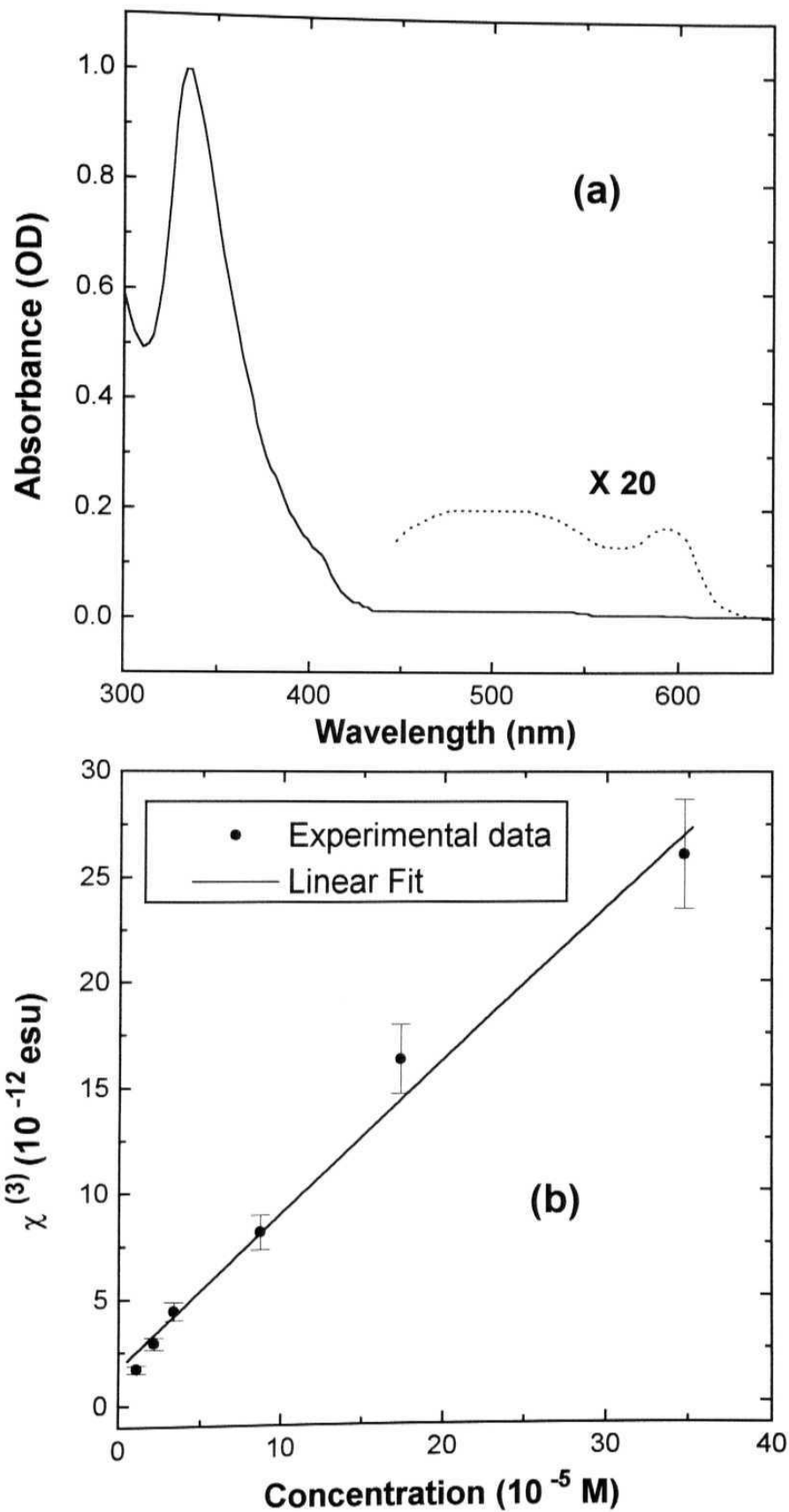
Fig. 6.1 (a) Absorption spectrum of the sample C_{60} (Xylene).(b) Concentration dependence of $\chi^{(3)}$. Solid dots are experimental data and line is a linear fit.

to be $5.388*10^{-30}$ esu using a $\chi^{(3)}$ value for reference sample CS_2 as $1.7*10^{"12}$ esu. When the polarization of the probe beam is crossed with respect to pump beams, the PC signal dropped by 6-7 times indicating a part of thermal contribution to the nonlinearity (for pure electronic contribution the signal drops down by 3 times and for orientational type it drops down by three-fourths). This large value of $\chi^{(3)}$ could be also attributed to strong Two Photon Absorption (TPA) at this wavelength. As shown in the later part of this chapter there is a strong TPA at and around this wavelength, exciting the molecules directly into the S_n states. Lee et. al. [41] have identified the energy of the singlet states in C_{60} S_1 state falls in $\sim 16,000$ cm^{-1} range and the S_n state falls in $\sim 29,000$ cm^{-1} range. We work at the wavelength of ~ 595 nm (16,800 $cm^{"1}$) and the two photon energy corresponds to $\sim 33,600$ cm^{-1} leading the population directly into S_n states. The measured nonlinearity, then, will have contributions from nonlinearities due to the ground state and the excited states. Moreover the singlet state excited state absorption is stronger than the ground state absorption forcing the population to be distributed among the different excited states. As argued in the earlier chapter this enhanced $\chi^{(3)}$ value could be a result of strong ESA/TPA with contribution from thermal part as well.

Comparing our value with those obtained in literature, Henari et al. [7] working with 5 ns pulses at 580 nm obtained a high value of $\sim 8.8*10^{"}$ esu. Ji et al. [11] obtained a value of $\sim 10^{-10}$ esu for $\chi^{(3)}$ and $\sim 10^{-31}$ esu for y at 608 nm using 6 ns pulses for thin films and conclude that $\chi^{(3)}$ is dominated by its imaginary part (which again is due to excited state absorption). They assume a refractive index of 1.49 for the films. We assume a value of 2 for the solutions. Flom et al. [13] working with 1.2 ps pulses at 597 nm, and in the phase conjugate geometry, obtains a $\chi^{(3)}$ value of $(38 \pm 9)*10^{-11}$ esu (in the *xxxx* configuration, where all the beams have same polarisation) for C_{60} pure film. By looking at the temporal response of the PC signal the high value observed for $\chi^{(3)}$ is attributed to the participation of the excited states in the nonlinear process. They observe a short lifetime of ~ 43 ps which is due to the first excited singlet state occurring due to the exciton-exciton annihilation and a long lived component which is due to the triplet state. Flom et al. [13] again working with 1.2 ps pulses at 590.5 nm report a value of $52*10^{-11}$ esu for $\chi^{(3)}$ in the *xxxx* configuration.

J. Li et al. [21] working at a non-resonant wavelength, 810 nm, reports an upper limit for γ as $9.0 * 10^{-35}$ esu which is very low.

6.2.2 Temporal response of the DFWM signal

We employ the standard DFWM in the phase conjugate geometry and delay the probe beam (beam 3) with backward pump and forward pump at zero delay. We observe two peaks in the phase conjugate signal when the probe is delayed with respect to the forward and backward pump beams. From the widths and ratio of these peaks we estimate T_1 and T_2 values for the S_1 and S_n states respectively [42]. We also estimate the vibrational relaxation time in the S_1 state. Fig. 6.2 shows the phase conjugate signal as the probe beam is delayed with respect to beam 1, with beam 2 kept at delay of 5 with respect to beam 1 (Inset shows the schematic of the configuration used, briefly) We see a sharp coherence peak at $\tau = 0$ due to beams 1 and 3 with beam 2 probing the grating, and another at $x = 8 = 9$ ps due to beams 2 and 3 with beam 1 probing the grating. For different δ values the broad peak shifted symmetrically across the first coherence peak. It has been shown that the ratio of these peaks would give information on the population relaxation time of the lower excited state and the line widths give information on the dephasing of the S_n and S_1 states [43]. From the width (FWHM) of the first coherence peak at $\tau = 0$ (~ 170 fs), the width (FWHM) of the second peak at $\tau = \delta$ (~ 5 ps), the ratio of the two peaks (~ 450) we estimate the phase relaxation time T_2 of the S_n states as < 170 fs, vibrational relaxation in the S_1 state ($S_{1v} - S_{10}$) as ~ 5 ps, and population relaxation (T_1) time as ~ 70 ps (Ratio* τ_c) respectively.

We compare our results with those obtained using 150 fs pulses at 633 nm and are find that they are in excellent agreement with them. Rosker et al. [8] employ the standard backward DFWM using 150 fs pulses at 633 nm and recorded the phase conjugate signal by delaying the backward pump beam, with other two beams at zero delay, which would give information on the population relaxation time of the material [44]. They observe three different decay times, 260 fs, 4.6 ps and 64 ps, in the signal and could not account for their observation. The longer component was
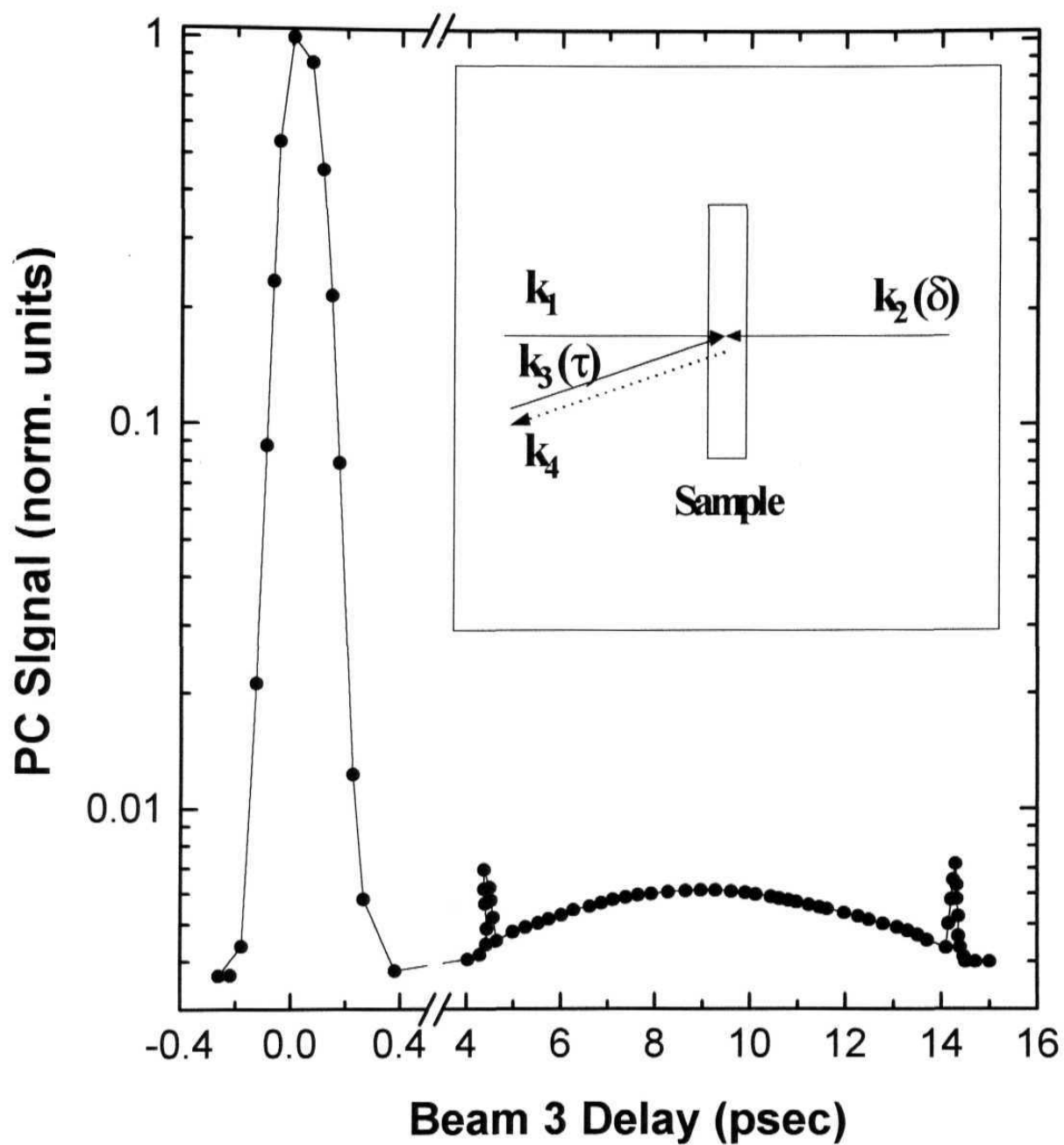
Fig. 6.2 Time resolved spectrum of the PC signal for 6 = 9 psec. Inset shows the FWM schematic

found to be sensitive to both the input intensity and the temporal overlap of the writing pulses suggesting that they are most likely due to presence of an excited state population grating. Also it was observed that the long-lived component vanishes for wavelengths longer than 650 nm clearly suggesting the involvement of S_1 state. However, in our present study, the three different time scales could be successfully assigned to the different relaxation processes in the upper and the lower excited states.

Since the input pulses have a correlation time of ~ 170 fs, the intersystem crossing rate, which is in the order of few hundred ps (~ 650 ps), would not play an important role in these studies. Two photon / excited state absorption takes the molecules from the vibrational manifold of the ground state to the upper states of S_n. The upper states S_n will relax back to the S_1 state on fs time scale and in the process generate a vibrationally excited S_1 state (Kasha's rule). Peak 1, which has a fast response time in fs, is attributed to the dephasing of the excited states S_n. The width of the second peak, of the order of few ps, is attributed to the vibrational relaxation or the vibrational dephasing time within the S_1 state (S_{1v} to S_1). The ratio of the peaks is related to the population relaxation time of the lower excited state. Thus from the observed line widths and the ratio of the DFWM signal, we estimate the dephasing time of the S_n states to be less than 180 fs, the vibration relaxation time in the S_1 state as ~ 5 ps, the population relaxation time as ~ 70 ps ($450*\tau_c$). Apart from the two coherence peaks we also observed two sharp peaks overriding the broader peak (Fig. 6.2). These sharp peaks observed on the shoulders of the broad peak are found to be due to coherence of probe beam (beam 3) and the reflections of the backward pump (beam 2) from the surfaces of the cell. This was confirmed by using cuvettes of different size. The broader peak appears exactly at x = |5| and therefore its position is dependant on the delay of second beam (beam 2).

The PC signal recorded with a grating in the cavity of the dye laser is shown in fig. 6.3 (a). Since τ_c is now 2.6 ps, the ratio of the two peaks will be reduced. The widths of the first peak and the second peak remained same within the experimental errors. The width of first coherence peak is ~ 2.7 ps and there is no decay observed within experimental errors indicating that the value of T_2 is much smaller than τ_c.
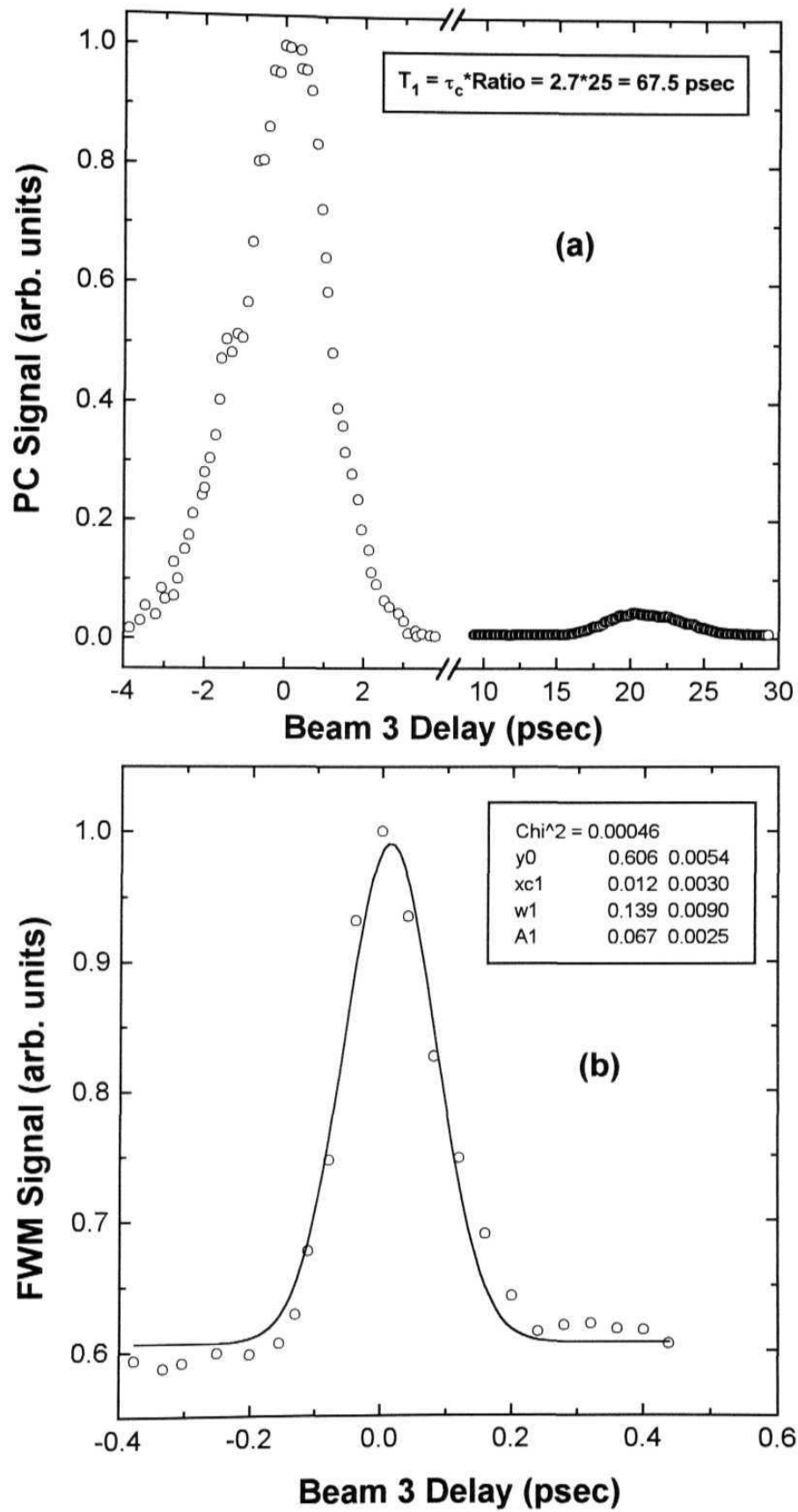
Fig. 6.3 (a) PC signal in the sample C_{60} with grating in the cavity. τ_c in this case is ~ 2.7 psec (b) Self diffracted signal in the $k_1 - 2k_2$ direction. Dots are experimental data and line is a gaussian fit

The value of T_1 calculated in this case is ~ 67.5 ps (25*2.7 ps). This result corroborates our earlier result, of T_1 ~ 70 ps, on the same sample using pulses having τ_c of 170 fs. Both the measurements are performed under identical conditions of input intensity, concentration of the sample to avoid any other complications arising from these factors. The values quoted above have an error bar of approximately 25 %. The major sources of error arise from the calibration of the neutral density filters used, the stepper motor movement, linearity of the photodiode.

There are several reports on the S_1 excited state dynamics in C_{60} in solution and thin film forms. As the excited singlet state has shorter lifetime compared to the metastable triplet state, different excited state populations are prepared if different pulse widths are used. Ishihara et al. [45] reports the relaxation dynamics of photoexcitations in polycrystalline C_{60} thin films using fs pump-probe spectroscopy. They observe the decay times of self-trapped excitons and polarons as 570 ± 120 fs and 54 ± 7 ps respectively. Schell et al. [46] working with C_{60}-doped solid xerogel matrices observe a depopulation rate of ~ 150 ps for the S_1 state. They indicate the reason for the observation of short lifetime compared to intersystem crossing rate could be due to the increased interaction between the C_{60} molecules and the surrounding glass matrix. Juhasz et al. [47] reports the dynamics of photoexcited carrier relaxation obtained through measurement of time-resolved transmissivity. They observe a decay time of ~ 18 ps at room temperature and ~ 120 ps at 5° K. They indicate that carrier trapping plays an important role in the relaxation mechanism. Dexheimer et al. [48] working with 60 fs at 620 nm observe the dynamics of C_{60} in both solid and liquid forms using the time-resolved pump-probe technique. In the solid form, they observe a non-exponential decay of the induced absorption, which is intensity dependent. For C_{60} in solution, because of the limited solubility, the molecules are well separated and the fast intensity dependent component is not observed. The dynamics are dominated by the intersystem crossing occurring on the time scale of few hundred ps.

Farztdinov et al. [49] report the slowing-down of ultrafast relaxation in C_{60} thin films at high fs pump intensities and suggest that this slowing-down results from

two-step photon absorption of the high-intensity pulse. Palit et al. [50] investigating the Photophysical properties of C_{60} and C_{70} report the S_1 state lifetime in C_{60} as 1.4 ns and is found to be solvent independent. Cheville et al. [51] report the time-resolved carrier relaxation in solid C_{60} thin films at 605 nm and observe a decay time of 43 ps which is temperature independent. They identify the two processes, carrier trapping and carrier hopping, relevant for the understanding of carrier relaxation. Chekalin et al. [52] performed fs measurements of relaxation in thin film and solution forms at different excitation intensities. They observe sharp differences in the relaxation mechanism in solid and solution forms. They do not observe any short-lived component in solution form (except for the 1.2 ps rise time, because of the disruption of the symmetry of the molecule as its structure changes). For thin films they observe the photo-induced absorption relaxes in a non-exponential way, at a rate which increases with increasing excitation intensity along with the spectral dependence peaking at 650 nm. Kardash et al. [53] reports their fs laser spectroscopic studies on ultrafast relaxation of photo-induced darkening in fullerite (C_{60} on a quartz substrate). They observe electronic-vibrational relaxation with time scales of ~ 1 ps and 30 ps. Wasielewski et al. [54] report fist excited singlet state lifetime of ~ 34 ps observed from their transient absorption measurements.

Yang et al. [55] performed time-resolved DFWM measurements with 32 ps pulses at 532 nm in the boxcar geometry. The time response was measured for different polarization configurations of the probe beam to extract the singlet S_1 state lifetime. They observe that dynamics exhibit a strong dependence on the incident energy. In the *yxxy* (probe polarization orthogonal to the pump beams) they observe a single decay in the DFWM signal with a decay time of ~ 650 ps. After excitation, the first excited state S_1 is populated, immediately opening up the S_1 to S_n transitions. At low pump intensities the lifetime of the S_1 state is mostly governed by the intersystem crossing rate from S_1 to T_1 state. They also argue that the most likely path for fast depletion of S_1 within a faster time scale (< 1 ns) is the strong singlet-singlet excited state absorption S_1 to S_n of the pump beams with subsequent non-radiative decay to the ground state. Flom et al. [56] performed time-resolved DFWM measurements on thin films of C_{60} and observed a lifetime of ~ 650 ps for the first excited singlet state.

A non-exponential decay is observed for low laser fluences, which is consistent with the pump-probe studies. The dynamics exhibit strong dependence on the laser fluence with decay becoming much faster at higher fluences. They also suggest that lifetime of the singlet state is governed by the intersystem crossing and strongly dependent on the excited-state population density. At lowest excitation densities the decay of the NLO signal was consistent with the 43 ps lifetime previously reported at 605 nm. The shortening of the lifetime of the electronic excited state, observed at high fluence, is attributed to an excitonic singlet-singlet annihilation mechanism. Sension et al. [57] reports the results of their transient absorption studies of C_{60} in solution using second and third harmonics of a Nd: YAG laser. A 100 ps component and a 650 ps growth component were observed in kinetics measurement performed using a 600 nm probe. They indicate that the 100 ps component is possibly due to the relaxation of the low-lying singlet states contributing to the broad ground state absorption between 440 and 660 nm. Ebbesen et al. [58] reports their excited state properties using ns and ps laser flash photolysis. They obtain S_1 state lifetime as 1.2 ns. Tanigaki et al. [59] reports the S_1 state lifetime as ~ 670 ps from their ps and ns laser flash photolysis studies. Brorson et al. [60] working with 80 fs pulses at 620 nm report their pump-probe investigations. In the forward FWM geometry (also known as self-diffraction geometry) they observe that the signal does not show any decay suggesting the phase relaxation time $\mathbf{T_2}$ to be < 100 fs. In our case we *do* observe two orders of the self-diffracted signals when the backward pump is blocked. The signal recorded by delaying the probe beam (beam 3 in this case) in either of $\mathbf{2k_2}$ - $\mathbf{k_1}$ or $\mathbf{2k_2}$ - $\mathbf{k_1}$ directions, shown in fig. 6.3 (b), does not show any decay again suggesting that T_2 is less than correlation time, 170 fs. There are also several other reports $[61\text{-}64]$ on the dynamics of excited states in C_{60} and it's derivatives studied using different techniques and pulse widths.

6.3 Z-scan studies

6.3.1 Reverse Saturable Absorption in C_{60}

The ability to control the intensity of light in a predetermined and predictable

manner is one of the most fundamental and important of manipulations, with applications ranging from optical communications to optical computing. There are many methods that can be used to switch, limit, amplify, or modulate the amplitude of an optical signal. All of these methods may be broadly categorised into two groups: dynamic and passive methods. In the dynamic methods, a device that uses some form of active feedback achieves control on the light intensity. For example a photo-sensor, which controls an iris that, restricts the intensity of light, incident on an optical system. There are an infinite number of schemes and devices that can be constructed to control light in this manner. But all these dynamic devices suffer a number of disadvantages. One of them is higher complexity, which results from the need for multiple components that must communicate with one another. Passive control is typically accomplished using a nonlinear optical material in which the sensing, processing and actuating functions are inherent. The optical control function is part of the physical characteristics of the material, so the speed is not limited by communication between individual modules and the device can be potentially very simple and fast.

Two important and different types of passive devices used to control the amplitude of an optical signal are optical limiters and switches. Both have many realised and potential applications. An ideal passive optical switch is a nonlinear optical device that is activated at a set intensity or fluence (Energy/Unit Area) threshold, after that the device becomes completely opaque. Whereas the optical limiters exhibits linear response at low input levels and for inputs above some threshold level the output is clamped. For some materials, e.g., two photon absorbers, this transmittance may be near 100%, and the input-output curve would have a slope of 1. On the other hand, RSA materials require a certain amount of linear absorption, and thus the input-output slope in the linear regime would be less than 1. At certain critical intensity in an ideal optical limiter the transmittance changes abruptly and exhibits an inverse intensity or fluence dependence. Thus the output is clamped at some value that would be less than the amount required damaging the sensor. This critical point is known as threshold of the device, and the clamped out put value is called as the limiting value of intensity or fluence. In a real material the transition is not so abrupt as in ideal optical limiter. In realistic conditions the definitions of threshold is not quite

as precise and in a real material, the output is not always clamped at a constant value.

An optical limiter must provide protection over a wide range of incident intensity or fluence. To achieve this task the optical limiter should possess two desirable qualities, such as low threshold and wide dynamic range, which is the ratio of the damage threshold (ED) to the threshold limiting value (EL). One of the most important applications for optical limiters is eye and sensor protection in optical . systems, such as direct viewing devices, night vision systems, etc. Such devices are useful for the protection of human eye and optical sensors from intense laser beams. Development of materials for optical limiting is based on various mechanisms [65] such as free-carrier absorption and refraction in semiconductors, optical breakdown-induced scattering, thermal refractive beam spreading, two-photon absorption (TPA) and excited state absorption (ESA). C_{60} was one of the first compounds to be identified as a potential candidate for optical limiting [22]. There have been series of other studies involving C_{60} and it's derivatives for realisation of optical limiter. The most important mechanisms responsible for limiting behaviour in C_{60} are excited state absorption and scattering [22,30]. For realisation of practical devices a two-fold effort is necessary. In the first step one should identify and completely understand the underlying mechanisms responsible for optical limiting like the lifetimes of each state, different excited state cross-sections etc. The next step involves the structural/chemical modification of the material and to perform repeat studies for optimisation of the material properties. Among the different techniques for measuring the excited state parameters Z-scan [66] is a simple, single beam technique which provides deep insight into the nonlinear absorptive properties of the material.

The imaginary part of the third order nonlinear susceptibility is responsible for nonlinear absorption. Two-photon absorption, Saturable absorption and reverse Saturable absorption are the most relevant type of nonlinear absorption processes in our studies. In two-photon absorption process, a molecule makes a transition from its ground state to an excited state by the simultaneous absorption of two photons from the incident radiation field. TPA is an instantaneous nonlinearity, which involves the absorption of a photon from its initial state to a virtual intermediate state, followed by

the absorption of a second photon that takes the electron to its final sate [fig. 6.4 (a)]. Saturable absorption involves the saturation of a given transition [depicted in fig. 6.4 (b)]. If the excited state absorption is less than ground state absorption and a long-lived state, say T_1, is involved in transition the material becomes transparent which was earlier absorbing. Reverse Saturable Absorption (RSA) generally arises in a molecular system when the excited state absorption cross section is larger than the ground state cross section. Keyes et al. and Guiliano et al. [67] reported the first observation of RSA. RSA is illustrated in Fig 5c for the materials in which energy states involved in three and five vibronically broadened electronic energy levels. σ_0 is the absorption cross-section from the ground state, σ_1 is absorption cross section from the first excited state to second excited state and σ_2 is absorption cross section from the first triplet state to excited triplet state. If σ_1 is larger than σ_0 then the total absorption increases and the material is known as reverse saturable absorber. In the five-level model the excited state 4 is usually a triplet or other long-lived state. It acts as a metastable state that accumulates population. The basic difference between TPA and ESA is that former involves intermediate extremely short-lived virtual states, whereas the latter involves intermediate real states whose lifetimes are determined by the electronic structure of the molecules in the material. TPA depends on intensity whereas ESA depends on fluence of the incident light. ESA involves a sequential process in which a photon is initially absorbed and the molecule remain in an excited state for a finite length of time so that a second photon that arrives during that time is absorbed to put the molecule in to an even higher excited state. For TPA, the material response is on the order of an optical cycle and is, therefore independent of the pulse width for a fixed intensity. The mechanism of TPA can be visualised in terms of three level RSA model for the case where lifetime of the intermediate state approaches zero and the ground state absorption cross-section is extremely low.

6.3.2 Dispersion studies of nonlinear absorption

Recent studies show very high performance ESA or reverse saturable absorption (RSA) behaviour in C_{60} [22-36]. These materials are characterised by
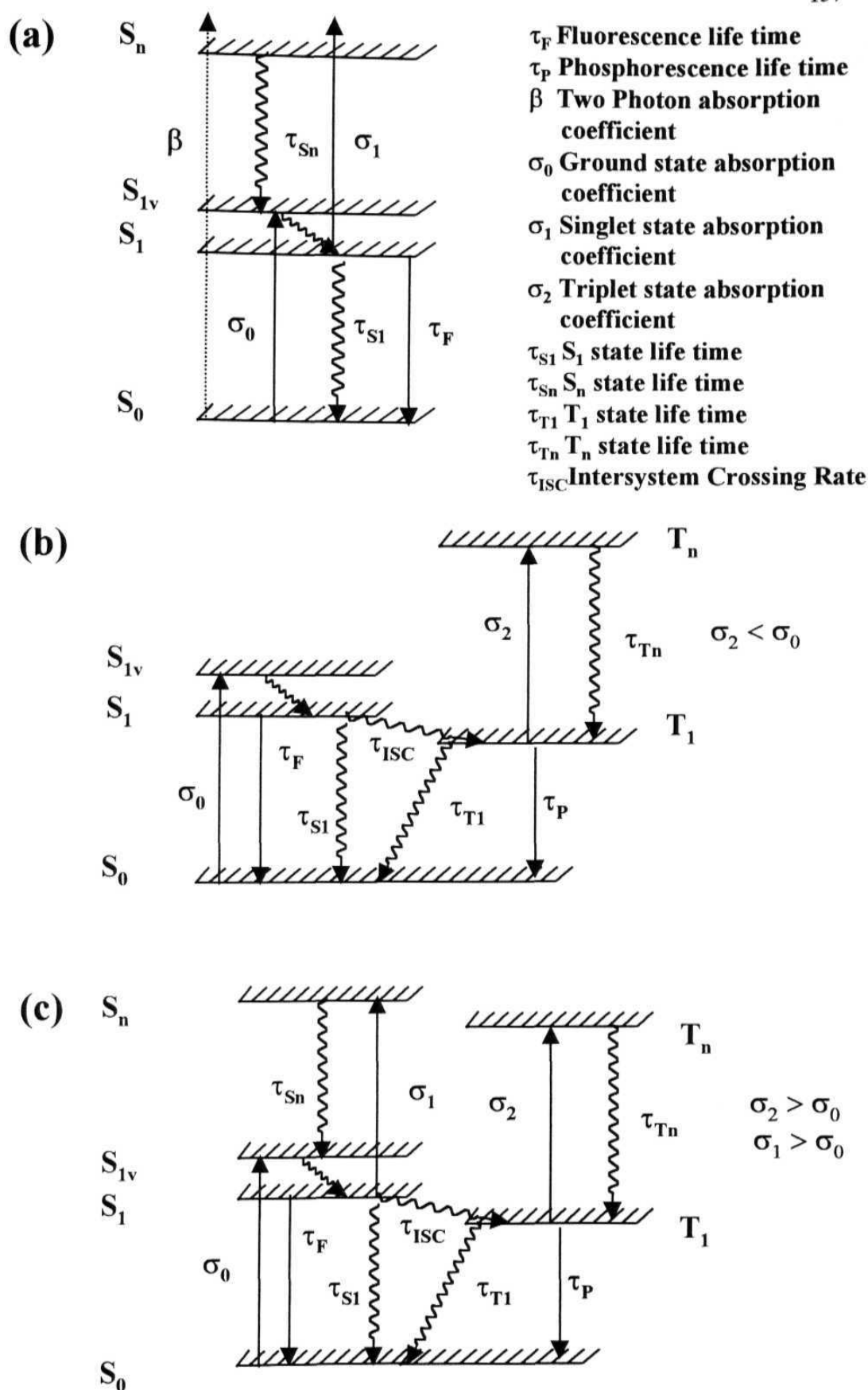
Fig. 6.4 (a) Two-photon Absorption (b) Saturable Absorption
(c) Excited State Absorption

their strong excited state absorption (σ_2 and CT]) compared to ground state absorption (σ_0). Most of these studies concentrated either at 532 nm or 600 nm and the models used to evaluate the photo-physical parameters are based on either 4-level (first excited singlet and triplet levels) or 3-level (singlet levels only) models. For fs and ps pulse excitation, triplet level contribution to the non-linear absorption can be neglected due to the slower intersystem crossing (~ 650 ps). Whereas, with ns pulses the triplet levels do play an important role. Depending on the pump intensity and wavelength, the absorption could be (1) from ground state S_o to the first excited singlet state S_1 and then to T_1 state through inter-system crossing (2) directly from S_o to S_n states (TPA) (3) from first excited singlet sate S_1 to higher excited states S_n (ESA/RSA) (4) from T_1 to T_n states (ESA/RSA). One has to incorporate all these absorption phenomena in rate equations in order to obtain exact contribution from each of these processes. Earlier reports [68-72] on dispersion studies of non-linear absorption do not take into consideration the contribution of two-photon absorption. We have performed open aperture Z-scan of C_{60} (in toluene) in the visible region from 440 nm to 660 nm. To fit our experimental data we consider a theoretical model where contribution to the non-linear absorption could be from S_o to S_n states (due to direct TPA), S_1 to S_n states (due to ESA/RSA) or T_1 to T_n states (due to ESA/RSA). Different curves are theoretically obtained by varying the ESA and TPA coefficients and the input intensity. The behaviour of the open aperture Z-scan curve with changes in the above parameters is investigated in detail.

We employ a commercial OPO (MOPO laser by Spectra Physics) pumped by the third harmonic (355 nm) from the Quanta Ray Nd: YAG laser with a repetition rate of 10 Hz and tunable in the range of 380-1000 nm for the open aperture Z-scan [66] studies. The pulse duration of the laser is 6 ns. The experimental set-up consists of a lens, sample, and a large area detector. The sample cell is moved along a rail, using a computer controlled stepper motor, to vary the intensity of light in the sample. An aperture of 1.4 mm is used at the output of the MOPO laser to obtain a smooth profile in the far field. Energy after the aperture varied from 0.2 to 2 mJ/pulse depending on the wavelength. The focal length of the lens used for focusing the beam into the sample is 50 mm. 1-mm glass cuvettes are used for the sample solutions. The input

energy is monitored using a fast photo-diode and the total output collected using a large area lens is measured using a similar photo-diode. The data is collected from -40 mm to +40 mm in steps of 2 mm. Fig. 6.4 (c) details the 5-level model used for theoretical simulations and fitting of the data. C_{60} dissolved in toluene is sonicated to obtain a clear solution. The concentrations used for the studies are in the range $\sim 10^{-4}$ - 10^{-3} M. Open aperture Z-scans are obtained in the wavelength region covering from 440 nm to 680 nm. Immediate scans obtained in opposite direction (+Z to -Z) show , similar structure verifying that there is no damage to the sample or the cell. The calculated values of beam waist at focus are $\sim$ 30 - 50 μ and the corresponding peak intensities are $\sim 10^8$ to 10^9 W/cm^2. The Rayleigh ranges are $\sim$ 6.5 to 8 mm depending on the wavelength. Rate equations for the 5-level model shown in fig. 6.4 (c) are:

$$\frac{dN_0}{dt} = -\frac{\sigma_0 I\, N_0}{\hbar\omega} - \frac{\beta I^2}{2\hbar\omega} + \frac{N_1}{\tau_1} + \frac{N_3}{\tau_4} \tag{1}$$

$$\frac{dN_1}{dt} = -\frac{\sigma_1 I\, N_1}{\hbar\omega} + \frac{\sigma_0 I\, N_0}{\hbar\omega} - \frac{N_1}{\tau_1} - \frac{N_1}{\tau_{ISC}} + \frac{N_2}{\tau_2} \tag{2}$$

$$\frac{dN_2}{dt} = \frac{\sigma_1 I\, N_1}{\hbar\omega} + \frac{\beta I^2}{2\hbar\omega} - \frac{N_2}{\tau_2} \tag{3}$$

$$\frac{dN_3}{dt} = -\frac{\sigma_2 I\, N_3}{\hbar\omega} - \frac{N_3}{\tau_4} + \frac{N_1}{\tau_{ISC}} + \frac{N_4}{\tau_3} \tag{4}$$

$$\frac{dN_4}{dt} = \frac{\sigma_2 I\, N_3}{\hbar\omega} - \frac{N_4}{\tau_3} \tag{5}$$

and the intensity transmitted through the sample is given by

$$\frac{dI}{dz} = -\sigma_0 I\, N_0 - \sigma_1 I\, N_1 - \sigma_2 I\, N_3 - \beta I^2 \tag{6}$$

with

$$I = I_{00} * \left(\frac{\omega_0^2}{\omega^2(z)}\right) * \exp\left(-\frac{t^2}{\tau_p^2}\right) * \exp\left(-\frac{2*r^2}{\omega^2(z)}\right) \tag{7}$$

and

$$\omega(z) = \omega_0 \left\{1 + \left(\frac{z}{z_0}\right)^2\right\}^{\frac{1}{2}} \; ; \; z_0 = \frac{\pi * \omega_0^2}{\lambda}$$

where σ_0 is the ground state absorption cross-section, CTi and σ_2 are the excited state absorption cross-sections from S_1 and T_1 states respectively, N_i's are the corresponding populations in the different states, Xj's are the lifetimes of the excited states, z_0 is the Rayleigh range, ω_0 is the beam waist at focus, 1 is intensity as a function of r, t, and z, I_{00} is peak intensity at the focus of the Gaussian beam, τ_p is the input pulse width used, (3 is the two-photon cross-section, and τ_{ISC} is the intersystem crossing rate. The differential equations are solved numerically using Runge-Kutta fourth order method. The equations are first de-coupled and then integrated over time, length, and along the radial direction. Assuming the input beam to be a Gaussian, the limits of integration for r, t, and z are varied from 0 to ∞, -00 to 00, and 0 to L (length of the sample) respectively. Typical number of slices used for r, t, and z are 60, 30, and 5 respectively. $G\backslash$, σ_2, and β are then estimated through least square fit of the experimental data.

Fig. 6.5 shows the experimental data (scattered points) and the theoretical fits (solid lines) obtained using the five level model for wavelengths ranging from 440 nm to 640 nm. Ground state absorption cross-sections for different wavelengths are calculated using $\sigma_0 = (a/N)$ where a is the linear absorption and N is the density of molecules per cm. Depending on the wavelength, I_{00} is found to be ~ 10 - 10 W/cm^2, ω_0 ~ 30 - 50 μm, z_0 ~ 6.5 - 8 mm. The relaxation time of the first excited singlet state τ_{S1}, intersystem crossing time τ_{ISC}, and the lifetime of the first excited triplet state τ_{T1} are taken as 70 ps, 650 ps, and 280 μs respectively. The relaxation times of S_n and T_n states are taken as ~ 100 fs. Excitation wavelengths are indicated for each Z-scan curve. In the wavelength region from 440 nm to 540 nm, experimental data fits better with $\beta = 0$ and in the wavelength region 580 nm to 640 nm, β dominates with smaller contribution from CT2 or σ_1. Effect of σ_1 on the Z-scan curves is shown in fig. 6.6 for two arbitrary wavelengths, one in 440 - 540 nm range and the other in 580 - 640 nm range.

Fig. 6.6 (a) shows the theoretical curves generated at 480 nm for $\sigma_0 = 3.0*10^-$ cm^2, a, $=15.0*10^{-18}$ cm^2, $\sigma_2 = 12.0*10^{-18}$ cm^2, (3 $=0.0$ (solid line); $\sigma_0 = 3.0*10^{18}$ cm^2,
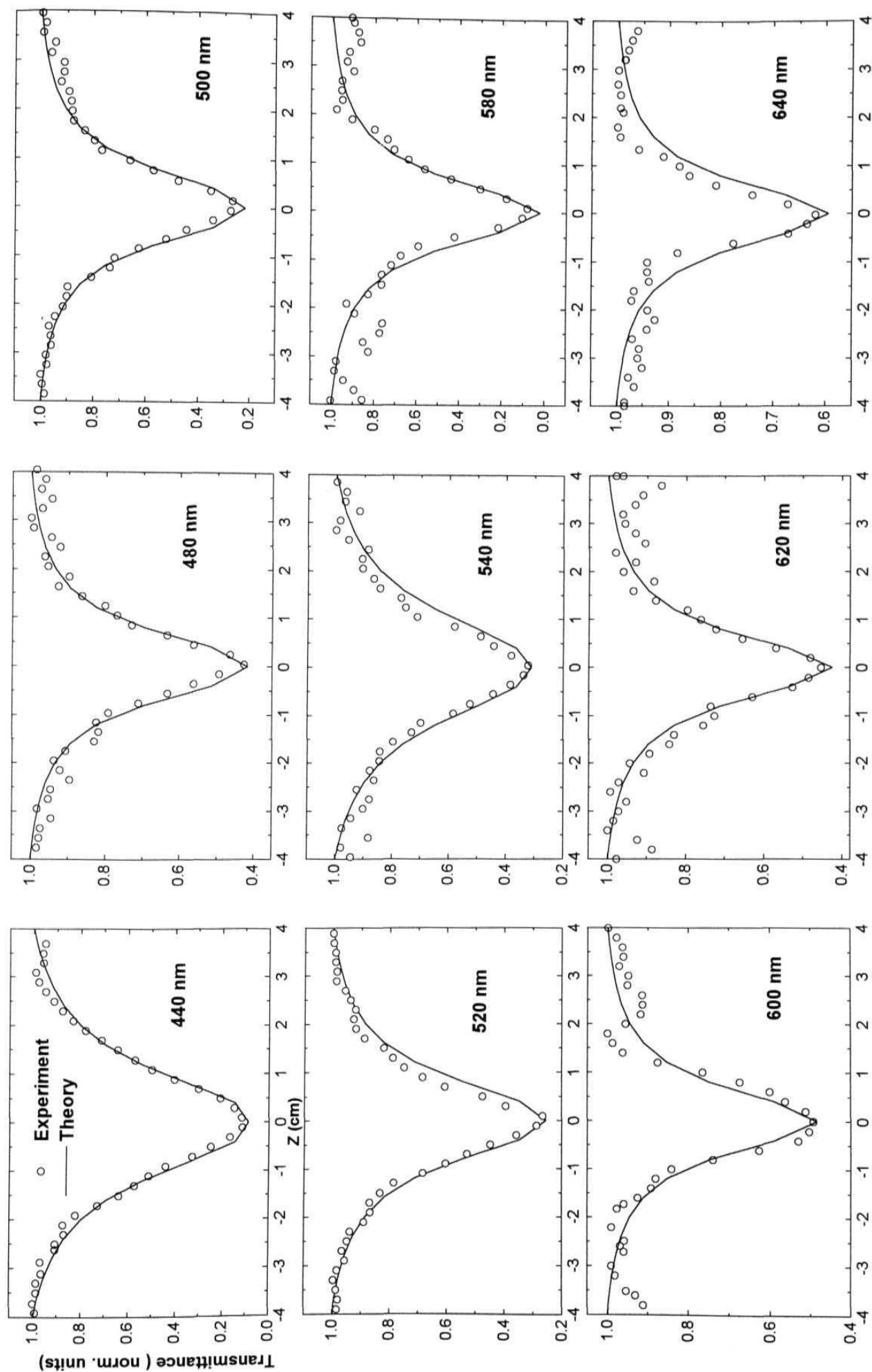
Fig. 6.5 Experimental data (open circles) and fitted curve (solid line) using the 5-level model for different wavelengths

Fig 6.6 Theoretical curves showing the effect of σ_1 at two wavelengths

(a) $\sigma_0 = 2.99*10^{-18}$ cm^2, $\sigma_2 = 12.0*10^{-18}$ cm^2, p = 0, $I_{00} = 10^9$ W/cm^2

(b) $\sigma_0 = 1.65*10^{-18}$ cm^2, $\sigma_2 = 2.40*10^{-18}$ cm^2, p = 2.25*10^{-8} cm/W,

$I = 4*10^8$ W/cm^2. The scattered points are the experimental data.

$\sigma_1 = 0.0$, $\sigma_2 = 12.0 \times 10^{-18}$ cm^2, $\beta = 0.0$ (dotted line). Fig. 6.6 (b) shows the theoretical curves generated at 600 nm for Go $= 1.65 \times 10^{-18}$ cm^2, $\sigma_1 = 6.60 \times 10^{-18}$ cm^2, $\sigma_2 = 6.60 \times 10^{-18}$ cm^2, ($3 = 2.25 \times 10^{-8}$ 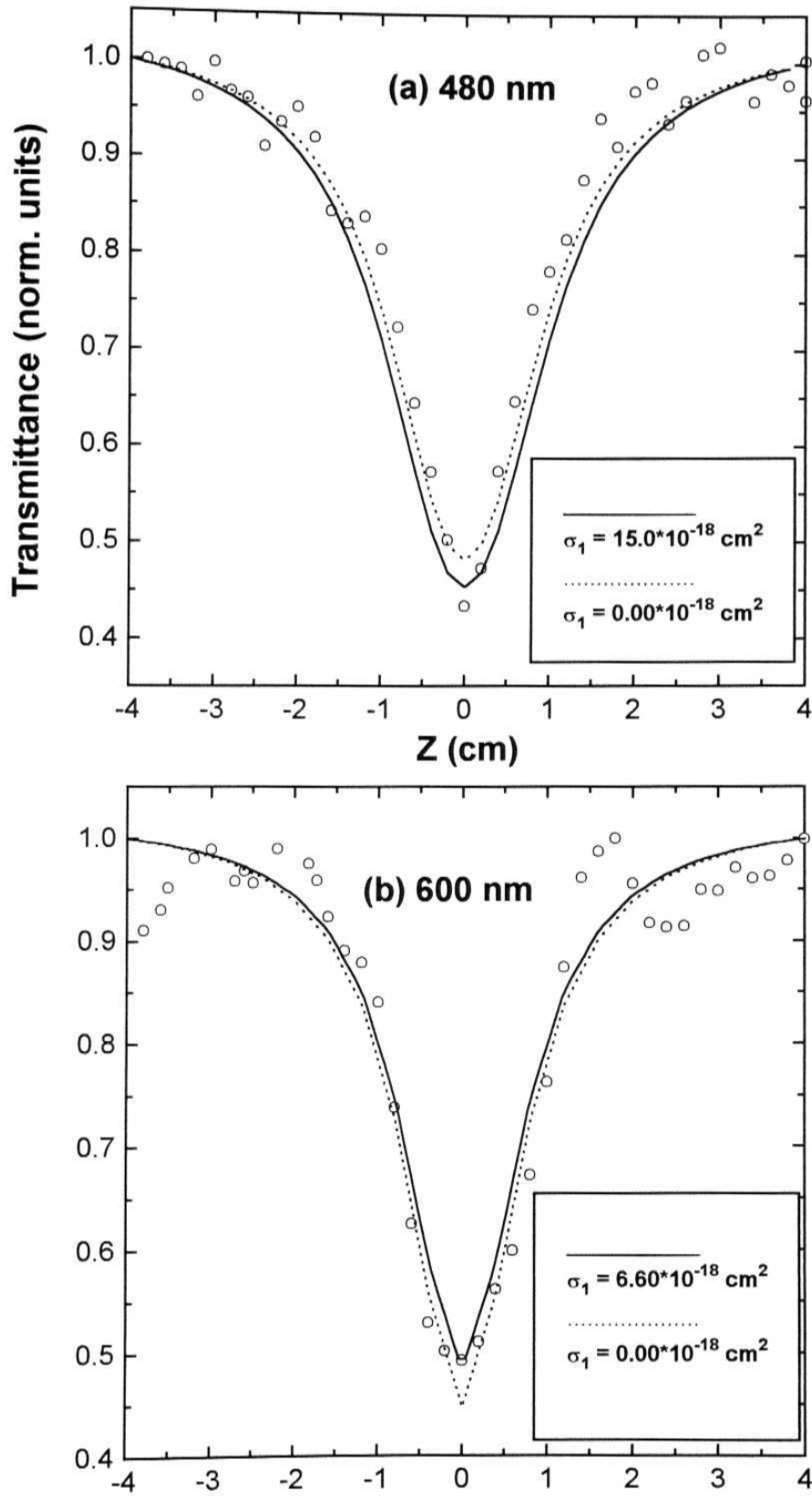cm/W (solid line); $\sigma_0 = 1.65 \times 10^{-18}$ cm^2, $\sigma_1 = 0.0$, $\sigma_2 = 6.60 \times 10^{-18}$ cm^2, $\beta = 2.25 \times 10^{-8}$ cm/W (dotted line). As we can see, there is very little effect on the open aperture Z-scan curves due to σ_1, which is mainly due to the fact that we have taken τ_{S1} to be 70 ps. Lifetimes of S$_1$ state have been reported to be ~ 100 ps, ~ 650 ps and ~ 1.2 ns by several groups [44-56]. Our studies performed through incoherent laser spectroscopy [42] have shown a lifetime for the S$_1$ state as 70 ps. We could obtain a reasonably good fit for σ_1 varying from 15×10^{-18} cm^2 to 20×10^{-18} cm^2 with σ_2 around 12×10^{-18} cm^2. Therefore, there could be larger error in the values of σ_1 compared to σ_2. If fs pulses are used for excitation we expect the contribution of σ_1 alone to the non-linear absorption as the intersystem crossing would be too slow compared to the pulse duration. From the fs data, one can then exactly find out the contribution of σ_1. Effect of varying τ_{S1} on the Z-scan curves is shown in fig. 6.7. Simulated curves for $\tau_{S1} = 1.2$ ns and 70 ps are shown in fig.'s 6.7 (a) for 480 nm and 6.7 (b) for 600 nm. Dotted line is the curve with $\tau_{S1} = 1.2$ ns and solid line is the curve with $\tau_{S1} = 70$ ps with all other parameters remaining same. We clearly see that for $\tau_{S1} \sim 1.2$ ns, the curves become very broad indicating that for the C$_{60}$ sample, that has been used in our system, $\tau_{S1} = 70$ ps. For longer wavelengths [fig. 6.7 (b)], the effect of τ_{S1} is small because of the domination of TPA in this range. The present results are therefore consistent with our earlier studies reported through DFWM experiments done with a broad band laser [42]. The sample that has been used in both the experiments is from the same batch and company.

In the above theoretical calculations we have assumed that the scattering from the sample, responsible for nonlinear absorption, is minimum. Mishra et al. [30] reports nonlinear scattering as the main mechanism responsible for optical limiting in C$_{60}$ in their experiments performed at 527 nm using 30 ns pulses. They also argue that the scattering arises from the thermally induced inhomogeneties and has been observed for fluences larger than 4 J/Cm^2 only. In our case the transmission measured with and without an aperture in the path of the transmitted remained almost the same, within

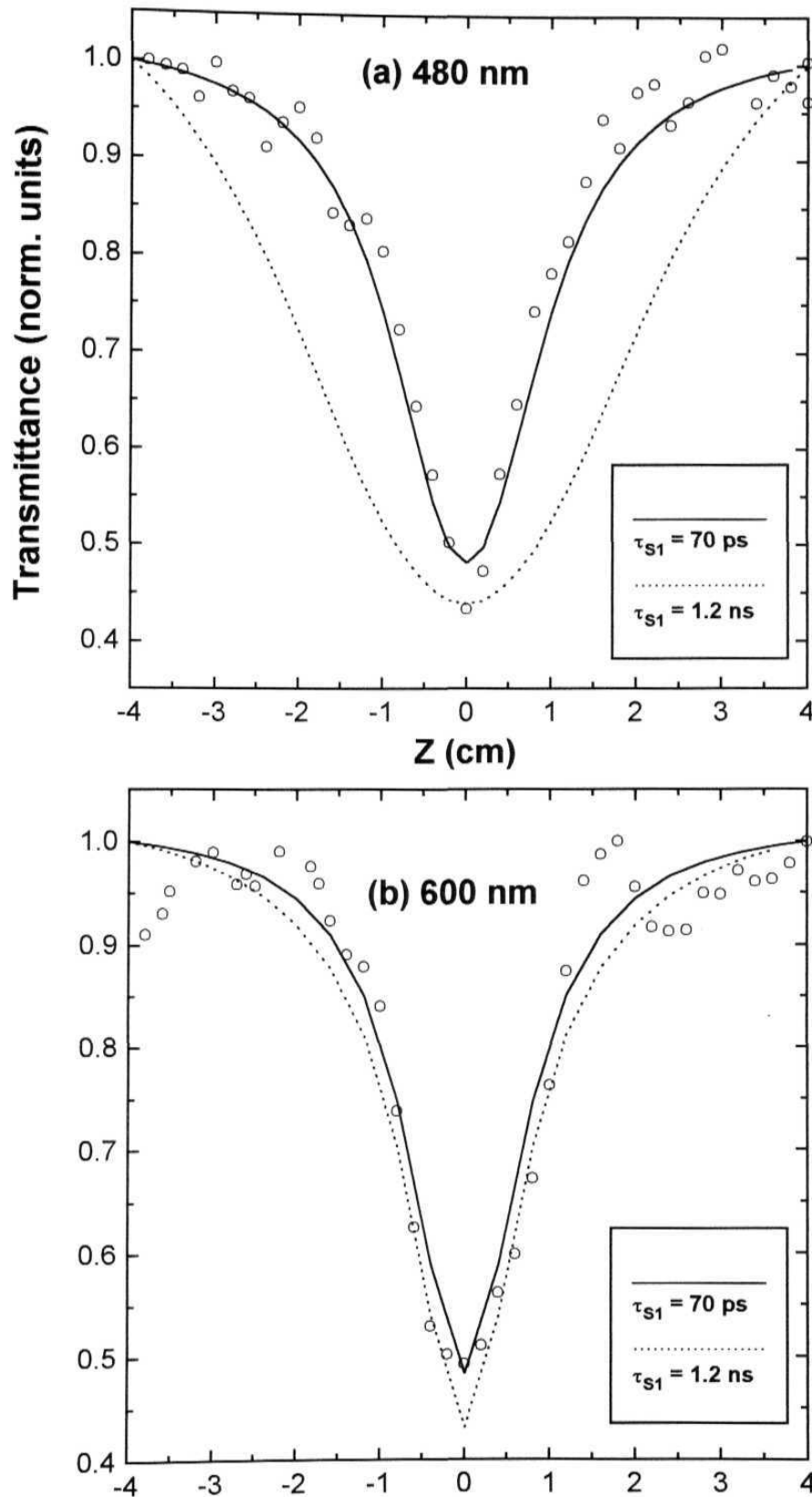Fig. 6.7 Theoretical curves showing the effect of τ_S at two different wavelengths.

(a) $\sigma_0=2.99*10^{-18}$ cm^2, $\sigma_1=0.0$, $\sigma_2=12.0*10^{-18}$ cm^2, $\beta=0.0$, $I_{00}=10^9$ W/cm^2

(b) $\sigma_0=1.65*10^{-18}$ cm^2 $\sigma_1=6.6*10^{-18}$ cm^2, $\sigma_2=2.4*10^{-18}$ cm^2, $\beta=2.25*10^{-8}$ cm/W,

$I=4*10^8$ W/cm^2. The scattered points are the experimental data

experimental error, indicating the negligible contribution of scattering, Also the solution obtained by dissolving in toluene is a clear solution and visual observation of the transmitted beam does not show any distortion in the beam profile.

σ_1, σ_2, and β obtained from our results are given in table 1 along with those reported in literature [74]. There is no contribution from TPA (P) to the non-linear absorption till 540 nm. From 580 nm to 640 nm the non-linear absorption appears to be dominated by TPA. Fig. 6.8 shows the influence of CT_2 and β on the theoretical curves. Figure 6.8 (a) shows the theoretical curves with and without σ_2 for 600 nm. Though both the fits can be seen to be close to the experimental data (open circles), curve generated with non-zero σ_2 and |3 has lower chi-square value. CTi has been taken as zero in this region as we see from fig. 6.8 (b) that the contribution of σ_1 on the curves is negligible. S_n and S_1 energies of C_{60} fall in the region of $\sim 29,000$ cm^{-1} and $\sim$ 16,000 cm^{-1} respectively [41]. Excitations longer than 580 nm fall either on the lower edge of the absorption curve or below it. Since at such excitations, it is expected that the molecule remains localised without diffusing into the higher levels [75] eventually decaying into the S_0 level through τ_{S1} or crossover to T_1 through τ_{ISC} Under such circumstances σ_1 and β would have the same effect. A complete reversal in the domination of a and β are observed in the region of short wavelengths. Below 580 nm [fig. 6.8 (b) at 480 nm] introduction of a small value of β leads to a sharper valley in the curve, deviating from the experimental points. Dotted curve is obtained with non-zero values of σ_1, σ_2 and $\beta = 0.5 * 10^{-8}$ cm/W and dashed curve is obtained for $\sigma_1 - \sigma_2$ = 0.0 and p = 2.25 * 10^{-8}. This clearly shows the domination of σ_1, CT_2 in the shorter wavelength region.

The values of different excited state parameters obtained by different groups, working with different pulse widths, are summarised in table 1. The value of β_{eff} obtained by Gu et al. [70] at 630 nm using CW beam is eight orders of magnitude larger than our value. Although they consider that large nonlinear absorption is dominated by triplet-triplet absorption, there is no experimental evidence that the triplet state T_1 is actually populated. Moreover the ground state absorption of C_{60} is notably increased in thin films as compared with dilute solutions. They have
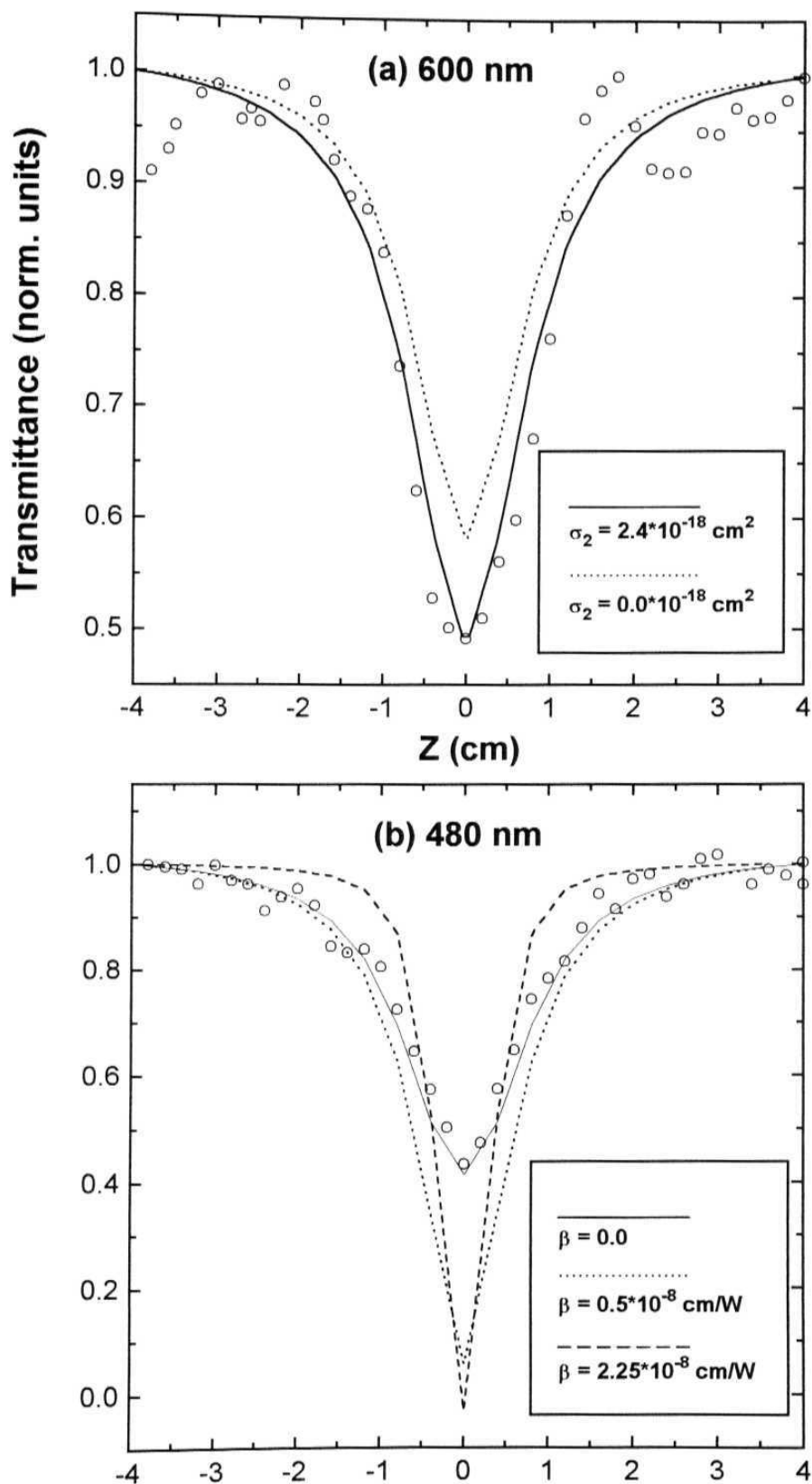
Fig. 6.8 Theoretical curves showing the effect of (a) σ_2 at 600 nm with $\sigma_0 = 1.65 \times 10^{-18}$ cm^2, $_{CTI}= 0$, $\beta = 2.25 \times 10^{-8}$ cm/W, $I_{00} = 4.6 \times 10^8$ W/cm^2 (b) p at 480 nm with $\sigma_0 = 2.99 \times 10^{-18}$ cm^2, $\sigma_1 = 12.8 \times 10^{-18}$ cm^2, $\sigma_2 = 9.6 \times 10^{-18}$ cm^2, $I_{00} = 9.5 \times 10^8$ W/cm^2 and for dashed curve $\sigma_1 = 0$, $\sigma_2 = 0.0$, $I_{00} = 9.5 \times 10^8$ W/cm^2. The scattered points are the experimental data

also suggested that thermal effects play a crucial role in self-focusing observed for their thin-films using CW beams. Bezel et al. [71] working with 300 fs pulses at 612 nm report a β value of $< 3 \pm 1.5*10^{-8}$ cm/W which is in good agreement with our value. Henari et al. [72], using Z-scan measurements, report a value of $1\ 2*10^{-3}$ cm/W at 488 nm for C6o-benzene/toluene solutions using CW beam, chopped at frequencies from 50 to 400 Hz, which is again five orders of magnitude larger than our value. The typical power density they used was ~ 100 W/cm^2. For longer duration pulses the population transfer to the triplet state is more efficient and therefore the optical limiting action will be observed at lower intensities. From viewpoint of practical optical limiting high-intensity pulse laser results are more relevant than the low-intensity chopped CW beams. The σ_{cx} values reported by Henari et al. [73], working with 5 ns pulses, are two orders of magnitude large than our value. Their ground state cross-sections (σ_0) are also two orders of magnitude larger than most of the earlier reported values.

Ebbesen et al., Tanigaki et al., and Barosso et al. [58,59,69] report a value of σ_1 as $\sim 1.6*10^{-17}$ cm^2 at 534 nm. We obtain a value of $1.82*10^{-17}$ cm^2, which is in good agreement with theirs. The values reported by Chunfei Li et al. [38] also match well with our results. Kardash et al. [53] report β value of $\sim 2.0*10^{-8}$ cm/W for C$_{60}$ film on quartz substrate excited with light pulses of frequency ~ 2.02 eV corresponding to ~ 600 nm. Yang et al. [55] carried out Z-scan measurements using 32 ps pulses at 532 nm and found out that S_1 state is the dominant absorption intermediate, with triplet states playing minor role in nonlinear absorption. Justus et al. [32] investigated the C∞ solutions dissolved in 1-chloronaphthalene with Z-scan using 6 ns pulses at 532 nm. Nonlinear phase change of several radians was observed and concluded that both sequential TPA and thermally induced refraction contribute to the nonlinear response. They also suggest developing optical limiting materials based on hybrid mechanism involving both STPA and thermal lensing.

6.3.3 Z-scans at 532 nm and 600 nm using Nd: YAG laser

We have performed open aperture Z-scans at 532 nm [fig. 6.9 (a)] and 600 nm [fig. 6.9 (b)] using the Nd: YAG laser and the broadband dye laser (centred at 595
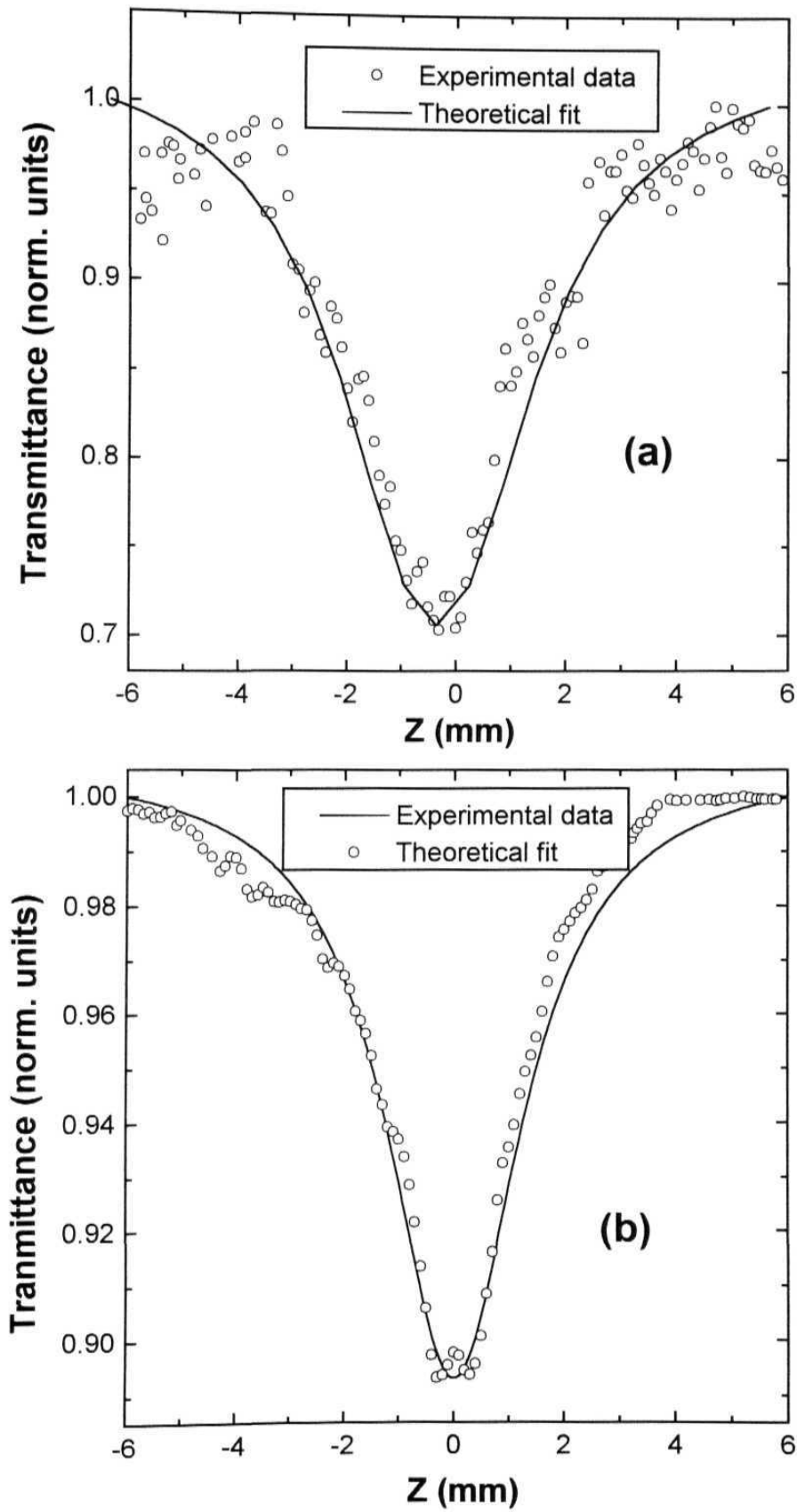
Fig. 6.9 (a) Open aperture Z - scan at 532 nm (6 ns pulses). Solid line is the fit to the data using 5-level model. (b) Open aperture Z - scan data at 600 nm using broadband dye laser. The solid line is fit to the data using 5-level model

nm). The set-up is similar to the one described in earlier section. Input beam diameter in this case is $\sim$ 2.5 mm and a lens of focal length of $\sim$ 80 mm is used to focus the beam into the sample. The scans are obtained from -6 mm to +6 mm using solutions in the concentration range of 10^{-4} to 10^{-3} M. Typical peak intensities are again in the range of 10^{8} - 10^{9} W/cm^2. The Rayleigh range is found to be $\sim$ 3 mm, larger than the thickness of the sample (1-mm), validating the thin sample approximation. The obtained data is fitted to the above 5-level model [fig. 6.9 (a) and (b)] and the different excited state parameters evaluated are found to be of the same order. Two photon absorption coefficient, (3, is found to be $\sim$ 2.5*10^{-8} cm/W at 600 nm with very small contribution from $\sigma_2 \sim$ 2*10^{-18} cm^2. At 532 nm we obtain σ_1 as $\sim$ 16.0*10^{-18} cm^2 and σ_2 as $\sim$ 10.0*10^{-18} cm^2. Both the values match very well with those obtained using an OPO.

6.4 Conclusions

1. We observe large third-order nonlinearity at 600 nm ($Y \sim 5.388 * 10^{-30}$ esu) obtained using broadband ns pulses. The high value is attributed to the strong TPA combined with contribution from the thermal part.

2. The excited state lifetimes measured using incoherent light are found to be < 170 fs, ~ 5 ps, and ~ 70 ps for the S_n state dephasing, S_{1v}-S_{10} vibrational relaxation and the S_1 state population relaxation respectively. The above results match very well with those obtained using the DFWM technique with 150 fs pulses at 633 nm.

3. From the dispersion studies of nonlinear absorption and theoretical modelling of the experimental data we evaluate the different excited state parameters for C_{60} in toluene. For the first time in the theoretical modelling we include the contribution of two-photon absorption, apart from excited absorption, to the total nonlinear absorption and solve the equations numerically. The values so obtained are in good agreement with those reported in literature.

4. From the dispersion studies we conclude that for optical limiting the main advantage of C_{60}, in comparison to Porphyrins and Phthalocyanines, is it shows RSA behaviour over the entire visible region, either through ESA in the shorter wavelengths or through TPA in the longer wavelength region. A proper chemical manipulation of this material could result in a practical optical limiter.

σ_0 (10^{-18} cm²)	σ_1 (10^{-18} cm²)	σ_2 (10^{-18} cm²)	$\beta*10^{-8}$ (cm/W)	References
296 520 350	-	$(\sigma_{ex})^*$ 802 149 724	-	Henari etal. [69], 5 ns 440 nm 520 nm 580 nm
1.21	8.07	5.35	-	Kost et al. [22] 532 nm, 8 ns
2.87	15.7	9.22	-	Chunfei Li [38] 532 nm, 15 ns
3.2	16.0	14	-	Barosso et al.[68] 534 nm, 6 ns
				Our study
1.79	22.0	14.0	-	440 nm
2.99	12.8	9.6	-	480 nm
2.69	14.8	11.6	-	500 nm
2.70	22.2	11.4	-	520 nm
2.69	18.2	11.4	-	540 nm
1.445	-	3.0	2.45	580 nm
1.65	-	2.4	2.25	600 nm
1.03	-	3.6	1.95	620 nm
0.724	-	2.2	1.85	640 nm
$^@\alpha$ 3.4 /cm 3.4/cm 0.45/cm	-	$(\sigma_{ex})^*$ 0.39 0.72 0.45	(β_{eff}) 0.96 1.85 0.18	McBranch et al.[27] 6 ns 561 nm 575 nm 680 nm
-	-	(σ_2/σ_0) - 8.3 7.5	(β_{eff}) 3.9 3.14 1.9	Couris et al. [17], 15ns 620 nm 630 nm 640 nm
-	-	-	(β_{eff}) $8.0*10^8$	Gu et al. [70] CW, 633 nm
-	-	-	(β_{eff}) $1.2*10^5$	Henari et al. [72] CW, 488 nm
5.0	-	-	$\leq(3\pm1.5)$	Bezel et al. [71] 300fs, 612 nm

$^@$ **linear absorbance** * **effective excited state cross-section**

Table 6.1 Comparison of the values obtained using our five-level model and those reported in literature

6.5 References

1. W. Kratschmer, L.D. Lamb, K. Fostiropolous, DR. Huffman, *Nature* **347,** 354, 1990; W. Kratschmer, L.D. Lamb, K. Fostiropolous, DR. Huffman, *Chem. Phys. Lett,* **170,** 167, 1990.

2. DS. Chemla, J. Zyss, Eds., *Nonlinear Optical Properties of Organic Molecules and Crystals,* Vols., 1 and 2, Academic Press, Orlanda, FL, USA, 1987; S.R. Marder, J.E. Sohn, G.D. Stucky, Eds., *Materials for Nonlinear Optics: Chemical Perspectives*, ACS Symposium Series, American Chemical Society, Washington , DC 1991; P.N. Prasad and D.J. Williams, *Introduction to Nonlinear Optical Effects in Molecules and Polymers,* Wiley, New York, 1991; J.L. Bredas, C. Adant, P. Tackx, and A. Persoons, *Chem. Rev.* 94, 243, 1994.

3. Q. Gong, Y. Sun, Z. Xia, Y.H. Zhou, Z. Gu, X. Zhou, and D. Qiang,./. *Appl. Phys.* **71(6),** 3025, 1992.

4. W.J. Blau, H.J. Byrne, D.J Cardin, T.J Dennis, J.P. Hare, H.W. Kroto, R Taylor and D.RM Walton, *Phys. Rev. Lett.* **67,** 1423, 1991; W.J. Blau and D.J. Cardin, *Mod. Phys. Lett.* **B6(22),** 1351, 1992; R.J. Knize and J.P. Partanen, *Phys. Rev. Lett.* 68, 2704, 1992; Z.H.Kafafi, F.J. Bartoli, J.R. Lindle, and R.G.S. Pong, *Phys. Rev. Lett,* 68,2705, 1992.

5. Z. Zhang, D. Wand, P. Ye, Y. Li, P. Wu and D. Zhu, *Opt. Lett.* **17(14),** 973, 1992; R.Vijaya, Y.V.G.S. Murthy, G. Sundararajan, C.K. Mathews and P.R. Vasudeva Rao, *Opt. Commun.* 94, 353, 1992.

6. F. Henari, J. Callaghan, H. Stiel, W. Blau and D.J. Cardin, *Chem. Phys. Lett.* **199,** 144, 1992; Z.H. Kafafi, J.R. Lindle, R.G.S. Pong, F.J. Bartoli, L.J. Lingg and J. Milliken, *Chem. Phys. Lett.* **188,** 492, 1992.

7. J.S. Meth, H. Vanherzeele, and Y. Wang, *Chem. Phys. Lett.* **197,** 26, 1992; Y. Wang and L.-T. Cheng, *J. Phys. Chem.* 96, 1530, 1992.

8. M.J. Rosker, HO. Marcy, Tallis Y. Chang, J.T. Khoury, K. Hansen, and R.L. Whetten, *Chem. Phys. Lett.* **196,** 427, 1992.

9. D. Neher, G.I. Stegeman, F.A. Tinker, N. Peyghambarian, *Opt. Lett.* **17,** 1491, 1992; GB. Talapatra, N. Manickam, M. Samoc, ME. Orczyk, S.P. Karna, and P.N. Prasad,./. *Phys. Chem.* **96,** 5206, 1992; K.C. Rustagi, L.M. Ramaniah, and

S.V. Nair, *Int, J. Mod. Phys.* **B6(23,24),** 3941, 1992.

10. F.J. Aranda, D V.G.L.N. Rao, J. F. Roach and P. Tayebati, *J. Appl. Phys.* **73,** 7941, 1993.

11. W. Ji, S.H. Tang, G.Q. Xu, H.S.O. Chan, S.C. Ng, and W.W. Ng, *J. Appl. Phys.* **74,** 3669, 1993; H. Liu, B. Taheri and W. Jia, *Phys. Rev.* **B49,** 10166, 1994.

12. F. Kazjar, *Proc. SPIE* **2025,** 352, 1993; F. Kazjar, C. Taliani, R. Danieli, S. Rossini, and R. Zamboni, *Chem. Phys. Lett.* **217(4),** 418, 1994.

13. S.R. Flom, R.G.S. Pong, F.J. Bartoli, and Z.H. Kafafi, *Phys. Rev.* **B46,** 15598, 1992; S.R.Flom, F.J.Bartoli, H.W.Sarkas, C.D.Merritt, and Z.H.Kafafi, *Phys. Rev.* **B51,** 11376, 1995.

14. D. Zhou, L. Gan, C. Luo, H. Ton, C. Huang, Z. Liu, Z. Wu, X. Zhao, X. Xia, S. Zhang, F. Sun, Z. Xia, Y. Zou, *Chem. Phys. Lett.* **235,** 548, 1995.

15. L. Geng, J.C. Wright, *Chem. Phys. Lett.* **249,** 105, 1996; H. Kanbara, T. Maruno, A. Yamashita, S. Matsumoto, T. Hayashi, H. Konami, and N. Tanaka, *J. Appl. Phys.* 80,3674, 1996.

16. F. Li, Y. Song, K. Yang, S. Liu, and C. Li, *Appl. Phys. Lett.* 71, 2073, 1997; H. Huang, G. Gu, S. Yang, J. Fu, P. Yu, G. K.L.Wong, and Y. Du, *J. Phys. Chem.* **B102,** 61, 1998; B.C. Hess, D.V. Bowersox, S.H. Mardirosian, L.D. Unterberger, *Chem. Phys. Lett.* 248, 141, 1996.

17. S. Couris, E. Koudoumas, A.A. Ruth, and S. Leach, *J. Phys. B: At. Mol. Phys.* 28, 4537, 1995; E. Koudoumas, F. Dong, S. Couris, and S. Leach, *Opt. Com/nun.* **138,** 301, 1997.

18. F.P. Strohkendl, L.R. Dalton, R.W. Hellwarth, H.W. Sarkas, and Z.H. Kafafi, *J. Opt. Soc. Am.* **B14,** 92, 1997; A. Costela, I. Garcia-Moreno, and J.L. Saiz, *J. Opt. Soc. Am.* **B14,** 615, 1997; J. Li, S. Wang, H. Yang, Q. Gong, X. An, H. Chen, and D. Qiang, *Chem. Phys. Lett.* **288,** 175, 1998.

19. K. Harigaya and S. Abe, *Jap..J. Appl. Phys.* **31,** L887, 1992.

20. S.J.A. van Gisbergen, J.G. Snijders, and E.J. Baerends, *Phys. Rev. Lett.* **78(16),** 3097, 1997.

21. J. Li, J. Feng, and J. Sun, *Chem. Phys. Lett.* **203,** 560, 1993; N. Tang, J P. Partanen, R.W. Hellwarth, and R.J. Knize, *Phys. Rev.* **B48,** 8404, 1993.

22. L.W. Tutt and A. Kost, *Nature* **356,** 225, 1992; A. Kost, L.W. Tutt, M.B.

Kelvin, T. K. Dougherty and W.E. Elias, *Opt. Lett.* **18,** 334, 1993.

23. Y.N. Han, W.J. Zhang, X.M. Gao, Y.B. Cui, Y.X. Xia, G. Gu, W.C. Zang, P. Yang, Y.W. Du, and D. Feng, *Appl. Phys. Lett.* 63, 447, 1993

24. L.W. Tutt and T.F. Bogges, *Prog. Quant. Elcetron.* 17, 299, 1993; A. Kost, L.W. Tutt, M.B. Kelvin, T.K. Dougherty and W.E. Elias, *Opt. Lett.* **18,** 334, 1993.

25. Y. Sun, Q. Gong, S.C. Yang, Y.H. Zou, L. Fei, X. Zhou and D. Qiang, *Opt. Commun.* **102,** 205, 1993; J.E. Wray, K.C. Liu, C.H. Chen, W.R. Garrett, MG. Payne, R. Goedert, and D. Templeton, *Appl Phys. Lett.* **64,** 2785, 1994; D. Vincent and J. Cruickshank, *Appl. Opt.* 36, 7794, 1997.

26. M. Cha, N.S. Saricifici, A.J. Heeger, J.C. Hummelen, and F. Wudl, *Appl. Phys. Lett.* 67 (1995) 3580; K.M. Nashold and D.P. Walter, *J. Opt. Soc. Am.* **B12,** 1228, 1995.

27. D. McBranch, L. Smilowitz, V. Klimov, A. Koskelo, J.M. Robinson, B.R Mattes, J.C. Hummelen, F. Wudl, J.C. Withers, and N.F. Borrelli, *Proc. SPIE* **2530,** 196, 1995; R. Signorini, M. Zerbetto, M. Meneghetti, R. Bozio, M. Maggini, CD. Faveri, M. Prato, and G. Scorrano, *Chem. Commun.* 1891, 1996; J. Schell, D. Brinkmann, D. Ohlmann, B. Honerlage, R. Levy, M. Joucla, J.L. Rehspringer, J. Serughetti, and C Bovier, *J. Chem. Phys.* **108,** 8599, 1998; L. Smilowitz, D. McBranch, V. Klimov, M. Grigorova, J.M. Robinson, B.J. Weyer, A. Koskelo, BR. Mattes, H. Wang, and F. Wudl, *Synthetic Metals,* **84,** 931, 1997.

28. F. Bentivegna, M. Canve, P. Georges, A. Brun, F. Chaput, L. Mailer, and J.-C. Boilot, *Appl. Phys. Lett.* 62, 1721, 1993; L. Smilowitz, D. McBranch, V. Klimov, J.M. Robinson, A. Koskelo, M. Grigorova, B.R. Mattes, H. Wang, and F. Wudl, *Opt, Lett.* 21,922, 1996.

29. Y. Song, G. Fang, Y. Wang, S. Liu, C. Li, L. Song, Y. Zhu, and Q.M. Hu, *Appl, Phys. Lett.* 74, 332, 1999; N.V. Kamanina, *Opt Commun.* **162,** 228, 1999; T. Zhang, J. Li, P. Gao, Q. Gong, K. Tang, X. Jin, S. Zheng, and L. Li, *Opt. Commun.* **150,** 201, 1998.

30. M.P.Joshi, S.R.Mishra, H.S.Rawat, S.C. Mehendale and K.C. Rustagi, *Appl. Phys. Lett* **62,** 1763, 1993; S.R. Mishra, H.S. Rawat, MP. Joshi and K.C. Rustagi, *J. Phys. B: At Mol. Phys.* 27, L157, 1994; S.R. Mishra, H.S. Rawat, M.P. Joshi, S.C. Mehendale, K.C.Rustagi, *Proc. SPIE* **2284,** 220, 1994; S.R. Mishra,

H.S. Rawat, MP. Joshi, SC. Mehendale, *Appl. Phys.* **A63,** 223, 1996; S.R. Mishra, H.S. Rawat, and S.C. Mehendale, *Appl. Phys. Lett.* **71(1),** 46, 1997.

31. D.G. McClean, R.L Sutherland, M.C Brant, D.M. Brandelik, P.A. Fleitz, and T. Pottenger, *Opt. Lett.* **18,** 858, 1993; D.G. McClean, M.C. Brant, *Proc. SPJE* **162,** 1856, 1993; M.C. Brant, *DM.* Brandelik, D.G. McClean, R.L. Sutherland, P.A. Fleitz, *Mol. Cryst, Liq. Cryst,* **256,** 807, 1994.

32. B.L. Justus, Z.H. Kafafi, and AL. Huston, *Opt. Lett.* **18,** 1603, 1993; Riju C. Issac, C.V. Bindhu, SS. Harilal, Geetha K. Varier, V.P.N. Nampoori and C.P.G. Vallbhan, *Mod. Phys. Lett.* **B10**, 61, 1996.

33. J.R. Lindle, R.G.S. Pong, F. Bartoli, Z.H. Kafafi, *Phys. Rev.* **B48,** 9447, 1993; C. Li, L. Zhang, R. Wang, Y. Song and Y. Wang, ./. *Opt, Soc. Am.* **B11,** 1356, 1994; V.V. Golovlev, W.R. Garrett, and C.H. Chen, *J. Opt, Soc. Am.* **B13,** 2801, 1996; S. Guha, W. T. Roberts, and B.H. Ahn, *Appl. Phys. Lett,* **68,** 3686, 1996.

34. R. Gvishi, J.D. Bhawalkar, N.D. Kumar, G. Ruland, U. Narang, P.N. Prasad, and B.A. Reinhardt, *Chem. Mater.* 7, 2199, 1995; P.N. Prasad, R. Gvishi, N.D. Kumar, J.D. Bhawalkar, U. Narang, *Proc. SPIE,* **2530,** 128, 1995.

35. B Ma, J. E. Riggs, and Y. -P. Sun, *J. Phys. Chem.* **B102,** 5999, 1998; Y. -P. Sun, J.E Riggs, and B. Liu, *Chem. Mater.* 9, 1268,1997; J.E. Riggs and Y. -P. Sun, ./. *Phys. Chem.* **A103,** 485,1999.

36. B.Z. Tang, H. Peng, S.M. Leung, N.-T. Yu, H.Hiroka, and M.W. Fok, *Mat. Res. Soc. Symp. Proc.* 479, 69, 1997.

37. F. Lin, J. Zhao, T. Luo, M. Jiang, Z. Wu, Y. Xie, Q. Qian and H. Zeng, ./. *Appl. Phys.* 74,2140, 1993.

38. C. Li, L. Zhang, R. Wang, Y. Song and Y. Wang, ./. *Opt. Soc. Am.* B H, 1356, 1994; C. Li, M. Yang, F. Guo, and Y. Wang, *Int, J. Nonlin. Opt. Phys.* 2, 551, 1993; F.Z. Henari, K.H. Cazzini, D.N. Weldon, and W.J. Blau, *Appl. Phys. Lett.* 68,619, 1996.

39. H. Hoshi, N. Nakamura, Y. Marayuma, T. Nakagawa, S. Suzuki, H. Shiromaru, and Y. Achiba, *Jap. J. Appl. Phys.* **30,** L1397, 1991; X.K. Wang, T.G. Zhang, W.P. Lin, S.Z. Liu, G.K. Wong, MM. Kappes, R.P.H. Chang, and J.B. Ketterson, *Appl. Phys. Lett.* 60, 810, 1992.

40. F. Diederich and Y. Rubin, *Angewandte Chemie,* **31,** 1101, 1992; M.

Prato, *J. Mater. Chem.* 7, 1097, 1997 and references therein.

41. M. Lee, O. -K. Song, J. -C. Seo, D. Kim, YD. Suh, S.M. Jin, and S.K. Kim, *Chem. Phys. Lett.* **196**, 325, 1992.

42. D. Narayana Rao, S. Venugopal Rao, F. J. Aranda, D.V.G.L.N. Rao and M. Nakashima, *J. Opt. Soc. Am.* B14, 2710, 1997; S. Venugopal Rao, L. Giribabu, B.G. Maiya, D. Narayana Rao, *Current Science,* 72, 957, 1997; S. Venugopal Rao and D. Narayana Rao, *Chem. Phys. Lett.* 283, 227, 1998.

43. H. Okamoto, *J. Opt. Soc. Am.* **B10,** 2353, 1993.

44. N. Morita and T. Yajima, *Phys. Rev.* A30(5), 2525, 1984; N. Morita, T. Tokizaki, and T. Yajima, *J. Opt. Soc. Am.* B4(8), 1269, 1987; T. Kobayashi, A. Terasaki, T. Hattori, K. Kurokawa, *Appl. Phys.* B47, 107, 1988 and references therein.

45. S. Ishihara, I. Ikemoto, S. Suzuki, K. Kikuchi, Y. Achiba, and T. Kobayashi, *Chem. Phys. Lett.* 295, 475, 1998.

46. J. Schell, D. Brinkmann, D. Ohlmann, B. Honerlage, R. Levy, M. Joucla, J.L. Rehspringer, J. Serughetti, and C. Bovier, *J. Chem. Phys.* 108, 8599, 1998

47. T. Juhasz, X.H. Hu, C. Suarez, WE. Bron, E. Maiken, and P. Taborek, *Phys. Rev.* B48, 4949, 1993.

48. S.L. Dexheimer, WA. Vareka, D. Mittleman, A. Zettl, and C.V. Shank, *Chem. Phys. Lett.* 235,552, 1995.

49. V.M Farztdinov, S.A. Kovalenko, Yu A. Matveets, N.F. Staodubtsev, and G. Marowsky, *Appl. Phys.* B66, 225, 1998; V.M. Farztdinov, Y.E. Lozovik, Y.A. Matveets, AG. Stepanov, and VS. Letokhov, *J. Phys. Chem.* 98, 3290, 1994.

50. D.K. Palit, A.V. Sapre, J.P. Mittal, and C.N.R Rao, *Chem. Phys. Lett,* 195, 1, 1992.

51. R.A. Cheville and N..I. Halas, *Phys. Rev.* B45, 4548, 1992.

52. S.V. Chekalin, V.M. Farztdinov, E. Akesson, and V. Sundstrom, *JETP Lett.* 58, 295, 1993; X. Wei, Z.V. Vardeny, D. Moses, V.I. Srdanov, and F. Wudl, *Synthetic Metals,* 49-50, 549, 1992.

53. I.E. Kardash, V.S. Letokhov, Y.E. Lozovik, Y.A. Matveets, A.G. Stepanov, and V.M. Farztdinov, *JETP Lett.* 58, 138, 1993

54. MR. Wasielewski, MP. O'Neil, K.R. Lykke, M.J. Pellin, and D.M. Gruen, *J. Am. Chem. Soc.* 113,2774, 1991.

55. Lina Yang, R. Dorsinville, and R. Alfano, *Chem. Phys. Lett.* **226,** 605, 1994.

56. S.R. Flom, R.G.S. Pong, F.J. Bartoli, and Z.H Kafafi, *Phys. Rev.* **B46,** 15598, 1992; S.R. Flom, F.J. Bartoli, H.W. Sarkas, CD. Merritt, and Z.H. Kafafi, *Phys. Rev.* **B51,** 11376, 1995.

57. R J Sension, CM. Phillips, A.Z. Szarka, W.J. Romanow, A.R. McGhie, J.P. McCauley, Jr., A.B. Smith III, and M. Hochstrasser, *J. Phys. Chem.* 95, 6075, 1991.

58. T.W. Ebbesen, K. Tanigaki, and S. Kuroshima, *Chem. Phys. Lett,* **181,** 501, 1991.

59. K. Tanigaki, T.W. Ebbesen, and S. Kuroshima, *Chem. Phys. Lett.* **185,** 189, 1991.

60. SD. Brorson, M.K Kelly, U. Wenschuh, R. Buhleier, and J. Kuhl, *Phys. Rev.* **B46(ll),** 7329, 1991.

61. T.N. Thomas, J.F. Ryan, R.A. Taylor, D. Mihailovic, and R. Zamboni, *Int. J. Mod Phys.* **B6(23,24),** 3931, 1992.

62. B. Fleischer, E.P. Ippen, G. Dresselhaus, M.S. Dresselhaus, A.M. Rao, P. Zhou, and P.C Elkund, *Appl. Phys. Lett,* **63,** 3241, 1993.

63. J.W. Arbogast, A.P. Darmanyan, C.S. Foote, Y. Rubin, F.N. Diederich, M.M. Alvarez, SJ Anz, and R.L. Whetten, *J. Phys. Chem.* 95, 11, 1991.

64. M. Terazima and N. Hirota, *J. Phys. Chem.* 96, 7147, 1992.

65. L.W. Tutt and T.F. Boggess, *Prog. Quant. Electron.* 17, 299, 1993 and references therein.

66. M. Sheik-Bahae, A.A. Said, T. -H. Wei, D.J. Hagan, E.W. VanStryland, *IEEE J. Quant. Electron,* 26, 760, 1990.

67. R.W. Keyes, *IBM Journal,* 334, 1963; C.R. Giuliano and L.D.Hess, *IEEE J. Quant. Electron.* **QE-3(8),** 358, 1967.

68. G.P. Banfi, D. Fortusini, M. Bellini, and P. Milani, *Phys. Rev.* **B52,** R10075, 1997

69. J. Barroso, A. Costela, I.G. Moreno, and J.L. Saiz, *J. Phys. Chem.* **A102,** 2527, 1998.

70. G. Gu, W. Zhang, H. Zen, Y. Du, Y. Han, W. Zhang, F. Dong, and Y. Xia, *J. Phys. B: At. Mol. Phys.* **26,** L451, 1993; B. Taheri, H. Liu, B. Jassemnejad, D. Appling, R.C. Powell and J.J. Song, *Appl. Phys. Lett.* **68,** 1317, 1996.

71. I.V. Bezel, S.V. Chekalin, Y.A. Matveets, AG. Stepanov, A.P. Yartsev and V.S. Letokhov, *Chem. Phys. Lett.* **218,** 475, 1994.

72. F.Z. Henari, S. MacNamara, 0. Stevenson, J. Callaghan, D. Weldon and W.J. Blau, *Adv. Mater.* 5, 930, 1993.

73. F. Henari, J. Callaghan, H. Stiel, W. Blau and D.J. Cardin, *Chem. Phys. Lett.* 199, 144, 1992; S. Couris, E. Koudoumas, A.A. Ruth, and S. Leach, *./. Phys. B: At. Mol. Phys.* 28, 4537, 1995

74. S. Venugopal Rao, D. Narayana Rao, J.A. Akkara, B.S. DeCristofano, and D.V.G.L.N. Rao, *Chem. Phys. Lett.* 297, 491, 1998.

75. G.B. Talapatra, D.N. Rao, and P.N. Prasad, *J. Phys. Chem.* 88, 4636, 1984.

CHAPTER 7

Phthalocyanines: DFWM-IL Results

This chapter presents some results of our DFWM-IL measurements on few Phthalocyanines (PC, CuPc, FePc, and ZnPc). The major conclusions of the studies carried out in this thesis are highlighted. Future prospects for the materials used and the different techniques, their drawbacks, further improvements and suggestions are also presented.

7.1 Introduction

Metallophthalocyanines and related compounds hold a considerable promise for the development of many nonlinear optical devices because of their large third-order nonlinearity, fast response time, unique electronic absorption characteristics, high thermal stability and environmental stability [1-3]. The large nonlinearity originates from their extensively delocalized π-electron distribution. They are highly stable and versatile compounds, capable of including more than 70 different metallic and non-metallic ions in the ring cavity. It is also possible to incorporate a variety of peripheral substituents around the phthalocyanine core, as well as replace some of the isoindole units by other heterocyclic moieties, giving rise to different phthalocyanine analogues. Another peculiar and useful feature of these compounds is their ability to form different kind of condensed phases. It is possible to make thin films by several techniques such as spin-coating, Molecular Beam Epitaxy (MBE), and Langmuir Blodgett (LB) technology that allow fabrication of practical devices. Phthalocyanine-based thin films have been successfully applied to a wide range of technological areas: Gas sensors, Electro-chromic devices, Field Effect Transistors, and Photovoltaic cells [4]. Harmonic generation [5], Wave mixing [6], optical limiting and switching [7] have been investigated in these molecules for a wide spectrum. There have been several papers on the measurement of third-order nonlinearity [8-9] in phthalocyanine, related compounds and their derivatives. The effect of central metal atom [10], peripheral substituents [11], and additional conjugations [12] on the third-order nonlinearity have been extensively investigated. The excited states of Phthalocyanines are expected to play an important role in various applications. Here we study the dynamics of excited state through DFWM with incoherent light.

7.2 Experimental Details

Two intense bands characterize the linear absorption spectra of these compounds, the Q-band (centered around 670 nm) and the B-band in the near UV region (centered around 340 nm) and both are correlated to π-π^* transitions. We have performed DFWM-IL measurements on three Phthalocyanines viz. Pc, CuPc, FePc and ZnPc. Figure 7.1 shows the linear absorption spectra of the samples, ZnPc and CuPc, used in DFWM-IL studies. All the samples are dissolved in spectroscopic grade, highly purified solvents. CuPc is dissolved in 16 % concentrated H_2SO_4, FePc is dissolved in DMSO, Pc and ZnPc are dissolved in toluene. CuPc and FePc gave clear solutions where as the samples dissolved in toluene are placed in a sonicator, for about half an hour, to achieve better solubility.

7.3 DFWM-IL Results on Phthalocyanines

Figure 7.2 (a) and (b) shows the DFWM-IL signals in the samples CuPC and FePC for 5 = 8 ps and 5 = 9 ps respectively. The signal structure remained the same as observed in Porphyrins. The different lifetimes calculated, from the widths and ratio of two peaks, for different samples are summarized in table 7.1. The population relaxation times measured are found to be $\sim$ 25 - 50 ps. Previous measurements on population relaxation times in various Phthalocyanines indicate similar lifetimes. Comparing the values obtained with our technique with those reported in literature, for similar compounds, Asahi et al. [13] working with copper phthalocyanine performed femtosecond transient grating spectroscopy and obtains a 100 ps component in their excited state dynamics measurements which they attribute to the intrinsic lifetime of the exciton. Zhenrong et al. [8] reports a 100 ps component in their time-resolved Z-scan measurements on a copper phthalocyanine thin film. Howe et al. [14] reports their ultra-fast studies of excited state dynamics of Pc and ZnPc tetrasulfonate in solution and they observe lifetimes of $\sim$ 130 ps and $\sim$ 160 ps for the S_1 state respectively. For our samples Pc and ZnPc we observe lifetimes of 55 ps and 35 ps respectively through DFWM-IL studies which are in consistent agreement with the reported values. There have been several other experimental results on the dynamics of various Phthalocyanines [15-22].
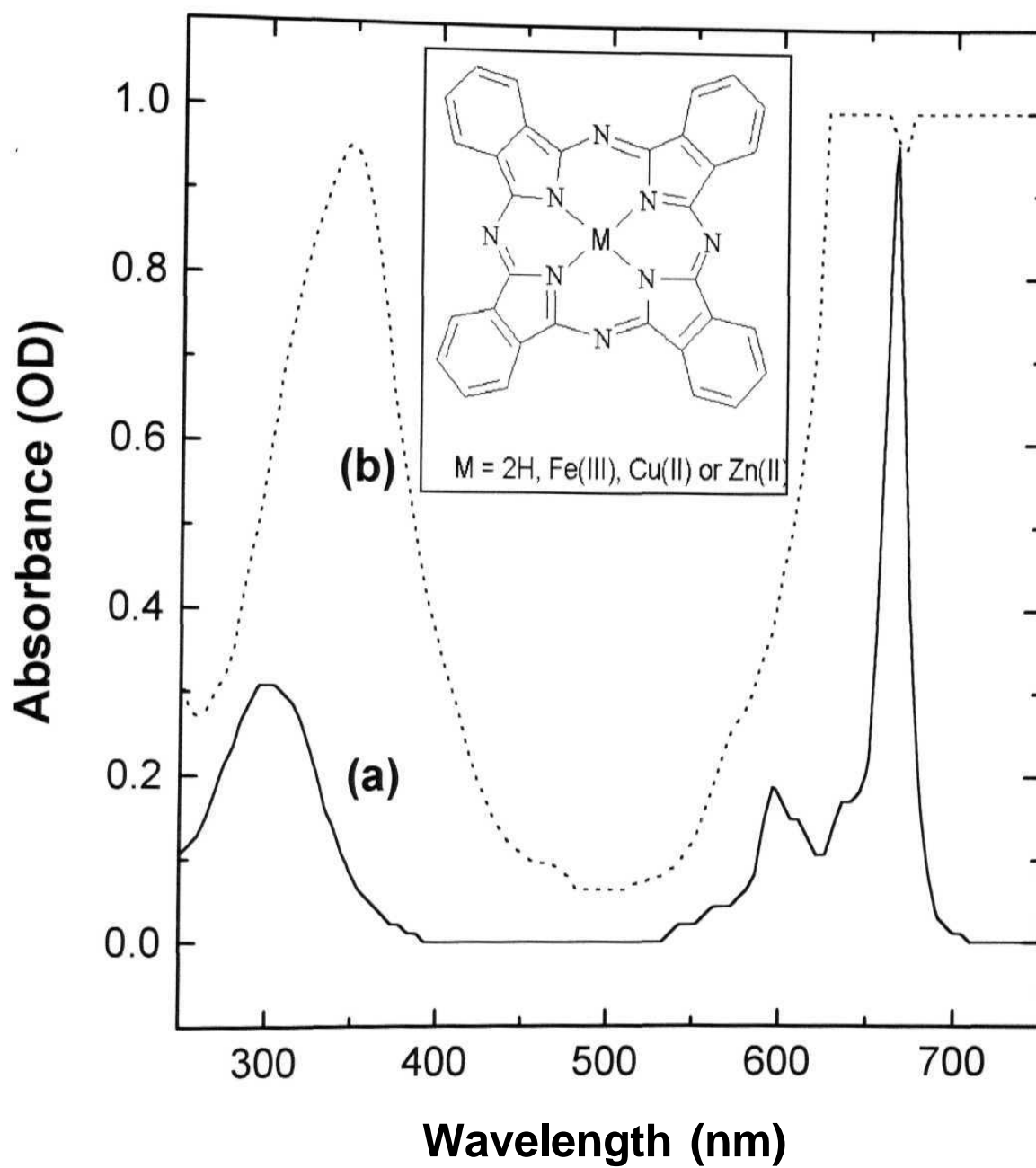
Fig. 7.1 Absorption spectra of the samples (a) ZnPc (DMSO) and (b) CuPc (H_2SO_4). **Inset shows the structure of the compounds.**
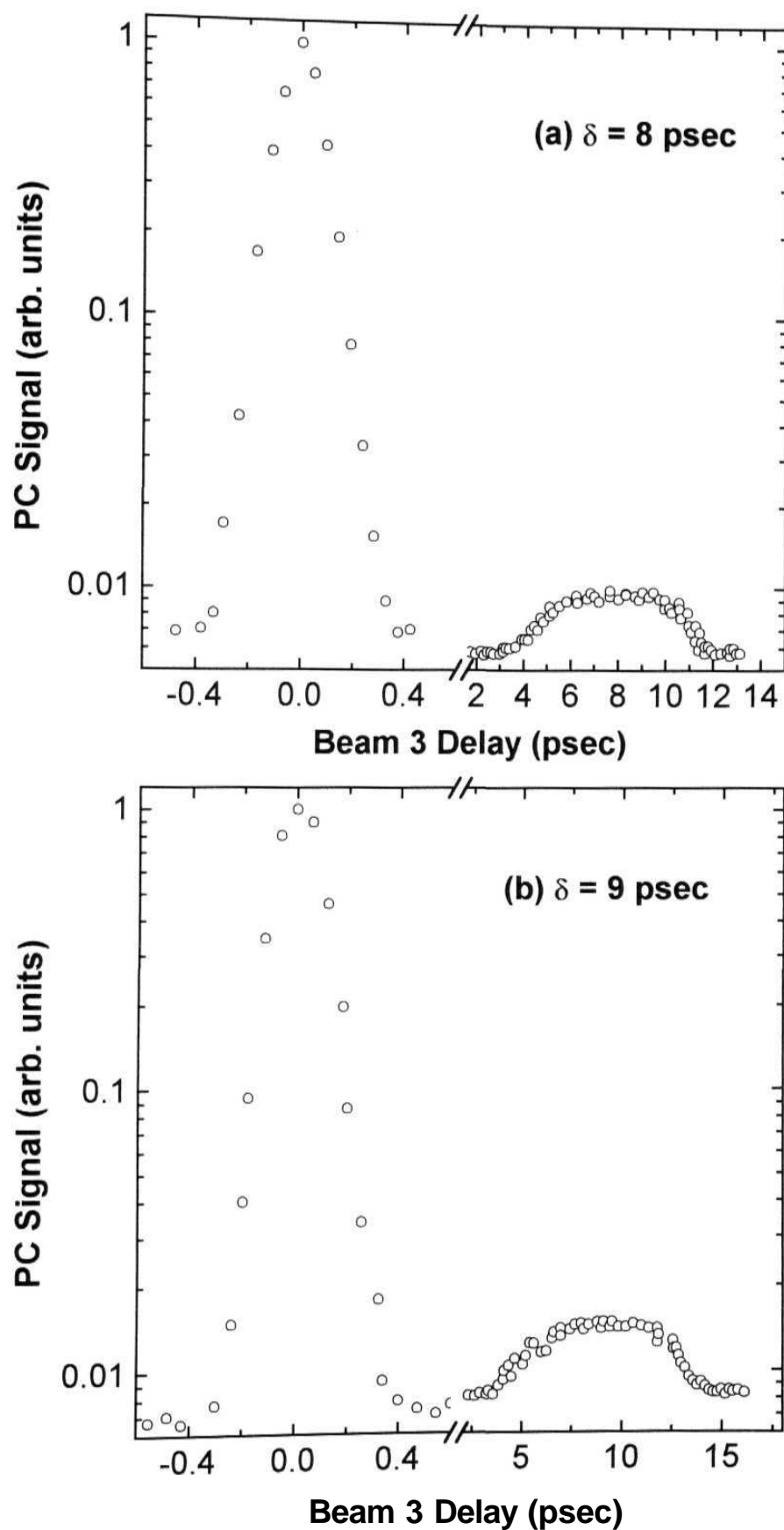
Fig. 7.2 (a) PC Signal in Copper Phthalocyanine (Conc. H_2SO_4)

(b) PC signal in the sample Iron Phthalocyanine (DMSO)

Sample	Dephasing of the S_n state (T_2) in fs	Vibrational Relaxation in S_1 state (τ_{Vib}) in ps	Population Relaxation time (T_1) in ps
Phthalocyanine (Toluene)	< 170	3.80 ± 0.76	55.0 ± 11.0
Copper Phthalocyanine (Conc. H_2SO_4)	< 170	4.30 ± 0.86	46.0 ± 9.20
Iron Phthalocyanine (DMSO)	< 170	4.00 ± 0.20	40.0 ± 8.00
Zinc Phthalocyanine (Toluene)	< 170	3.50 ± 0.70	35.0 ± 7.00

Table 7.1 The transverse and longitudinal lifetimes calculated for different samples using DFWM-IL

7.6 References

1. H.S. Nalwa, J.S. Shirk, in: C.C. Leznoff, A.B.P. Lever Eds., *Pthalocyanines: Properties and Applications,* Vol. 4, VCH, New York, 1996, p. 79; H.S. Nalwa, S. Miyata Eds., *Nonlinear Optics of Organic Molecules and Polymers,* Chap.] 1, CRC Press, Boca Raton, FL, 1997; H.S. Nalwa, *Appl. Organomet. Chem.* 5, 3493, 1991.

2. H.S. Nalwa, *Adv. Mater.* 5, 341, 1993; J. -L. Bredas, C. Adant, P. Tackx, A. Persoons, B.M. Pierce, *Chem. Rev.* 94, 243, 1994.

3. S.R. Marder, J.E. Sohn, G.D. Stucky Eds. , Materials for Nonlinear Optics - Chemical Perspectives, ACS Symposium Series 455, American Chemical Society, Washington, DC, 1991.

4. G. de la Torre, P. Vazquez, F. Agullo-Lopez, and T. Torres, *./. Mater. Chem.* 8, 1671, 1998 and reference there in.

5. MLA. Diaz-Garcia, 1. Ledoux, F. Fernandez-Lazaro, A. Sastre, T. Torres, F. Agullo Lopez, J. Zyss, *J. Phys. Chem.* 98, 4495, 1994; Z.Z. Ho, C.Y. Ju, W.M. Hetherington **III,** *./. Appl. Phys.* 62, **716,** 1987.

6. R.A. Norwood, J.R. Sounik, *Appl. Phys. Lett.* 60, 295, 1992; D.V.G.L.N. Rao, F.J. Aranda, J.F. Roach, D.E Remy, *Appl. Phys. Lett.* 58, 1211, 1991.

7. S. Guha, K. Kang, P. Porter, J.F. Roach, D.E. Remy, F.J. Aranda, D.V.G.L.N. Rao, *Opt. Lett.* 17, 264, 1992; C. Li, L. Zhang, M. Yang, H. Wang, Y. Wang, *Phys. Rev. A* 49, 1149, 1994; A. Sevian, M. Ravikanth, G. Ravindra Kumar, *Chem. Phys. Lett.* **263,** 241, 1996; J.W. Perry, K. Mansour, S.R. Marder, KJ. Perry, D. Alvarez Jr., 1. Choong, *Opt. Lett,* 19, 625, 1994; M. Sanghadasa, C.C. Sung, 1. -S. Shin, B.C. Penn, R.D. Clark, H. Guo, and A. Martinez, *Proc. SPIE* 3472, 116, 1998; K. Mansour, P. Fuqua, S.R. Marder, B. Dunn, and J.W. Perry, *Proc. SPLE* **2143,** 239, 1994; T.C. Wen and I.D. Lian, *Synth. Met.* 83, 111, 1996.

8. J.S. Shirk, J.R. Lindle, F.J. Bartoli, Z.H. Kafafi, A.W. Snow, in: S.R. Marder, J.E. Sohn, G.D. Stucky Eds., *Materials for Nonlinear Optics-Chemical Perspectives,* ACS Symposium Series 455, American Chemical Society, Washington, DC, 1991; J.S. Shirk, J.R. Lindle, F.J. Bartoli, ME. Boyle, *J. Phys. Chem.* 96, 5847, 1992; S. Zhenrong, D. Liangen, H. Yanping, Q. Lijuan, and W. Zugeng, *Chin. J. Lasers.* B7, 241, 1998; R, Philip, M. Ravikanth, and G.R. Kumar, *Opt. Commun.*

165, 91, 1999; M. Tian, S. Yanagi, K. Sasaki, T. Wada, and H. Sasabe, *J. Opt. Soc. Am.* **B15,** 846, 1998.

9. H.S. Nalwa, T. Saito, A. Kakuta, and T. Iwayanagi, *J. Phys. Chem.* 97, 10515, 1993; M. Hosoda, T. Wada, T. Yamamoto, A. Kaneko, A.F. Garito, and H. Sasabe, *Jap. J. Appl. Phys.* 31, 1071, 1992; A. Yamashita, S. Matsumoto, S. Sakata, T. Hayashi, and H. Kanbara, *Opt. Commun.* **145,** 141, 1998; A. Yamashita, S. Matsumoto, S. Sakata, T. Hayashi, and H. Kanbara,*./. Phys. Chem.* **B102,** 5165, 1998; R. Rangel-Rojo, S. Yamada, H. Matsuda, H. Kasai, Y. Komai, S. Okada, H. Oikawa, and H. Nakanishi, *Jap. J. Appl. Phys.* 38, 69, 1999; M.A. Diaz-Garcia, G. Rojo, and F. Agullo-Lopez, *Proc. SPIE* **3473,**91, 1998.

10. J.S. Shirk, JR. Lindle, F.J. Bartoli, Z.H. Kafafi, A.W. Snow, ME. Boyle, *Int. J. Opt. Phys.* 1, 699, 1992.

11. H.S. Nalwa, A. Kakuta, A. Mukoh, *Chem. Phys. Lett.* 203, 109, 1993 and references therein.

12. H.S. Nalwa, A. Kakuta, A. Mukoh,*./. Phys. Chem.* 97, 1097, 1993.

13. T. Asahi, N. Tamai, T. Uchida, N. Shimo, and H. Masuhara, *Chem. Phys. Lett.* **234**, 337, 1995.

14. L. Howe and J.Z Zhang,*./. Phys. Chem.* **A101,** 3207, 1997.

15. P.S. Vincett, E.M. Voigt, and K.E. Rieckhoff,*J. Chem. Phys.* 55, 4131, 1971.

16. Z.Z. Ho and N. Peyghambarian, *Chem. Phys. Lett.* **148,** 107, 1988

17. A. Terasaki, M. Hosoda, T. Wada, H. Tada, A. Koma, A. Yamada, H. Sasabe, A.F. Garito, and T. Kobayashi,*./. Phys. Chem.* 96, 10534, 1992.

18. JH. Brannon and D. Magde, *J. Am. Chem. Soc.* 102, 62, 1980.

19. VS. Williams, S. Mazumdar, N.R. Armstrong, Z.Z. Ho and N. Peyghambarian, *J. Phys. Chem.* 96, 4500, 1992.

20. R.R. Millard and B.I. Greene, *J. Phys. Chem.* 89, 2976, 1985.

21. V. Gulbinas, M. Chachisvillis, L. Valkunas, and V. Sundstrom, *./. Phys. Chem.* 100,2213, 1996.

22. M.K. Casstevens, M. Samoc, J. Pfleger, and P.N. Prasad, *J. Chem. Phys.* 92, 2019, 1990.

Conclusions

1. Degenerate Four-Wave Mixing measurements are performed, using incoherent light (with τ_c = 170 fs and 2.7 ps), on different samples like RhB, Black Ink, Cresyl Violet, DQOCI, Porphyrins, C60 and Phthalocyanines. A double peak structure is observed in the PC signal for all the samples, except for RhB and CS2. The width of the first peak, which is limited by correlation time in our case, is characterized as due to the dephasing time (T_2) in the excited states S_n. The width of the second peak, which is unusually large in Porphyrins, C_{60}, and Phthalocyanines compared to other samples, is attributed to the vibrational relaxation in the S_1 states (τ_{vib}). The ratio of the two peaks is used to calculate the population relaxation time (T_1) of these samples.

2. Earlier theoretical models were based on two-level (Morita et al. and Kobayashi et al.) or open three-level (Okamoto et al.) systems. While Okamoto's theory is being used for calculating the population relaxation time, we have proposed a theory, based on four-level model and comprising of the So, S10, S_{1v}, and S_n states, to explain the widths of the two peaks observed in DFWM -IL experiments.

3. A new series of metalloporphyrins, with sixteen different metal ions, have been synthesized in order to see the effect of the metal complexes on the third-order nonlinearity and bring out a relation between the structure and $\chi^{(3)}$. They have also been chosen for their higher damage threshold, large nonlinearity compared to other class of Porphyrins, and the simplicity in preparation. The values of $\chi^{(3)}$ and $<y>$ are evaluated using the DFWM technique with 35 ps and 6 ns pulses at 532 nm. These studies indicate very large nonlinearity, y ($\sim 10^{-28}$ esu), in the ns regime and reasonable large values ($\sim 10^{-30}$ esu) in the ps domain. The large value of nonlinearity, in the ns domain, has been identified as due to the enhancement by participation of the high lying singlet and triplet states to the total nonlinearity with part of thermal contribution. Our preliminary studies also suggest a large value at 600 nm, which could be due to strong TPA. Closed aperture Z-scan studies indicate large negative nonlinearity. Nonlinear absorption studies using the open aperture Z-scan technique indicate a large excited state absorption and/or two-photon absorption.

4. Excited state dynamics obtained using incoherent light for all the samples and 35 ps pulses for few Porphyrins show fast response times in the order of ps and fs. The results obtained with both the pulses match well with each other and also with previously reported values on similar class of Porphyrins. These porphyrins with their large nonlinearity and fast response times could be potential candidates for applications in optical limiting, optical communications, and optical data processing provided they are thoroughly optimized in their performance.

5. Large third order nonlinearity has been estimated for the sample C_{60} at 600 nm, which has been attributed to the strong two-photon absorption at this wavelength. The excited state dynamics obtained with incoherent light matches very well with those obtained using 150 fs pulses at 633 nm. Dispersion studies of nonlinear absorption have been carried out using a ns OPO and the obtained open aperture Z-scan data is theoretically fitted, using a 5-level model, to evaluate the different excited state absorption cross-sections. The results indicate that σ_2 (excited singlet state absorption) dominates at lower wavelengths and β (two-photon absorption) dominates at higher wavelengths.

6. DFWM-TL studies are extended to Phthalocyanines to estimate the different lifetimes and we observe similar time scales compared to Porphyrins.

Future Scope

1. Our extensive DFWM-IL studies suggest that Incoherent Laser Spectroscopy is still a powerful tool in measuring the excited state dynamics of different materials. The technique is attractive with different configurations (Forward FWM, Backward FWM, Forced Light Scattering, Photon Echoes etc.) offering number of options for measuring various relaxation times in the ps and fs domain with ns pulses. Though there are a few drawbacks like the small dynamic range (not suitable for very long relaxation times measurement) in the technique it can be made more powerful by appropriately choosing the source with proper correlation time (i.e. to choose a very short correlation time for ultra-short measurements and long correlation time for population kind of relaxation measurements) and the working wavelength.

2. A more rigorous DFWM theory, based on five-level model, has to be developed for these materials including the singlet as well as triplet states and all the decay processes.

3. Our studies prove that Tetra Tolyl Porphyrins possess very strong third-order nonlinearity, nonlinear absorption and fast response times. By doping these materials in suitable hosts, making thin films may result in practical NLO devices such as optical limiter and switches. Suitable chemical modifications of these molecules would enable to increase the intersystem crossing rate leading to the improvement in the effective nonlinearity.

4. Excited-state enhancement is a powerful tool to increase the nonlinearity of materials in the absence of any external pump beams. A proper theoretical and experimental understanding is necessary in this direction to identify materials with largest nonlinearity.

5. Our dispersion studies indicate that C_{60} is a potential candidate for broadband optical limiter in the visible region (440 to 660 nm). A proper combination of synthetic chemistry (to modify the excited state absorption and make it much stronger), characterization (through Z-scan and optical limiting techniques) would lead to a practical optical limiter.

H. No.1-6-146 (I floor),   **Phone**: 91-40-781-6121
Kandoji Bazaar,   **E-mail:**
Secunderabad - 500003   dnrsprs@uohyd.crnct.in
Andhra Pradesh   soma_venu@yahoo.com
India.   Fax: 91-40-301-0120/145

Venugopal Rao Soma

Summary

I have over five and half years of research experience in the area of experimental Non-linear Optics. I have obtained my Master's degree from University of Hyderabad. India with specialization in the area , of Advanced Electronics. I have significant practical experience in the areas of Solid State Physics, Analog and Digital Electronics, Laser Physics, Modern Optics, Microwave Techniques, Modern Physics and Nuclear Physics. I underwent a rigorous training in theoretical areas of Classical Mechanics, Quantum Mechanics, Solid State Physics, Mathematical Physics, Computational Physics, Electro-Magnetism, Statistical Mechanics, Particle and Nuclear Physics, Currently I have been working in the area of Incoherent Laser Spectroscopy for measurement of ultra-fast relaxation times using *ns* laser.

Research Experience

- ## University of Hyderabad, India
(1994 – 2000)

I have over five years of research experience in the area of experimental Nonlinear Optics. The title of my thesis is *Studies of excited state dynamics, third-order nonlinearity, and nonlinear absorption in* C_{60}, *Porphyrins, and Phthalocyanines using Incoherent Laser Spectroscopy.* The lifetimes of different excited states in these materials, which are in the ps and fs domain, are measured using DFWM technique with incoherent light and compared with those obtained with 35 ps pulses. The sign and magnitude of third order non-linearity measurements are performed at 532 nm and 600 nm with ns and ps pulses. A more general 4-level model is used theoretically to simulate the observed DFWM signals. The nonlinear absorption is measured using the Z-scan technique and a 5-level theoretical model is developed to satisfactorily explain the observed results.

Other Experience

1 am well versed with different techniques for the measurement of excited state dynamics, third order nonlinearities, second order non-linearity, nonlinear absorption which includes Degenerate Four Wave Mixing (backward, forward and boxcar configurations using coherent and incoherent light). 1 have an extensive experience with other techniques such as Z-Scan (open and closed aperture), Optical Limiting, Electric Field Induced Second Harmonic Generation (EFISHG), Kurtz-Perry powder SHG measurements, Optical Interferometry using white light (Michelson and Mach-Zchnder).

I have comprehending experience in handling/maintaining high power Nd: YAG (6 ns and 35 ps), Dye (RhB/Rh6G/DCM), high power and low power He-Ne and Diode (AlGaAs) lasers. Also, I have significant experience handling different data acquisition and processing apparatus such as Lock-in Amplifiers (SRS 830, Ithaco, Princeton Applied Research). The other apparatus include Boxcar Integrators (SRS), Oscilloscopes (Tektronix 2465B, 400 MHz, TDS 210), ADC cards, Stepper Motor Controllers, Monochromators (Jobin Yvon, SM 240 CVI), CCD cameras, Power Meters (Scientech), High Voltage Pulsers (Velonex), Spin Coating Unit, UV-Visible absorption spectrometers (Jasco 7800), and high power optics.

I have good knowledge in computer programming using various computer languages and handling various computer systems (Pentium II/III, Unix, μ-Vax, and Linux). The mathematical packages I used extensively include Origin, Sigmaplot, IMSL, NAG, Grapher, Genplot, Gnuplot, and Matlab. Also word processing packages such as MS-Word and Chi-Writer. I have one year of experience in teaching Laser Laboratory course for the under-graduate students in University of Hyderabad. I have

been involved in the 'Laser Fundamentals'. 'Fiber Optics' training courses and 'National Laser Symposium' conducted by University of Hyderabad.

List of Publications

1. *"Ultra-fast relaxation times of metalloporphyrins by time resolved degenerate four wave mixing with incoherent light,"* D. Narayana Rao, S. Venugopal Rao, F.J. Aranda, M. Nakashima and J.A. Akkara, J. Opt. Soc. Am. **B14(10)**, 2710-2714, 1997.

2. *"A novel observation in the measurement of ultrafast relaxation times using incoherent light,"* S, Venugopal Rao, L. Giribabu, B.C Maiya and D, Narayana Rao, Current Science **72(12)**, 957-960, 1997.

3. *"Excited state dynamics of C_{60} studied using incoherent light,"* S. Venugopal Rao and D. Narayana Rao, Chem. Phys. Lett. **283(3-4)**, 227-230, 1998.

• 4. *"A comparative study of C_{60} phthalocyanine and a porphyrin for optical limiting over the visible region"* D. Narayana Rao, S. Venugopal Rao, E. Blanco, F.J. Aranda, D.V.G.L.N. Rao, and Joseph A. Akkara, J. Sci. Ind. Res. (special issue on frontiers in bio-technology) **57(10,11)**, 664-667, 1998.

5. *"Dispersion studies of nonlinear absorption in C_{60} using Z-scan,"* S. Venugopal Rao, D. Narayana Rao. J.A. Akkara, B.S. DeCristofano, and D.V.G.L.N. Rao, Chem. Phys. Lett. 297, 491-498, 1998.

6. *"N-Alkyl-p-nitroanilines:Impact of alkyl chain length on crystal structures and optical SHG"* P. Gangopadhyay, S. Venugopal Rao, D. Narayana Rao and T.P. Radhakrishnan, J. Mater. Chem.. 9(8), 1699-1706, 1999.

7. *"Studies of third-order optical nonlinearity and nonlinear absorption in Tetra Tolyl Porphyrins using degenerate four wave mixing and Z-scan,"* S. Venugopal Rao, N.K.M.N. Srinivas. L. Giribabu. B.G. Maiya, D. Narayana Rao. Reji Philip, and G. Ravindra Kumar, Submitted to Optics Communications.

8. *"Excited state dynamics in Tetra Tolyl Poprhyrins studied using DFWM with incoherent light and ps pulses,"* S. Venugopal Rao, N.K.M.N. Srinivas, L. Giribabu, B.G. Maiya, D. Narayana Rao, Reji Philip, and G. Ravindra Kumar, Submitted to JOSA B.

9. *"Wavelength dependent studies of nonlinear absorption in ZnmpTBP using Z-scan,"* S. Venugopal Rao, N.K.M.N. Srinivas, and D. Narayana Rao, Submitted to Journal of Porphyrins and Phthalocyanines

10. *"Theoretical Modelling of DFWM signals observed in materials with excited state absorption using an incoherent laser source,"* S. Venugopal Rao, Suneel Singh, and D. Narayana Rao, Manuscript under preparation.

Conferences/Proceedings/Talks

1. *"Femtosecond transient kinetics of Zn-Tetrabenzporphyrin using incoherent laser spectroscopy,"* S. Venugopal Rao, International Conference on Spectroscopy - Perspectives and Frontiers, January 3- 5, 1996, BARC, Bombay, 182.

2. *"Ultrafast population relaxation times of metalloporphyrins using DFWM-IL"* S. Venugopal Rao, **30** min. **talk** presented al "Workshop on Nonliear Optics," Center for Advaned Technology, Indore, July 21-26, 1996.

3. *""Nonlinear Optical properties of Indian Ink."* S. Venugopal Rao and D. Narayana Rao, Proceedings of National Laser Symposium, CAT, Indore, February 6-8, 217, 1996.

4. *""The study of ultrafast relaxation times using DFWM-IL"* S. Venugopal Rao and D. Narayana Rao, 30 min. talk presented at SERC school on "Nonlinear Optics and Laser Spectroscopy" held at IIT Delhi, March 10-27, 1997.

5. *"Ultrafast relaxation times of metalloporphyrins by time resolved degenerate four wave mixing with incoherent light,"* D. Narayana Rao, S. Venugopal Rao, F.J. Aranda, D.V.G.L.N. Rao, M. Nakashima, J.A. Akkara. International Conference on Nonlinear Optical Materials, Cairo, January 4-9, 1997.

6. *"Picosecond time resolved four wave mixing studies using a nanosecond laser light source,"* D. Narayana Rao. S. Venugopal Rao, Ram Mohan, Joseph A. Akkara, International Conference on Frontiers in Biotechnology. Trivandrum, India, November 26 - 29, 1997.

7. *"A theoretical model for the measurement of ultrafast population relaxation times in organic molecules using incoherent light,"* S. Venugopal Rao, Suneel Singh, D.Narayana Rao, Proc. of National Laser Symposium, Physical Research Laboratory, Ahmedabad, 139-140, December, 1997

8. *"Excited state dynamics of C_{60} studied using DFWM – IL."* S. Venugopal Rao, **Suneel Singh. D.** Narayana Rao, Proceedings of National Laser Symposium. Physical Research Laboratory, Ahmedabad, 133-134, December. 1997

9. *"Electricfield induced second harmonic generation study of novel quinonoid molecules."* M. Ravi. S. Venugopal Rao, P. Gangopadhyay, T.P. Radhakrishnan, Proceedings of National Laser Symposium, Physical Research Laboratory, Ahmedabad, 187, December. 1997

10. *"Quinonoid molecular materials for Nonlinear optics-EFISHG study of molecular hyperpolarizabilities.,"* M. Ravi. S. Venugopal Rao, V. Nirmal Kumar, and T.P. Radhakrishnan. Page No.P1-33 Proceedings of the "Symposium on current topics in Physics of Materials," University of Hyderabad, Hyderabad, March 27-29, 1997

11. *"Theoreticalmodel for the measurement of ultrafast relaxation times in organic materials using incoherent light"* S. Venugopal Rao, Suneel Singh and D. Narayana Rao, Seminar on selected topics in theoretical physics, September 15-17, 1998, University of Hyderabad, Hyderabad.

12. *"Theoretical and experimental study of the excited state dynamics in reverse Saturable absorbers using Z-scan technique,"* S. Venugopal Rao, Suneel Singh. B.S. DeCristofano and D. Narayana Rao. Proceedings of International Conference on Optics and Lasers. 167-172. Dehradun. December 1998.

13. *"Dispersion studies of nonlinear absorption in zinc tetrabenzporphyrin (ZnmpTBP) using Z-scan,"* S. Venugopal Rao. Suneel Singh and D. Narayana Rao, Proceedings of National Laser Symposium. 169-170, IIT Kanpur, December 1998.

14. *"Wavelength dependence of nonlinear absorption in copper phthalocyanine using Z-scan,"* S. Venugopal Rao, Suneel Singh and D. Narayana Rao. Proceedings of National Laser Symposium, 171-172, IIT Kanpur, December 1998.

15. *"Studies of third-order optical nonlinearity, excited state dynamics, and nonlinear absorption in Tetra Tolyl Porphyrins using DFWM and Z-scan with incoherent light and ps pulses,"* S. Venugopal Rao, N.K.M.N. Srinivas, L. Giribabu, B.C Maiya. R. Philip. G.R. Kumar, and D. Narayana Rao. Submitted to International Conference on Nonlinear Optics. Davos. Switzerland, March 2000.

16. *"Excitedstate dynamics in Tetratolyl Porphyrins studied using DFWM with incoherent light and 35 ps pulses,"* S.Venugopal Rao, N.K.M.N. Srinivas. L. Giribabu. B.G. Maiya, R. Philip. G.R. Kumar, and D. Narayana Rao. Proc. of National Laser Symposium, Pg. 165. University of Hyderabad. December 15-17, 1999.

17. *"Studies of third-order optical nonlinearity and nonlinear absorption in Tetra Tolyl Porphyrins using degenerate four wave mixing and Z-scan",* S.Venugopal Rao, N.K.M.N. Srinivas, L. Giribabu. B.G. Maiya, R. Philip, G.R. Kumar, and D. Narayana Rao. Proceedings of the National Laser Symposium. Pg. 163. University of Hyderabad. Hyderabad, December 15-17, 1999.

18. *"Alkyl chain length as a design element in molecular materials for optical second harmonic generation",* P. Gangopadhyay, S. Venugopal Rao, D. Narayana Rao, and T.P. Radhakrishnan, Proc. of National Laser Symposium, Pg. 143, University of Hyderabad, December 15-17, 1999.

19. *"Excited stale enhancement of third-order optical nonlinearity in AuTTP studied by Degenerate Four Wave Mixing at 532 nm".* D. Narayana Rao and S. Venugopal Rao, To be presented at International Conference on Lasers and Applications, St. Joseph's College, Trichy, March 1-4, 2000.

20. *"Wavelength dependent studies of nonlinear absorption in ZnmpTBP using Z-scan with a ns OPO",* S. Venugopal Rao, N.K.M. Naga Srinivas, and D. Narayana Rao, To be presented at the XXVI National Symposium on Optics and Opto-electronics, REC, Warangal, Feb 4-6, 2000.

Achievements/Distinctions

- Recipient of UGC-Senior Research Fellowship, Govt. of India.
- Recipient of UGC-Junior Research Fellowship, Govt. of India.
- Qualified the UGC-GATE exam with an overall percentile of 88.
- Fourth Rank in M.Sc in the university.
- Recipient of Merit Scholarship from Government of Andhra Pradesh in M.Sc and B.Sc.
- Second Rank in B.Sc in the college
- Life Member of the Indian Laser Association.
- Student Member, SPIE.
- Member of the Indian Physics Association

Academic Interests

- Nonlinear Optical Phenomena in novel materials (Organic, Biological and nano-structures).
- Studies of excited state dynamics in the psec/.fsec domain using incoherent and coherent light
- Optical Limiting
- Transient absorption and pump-probe studies

References

1. Dr. D. Narayana Rao
   School of Physics
   University of Hyderabad,
   Hyderabad - 500 046. India.
   E-mail: dnrsp@uohyd.crnct.in
   Phone: +91-40-301-1230(O), +91-40-300-1084 (R)
   Fax; +91-40-301-0120 (145).

2. Prof. Surya P. Tewari
   School of Physics
   University of Hyderabad,
   Hyderabad - 500 046, India.
   E-mail: sptsp@uohyd.ernet.in
   Phone: +91-40-301-0500 (X-4303), +9140-301-0634 (R)
   Fax:+91-40-301-0120 (145).

3. Dr. G. Ravindra Kumar
   Atomic and Molecular Physics Group
   Tata Institute of Fundamental Research, Colaba,
   Mumbai - 400 005, India
   E-mail: grk@tifrvax.tifr.res.in
   Phone: +91-22-215-2971 (X-2381)
   Fax: +91-22-215-2110/2181

4. Dr. Bahaskar G. Maiya
   School of Chemistry
   University of Hyderabad,
   Hyderabad - 500 046, India.
   Phone: +91-40-301-0500 (x-4831), +91-40-301-0714 (R)
   E-mail: bgmsc@uohyd.ernet.in
   Fax: +91-40-301-0120 (145).

5. Dr. Ranjit Singh Pandher
   Department of Engineering Sciences and Physics
   1N-225, CS1/CUNY
   2800 Victory Blvd.,
   Staten Island, NY 10314
   USA
   E-mail: pandher@postbox.csi.cuny.edu
   Phone:001-718-982-2805